1-1-2017

Novel Functions Of Cardiolipin Remodeling In Saccharomyces Cerevisiae And Mammalian Cells: Implications For Barth Syndrome

Wenjia Lou
Wayne State University,

NOVEL FUNCTIONS OF CARDIOLIPIN REMODELING IN *SACCHAROMYCES CEREVISIAE* AND MAMMALIAN CELLS: IMPLICATIONS FOR BARTH SYNDROME

by

WENJIA LOU

DISSERTATION

Submitted to the Graduate School

of Wayne State University,

Detroit, Michigan

in partial fulfillment of the requirements

for the degree of

DOCTOR OF PHILOSOPHY

2017

MAJOR: BIOLOGICAL SCIENCES

Approved By:

_____

Advisor Date

_____

_____

_____

DEDICATION

谨以此书献给我的妻子陈青，儿子岚笛和我的父母，岳父母

I am grateful for my wife Qing Chen, my son Landi Lou, my parents, and my parents-in-law, without whom this dissertation would never be completed.

ACKNOWLEDGEMENTS

I owe my genuine gratitude to my advisor Dr. Miriam L. Greenberg for marvelous mentorship and support. Her passion for science and confidence inspired me to keep moving in the academic field. Her guidance encouraged me to not only be a good researcher but also develop social and written skills. She is an admirable friend who is willing to share my happiness and sadness. Finally, without access to a mentor who is both patient and inspiring, while astutely guiding me throughout this process, and her demand for perfect English composition, I can never finish my projects, convert them to published papers, and write this dissertation.

I would like to extend my sincerest gratitude and appreciation to my previous and current committee members: Dr. David Njus, Dr. Xiang-Dong Zhang, Dr. Weilong Hao, and Dr. Maik Hüttemann for their notable and valuable advice, and continuous support during my graduate studies. I would like to thank all collaborators and coauthors of my published papers for their great support.

I would like to thank and acknowlege my friends and colleagues: Dr. Christian Reynolds, Dr. Cunqi Ye, Dr, Rania Deranieh, Dr. Wenxi Yu, Dr. Shyamala Jadhav, Dr. Vaishnavi Raja, Michael Salsa, Yiran Li, Jiajia Ji, and Zhuqing Liang; for discussions on my research, and for making our lab sympathetic and cheery. Thanks to Keanna McCain for helping me with English and writing. Special thanks to Dr. Shuliang Chen for inviting me to join the lab.

Finally, I would like to thank my wife, Qing Chen; my son, Landi Lou; my parents, Minjie Zhang and Zhongchen Lou; and my in-laws, Jun Zhong and Qiping Chen for their unlimited love and support.

Thank you all very much!

TABLE OF CONTENTS

LIST OF TABLES

LIST OF FIGURES

CHAPTER 1 INTRODUCTION

The mitochondrion is one of the most important membrane-bound structures in eukaryotic cells. Mitochondria play a pivotal role in cellular energy production as well as metabolism. Mitochondria consist of outer and inner bilayer membranes, which constitute a unique composition of phospholipids and proteins. The lipid composition of the inner membrane determines its shape, which confers a functional role in anchoring proteins, modulating protein activity and signal transduction. The signature lipid of mitochondria is cardiolipin (CL), which is primarily localized in the inner membrane. In the presence of reactive oxygen species (ROS), which are known to accumulate in the mitochondria when the cells respire, CL acyl chains are peroxidized (Petrosillo et al., 2001). The activity of peroxidized CL, and products generated downstream, are intrinsic to mitochondrial signal transduction. The results of this dissertation research identify novel functions of CL remodeling in peroxidized CL removal and myotube differentiation.

1. Structure and cellular functions of CL

CL (1,3 diphosphatidyl-*sn*-glycerol) was first isolated from bovine cardiac tissue, in which it is most abundant (Pangborn, 1948; Shen et al., 2017). Unlike other phospholipids that have two fatty acyl chains and one phosphatidyl group, CL contains two phosphatidyl moieties, contributing two negative charges, and four acyl chains (Lecocq and Ballou, 1964) (Figure 1-1).

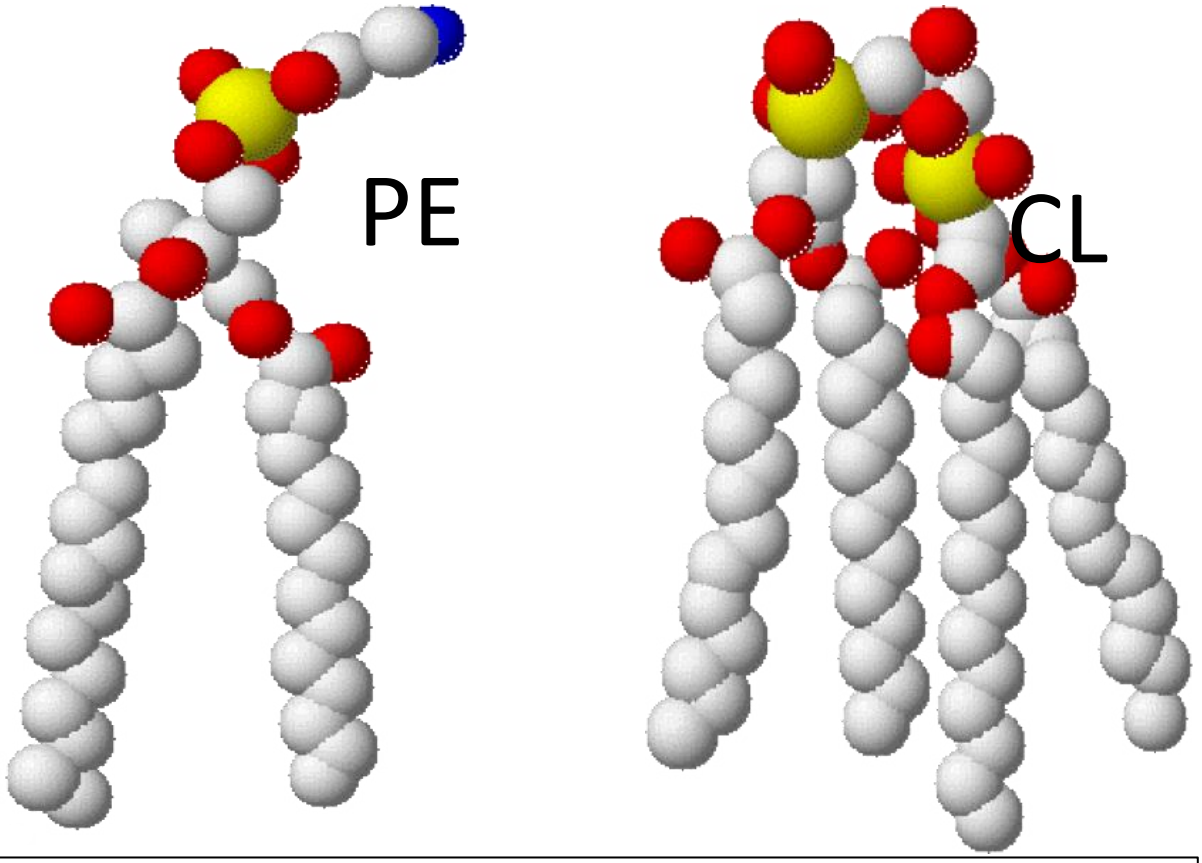

Figure 1-1 Cardiolipin (CL) has a unique structure

Unlike PE and other membrane phospholipids, CL has a dimeric structure in which two phosphatidyl moieties are linked by a glycerol. Consequently, it is hydrophobic and negatively charged due to the presence of four fatty acyl chains and two phosphate groups respectively. CL interacts with diverse mitochondrial proteins by hydrophobic and electrostatic interactions. The asymmetry of CL molecules, resulting from the diversity of fatty acyl chains, leads to a variety of CL species, which confer distinct functions of CL in different tissues. Symmetric CL molecules, in which all four fatty acid chains are linoleic acid, are common in heart and muscle. However, asymmetric CL molecules, with highly diversified acyl chains, are found in mammalian brain (Cheng et al., 2008; Kagan et al., 2014; Schlame et al., 2005).

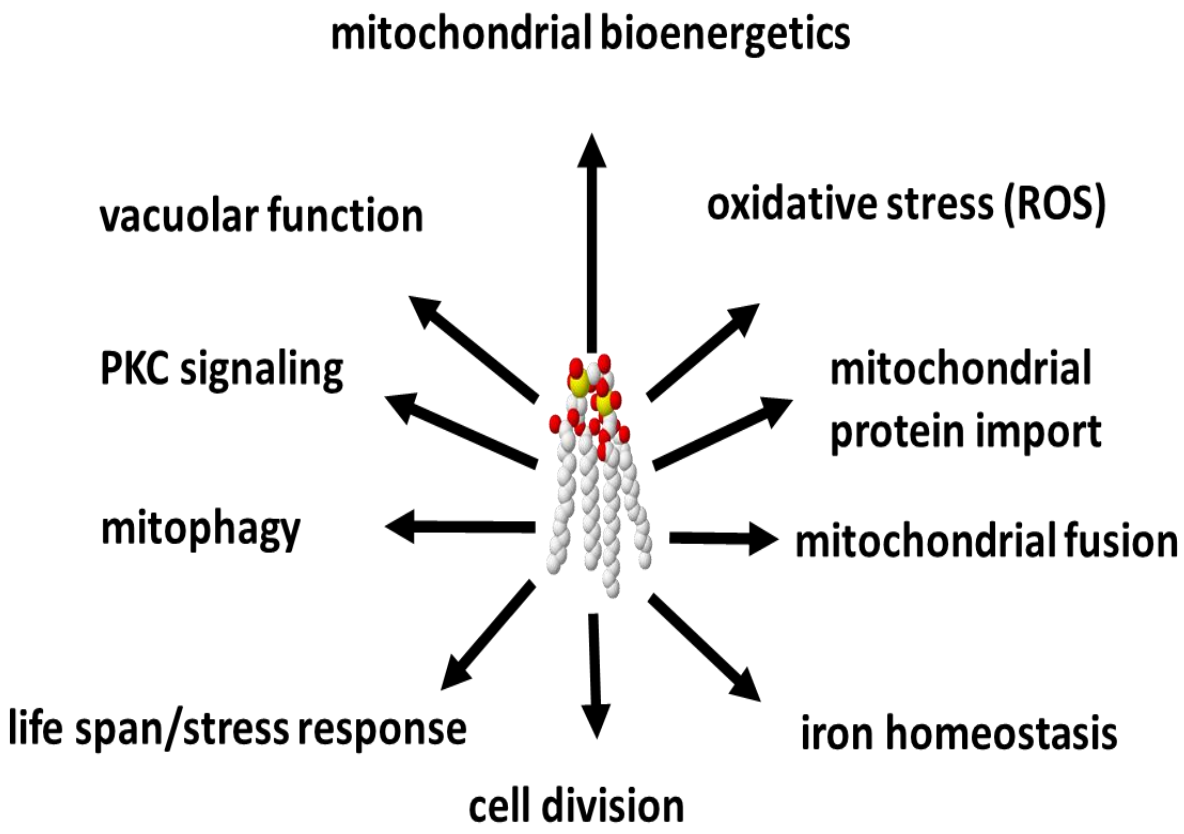

Figure 1-2 Various cellular functions of CL have been identified in yeast.

CL-protein interactions stabilize respiratory chain supercomplexes (Pfeiffer et al., 2003; Zhang et al., 2002), which is pivital to mitochondrial bioenergetics. Interestingly, CL is essential in cellular functions not generally associated with bioenergetics. Although the vacuolar concentration of CL is low, CL deficiency has been linked to vacuolar morphology and acidification defects at elevated temperature (Chen et al., 2008). The importance of CL to protein import is underscored by the finding that the absence of CL leads to a reduced membrane potential and decreased protein import (Jiang et al., 2000). Furthermore, CL is also required for assembly of outer membrane protein translocases (Gebert et al., 2009). Increasing evidence supports a role for CL in cellular signaling pathways, including PKC and HOG, which affact cell wall biogenesis, aging, and mitophagy (Zhong and Greenberg, 2005; Zhou et al., 2009). Additionally, functions of CL in life span/stress response (Gonzalvez and Gottlieb, 2007; Schug and Gottlieb, 2009), cell division (Chen et al., 2010), iron homeostasis (Patil et al., 2013), and mitochondrial fusion (Joshi et al., 2016) are now established.

CL comprises approximately 15% of total mitochondrial phospholipids (Jakovcic et al., 1971). CL interacts with a variety of mitochondrial proteins through both hydrophobic and electrostatic interactions (Schlame et al., 2000a), including the ADP/ATP carrier (Beyer and Klingenberg, 1985; Claypool et al., 2008b) and respiratory complexes (Eble et al., 1990; Lange et al., 2001; Palsdottir et al., 2003). CL-protein interactions stabilize and promote supramolecular associations such as respiratory chain supercomplexes and ADP/ATP carrier (Claypool et al., 2008b; Pfeiffer et al., 2003; Zhang et al., 2002). Additionally, CL deficiency leads to functional defects in diverse biochemical pathways other than mitochondrial bioenergetics, including mitochondrial dynamics (DeVay et al., 2009; Joshi et al., 2012); cell wall biogenesis (Zhong et al., 2005; Zhong et al., 2007); mitochondrial protein import (Gebert et al., 2009; Jiang et al., 2000); vacuolar function and morphology (Chen et al., 2008); aging (Zhou et al., 2009); cell cycle (Chen et al., 2010); mitophagy (Shen et al., 2017); iron homeostasis (Patil et al., 2013); and apoptosis (Gonzalvez and Gottlieb, 2007; Schug and Gottlieb, 2009). It is likely that this list will grow in the future (Figure1-2). The regulation of CL synthesis and remodeling is crucially important to the physiological state of an organism, as different CL species are engaged in diverse, yet significant cellular pathways (Kagan et al., 2014; Kagan et al., 2015).

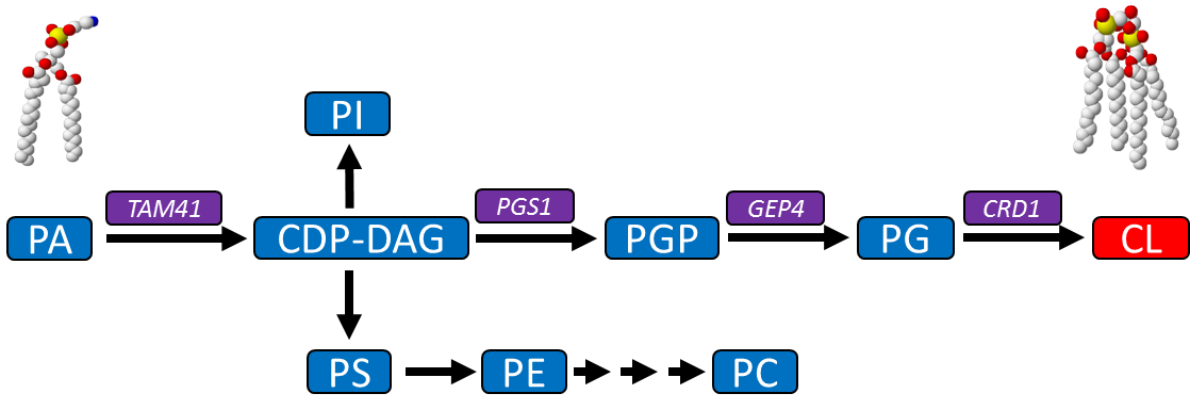

Figure 1-3 CL biosynthesis synthesis.

Prior to CL synthesis, CDP-DAG synthase (Tam41) catalyzes the transfer and conversion of phosphatidic acid (PA) from the outer membrane to the matrix face of inner mitochondrial membrane. To initiate CL synthesis, PGP synthase (Pgs1) catalyzes conversion of CDP-diacylglycerol (CDP-DAG) to phosphatidylglycerolphosphate (PGP). In the second step, PGP phosphatase (Gep4) dephosphorylate PGP to generate phosphatidylglycerol (PG). Lastly, CL synthase (Crd1) converts PG to nascent CL that contains saturated and unsaturated fatty acyl chains.

2. CL biosynthesis

According to current literature, “the life of a CL molecule can be divided into several discreet phases: biosynthesis, remodeling, peroxidation modification, translocation, and degradation” (Schlame and Greenberg, 2017). *TAM41*-encoded CDP-DAG synthase, located on the matrix side of the mitochondrial inner membrane, initiates CL biosynthesis through the conversion of phosphatidic acid (PA) to CDP-diacylglycerol (CDP-DAG) (Kutik et al., 2008; Tamura et al., 2013). PA is synthesized on the mitochondrial outer membrane and translocated to the inner membrane via the UPS1-encoded PA transfer protein (Athenstaedt and Daum, 1999). Secondly, CDP-DAG is converted to phosphatidylglycerol phosphate (PGP) by *PGS1*-encoded PGP synthase (Chang et al., 1998a), which is then dephosphorylated to phosphatidylglycerol (PG) by *GEP4*-encoded PGP phosphatase (Osman et al., 2010). CL synthase (Crd1) catalyzes the last step of CL synthesis by condensing CDP-DAG and PG to form CL (Figure 1-3) (Chang et al., 1998b; Jiang et al., 1997; Tamai and Greenberg, 1990; Tuller et al., 1998). Following *de novo* synthesis, CL undergoes a remodeling process in which saturated acyl chains are exchanged for unsaturated acyl chains.

3. CL remodeling

CL remodeling is a structural modification that follows *de novo* biosynthesis. This process facilitates fatty acyl chain transfer. The remodeled CL acyl chain species are organism and tissue specific. In the mammalian brain, the CL species are very diverse (Kiebish et al., 2008). However, in tissues with high energy turnover, such as the heart,

CL species are typically dominated by acyl groups with one or two double bonds (Schlame et al., 2005).

In yeast, a CL-specific phospholipase (Cld1) initiates CL remodeling as it deacylates CL to monolysocardiolipin (MLCL) on the matrix side of the inner mitochondrial membrane (Baile et al., 2013; Beranek et al., 2009). The CL transacylase, Taz1, utilizes donor phospholipids, particularly PC and PE, to reacylate MLCL and produce remodeled CL in the mitochondrial periphery (Figure 1-4) (Brandner et al., 2005; Gu et al., 2004; Testet et al., 2005). Remodeled CL contains more unsaturated acyl chains than CL synthesized *de novo* (Beranek et al., 2009; Gu et al., 2004; Vaz et al., 2003). Presently, the scientific community debates whether tafazzin transfers fatty acyl-chains from PE and PC to MLCL specifically. Although Abe et al. purport that purified yeast tafazzin catalyzes acyl-specific transacylation in bilayers, Schlame and Greenberg contend that tafazzin is simply a vehicle to facilitate fatty acid exchange between phospholipid molecules. Specifically, they argue that in order to generate specific CL species, the free energy of remodeled CL must be lower than the free energy of other molecular species (Abe et al., 2016; Schlame and Greenberg, 2017). These theories attempt to elucidate the mechanistic functions of Taz1 to further our understanding of the cellular role of CL remodeling. However, focus of my study was to elucidate the link between the cellular functions of Cld1 and CL remodeling.

The experiments described in Chapter 3 demonstrate that yeast Cld1 exhibits specificity for different CL molecular species. The observed molecular specificity suggests that the functional role of Cld1, with respect to CL remodeling, is to maintain

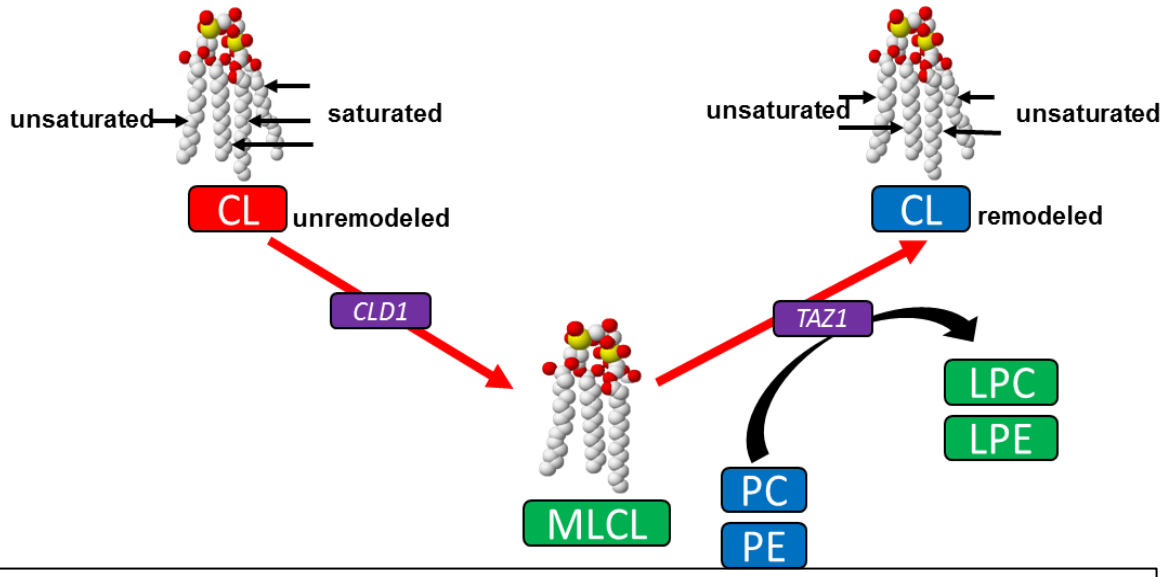

Figure 1-4 CL remodeling.

Unremodeled CL contains both saturated and unsaturated fatty acyl chains. Remodeling occurs in the outer leaflet of the inner membrane. *CLD1*-encoded phospholipase catalyzes the conversion of CL to monolyso-CL (MLCL). The transacylase, Taz1, utilizes donor phospholipids, particularly PC and PE, to reacylate MLCL to CL. Remodeled CL contains primarily unsaturated fatty acyl chains.

the levels of various molecular species within the CL pool. The study described in Chapter 2 identifies CL deacylation, catalyzed by Cld1, as the only step of CL remodeling significantly upregulated at the mRNA level. Taken together, my findings support this as a third possible explanation for the observed specificity of CL composition generated by CL deacylation. However, maintaining a CL pool of specified fatty acyl composition is not the only function of CL remodeling. My work also suggests that CL deacylation serves to specifically remove peroxidized acyl chains in response to oxidative stress.

4. CL peroxidation and translocation

In normally functioning mitochondria, the CL concentration is highest on the inner leaflet of the mitochondrial inner membrane (Hovius et al., 1990; Krebs et al., 1979). A

significant portion of CL is translocated to the mitochondrial outer membrane during mitochondrial injury and depolarization, which distorts the highly asymmetric distribution of CL between the outer and inner membranes (Baile et al., 2013; Garcia Fernandez et al., 2002; Gonzalvez and Gottlieb, 2007). Externalized CL signals autophagy machinery to remove damaged mitochondria (Chu et al., 2013). The translocation of CL from the inner to outer mitochondrial membrane, along with oxidative modification of CL acyl chains, leads to apoptotic death (Kagan et al., 2005b).

CL containing polyunsaturated fatty acyl chains are susceptible to oxidative modifications. This process is, under certain conditions, enzymatically catalyzed by the peroxidase function of an intermembrane space hemoprotein, cytochrome c (cyt c) (Atkinson et al., 2011; Kagan et al., 2009). In the absence of CL, cyt c peroxidase activity is negligible (Basova et al., 2007). Upon binding CL, cyt c undergoes a conformational change facilitating CL-specific peroxidation. Cyt c tyrosyl radicals are likely reactive intermediates of the peroxidase cycle, leading to CL peroxidation (Kapralov et al., 2011). Recent studies reveal that acute reperfusion injury, such as the massive apoptotic response observed during acute brain injury, is accompanied by the generation of multiple peroxidized CL (CLox) species (Chan and Di Paolo, 2012; Ji et al., 2012). The study also emphasizes that attenuating CL peroxidation confers a significant countermeasure against the biochemical and physiological effects of oxidative stress. Mammalian cells possess a similar mechanism to mitigate damage resulting from CL peroxidation. Liu's 2017 study reveals iPLA2γ, a gene product whose function is analogous to Cld1, as the major enzyme responsible for deacylation of oxidized

aliphatic chains from CL (Liu et al., 2017). Deletion of iPLA2γ results in the accumulation of peroxidized CL in mouse mitochondria when subjected to oxidative stress. There is mounting evidence to support CLs/CLox as necessitative signaling molecules for immune responses, cell death, and coordination of metabolism (Kagan et al., 2014; Maguire et al., 2017).

The physiological consequences and molecular mechanism of CL peroxidation remain poorly understood, and represent a significant gap in the field. My work, in part, focuses on the link between CL remodeling and peroxidation. Using the powerful yeast model, in which well-characterized mutants for every step of CL synthesis and remodeling are available, we are trying to elucidate the molecular mechanism of CL peroxidation.

5. CL and Barth Syndrome

The importance of CL remodeling is underscored by the X-linked mitochondrial disorder Barth syndrome (BTHS) (Figure 1-4). In 1983, Barth et al. identified a mitochondrial disease that negatively impacts bioenergetics of the heart, muscle and neutrophil leukocytes (Barth et al., 1983). Many abnormalities are well established in BTHS patients, including cardiomyopathy (Kelley et al., 1991; Spencer et al., 2006a); neutropenia (Kelley et al., 1991); underdeveloped skeletal musculature and weakness (Barth et al., 1983); growth delay (Kelley et al., 1991); exercise intolerance; and elevated urinary excretion of 3-methylglutaconic acid. Untreated BTHS patients die in infancy, or during early childhood, due to defective development of heart and skeletal muscle. Moreover, surviving BTHS patients are known to have a distinct cognitive

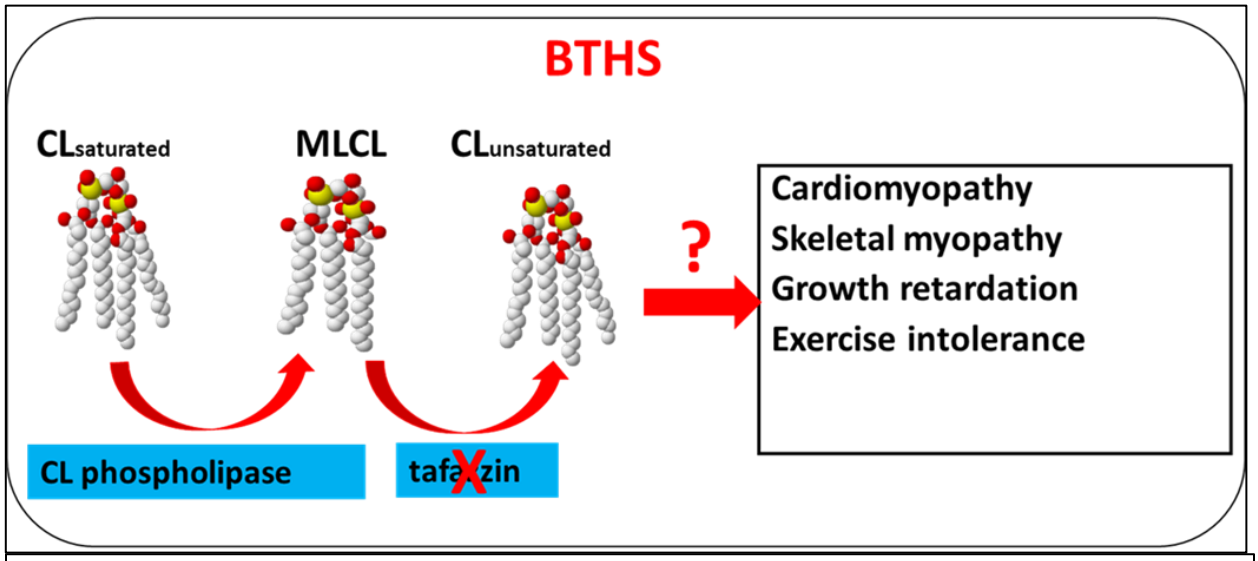

Figure 1-5 The cause of BTHS is not clear.

Mutations in tafazzin lead to perturbed CL remodeling resulting in decreased total CL, accumulation of MLCL, and aberrant CL acyl species that is associated with cardiomyopathy, skeletal myopathy, growth retardation and exercise intolerance. However, the link between CL deficiencies and the BTHS symptoms is not clear.

phenotype (Mazzocco et al., 2007a). After a decade, investigators mapped the mutant locus (Bolhuis et al., 1991), and the functional loss of tafazzin (TAZ) was identified as the genetic basis for clinical BTHS (Bione et al., 1996). Schlame and Ren showed that tafazzin reacylates monolyso-CL (MLCL) to CL (Schlame and Ren, 2006). The yeast and human tafazzin sequences are highly conserved, and encode a transacylase that catalyzes CL reacylation. Approximately 28 different TAZ mutations, resulting in single amino acid substitution, have been identified in BTHS patients (Schlame and Ren, 2006). These tafazzin mutations lead to either a complete loss of function, or expression of a severely truncated protein resulting in decreased total CL, accumulation of MLCL and aberrant CL acyl species (Schlame et al., 2002).

6. Yeast and mammalian BTHS models

The budding yeast, *Saccharomyces cerevisiae*, is an excellent eukaryotic model system (Botstein et al., 1997) because it is nonpathogenic, grows rapidly, and can be easily used for genetic analysis. More specifically, yeast is an excellent model for CL-focused research because deletion mutants for all CL biosynthetic genes are readily available and viable. Although the yeast model has clarified the role of CL in cell function and links the deficiency of CL to bioenergetic defects, a mammalian model organism is essential to test and confirm hypotheses regarding CL function in humans.

BTHS lymphoblasts, generated by EBV transformation, exhibit decreased mitochondrial membrane potential and abnormal mitochondrial proliferation (Xu et al., 2005). These cells exhibit phospholipid deficiencies similar to those seen in BTHS patients, namely impaired CL levels, increased MLCL, and aberrant acyl species. Lymphoblasts are relatively inexpensive and simply grown, which make them an easy model to work with. However, the disease phenotype may only manifest with a substantial metabolic demand beyond cell growth and division. BTHS lymphoblasts do not exhibit the same metabolic demand as cardiac and skeletal muscle cells. Most importantly, a congenic control cell line is not available for BTHS lymphoblasts.

Induced pluripotent stem cells (iPSCs) generated from BTHS patients exhibit mitochondrial defects similar to BTHS lymphoblasts (Dudek et al., 2013b). These cells can readily differentiate into muscle cells that exhibit the same metabolic demand as muscle cells. Unfortunately, they share the same disadvantage with BTHS lymphoblasts: the lack of a congenic control cell line.

Inducible short hairpin RNA (shRNA)-mediated tafazzin knockdown mice, and tafazzin knockout mouse embryonic stem cells are very powerful models for BTHS research (Acehan et al., 2009; Acehan et al., 2011; Soustek et al., 2011). Murine tafazzin knockdown resulted in a dramatic decrease of tetralinoleoyl CL and accumulation of MLCL. When tafazzin is knocked down, mitochondria, myofibrils, and mitochondrial-associated membranes of murine skeletal and cardiac muscles exhibit pathological changes similar to BTHS patients. Additionally, the congenic control is available for both of these models. However, mice and stem cells are relatively expensive and laborious to handle.

To circumvent the drawbacks of current mammalian models, I constructed a stable mammalian cell line using C2C12 mouse myoblasts, which will be described in Chapter 6. The C2C12 mouse skeletal muscle cell line is maintained as myoblasts under high serum conditions, and is easily differentiated into myotubules under low serum conditions. It is often employed in studies of mitochondrial bioenergetics (Leary et al., 1998; Liu and Brooks, 2012; Nicholls et al., 2010). The TAZ-KO C2C12 cells exhibit similar mitochondrial defects observed in other BTHS models such as decreased membrane potential and respiration. Additionally, the TAZ-KO C2C12 cells exhibit the same metabolic demand as skeletal muscle cells, have a congenic control cell line, and are relatively inexpensive and easy to handle.

7. Project outline

The objectives of the studies described in this thesis were to elucidate functions of *CLD1* and CL remodeling in the yeast *S. cerevisiae* and murine myoblasts.

In the studies summarized in **Chapter 2**, we assayed the regulation of yeast CL phospholipase, Cld1. Our data indicated that an increased MLCL/CL ratio, but not decreased CL unsaturation, is likely the primary cause of decreased respiratory growth and chronological life span observed in *taz1Δ*. This suggests that the physiological defects of BTHS patients is possibly due to increased MLCL/CL rather than decreased unsaturated CL, and that attenuation of CL phospholipases may potentially treat BTHS.

If unsaturated CL is not essential, as suggested by our finding, what is the function of CL remodeling? Our finding that *CLD1* expression was upregulated under respiratory conditions suggests the possibility that *CLD1* expression is upregulated in response to oxidative stress. CL peroxidation, resulting from oxidative stress, has been described in mammalian cells (Bayir et al., 2007; Kriska et al., 2005; Petrosillo et al., 2001). Based on this, one of the physiological roles of CL remodeling may be to remove peroxidized CL. To address this possibility, it was necessary to determine whether CL species can be altered by nutritional supplementation of PUFA, because yeast does not synthesize oxidizable CL **(Chapter 3).** Liquid chromatography−mass-spectrometry-based phospholipidomics was combined with genetic and nutritional manipulations to assay CL incorporation of PUFA during the CL biosynthetic and post-synthetic remodeling processes in yeast. Our results demonstrated that yeast readily incorporated PUFA to synthesize oxidizable CL. To genetically manipulate CL species, the *H. brasiliensis* Δ^{12}-desaturase gene was expressed in yeast **(Chapter 4).** Lipidomic analysis of this strain confirmed the presence of PUFA within molecular species of CL. Although multiple CL-hydroperoxides and CL-dihydroperoxides were readily detected in

these cells, cell growth and life span were not impacted. Using this novel yeast model, in which cells expressed Δ^{12}-desaturase, the specificity of Cld1 for peroxidized CL, and its role in deacylating peroxidized CL, was determined **(Chapter 5)**. *cld1Δ* cells expressing Δ^{12}-desaturase were utilized to determine the effect of peroxidation on CL remodeling. In cells expressing desaturase, loss of *CLD1* led to increased peroxidized CL species, as well as decreased cell growth and life span. The findings from this study may help to clarify the role of CL remodeling and its mechanistic roles in mitigating oxidative stress.

To probe defects resulting from CL deficiency in mammalian cells **(Chapter 6)**, I constructed a tafazzin knockout C2C12 cell line, which exhibits an increased MLCL/CL ratio, decreased respiration capacity, increased ROS generation and decreased membrane potential. Although WT and TAZ-KO C2C12 cells can differentiate into myotubes, differentiation was significantly decreased in TAZ-KO C2C12 cells under certain conditions. Taken together, these findings indicate that CL remodeling plays a role in myotube differentiation.

While the studies described here identify various functions of CL, many questions remain unanswered. Future studies to elucidate functions of CL are suggested in **Chapter 7**.

CHAPTER 2 DELETION OF THE CARDIOLIPIN-SPECIFIC PHOSPHOLIPASE *CLD1* RESCUES GROWTH AND LIFESPAN DEFECTS IN THE TAFAZZIN MUTANT: IMPLICATIONS FOR BARTH SYNDROME

The work described in this chapter has been published in Ye*, C**., W. Lou***, Y. Li, I.A. Chatzispyrou, M. Huttemann, I. Lee, R.H. Houtkooper, F.M. Vaz, S. Chen, and M.L. Greenberg. 2014. Deletion of the cardiolipin-specific phospholipase Cld1 rescues growth and life span defects in the tafazzin mutant: implications for Barth syndrome. *The Journal of biological chemistry.* 289:3114-3125. ***Equal contributors** http://www.ncbi.nlm.nih.gov/pubmed/24318983

It has also been published in Ye, Cunqi, "Characterization And Identification Of Novel Regulators Of The Synthesis Of Phospholipids" (2014). *Wayne State University Dissertations*. Paper 1036.

INTRODUCTION

Cardiolipin (CL) is a unique phospholipid that is predominant in mitochondrial membranes (Hostetler et al., 1972; Joshi et al., 2009a). Unlike other membrane phospholipids, it contains two phosphatidyl moieties, four acyl chains and two negative charges (Lecocq and Ballou, 1964; Pangborn, 1947). As the signature lipid of mitochondria, it comprises about 15% of total mitochondrial phospholipids (Jakovcic et al., 1971) and interacts with a wide range of mitochondrial proteins (Claypool, 2009; Klingenberg, 2009; Schlame and Ren, 2009; Schlame et al., 2000a), including the ADP/ATP carrier (Beyer and Klingenberg, 1985; Claypool et al., 2008b) and respiratory complexes (Eble et al., 1990; Lange et al., 2001; Palsdottir et al., 2003; Shinzawa-Itoh et al., 2007). CL-protein interactions stabilize respiratory chain supercomplexes (Pfeiffer

et al., 2003; Zhang et al., 2002) and promote supramolecular associations between the ADP/ATP carrier and respiratory supercomplexes (Claypool et al., 2008b). Therefore, it is not surprising that mitochondrial respiration and energy production are highly correlated with CL biosynthesis (Claypool et al., 2008b; Gohil et al., 2004; Jiang et al., 2000). Interestingly, CL deficiency also leads to deficiencies in diverse cellular functions other than mitochondrial bioenergetics, including mitochondrial dynamics (DeVay et al., 2009; Joshi et al., 2012), mitochondrial protein import (Gebert et al., 2009; Jiang et al., 2000), cell wall biogenesis (Zhong et al., 2005; Zhong et al., 2007), vacuolar function and morphology (Chen et al., 2008), cell cycle (Chen et al., 2010), aging (Zhou et al., 2009), and apoptosis (Gonzalvez and Gottlieb, 2007; Houtkooper and Vaz, 2008; Schug and Gottlieb, 2009). As CL is engaged in a plethora of cellular activities, the regulation of CL synthesis is crucially important.

The synthesis of CL is well-characterized in *Saccharomyces cerevisiae*. As seen in Figure 2-1, Pgs1 catalyzes the committed step of CL synthesis by converting CDP-DAG and glyerol-3-phosphate to phosphatidylglycerolphosphate (PGP) (Chang et al., 1998a), which is dephosphorylated to phosphatidylglycerol (PG) by the PGP phosphatase Gep4 (Kelly and Greenberg, 1990; Osman et al., 2010). CL synthase (Crd1) catalyzes the final step of *de novo* CL synthesis by condensing PG and CDP-DAG to form CL with primarily saturated acyl chains (Chang et al., 1998b; Jiang et al., 1997; Tamai and Greenberg, 1990; Tuller et al., 1998). Following the *de novo* synthesis of CL on the matrix side of the inner mitochondrial membrane, CL undergoes remodeling in which acyl chains are exchanged. In this process, CL is deacylated to

monolysocardiolipin (MLCL) by the CL-specific lipase Cld1 on the matrix side of the inner mitochondrial membrane (Baile et al., 2013; Beranek et al., 2009). MLCL is reacylated by the transacylase Taz1 in the mitochondrial periphery (Brandner et al., 2005; Claypool et al., 2008a; Gu et al., 2004; Testet et al., 2005). Remodeled CL has more unsaturated acyl chains than CL synthesized *de novo* (Beranek et al., 2009; Gu et al., 2004; Vaz et al., 2003; Xu et al., 2003). Although the CL remodeling genes and enzymes have been identified in yeast, the function of CL remodeling and mechanisms underlying its regulation are not understood.

The importance of CL remodeling is underscored by the X-linked mitochondrial disorder Barth syndrome (BTHS), a cardioskeletal myopathy that results from mutations in the tafazzin gene (the homologue of yeast *TAZ1*) (Barth et al., 1983; Barth et al., 2004; Barth et al., 1999a). Tafazzin deficiency leads to a decrease in the CL/MLCL ratio and a decrease in CL species containing unsaturated fatty acids (Acehan et al., 2011; Gu et al., 2004; Houtkooper et al., 2009; Schlame et al., 2003; Valianpour et al., 2002; Vreken et al., 2000; Xu et al., 2006a). Which of these biochemical outcomes leads to the pathology in BTHS is not understood. Genetic inactivation of the CL-specific phospholipase iPLA2-GVIA rescued sterility defects associated with tafazzin deficiency in *Drosophila* (Malhotra et al., 2009). The mechanism underlying this rescue is not known. In mammals, CL-specific phospholipases have not been identified, and multiple phospholipases supposedly catalyze the deacylation of CL (Hsu et al., 2013), complicating experiments to elucidate the role of deacylation in mammalian cells. In

Table 2-1 Strains and plasmids used in this study

BY4741	*MATa his3Δ1 leu2Δ0 met15Δ0 ura3Δ0*	Invitrogen
BY4742	*MATα his3Δ1 leu2Δ0 lys2Δ0 ura3Δ0*	Invitrogen
crd1Δ	*MATa his3Δ1 leu2Δ0 met15Δ0 ura3Δ0 crd1Δ::KanMX6*	Invitrogen
cld1Δ	*MATa his3Δ1 leu2Δ0 met15Δ0 ura3Δ0 cld1Δ::KanMX6*	Invitrogen
taz1Δ	*MATa his3Δ1 leu2Δ0 met15Δ0 ura3Δ0 taz1Δ::KanMX6*	this study
cld1Δtaz1 Δ	*MATa his3Δ1 leu2Δ0 met15Δ0 ura3Δ0 cld1Δ::KanMX6 taz1Δ::KanMX6*	this study
mig1Δ	*MATα his3Δ1 leu2Δ0 lys2Δ0 ura3Δ0 mig1Δ::KanMX6*	Invitrogen
hap2Δ	*MATα his3Δ1 leu2Δ0 lys2Δ0 ura3Δ0 hap2Δ::KanMX6*	Invitrogen
hap3Δ	*MATα his3Δ1 leu2Δ0 lys2Δ0 ura3Δ0 hap3Δ::KanMX6*	Invitrogen
hap4Δ	*MATa his3Δ1 leu2Δ0 met15Δ0 ura3Δ0 hap4Δ::KanMX6*	Invitrogen
hap5Δ	*MATa his3Δ1 leu2Δ0 met15Δ0 ura3Δ0 hap5Δ::KanMX6*	Invitrogen
BY4741 *ρ°*	*ρ°* mutant derived from BY4741	this study
crd1Δ ρ°	*ρ°* mutant derived from BY4741 *crd1Δ*	this study
cld1Δ ρ°	*ρ°* mutant derived from BY4741 *cld1Δ*	this study
taz1Δ ρ°	*ρ°* mutant derived from BY4741 *taz1Δ*	this study
cld1Δtaz1Δ ρ°	*ρ°* mutant derived from BY4741 *cld1Δtaz1Δ*	this study
pYPGK18	*2μm, LEU2*	(Vaz et al., 2003)
pYPGK18CLD1	derived from pYPGK18, expression CLD1 from *PGK1* promoter	this study

contrast, *CLD1* is the only CL-specific phospholipase in *S. cerevisiae* (Beranek et al., 2009). The yeast *cld1Δ* mutant has decreased unsaturated CL compared to wild type cells, but the CL/MLCL ratio is not altered. In this study, we demonstrated for the first time that deletion of *CLD1* rescued both respiratory and fermentative growth defects as well as decreased chronological life span in yeast *taz1Δ* cells. This suggests that deacylation of CL in the absence of tafazzin is deleterious because it leads to a decrease in the CL/MLCL ratio. These findings argue against the current thought that defects in tafazzin deficient cells result from decreased unsaturated CL. We further show that expression of *CLD1* is regulated in response to conditions affecting mitochondrial respiration and controlled by the HAP transcriptional activator.

Overexpression of *CLD1* leads to decreased ATP production from mitochondrial respiration that is compensated by increased glycolysis. Based on these findings, we proposed that transcriptional regulation of *CLD1* controls deacylation of CL, and the regulation of this process modulates cellular energy production

METHODS AND MATERIALS

Yeast strains, plasmids and growth media—The yeast *S. cerevisiae* strains and plasmids used in this study are listed in Table 2-1 and Table 2-2. Single deletion mutants were obtained from the yeast knock-out deletion collection (Invitrogen). Double mutants were obtained by tetrad dissection. Parental ρ^+ cells were used to generate ρ° derivatives by growing in yeast extract peptone dextrose (YPD) medium containing 20 μg/ml ethidium bromide to the early stationary phase. ρ° strains were confirmed by inability to grow on yeast extract peptone glycerol ethanol (YPGE) medium, the absence of mitochondrial DNA by DAPI staining, and the failure to complement ρ^- tester strains for growth on YPGE medium. To construct a *CLD1*-overexpression plasmid, a 1338-bp sequence containing the entire open reading frame of *CLD1* was amplified from yeast genomic DNA using an EcoRI-tagged forward primer CLD1_EcoRI_F (5'-TATAGAACATGAATTCAAAAGTGAGCTGCAATGAGCA) and an XbaI-tagged reverse primer CLD1_XbaI_R (5′- ATTTTGAGATTCTAGAAAGAAGAAAAATAGCGGCGA -3′). The PCR products were purified using the Wizard SV Gel and PCR Clean-up System (Promega). The purified DNA fragments were ligated into pYPGK18 cut with EcoRI and XbaI, downstream of the *PGK1* promoter. All the plasmids were amplified and extracted

using standard protocols. The plasmids were transformed into yeast strains using a one-step transformation protocol.

Synthetic complete (SC) medium contained adenine (20.25 mg/L), arginine (20 mg/L), histidine (20 mg/L), leucine (60 mg/L), lysine (200 mg/L), methionine (20 mg/L), threonine (300 mg/L), tryptophan (20 mg/L), uracil (20 mg/L), yeast nitrogen base without amino acids (Difco), all the essential components of DIFCO vitamin (inositol-free), 0.2% ammonium sulfate, and glucose (2%). Inositol (75 μM) was supplemented in all media used in this study. Synthetic dropout media contained all ingredients mentioned above except for the amino acid used as a selectable marker, and were used to culture strains containing a plasmid.

Chronological life span—Yeast chronological life span is determined by survival of non-dividing cells in a prolonged stationary culture (Fabrizio and Longo, 2003). A standard protocol previously described was followed (Hu et al., 2013) to assess chronological life span. In brief, individual colonies were inoculated in 10 ml of SC glucose medium and incubated overnight. The cultures were then diluted in 50 ml of SC medium, and cells were allowed to grow until saturation. Viable cells were measured every 2 or 3 days by counting colonies that were serially diluted and plated on YPD plates and represented as percentage of cells at day 2. The viability is considered to be 100% at or before day 2.

Spotting assay—Cells were pre-cultured in SC medium to the early stationary growth phase at 30°C and washed with sterile water. Three μL aliquots of a series of 10-fold

dilutions of 0.5 units of A_{550} cells were spotted onto indicated plates and incubated at 30°C.

Real-Time quantitative PCR (RT-qPCR) analysis—Cells were grown to the indicated growth phase and harvested at 4°C. Total RNA was extracted using hot phenol (Kohrer and Domdey, 1991) and purified using the RNeasy Mini Plus kit (QIAGEN, Valencia, CA). Complementary DNA (cDNA) was synthesized using the First Strand cDNA Synthesis Kit (Roche Applied Science, Indianapolis, IN) according to the manufacturer's manuals. RT-qPCR reactions were performed in a 20 µL volume using Brilliant III Ultra-Faster SYBR Green QPCR Master Mix (Agilent Technologies, Santa Clara, CA). Triplicates were included for each reaction. The primers for RT-qPCR are listed in Table 2-2. RNA levels were normalized to ACT1. Relative values of mRNA transcripts are shown as fold change relative to indicated controls. Primer sets were validated according to Methods and Applications Guide from Agilent Technologies. Optimal primer concentrations were determined, and primer specificity of a single product monitored by a melt curve following the amplification reaction. All the primers were validated by measurement of PCR reaction efficiency and have calculated reaction efficiencies between 95-105%.

Measurement of respiration—Cell respiration was analyzed in a closed 500 µL chamber equipped with a micro Clark-type oxygen electrode (Oxygraph plus system, Hansatech) at 30°C. Cells grown to the logarithmic phase were mixed in fresh growing media using a

Table 2-2. Real-time PCR primers used in this study.

Gene	Primers	Sequence (5' to 3')	
ACT1	Forward	TCCGGTGATGGTGTTACTCA	this study
	Reverse	GGCCAAATCGATTCTCAAAA	
PGS1	Forward	TTTGCTCCAACTCACTCGTCCTCA	this study
	Reverse	ATTGCCAAATGGAGAAGGGTTCGC	
GEP4	Forward	AAAGGCCGTGGTCTTGGATAAGGA	this study
	Reverse	ATTGGAACCGGCGGTATTGCTAA	
CRD1	Forward	TGCGGCGATAATTCTGGGTAGAGA	this study
	Reverse	ATTCCATGCCACACGACCAGGATA	
CLD1	Forward	ACTGGCTTTGGCTTTATGGCGAT	this study
	Reverse	TCCAGGTACAAGTGATGCCCTGA	
TAZ1	Forward	CGAAGCCATCTTGGGTCCATGTT	this study
	Reverse	CAATGGGCGGCTTTGTTGCTTCT	
ADH1	Forward	GGTCTAGGTTCTTTGGCTGTT	this study
	Reverse	CACCACCGATGGATCTGAATAA	
ADH2	Forward	GTACTGTTGTCTTGGTTGGTTTG	this study
	Reverse	GTAAGAGCCGACAATGGAGATAG	
PGK1	Forward	AGGCTTCTGCCCCAGGTTC	(Szijgyarto et al., 2011)
	Reverse	CAGCACGTTGTGGCAAGTC	
GAPDH	Forward	AGTCTTTTGGGTGGCGGTCA	(Szijgyarto et al., 2011)
	Reverse	ACATTGACGCTGGTGCCAAG	

protein concentration of 2 mg/mL following measurements of basal respiration. State 4 and 3 respiration was determined in the presence of 4 μM oligomycin and 5 μM FCCP, respectively. KCN (0.2 mM) was added at the end of the experiment to inhibit cytochrome c oxidase to normalize for (subtract) cytochrome c oxidase independent oxygen consumption. Oxygen consumption was recorded on a computer and analyzed with the Oxygraph plus software. Respiration rates are defined as consumed O_2 (nmol)/min·total protein (mg).

Determination of ATP concentrations—Yeast cells were cultured to the logarithmic phase and flash-frozen with liquid nitrogen. ATP levels were determined by the bioluminescence method described previously (Lee et al., 2010).

Determination of ethanol concentrations—Yeast cells were cultured in 10-mL growth medium for the indicated times to the logarithmic phase after inoculation at A_{550} of 0.05, and cells were pelleted by a 5-min centrifugation at 3,000 rpm. Supernatants were used to determine ethanol concentrations in the media. An ethanol colorimetric assay kit from BioVision was used to assay ethanol concentrations according to the manufacturer's manual.

Mitochondrial aconitase activity—Cultures (2L) of yeast cells in the mid-logarithmic phase were harvested for isolation of mitochondria. Mitochondria were isolated as described previously (Diekert et al., 2001). Briefly, spheroplasts generated by zymolyase treatment were ruptured by Dounce homogenization, and mitochondria were obtained by differential centrifugation. Total mitochondrial protein concentration was determined using the BCA protein assay (Pierce Protein). Mitochondrial aconitase activity was determined in mitochondrial extracts (50-μg protein) using an aconitase-isocitrate dehydrogenase-coupled assay, in which NADPH formation was monitored at A_{340} for 1 h (Gardner, 2002).

Determination of CL by mass spectrometry —Total lipid extracts from 10 mg of cells (dry weight) were analyzed by HPLC-MS as described previously (Houtkooper et al., 2006).

RESULTS

Deletion of *CLD1* rescues growth and life span defects of the *taz1Δ* mutant.

Deacylation of CL in the absence of tafazzin leads to a decreased ratio of CL/MLCL and decreased unsaturated CL (Acehan et al., 2011; Gu et al., 2004; Valianpour et al., 2002; Xu et al., 2006a), either of which may be responsible for cellular defects in tafazzin-deficient cells. We wished to distinguish between decreased CL/MLCL ratio vs. decreased unsaturated CL as the mechanism underlying the defects in the *taz1Δ* mutant. Blocking CL deacylation by deletion of *CLD1* prevents the decrease in CL/MLCL ratio (Beranek et al., 2009). However, the CL that is synthesized *de novo* but not remodeled is mostly saturated, in contrast to remodeled CL in wild type (WT) cells, which is mostly unsaturated (Beranek et al., 2009). To determine if the decreased CL/MLCL ratio is responsible for *taz1Δ* defects, we determined the effects of *CLD1* deletion in *taz1Δ* mutants. Interestingly, deletion of *CLD1* rescued the respiratory growth defect of the *taz1Δ* mutant (Figure 2-2A). Because mitochondrial respiration varies in strains with different genetic backgrounds (Ocampo et al., 2012) and the presence of polymorphic mitochondrial DNA can contribute to differences in mitochondrial respiration (Dimitrov et al., 2009), we assayed the effects of *CLD1* deletion independent of mitochondrial respiration. To do so, we constructed ρ^0 strains (which lack mitochondrial DNA) of the WT and CL mutants. While CL deficient cells grow normally on glucose (Figure 2-2A), which can be fermented,

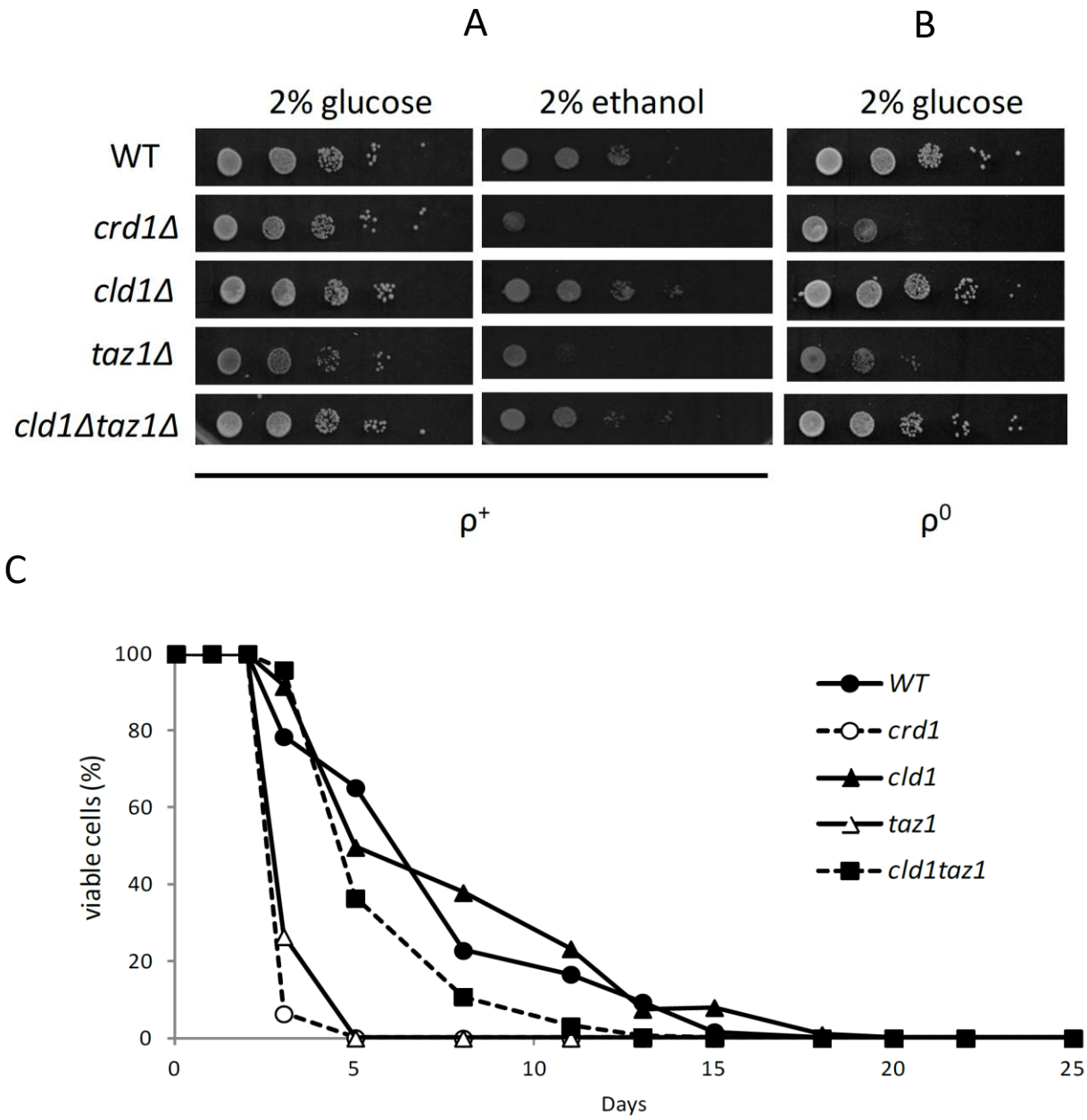

Figure 2-1. Deletion of *CLD1* rescues growth and chronological life span defects in *taz1Δ*.

(A) Serial 10-fold dilutions of WT, *crd1Δ*, *cld1Δ*, *taz1Δ*, and *crd1Δtaz1Δ* cells were spotted on synthetic complete medium with 2% glucose or 2% ethanol as carbon sources. Plates were incubated at 30°C for 3 days. (B) Serial 10-fold dilutions of respiration-incompetent (ρ^0) cells of the above mutants were spotted on synthetic complete medium with 2% glucose. (C) Chronological life span of WT, *crd1Δ*, *cld1Δ*, *taz1Δ*, and *crd1Δtaz1Δ* cells was determined as described under "Experimental Procedures." The data depicted in the figure is a representative of three experiments.

growth on glucose is compromised in the mutants if they lack mitochondrial DNA (Figure 2-2B). Deletion of *CLD1* rescued this growth defect (Figure 2-2B). We predicted that CL deficient cells would exhibit a decreased chronological life span similar to the decreased replicative life span observed in these cells (Zhou et al., 2009). As shown in Figure 2-2C, both *crd1Δ* and *taz1Δ* mutants exhibited a dramatic decrease in chronological life span. Deletion of *CLD1* partially rescued the decrease in *taz1Δ* life span, as the life span of *taz1Δcld1Δ* was almost similar to that of WT (Figure 2-2C). The observation that deletion of *CLD1* suppresses the defects in *taz1Δ* indicates that deacylation of CL is deleterious in the absence of tafazzin, and that the decreased CL/MLCL ratio but not decreased CL unsaturation is likely the primary cause of *taz1Δ* defects.

CLD1 expression is highly regulated in response to growth phase, glucose availability and respiratory activity.

The finding that *cld1Δ* rescued respiratory defects in *taz1Δ* suggested that *CLD1* expression plays a role in respiration. We first compared expression of CL biosynthetic genes, including *PGS1*, *GEP4*, *CRD1*, *CLD1*, and *TAZ1,* in logarithmically growing cells (in which energy is generated primarily from glycolysis) and in cells in the stationary phase (during which energy is generated from respiration). Expression of all the CL biosynthetic genes was increased in the stationary phase (Figure 2-3A). However, while *PGS1*, *GEP4*, *CRD1*, and *TAZ1* were increased about 3-5 fold, *CLD1* was increased by about 10-fold in the early stationary phase and more than 30-fold in the later stationary phase (Figure2-3A). The large increase in *CLD1* expression suggests that levels of

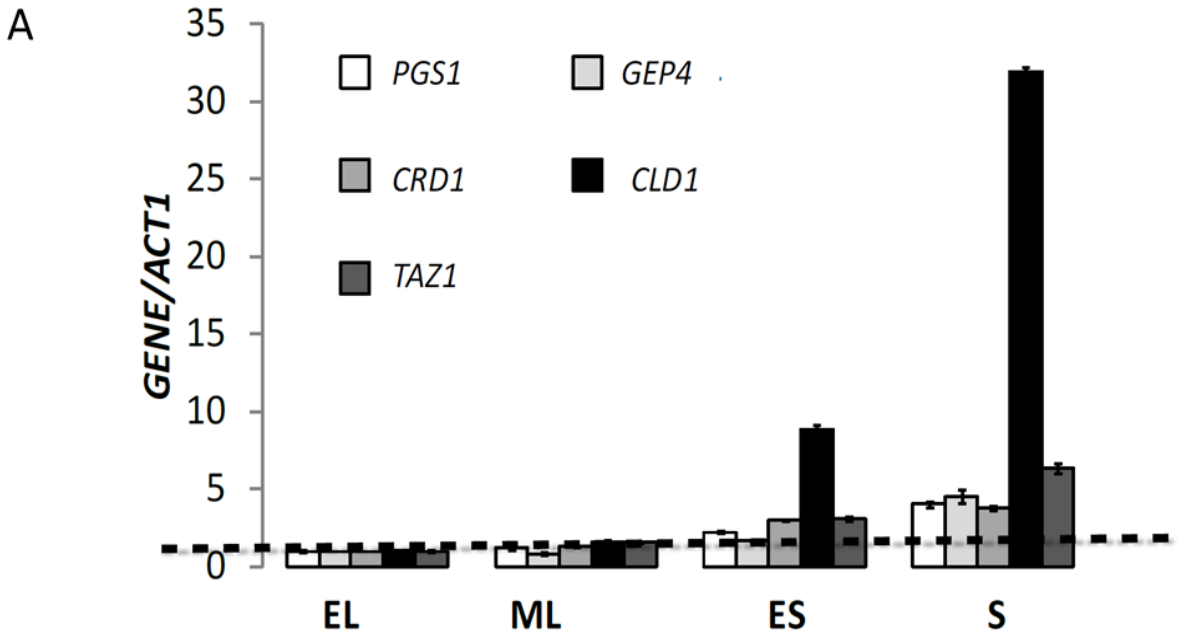
A
35
30
25
20
15
10
5
0
GENE/ACT1
PGS1
GEP4
CRD1
CLD1
TAZ1
EL
ML
ES
S

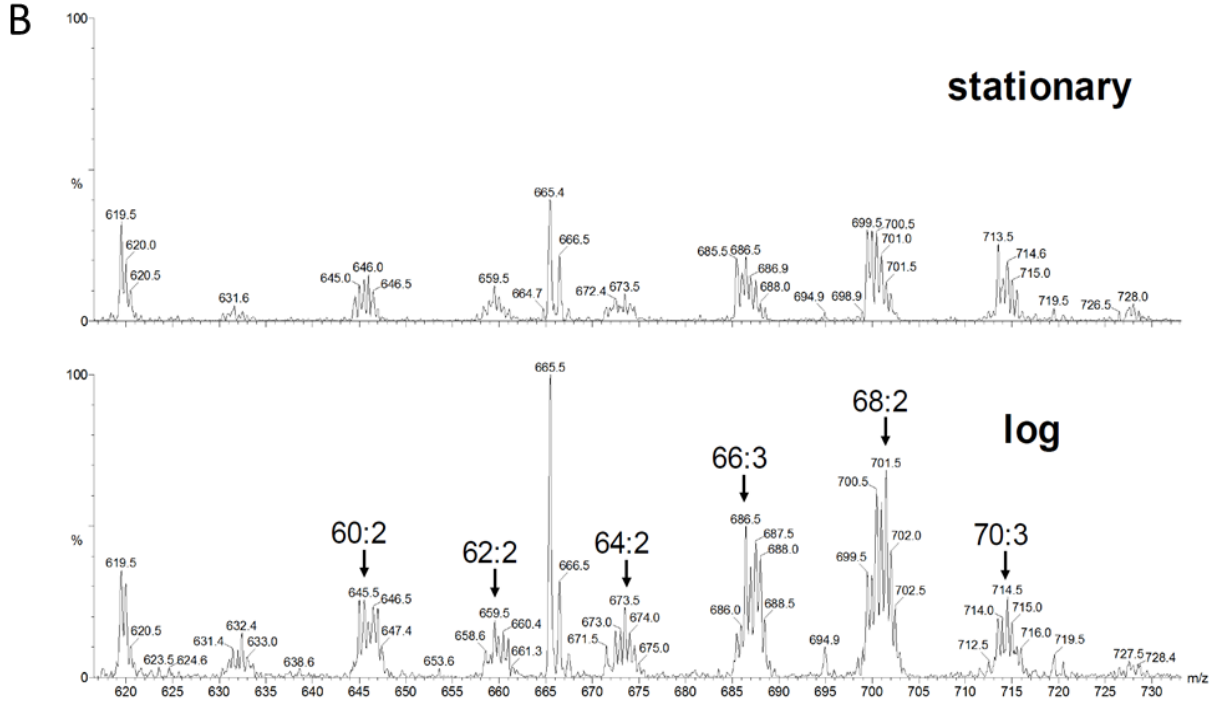
B
stationary
log
60:2
62:2
64:2
66:3
68:2
70:3
m/z

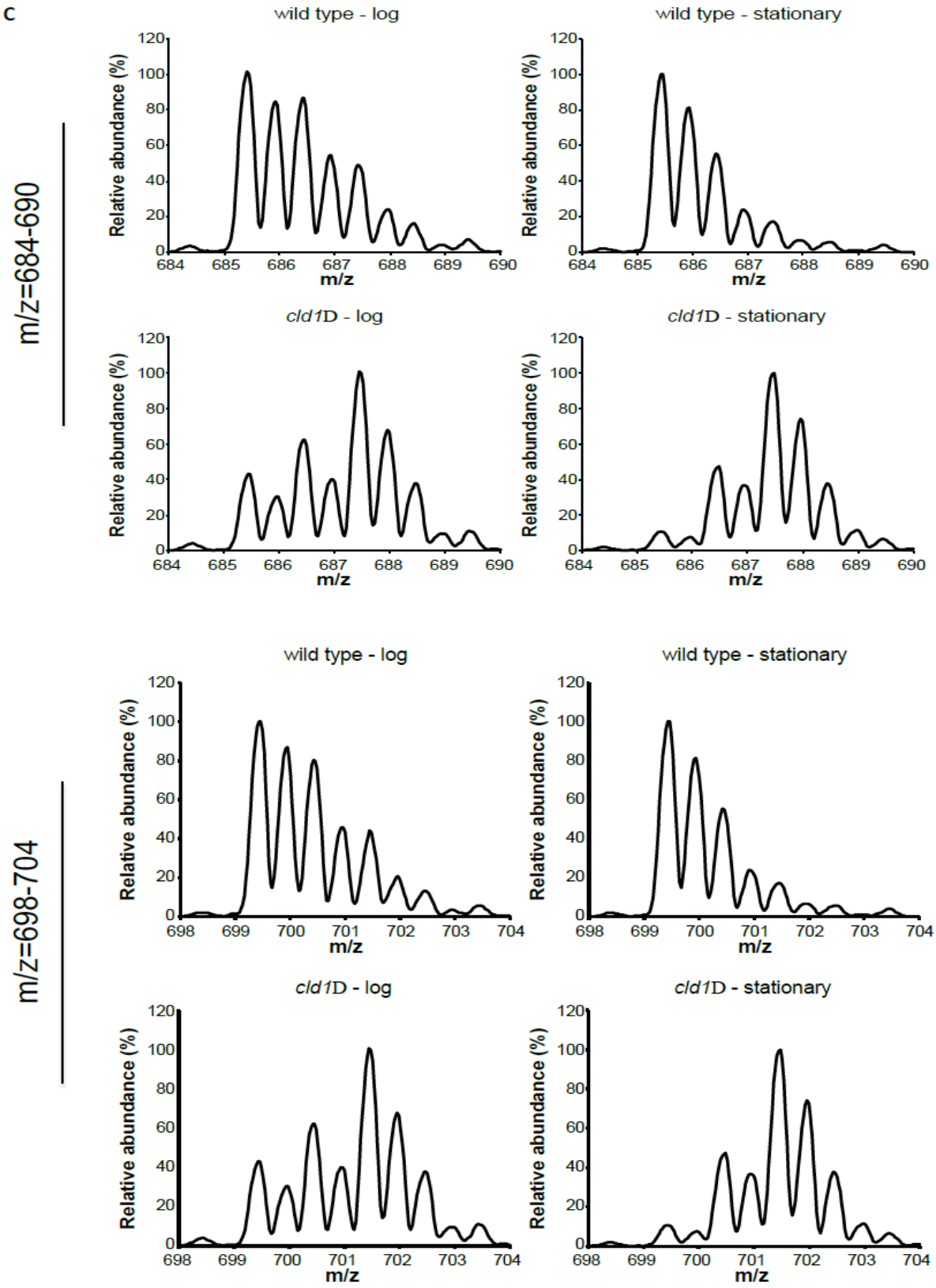
C
m/z=684-690
m/z=698-704
wild type - log
wild type - stationary
cld1D - log
cld1D - stationary
Relative abundance (%)
m/z

Figure 2-2. Increased *CLD1* expression in the stationary phase is concomitant with increased CL unsaturation.

(A) WT cells were grown in SC medium to the early-logarithmic (EL), mid-logarithmic (ML), early-stationary (ES), and stationary (S) growth phases, and *PGS1, GEP4, CRD1, CLD1,* and *TAZ1* expression was quantified by RT-PCR as described under "Experimental Procedures." Values of each gene were normalized to the internal control *ACT1* and are represented as fold change relative to those in EL. Data shown are mean ± S.E. (*n* = 3). (B) Cells grown in YPD in the logarithmic and stationary phases were extracted for CL acyl composition analysis by HPLC-mass spectrometry, described under "Experimental Procedures." (C) WT and *cld1Δ* cells grown in SC media in the logarithmic and stationary phases were extracted for CL acyl composition analysis by HPLC-mass spectrometry, described under "Experimental Procedures."

unsaturated CL may be increased during stationary phase. This was in fact observed (Figure 2-3B). Specifically, in the C68 cluster, the most unsaturated CL (C68:4, m/z 699.5) was abundant, while a more saturated species (C68:2, m/z 701.5) was less abundant in stationary phase cells. Conversely, the C68:4 CL was much less abundant than C68:2 in logarithmically growing cells. This is also evident in the C60 cluster as the most saturated CL (C60:0, m/z 647.4) was absent from stationary cells but clearly present in logarithmically growing cells. Deletion of *CLD1* prevents CL remodeling and leads to decreased unsaturated CL (Beranek et al., 2009). As expected, *cld1Δ* exhibited a decreased degree of unsaturated CL compared to WT regardless of growth phase (Figure 2-3C). Interestingly, unsaturated CL levels were greater in stationary phase than in log phase *cld1Δ* cells. This finding suggests that an as yet unidentified mechanism regulates CL saturation in the absence of Cld1.

Increased *CLD1* expression in the stationary phase, during which glucose is exhausted and cells shift from fermentation to oxidative phosphorylation, suggested that *CLD1* may be transcriptionally regulated in response to glucose availability and the

need to respire. To test this prediction, we examined the expression of *CLD1* in response to acute removal of glucose and in respiration-deficient cells (ρ^0 cells). As expected, expression of *CLD1* but not the other CL biosynthetic genes was greatly increased in response to glucose starvation, by 6-fold and 10-fold, during 30-min and 60-min starvation, respectively (Figure 2-4A). Furthermore, *CLD1* transcription was increased in the stationary phase in ρ^+ cells but not in respiration incompetent ρ^0 cells (Figure 2-4B). These findings indicate that *CLD1* expression is upregulated during respiratory conditions and in response to glucose deprivation.

Using the *Promoter Database of Saccharomyces cerevisiae* (SCPD) to search for putative regulatory elements in the upstream region of the *CLD1* gene, we identified consensus sequences for Hap2 and Mig1 (Figure 2-4C), transcription factors that mediate activation of respiratory gene expression and glucose repression, respectively (Nehlin and Ronne, 1990; Pfeifer et al., 1989; Santangelo, 2006). Consistent with this observation, the HAP complex regulates *CLD1*. As seen in Figure 2-4D, *CLD1* expression in the stationary phase was greatly reduced in *hap2Δ, hap3Δ, hap4Δ, and hap5Δ* mutants, indicating that the HAP complex up-regulates *CLD1* transcription. Mig1 has been shown to repress gene expression in the presence of glucose (Santangelo, 2006; Schuller, 2003). If Mig1 repressed *CLD1* transcription in the presence of glucose, *CLD1* transcription would be increased in *mig1Δ* cells. However, *CLD1* transcription in *mig1Δ* cells was decreased in these conditions (Figure 2-4E). Thus, Mig1 appears to be a positive regulator of *CLD1* expression. This is consistent with reported activator

A

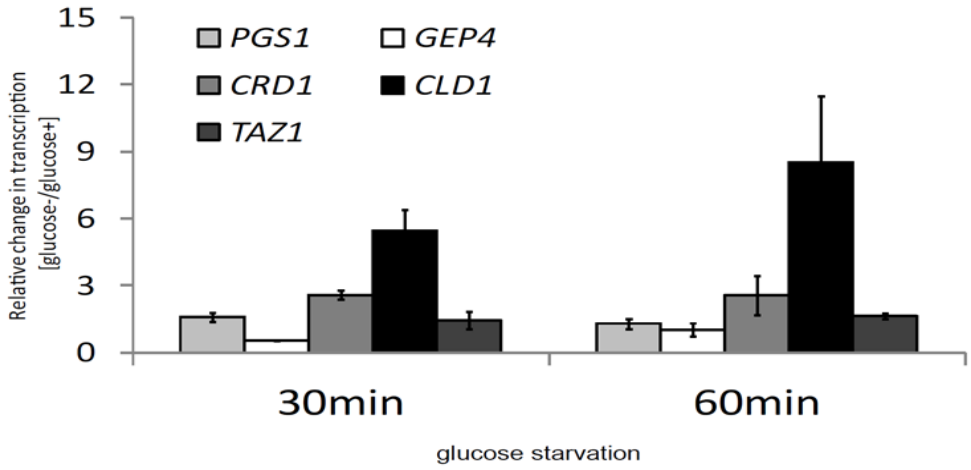

B

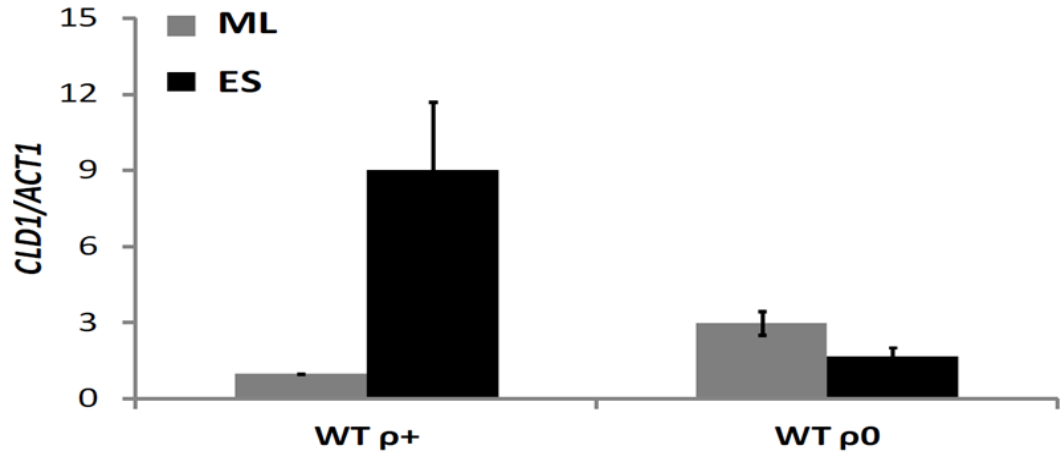

C

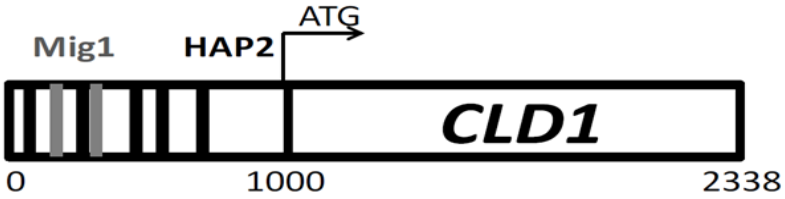

HAP2 ACCAATNA
MIG1 CCCCRNNWWWWW

-	(238, 245)	HAP2	ACCAATAA	1
+	(364, 371)	HAP2	ACCAAAAA	0.88
-	(793, 800)	HAP2	TCCAATAA	0.88
-	(632, 639)	HAP2	ACAAATTA	0.88
+	(581, 588)	HAP2	ACTAATCA	0.88
+	(291, 302)	MIG1	CCCCCCCTATAT	0.82
+	(376, 386)	MIG1	CTCCACTTTTAT	0.82

+: Watson strand
- : Crick strand

D

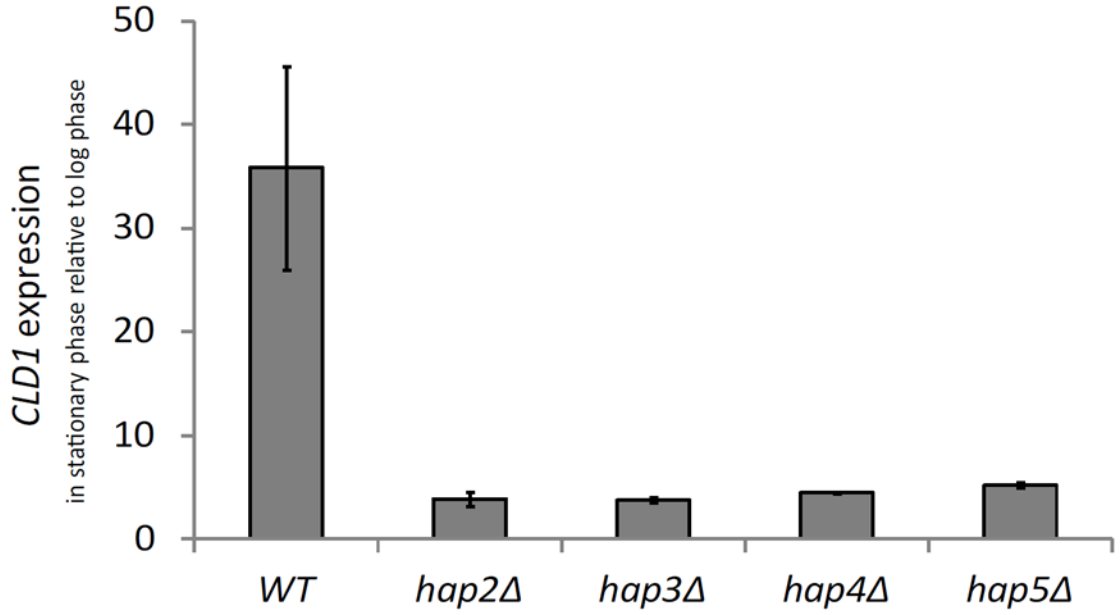
50
40
30
20
10
0
CLD1 expression
in stationary phase relative to log phase
WT
hap2Δ
hap3Δ
hap4Δ
hap5Δ

E

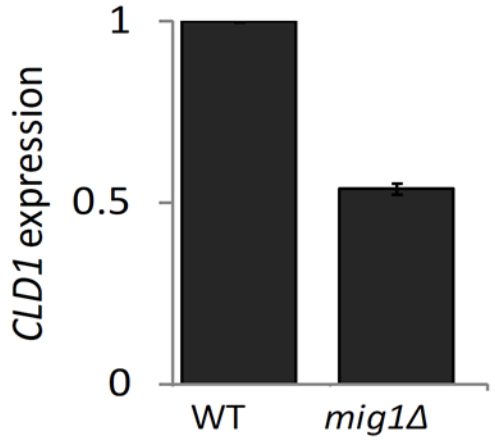
1
0.5
0
CLD1 expression
WT
mig1Δ

Figure 2-3. *CLD1* expression is increased in response to respiration and activated by HAP.

(A) Glucose limitation. WT cells harvested in the mid-logarithmic phase were washed with pre-warmed media with or without glucose and resuspended in fresh media with or without glucose for 30-min and 60-min. Analyses of *PGS1, GEP4, CRD1, CLD1*, and *TAZ1* expression was determined using RT-qPCR and normalized to *ACT1*, as described under "Experimental Procedures." The data represent as fold change relative to expression in media containing glucose and include the mean ± S.E. (n = 6). (B) Respiratory competency. ρ^+ and ρ^0 cells were grown to the mid-logarithmic (ML) and early stationary (ES) phases. The values shown represent the fold change relative to expression of WT ρ^+ cells in ML, and include mean ± S.E. (n = 6). (C) Sequence alignment depicting consensus sequences for Mig1 and Hap2 in the upstream region of the *CLD1* gene using the Promoter Database of Saccharomyces cerevisiae (SCPD). 1 indicates a 100% match with putative consensus sequences, and 0.88 and 0.82 indicates one mismatch. (D) Effect of the HAP complex. Expression was determined in *hap2Δ, hap3Δ, hap4Δ*, and *hap5Δ* cells grown to the mid-logarithmic phase. Data shown are mean ± S.E. (n = 6). (E) Effect of *MIG1*. Expression was determined in WT and mig1Δ cells grown to the mid-logarithmic phase. Data shown are mean ± S.E. (n = 3).

activity of Mig1 (Bu and Schmidt, 1998; Wu and Trumbly, 1998). Taken together, these findings indicate that expression of *CLD1* is increased in response to respiration conditions, and this increase is mediated by the HAP and Mig1 transcriptional factors.

Constitutive overexpression of *CLD1* leads to decreases in respiration and mitochondrial aconitase activity, and instability of mitochondrial DNA.

As expression of *CLD1* is deleterious to tafazzin-deficient cells, we predicted that increased *CLD1* expression alters metabolism and perturbs cell growth. Consistent with this, cell growth was decreased when *CLD1* was overexpressed (Figure 2-5A). One possible explanation for this is that increased *CLD1* expression perturbs respiration. In

A

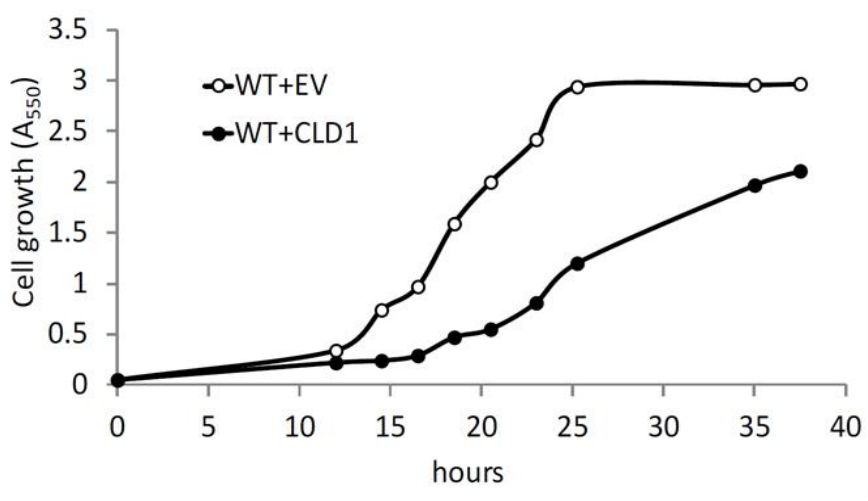
WT+EV
WT+CLD1
Cell growth (A_{550})
hours

B

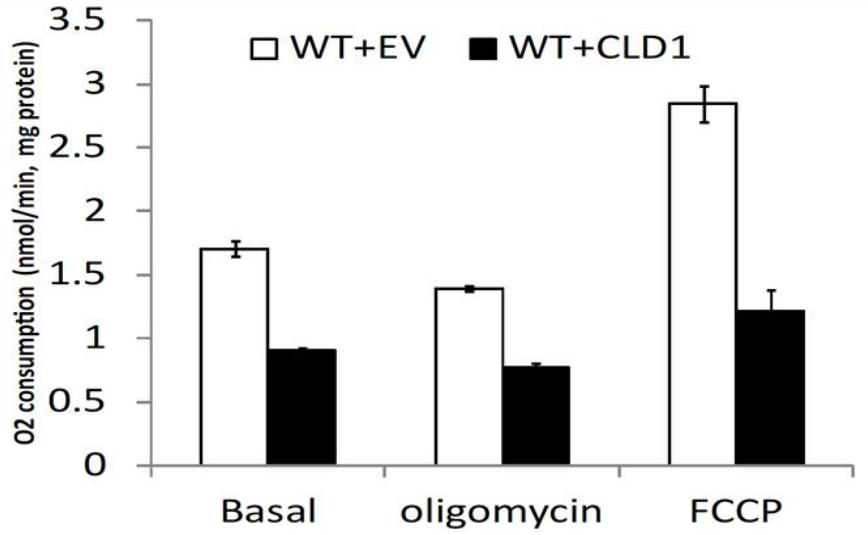
WT+EV
WT+CLD1
O2 consumption (nmol/min, mg protein)
Basal
oligomycin
FCCP

C

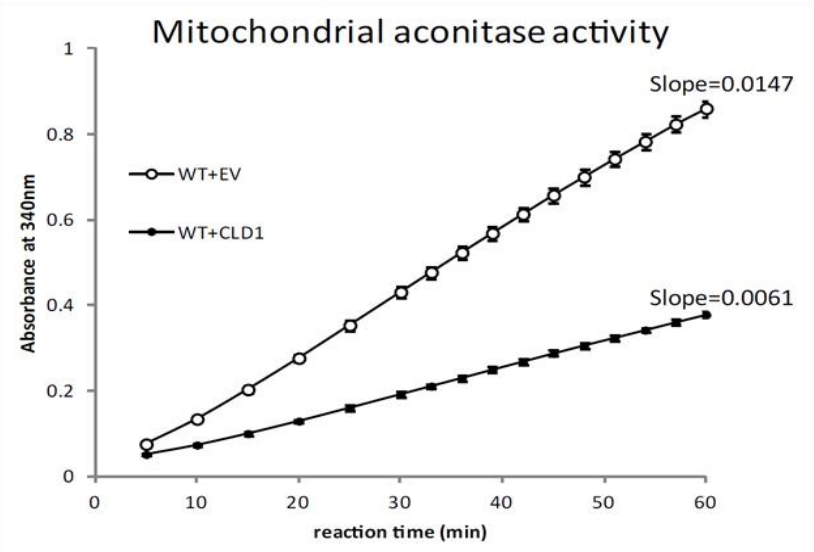
Mitochondrial aconitase activity
Slope=0.0147
Slope=0.0061
WT+EV
WT+CLD1
Absorbance at 340nm
reaction time (min)

Figure 2-4. Overexpression of *CLD1* decreases cell growth, respiration, and mitochondrial aconitase activity.

(A) Growth of WT cells in SC media overexpressing *CLD1* or empty vector (EV). Cells were inoculated at an initial A_{550} of 0.05, and A_{550} was measured at the indicated times. The growth curves shown in the figure are representative of three experiments. (B) Oxygen consumption was measured in logarithmically growing cells using a Clark-type electrode as described under "Experimental Procedures." Data shown are mean ± S.E. (n = 3-6). (C) The kinetics of aconitase enzymatic activity in mitochondria from control and *CLD1* overexpressing cells grown to the logarithmic phase were determined as described under "Experimental Procedures". Data shown are mean ± S.E. (n = 3).

support of this, basal respiration in mitochondria from cells that overexpressed *CLD1* was about half that of control cells (Figure 2-5B). This difference was even more pronounced comparing the maximum respiratory capacity that was achieved by uncoupling the respiratory chain with trifluorocarbonylcyanide phenylhydrazone (FCCP). Therefore, constitutive overexpression of *CLD1* decreases mitochondrial respiration.

A possible mechanism to account for decreased respiration in *CLD1* overexpressing cells is suggested by the observation that over 60% of cells became cytoplasmic petites. The respiratory growth deficiency of the petites was not complemented by crossing to ρ^- tester strains, and mitochondrial DNA was not observed in the petite cells stained with DAPI. As aconitase is required for mitochondrial genome maintenance (Chen et al., 2005b), we tested the possibility that aconitase activity might be decreased in cells overexpressing *CLD1*. In fact, the kinetics of aconitase enzymatic activity in mitochondria from *CLD1* overexpressing cells exhibited a 60% decrease compared to cells overexpressing empty vector (Figure 2-5C). Taken together, these studies indicate that increasing CL deacylation by constitutive

overexpression of *CLD1* impairs cell growth and respiration and decreases mitochondrial DNA stability, suggesting that deacylation of CL is an important control point for mitochondrial function.

Increased fermentation compensates for decreased respiration in cells overexpressing *CLD1*.

As respiration was decreased in cells overexpressing *CLD1*, we expected to see a concomitant decrease in ATP synthesis. The contribution of mitochondria to cellular ATP production can be estimated by the decrease in oxygen consumption resulting from the addition of oligomycin, an inhibitor of ATP synthesis. Under basal conditions, the decrease in respiration caused by oligomycin was significantly less in mitochondria from *CLD1* overexpressing cells than in controls (Figure 2-5B), suggesting that mitochondrial ATP synthesis was decreased. Interestingly, however, total ATP levels were actually higher in *CLD1* overexpressing cells (Figure 2-6A). This suggested that cells may compensate for the respiratory loss by increasing ATP generation from fermentation. Consistent with this, ethanol production was significantly higher in *CLD1*-overexpressing cells than in controls (Figure 2-6B). To determine if up-regulation of genes in glycolysis/fermentation could account for increased ethanol production, we analyzed expression of *GAPDH* and *PGK1,* which encode enzymes that catalyze key steps in glycolysis (glyceraldehyde-3-P dehydrogenase and phosphoglycerate kinase, respectively), as well as *ADH1* and *ADH2,* which encode the fermentation enzyme alcohol dehydrogenase. As seen in Figure 2-6C, expression of *ADH1* and *ADH2* was

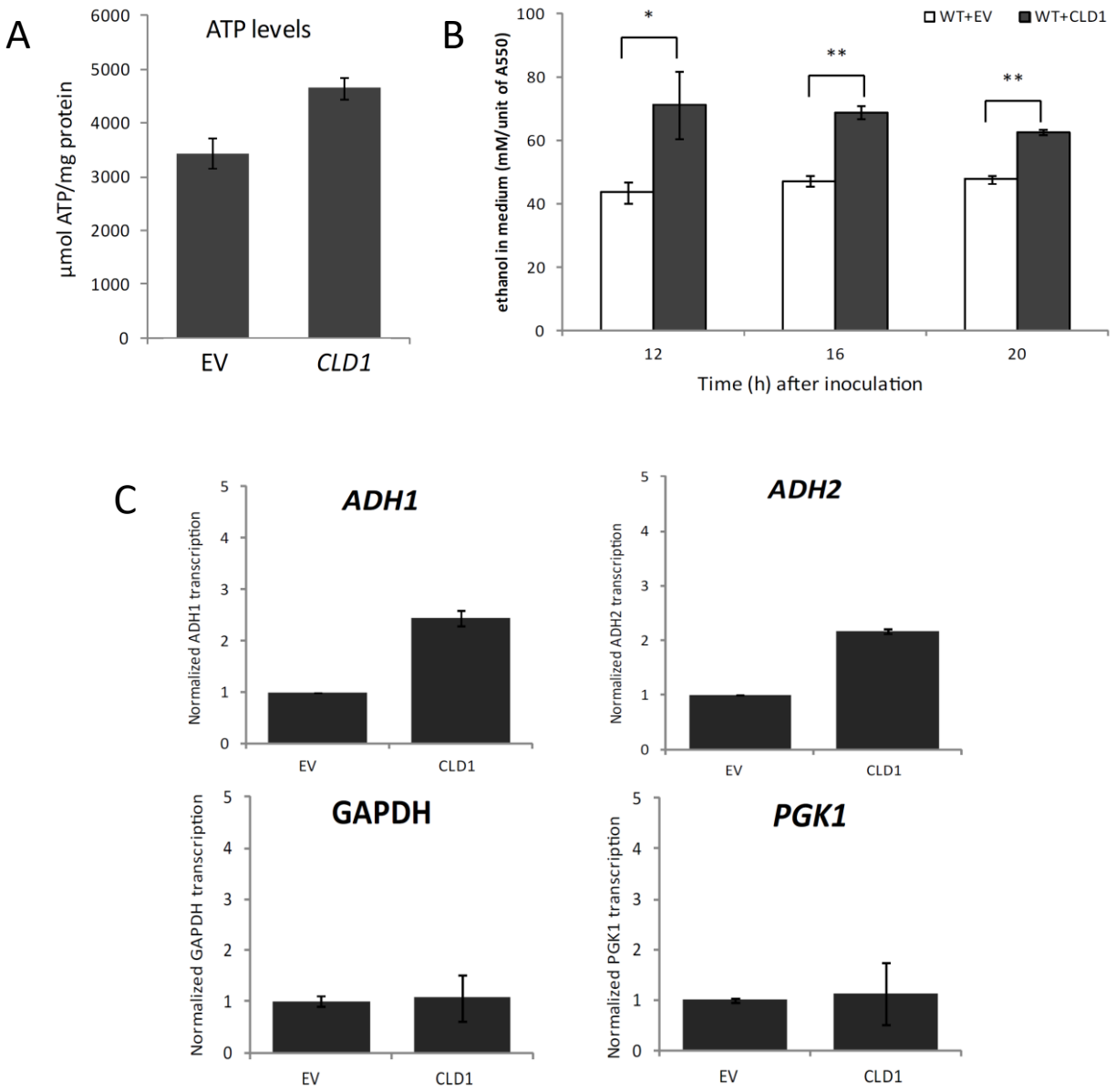

Figure 2-5. Overexpression of *CLD1* leads to increased ATP and ethanol.

(A) ATP levels in logarithmically growing cells overexpressing *CLD1* or empty vector (EV) were determined as described under "Experimental Procedures." Data shown are mean ± S.E. (*n* = 3). (B) Ethanol concentrations were determined as described under "Experimental Procedures". Data shown are mean ± S.E. (*n* = 6) (*p<0.05, **p<0.01). (C) WT cells overexpressing *CLD1* or EV grown to the logarithmic phase were harvested for mRNA extraction. Expression of *ADH1, ADH2, GAPDH,* and *PGK1* was determined using RT-qPCR as described under "Experimental Procedures". Values of each gene were normalized to the internal control *ACT1.* Transcripts normalized to *ACT1* are represented as fold change relative to those in control cells. Data shown are mean ± S.E. (*n* = 3)

increased 2-fold, which most likely accounts for the increase in ethanol production. Expression of *GAPDH* and *PGK1* was not altered. These findings indicate that overexpression of *CLD1* leads to decreased mitochondrial respiration and ATP synthesis, which is compensated by increasing glycolysis.

DISCUSSION

A deficiency in CL reacylation catalyzed by tafazzin is deleterious in eukaryotes (Acehan et al., 2011; Gu et al., 2004; Schlame et al., 2003; Valianpour et al., 2002; Vreken et al., 2000; Xu et al., 2006a), most notably in humans where it leads to the life-threatening disorder BTHS (Barth et al., 1983; Barth et al., 2004; Barth et al., 1999a). The loss of tafazzin results in perturbation of CL metabolism. Specifically, the CL/MLCL ratio is decreased, as are the levels of unsaturated CL species. Although many studies suggest that the deleterious effects of tafazzin deficiency result from the absence of unsaturated CL (Schlame et al., 2003; Schlame and Ren, 2006; Schlame et al., 2002; Valianpour et al., 2003; Xu et al., 2003), no reports to date have distinguished between decreased unsaturated CL and decreased CL/MLCL as the cause of the cellular defects. In the current study, we addressed this question by characterizing the effects of *CLD1* deletion on tafazzin deficient yeast cells. The *cld1Δ* mutant has decreased unsaturated CL (similar to the *taz1Δ* mutant), but the CL/MLCL ratio is not decreased. We report that *cld1Δ* rescues growth and respiration defects of the *taz1Δ* mutant, indicating that the decreased CL/MLCL ratio, and not decreased unsaturated CL, leads to the defects in tafazzin-deficient cells.

Interestingly, the double mutant *cld1Δtaz1Δ* exhibited defective growth in glycerol/ethanol medium at 37˚C as reported in Beranek et al (Beranek et al., 2009). We tested growth of WT, *crd1Δ*, *cld1Δ*, *taz1Δ*, and *cld1Δtaz1Δ* cells in media containing glucose, glycerol, ethanol, or glycerol/ethanol as carbon sources. Indeed, we found that the double mutant grew poorly compared to WT when glycerol/ethanol was used as carbon source, similar to the observation of Beranek et al. However, in these carbon sources, we did not observe respiratory growth defects in *taz1Δ* at 30˚C. Although *taz1Δ* exhibited decreased growth in glycerol/ethanol at 37˚C, high temperature stress complicates respiration defects. In marked contrast, we observed that *taz1Δ* cells exhibit a significant respiratory growth defect in ethanol medium at 30˚C. Under these conditions, we observed that the double mutant rescued the respiratory defects of *taz1Δ*. As *cld1Δ* restores CL levels but not unsaturated CL species in *taz1Δ*, this finding indicates that rescue of respiratory growth of *taz1Δ* by *cld1Δ* results from restoration of CL levels.

While deletion of *CLD1* does not appear to affect growth, expression of the gene is deleterious in the absence of reacylation, as *taz1Δ* cells that have the wild type *CLD1* gene are defective, while those carrying the *cld1Δ* mutation grow normally. To gain insight into the mechanism underlying the deleterious effects of increased *CLD1*, we characterized growth and mitochondrial function of cells overexpressing this gene. Interestingly, overexpression of *CLD1* resulted in increased ATP levels (Figure 2-6A) despite a significant reduction in mitochondrial respiration (Figure 2-5B). Two possibilities may explain this seemingly surprising finding. First, overexpression of

CLD1 leads to growth slowdown, therefore less ATP is required and utilized to maintain cellular functions. Second, *CLD1* overexpression shifts metabolism from respiration toward glycolysis and fermentation (Figure 2-7), compensating for defective oxidative phosphorylation. This indicates that regulation of Cld1-mediated deacylation of CL influences energy metabolism by modulating the relative contribution of glycolysis and respiration. CL is an essential component of oxidative phosphorylation complexes. For example, it was identified in the crystal structure of cytochrome *c* oxidase (Shinzawa-Itoh et al., 2007), the proposed rate-limiting enzyme of the electron transport chain (reviewed in (Huttemann et al., 2012)) and is required for optimal enzyme function and activity (Koshkin and Greenberg, 2000). Therefore, reduced mitochondrial respiration in *CLD1* overexpressing cells would be expected if the CL pool is modified. (We hypothesize that during stationary growth, when oxidative phosphorylation is used, CL may be tuned towards increased membrane fluidity or association with the supercomplexes). Furthermore, such alterations lead to mitochondrial DNA instability.

Apparently, there is yet another level of regulation of the CL metabolic pathway intersecting with cytochrome *c* oxidase regulation. We show here that *CLD1* gene regulation is mediated by the Hap2/3/4/5p transcription factor complex (Figure 2-4E), which is also a crucial regulator of cytochrome *c* oxidase subunit V isoforms Va and Vb (Kwast et al., 1999). These isoforms result in an enzyme with higher affinity for oxygen when the substrate is scarce. Furthermore, overexpression of components of the Hap2/3/4/5p complex rescues cytochrome *c* oxidase deficiencies (Fontanesi et al., 2008). In another example of coordinate control, regulation of *COX4* translation

requires Pgs1, the enzyme that catalyzes the committed step of CL synthesis (Su and Dowhan, 2006). Taken together these findings suggest an integrated and concerted response to environmental stress that affects the CL pathway and oxidative phosphorylation, both of which are interconnected.

Our findings suggest that increased *CLD1* is deleterious to cells because it decreases respiration. However, *CLD1* expression was increased during respiratory growth and regulated by the HAP complex (Figure 2-4), the transcriptional activator that responds to respiratory growth signals. This raises the question of what is the function of the CL remodeling pathway, and the corollary question of why is *CLD1* expression increased in response to respiratory conditions. We speculate that the function of CL remodeling is to remediate the deleterious effects of respiration (Figure 2-7). In support of this possibility, superoxides generated by respiratory complex III cause peroxidation of CL and decreased cytochrome *c* oxidase activity (Paradies et al., 2000; Paradies et al., 2001; Paradies et al., 1998). Exogenous supplementation of CL, but not peroxidized CL or other phospholipids, rescued both reduced activity of cytochrome c oxidase and increased generation of ROS in reperfused heart (Paradies et al., 2001; Petrosillo et al., 2007). In this light, CL remodeling may be a mechanism whereby damaged fatty acyl chains are replaced. Although different approaches have been used, this proposed model is similar to the model described in Baile et al (Baile et al., 2013), in which they suggested a feedback loop between oxidative phosphorylation and CL remodeling. Specifically, they found that *CLD1* expression is regulated by carbon sources, and the activity of Cld1 is increased by dissipating the mitochondrial membrane potential

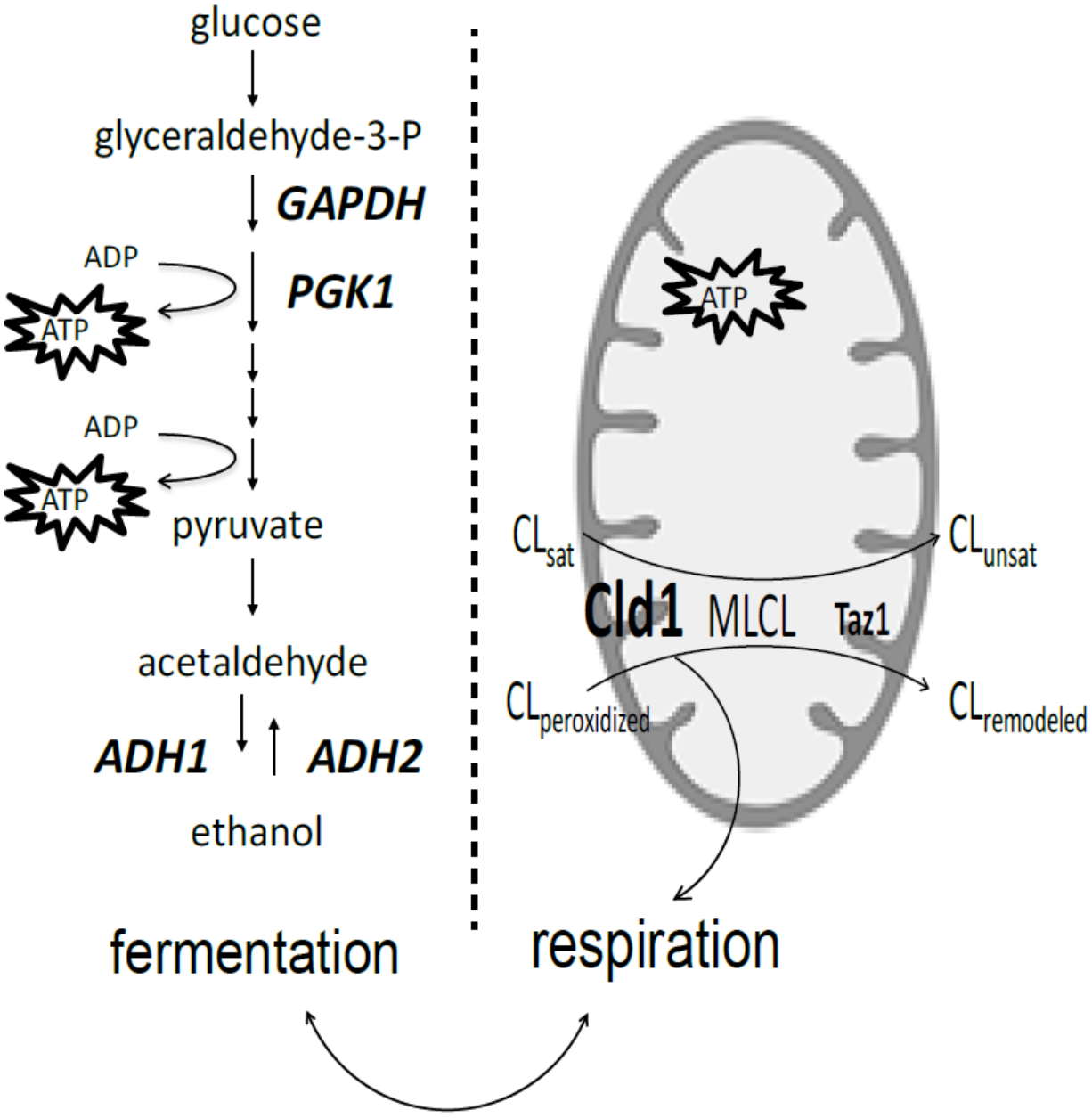

Figure 2-6. Proposed model.

Regulation of Cld1-mediated deacylation of CL influences energy metabolism. *CLD1* expression is upregulated in response to increased respiration. Increased *CLD1* expression modulates the relative contributions of oxidative phosphorylation and glycolysis to cellular energy production. We speculate that the function of CL deacylation, which is increased during respiratory conditions that are known to increase oxidative stress, is to remove peroxidized acyl chains from damaged CL.

(Baile et al., 2013). They suggested that CL remodeling functions to increase oxidative phosphorylation efficiency and/or replace peroxidized CL.

Our findings have implications for understanding the mechanism underlying BTHS. Many studies of BTHS have concluded that the disorder is due to the complete lack of the 'normal' unsaturated (tetralinoleoyl, or L4) CL in the heart (Schlame et al., 2003; Schlame and Ren, 2006; Schlame et al., 2002; Valianpour et al., 2003; Xu et al., 2003). However, the current study indicates that in yeast, a total lack of the 'normal' unsaturated CL species is not deleterious to cells. The large number of mammalian phospholipases complicates the ability to distinguish between decreased CL/MLCL vs. decreased unsaturated CL in human cells. Gross and co-workers (Kiebish et al., 2013b) reported that ablation of phospholipase iPLA$_2$g in the mouse reduced MLCL levels by only ~50% indicating that other phospholipases deacylate CL. Mass spectrometry analysis of phospholipase activity identified at least four phospholipases that deacylate CL in vitro (Hsu et al., 2013). The identification of mammalian CL-specific phospholipases may ultimately enable this question to be addressed.

ACKNOWLEGMENTS

I collaborated with Cunqi Ye to conceive and design the study in this chapter. We prepared the experimental samples and collected the data. Specifically, I constructed the *CLD1* expression plasmid and the *cld1Δtaz1Δ* strain; performed the experiments indicating effects of overexpression of *CLD1* on cell growth, respiration, mitochondrial aconitase activity, and ethanol production. qPCR experiments were carried by Yiran Li (Figures 2-4D, E and 2-6C). A mass spectrometry analysis of lipid profile was performed by Shuliang Chen and the Amsterdam AMC group several years ago and was included in this study (Figures 2-3). Oxygen consumption and ATP measurements were carried out by Maik Huttemann's lab (Figure 2-6A).

CHAPTER 3 LIPIDOMICS CHARACTERIZATION OF BIOSYNTHETIC AND REMODELING PATHWAYS OF CARDIOLIPINS IN GENETICALLY AND NUTRITIONALLY MANIPULATED YEAST CELLS

The work described in this chapter has been published in Tyurina* Y. Y., **W. Lou***, F. Qu*, V. A. Tyurin, D. Mohammadyani, J. Liu, M. Hüttemann, M. A. Frasso, P. Wipf, H. Bayir, M. L. Greenberg, and V. E. Kagan. 2016. Lipidomics characterization of biosynthetic and remodeling pathways of cardiolipins in genetically and nutritionally manipulated yeast cells. *ACS Chemical Biology*. ***Equal contributors**

http://pubs.acs.org/doi/pdf/10.1021/acschembio.6b00995#notes-1

INTRODUCTION

The well-established tissue specificity of cardiolipins (CL)s (Kagan et al., 2015; Schlame, 2008) has led to a paradigm that the molecular speciation of CLs – achieved through the process of remodeling of the nascent species - is defined by the unique mitochondrial demands of a particular tissue. This commonly accepted paradigm has been recently challenged by a clear demonstration that unremodeled CLs are functionally indistinguishable from remodeled CLs for yeast mitochondrial morphology and major bioenergetic functions, such as in oxidative phosphorylation (OxPhos) (Baile et al., 2014), where it is a required structural component of the individual OxPhos complexes as well as supercomplexes (Eble et al., 1990; Mileykovskaya and Dowhan, 2014; Pfeiffer et al., 2003; Poyry et al., 2013; Sharpley et al., 2006; Shinzawa-Itoh et al., 2007). Recent findings have demonstrated that respiratory supercomplexes are destabilized by disturbed CL remodeling in heart mitochondria from *tafazzin* knockdown mice, resulting in disruption of interactions between the electron transporting complexes

and the fatty acid (FA) oxidation enzymes (Huang et al., 2015).

The two major reactions in the remodeling process are a phospholipase-driven production of monolyso-CL (MLCL) intermediates followed by an acyltransferase (tafazzin) dependent “rebuilding” of the molecule that reacylates MLCL via the acyl-CoA-independent transfer of an acyl group from a donor phospholipid (Baile et al., 2014; Beranek et al., 2009; Gu et al., 2004).

Recent developments, elucidating the role of mitochondria as a platform coordinating many metabolic processes as well as life and death decisions, imply that essential functions not associated with bioenergetics may dictate the necessity for the highly diversified molecular speciation of CLs in tissues with signaling functions (e.g., in the brain). Not only has it been shown that mitochondria have functions other than bioenergetics, but CL in particular has extra-bioenergetic functions. The first demonstration of a role for CL in cell viability apart from bioenergetics was the demonstration that the *crd1Δ* (CL synthase) mutant has a temperature-sensitive growth defect, unlike yeast mitochondrial bioenergetics mutants which do not exhibit temperature sensitivity (Jiang et al., 1999). Perturbation of CL synthesis has been shown to affect MAPK signaling (Zhong et al., 2007; Zhou et al., 2009) and vacuolar function in yeast (Chen et al., 2008). This is in sharp contrast to such tissues as cardiac and skeletal muscles in which mitochondrial energy production dictates the dominance of homo-acylated tetraoleoyl-CL ($(C18:1)_4$-CL) or tetralinoleoyl-CL ($(C18:2)_4$-CL) species over a rich assortment of hetero-acylated CLs that may be required for signaling purposes (Patil and Greenberg, 2013; Tyurina et al., 2014).

CL signaling may be realized through the production of oxygenated lipid mediators (Tyurina et al., 2014), thus requiring CL species containing polyunsaturated fatty acids (PUFA). Therefore, the plasticity that is fine-tuned by adaptive changes in the microenvironment – rather than a rigid constitutive program – is likely to define the functions and mechanisms of CL remodeling. The machineries realizing these adaptive responses may include the availability of polyunsaturated fatty acids as well as enzymatic mechanisms involved in CL remodeling – including phospholipases A and acyl-transferases (Lu and Claypool, 2015; Schlame, 2013).

Yeast cells may be ideal organisms for the exploration of these pathways because they: i) can be grown on media completely devoid of PUFA or supplemented with PUFA, ii) rely on only one CL-specific phospholipase A, Cld1, iii) utilize Taz1 as the major tool for reacylation of MLCL, and iv) employ only one – Cld1/Taz1-dependent – pathway for CL remodeling. With this in mind, in the current work we employed detailed phospholipidomics analysis to explore the effects of PUFA supplementation as well as *cld1Δ* and *taz1Δ* mutants on the molecular speciation of CLs in *S. cerevisiae*. Herein, we report the results of differential phospholipidomics studies of *S. cerevisiae* that provide new insights into CL remodeling and biosynthesis. Our findings identified the roles of Cld1 and Taz1 as the major regulatory mechanisms, which are governed by the availability of PUFA esterified into phospholipids that act as donors for the Taz1-catalyzed reaction.

METHODS AND MATERIALS

Yeast strains, media, and growth conditions—The *Saccharomyces cerevisiae* strains used in this work are listed in Table 2-1. Single deletion mutants were obtained from the yeast knock-out deletion collection (Invitrogen). Double mutants were obtained by tetrad dissection. Complex media contained yeast extract (1%), peptone (2%), and glucose (2%) (YPD) or glycerol (3%) and ethanol (1%) (YPGE). The effect of fatty acids was determined in YPD or YPGE medium supplemented with 0.2% oleic, arachidonic, linoleic, or docosahexaenoic acid solubilized in the media with tergitol (1%). Unsupplemented controls contained only tergitol. Synthetic complete (SC) medium contained all the essential components of Difco yeast nitrogen base, 2% glucose, 0.2% ammonium sulfate, vitamins, adenine (20.25 mg/L), arginine (20 mg/L), histidine (20 mg/liter), leucine (60 mg/L), lysine (200 mg/liter), methionine (20 mg/L), threonine (300 mg/L), tryptophan (20 mg/L), uracil (20 mg/L), and inositol (75 μM). For solid medium, 2% agar was added. For selection of cells carrying plasmids, appropriate amino acids were omitted from the media. Yeast strains were grown at 30°C. *E. coli* strain DH5 was used for plasmid maintenance and amplification. Bacteria were grown at 37°C in LB medium (0.5% yeast extract, 1% tryptone, 1% NaCl), supplemented with ampicillin (100 μg/mL) for selection purposes. Solid medium contained 1.5% agar. Growth in liquid cultures was monitored spectrophotometrically. Cells were harvested and centrifuged at 4^{o}C (4,300 rpm, 5 min). Supernatant was discarded and glass beads (0.3g) were added to the centrifuge tubes. Samples were vortexed (5 X 1min intervals) and frozen at -80^{o}C for lipidomics analysis.

Construction of plasmids and expression of His_6-tagged *CLD1* in S. cerevisiae— To construct a His_6-tagged *CLD1* overexpression plasmid, a 1373-bp sequence containing the entire open reading frame without stop codon of *CLD1* was amplified from yeast genomic DNA using an *EcoR*I-tagged forward primer CLD1_*EcoR*I_F3 (5'-TGATTAATAAGAATTCAACACAATGTTCAAGTCAACTTTAAACTC-3') and an *Xba*I-tagged reverse primer CLD1_*Xba*I_R3 (5'-ATTTTGAGATTCTAGATATTTTTTGCATTTCTTTCG-3'). The PCR products were purified using the Wizard SV gel and PCR clean-up system (Promega). The purified DNA fragments were ligated into pYES2/CT cut with *EcoR*I and *Xba*I downstream of the *GAL1* promoter. All the plasmids were amplified and extracted using standard protocols. The plasmids were transformed into yeast strains using a one-step transformation protocol.

Purification of His_6-tagged Cld1—*S. cerevisiae* strain BY4741 was used to express the recombinant His_6-tagged Cld1. Cells were grown at 30°C in synthetic complete raffinose medium lacking uracil. Galactose (2%) was added to induce expression of the recombinant protein. Cell extracts were prepared by disrupting cells with glass beads (0.5 mm diameter), vortexing for 5 min intermittently in disruption buffer containing 50 mM Tris-Cl (pH 8.0) and 300 mM NaCl. Protease inhibitor (cOmplete EDTA-free, Roche) was added to the disruption buffer before breaking the cells. His_6-tagged Cld1 was purified with Millipore® PureProteome nickel magnetic beads following the manufacturer's instructions. Millipore® UFC503024 Amicon® Ultra-0.5 centrifugal filter concentrator (30 KD) was used to concentrate the protein and remove imidazole.

Protein concentration was determined with a BIO-RAD DC protein assay kit using bovine serum albumin as the standard.

LC/MS assessment of phospholipids—Lipids were extracted from yeast using the Folch procedure (Folch et al., 1957) and lipid phosphorus was determined by a micro-method (Boettcher et al., 1961). LC/MS of phospholipids was performed in negative mode using a Dionex UltimateTM 3000 RSLCnano system coupled online Q-Exactive hybrid quadrupole-orbitrap mass spectrometer (ThermoFisher Scientific, San Jose, CA). Total lipids were separated on a normal phase column (Silica Luna 3 µm, 100A, 150x2 mm, (Phenomenex, Torrance CA)) with flow rate 0.2 mL/min using gradient solvents containing 5 mM CH_3COONH_4 (A – *n*-hexane:2-propanol:water, 43:57:1 (v/v/v) and B - *n*-hexane:2-propanol:water, 43:57:10 (v/v/v). The gradient conditions (all linear) were as follows: 0-23 min (10%B to 32%B); 23-32 min (32%B to 65%B); 32-35 min (65%B to 100%B) 35-62 min (hold at 100%B); 62-64 min (100%B to 10%B); 64-80 min (10%B). Flow rate was maintained at 200 microliters/min except for the 35-62 min time frame where the flow rate was increase to 225 microliters/min. MS analysis was performed in negative ion mode (profile) at a resolution of 140,000 for the full MS scan and 17,500 for the MS^2 scan in a data-dependent mode with appropriate inclusion and exclusion lists. The scan range for MS analysis was 400-1800 m/z with a maximum injection time of 128 ms using 1 microscan. A maximum injection time of 500 ms was used for MS^2 (high energy collisional dissociation (HCD)) analysis with collision energy set to 24. An isolation window of 1.0 Da was set for the MS^2 scans. Capillary spray voltage was set at 3.5 kV, and capillary temperature was 320 ^oC. The S-lens Rf level was set to 60 with a

sheath gas flow of 8. To quantitatively assess phospholipids, PE-(17:0/17:0); PC-(17:0/17:0); CL-(14:0/14:0/14:0/14:0); LPE-(17:1/0:0); LPC-(17:1/0:0) from Avanti Polar Lipids have been used as internal standards. Reference standards PE-(18:1/18:1); PC-(18:1/18:1); CL-(18:2/18:2/18:2/18:2); LPE-(18:0/0:0); LPC-(18:0/0:0) were used for calibrations and were also from AvantiPolar Lipids. Both Internal and reference standards of MLCLs were prepared from CL-(14:0/14:0/14:0/14:0) CL-(18:2/18:2/18:2/18:2), respectively as described (Kim and Hoppel, 2011). Precursor ions [M-H]- were identified with mass accuracy less than 5ppm. Therefore, phospholipids, including CL, were identified by accurate mass and MS^2 fragmentation analysis. The fragmentation pattern provided information on fatty acids but not on their position. Assuming that sn-1 position in phospholipids is commonly occupied by saturated and monounsaturated acids we used this information to identify PE and PC molecular species. Clearly, this is a more difficult task for CL molecular species with four acyl chains in the molecule. Therefore, we presented CL molecular species based on the information provided in the paper by Liebisch et al.(Liebisch et al., 2013). Spectra subtraction was done by Background Subtraction Module in Xcalibur (Thermo Fisher Scientific). By defining one file as background (subtractor) and another file as foreground (minuend), the difference can be evaluated from the differential spectra. Since negative spectra cannot be calculated and exported from Xcalibur, we performed swapping of the subtractor and the minuend which afforded the calculations and presentation of the negative spectra.

Respiration measurements—Oxygen consumption rate (OCR) of intact yeast cells was analyzed via the polarographic method in a closed 500 μL chamber equipped with a micro Clark-type oxygen electrode (Oxygraph Plus System, Hansatech Instruments) at 30°C. Yeast cells were grown in synthetic YPD media supplemented with oleic acid, linoleic acid, or arachidonic acid. Cells were harvested during the stationary phase. Cells were mixed in fresh media using a final protein concentration of 0.5 mg/mL following measurements of respiration. KCN (0.2 mM) was added at the end of the experiment to inhibit cytochrome *c* oxidase to correct for cytochrome *c* oxidase-independent oxygen utilization. Oxygen consumption was recorded on a computer and analyzed with the Oxygraph plus software. Oxygen consumption rate (ORC) is defined as consumed O_2 (nmol)/min/total protein (mg).

Synthesis of Cardiolipins—General Experimental Conditions. All air and moisture sensitive reactions were carried out under a nitrogen or argon atmosphere. All reactions carried out above room temperature were performed using an oil bath set to the specified temperature and monitored with an external thermometer. THF and diethyl ether were distilled from sodium/benzophenone ketyl. Dichloromethane was distilled from CaH_2. Diisopropylethylamine (DIPEA) and diisopropylamine were distilled from and stored over KOH. Pyridine was filtered through activated basic alumina and stored over freshly activated 4 Å molecular sieves for at least 24 h prior to use. Amberlite-IR120H resin was activated by stirring with 6 N HCl for 30 min, filtering, and rinsing once with equal volumes of water and methanol. All other reagents were used as received. Concentrating under reduced pressure refers to removing solvents by the use of a

rotary evaporator connected to a PIAB Lab Vac H40. Reactions were monitored by thin layer chromatography analysis (pre-coated silica gel 60 F254 plates, 250 μm layer thickness) and visualized with a 254 nm UV light or by staining with a $KMnO_4$ solution. Flash chromatography on SiO_2 (Silicycle, 40-63 μm) was used for purification where indicated. All products were placed under high vacuum to remove trace solvents. Melting points were determined using a Laboratory Devices Mel-Temp II and are uncorrected. Infrared spectra were obtained from neat solids or oils on a Perkin Elmer ATR IR or Smiths Detection IdentifyIR FT-IR spectrometer. High-resolution mass spectra were obtained on a Thermo Scientific Exactive Orbitrap mass spectrometer using electrospray ionization. Low-resolution mass spectra were obtained on an Advion Expression L compact mass spectrometer using electrospray ionization. ^{1}H NMR spectra were obtained on a Bruker Avance at 300 MHz, 400 MHz, or 500 MHz in $CDCl_3$, CD_2Cl_2, or CD_3OD. Chemical shifts were reported in parts per million with the residual solvent peak used as an internal standard ^{1}H / ^{13}C (solvent): 7.26 / 77.00 ($CDCl_3$); 5.32/53.84 (CD_2Cl_2). ^{1}H NMR spectra were obtained and are tabulated as follows: chemical shift, multiplicity (s = singlet, d = doublet, t = triplet, q = quartet, dd = doublet of doublets, m = multiplet, bs = broad singlet), number of protons, and coupling constant(s). ^{13}C NMR spectra were recorded using a proton-decoupled pulse sequence run at 100 MHz or 125 MHz and are tabulated by observed peaks. ^{31}P NMR spectra were recorded using a complete decoupled pulse sequence run at 162 MHz.

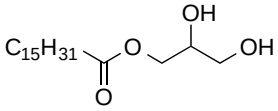

1-*O*-Palmitoylglycerol (1a) (Lok et al., 1985; Mori, 2012). General Procedure A. A solution of palmitic acid (5.5 g, 21.4 mmol, 1.0 eq.), 50% glycidol in CH_2Cl_2 (3.0 mL, 22.8 mmol, 1.06 eq.) and tributylamine (0.1 mL, 0.4 mmol, 0.02 eq.) was heated to 85 °C and stirred for 5 h. The crude product was recrystallized from *i*-Pr_2O:Et_2O (1:1) to yield 1-*O*-palmitoylglycerol (**1a**, 4.88 g, 14.8 mmol, 69%) as a colorless solid: Mp 71.9-72.5 °C; IR 3293, 2913, 2848, 1728 cm^{-1}; ^1H NMR ($CDCl_3$, 300 MHz) 4.22 (dd, 1 H, *J* = 4.8, 11.7 Hz), 4.15 (dd, 1 H, *J* = 6.0, 11.4 Hz), 3.97-3.90 (m, 1 H), 3.70 (dd, 1 H, *J* = 4.2, 11.7 Hz), 3.60 (dd, 1 H, *J* = 5.7, 11.4 Hz), 2.35 (t, 2 H, *J* = 7.7 Hz), 1.66-1.58 (m, 2 H), 1.28-1.25 (m, 25 H), 0.85 (t, 3 H, *J* = 6.8 Hz); ^{13}C NMR ($CDCl_3$, 100 MHz) 174.4, 70.3, 65.2, 63.3, 34.1, 31.9, 29.7-29.6 (multiple peaks), 29.4, 29.3, 29.1, 24.9, 22.7, 14.1.

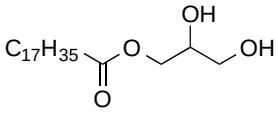

1-*O*-Stearoylglycerol (1b) (Lok et al., 1985; Mori, 2012). According to General Procedure A but using stearic acid, 1-*O*-stearoylglycerol (**1b**, 4.36 g, 12.2 mmol, 71%) was obtained as a colorless solid: ^1H NMR ($CDCl_3$, 300 MHz) 4.21 (dd, 1 H, *J* = 4.8, 11.7 Hz), 4.14 (dd, 1 H, *J* = 5.7, 11.4 Hz), 3.96-3.90 (m, 1 H), 3.70 (dd, 1 H, *J* = 3.9, 11.4 Hz), 3.60 (dd, 1 H, *J* = 6.0, 11.4 Hz), 2.71 (bs, 2 H), 2.35 (t, 2 H, *J* = 7.7 Hz), 1.65-1.60 (m, 2 H), 1.28-1.25 (m, 29 H), 0.88 (t, 3 H, *J* = 6.6 Hz).

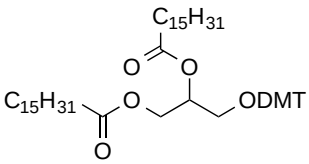

1,2-*O*-Dipalmitoyl-3-*O*-dimethoxyltriylglycerol (2a). General Procedure B. To a solution of **1a** (4.57 g, 13.8 mmol, 1.0 eq.) in pyridine:CH_2Cl_2 (1:2, 35 mL) at 0 °C was added

dimethoxyltrityl chloride (DMTCl, 4.82 g, 14.1 mmol, 1.0 eq.) and dimethylaminopyridine (DMAP, 0.177 g, 1.43 mmol, 0.1 eq.) The orange solution was stirred at this temperature for 15 min., then warmed to room temperature and stirred for 13 h. The orange reaction mixture was quenched with water (30 mL) and extracted with CH_2Cl_2 (2x50 mL). The organic portion was rinsed with water (40 mL), brine (40 mL), dried ($MgSO_4$), and concentrated. The residue was then concentrated from toluene (2x20 mL) and the resulting orange oil used without further purification. A solution of 1-ethyl-3-(3-dimethylaminopropyl) carbodiimide (EDCI, 2.93 g, 15.3 mmol, 1.1 eq.), palmitic acid (3.91 g, 15.3 mmol, 1.1 eq.) and DMAP (0.851 g, 6.90 mmol, 0.5 eq.) in CH_2Cl_2 (60 mL) was allowed to stir at room temperature under nitrogen for 15 min. Then, a solution of the previously obtained oil from the dimethoxyltrityl protection (8.77 g, 13.9 mmol 1.0 eq) in CH_2Cl_2 (30 mL) was added and stirring was continued for 4 h. The reaction mixture was diluted with water (50 mL) and the organic layer was rinsed with water (50 mL), brine (50 mL), dried ($MgSO_4$), and concentrated. Purification by filtration through SiO_2 (9:1 CH_2Cl_2:hexanes) gave 1,2-*O*-dipalmitoyl-3-*O*-dimethoxyltriylglycerol (**2a**, 7.94 g, 9.11 mmol, 66%) as a colorless solid. Pure **2a** can also be obtained by repeated trituration with MeOH. Mp 64.5-66.0 °C; IR 2915, 2846, 1729 cm^{-1}; ^1H NMR ($CDCl_3$, 300 MHz) 7.42 (d, 2.0 H, *J* = 2 Hz), 7.40-7.20 (m, 7 H), 6.82 (d, 4 H, *J* = 8.7 Hz), 5.28-5.22 (m, 1 H), 4.34 (dd, 1 H, *J* = 3.6, 11.7 Hz), 4.25 (dd, 1 H, *J* = 6.6, 11.7 Hz), 3.79 (s, 6 H), 3.22 (d, 2 H, *J* = 5.1 Hz), 2.33 (t, 2 H, *J* = 7.5 Hz), 2.23 (t, 2 H, *J* = 7.5 Hz), 1.65-1.53 (m, 4 H), 1.28-1.25 (m, 48 H), 0.91 (t, 3 H, *J* = 6.6 Hz); ^{13}C NMR ($CDCl_3$, 125 MHz) 173.4,

173.0, 158.5, 144.5, 135.7, 130.0, 128.1, 127.8, 126.8, 113.1, 86.0, 70.5, 62.9, 62.0, 55.1 34.4, 34.1, 31.9, 29.7-29.1 (multiple peaks), 25.0, 24.8, 22.7, 14.1.

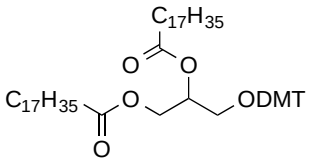

1,2-*O*-Distearoyl-3-*O*-dimethoxyltriylglycerol (2b). According to General Procedure B but using **1b** and purification by trituration with MeOH gave 1,2-*O*-distearoyl-3-*O*-dimethoxyltriylglycerol (**2b**, 6.68 g, 6.48 mmol, 53%) as a colorless solid: Mp 67-68.4 °C; IR 2915, 2848, 1730 cm^{-1}; ^{1}H NMR ($CDCl_3$, 300 MHz) 7.45 (d, 2 H, *J* = 7.2 Hz), 7.35-7.24 (m, 7 H), 6.85 (d, 4 H, *J* = 9.0 Hz), 5.29-5.28 (m, 1 H), 4.35 (dd, 1 H, *J* = 8.1, 11.7 Hz), 4.25 (dd, 1 H, *J* = 6.6, 11.7 Hz), 3.82 (s, 6 H), 3.25 (d, 2 H, *J* = 3.3 Hz), 2.36 (t, 2 H, *J* = 7.5 Hz), 2.27 (t, 2 H, *J* = 7.5 Hz), 1.69-1.56 (m, 4 H), 1.29 (m, 58 H), 0.91 (t, 3 H, *J* = 6.6 Hz); ^{13}C NMR ($CDCl_3$, 125 MHz) 173.4, 173.0, 158.5, 144.6, 135.8, 130.1, 128.1, 127.8, 126.8, 113.1, 113.0, 86.1, 70.5, 62.9, 62.1, 55.2, 34.4, 34.1, 31.9, 29.7-29.1 (multiple peaks), 25.0, 24.8, 22.7, 14.1.

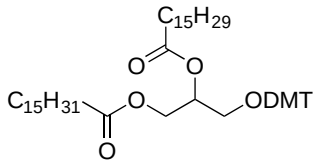

1-*O*-Palmitoyl-2-*O*-palmitoleoyl-3-*O*-dimethoxyltriylglycerol (2c). According to General Procedure B but using **1a** and purification by chromatography on SiO_2 (95:5, hexanes:ethyl acetate) gave 1-*O*-palmitoyl-2-*O*-palmitoleoyl-3-*O*-dimethoxyltriylglycerol (**2c**, 0.619 g, 0.712 mmol, 65%) as a clear colorless oil: IR 2923, 2853, 2093, 1741, 1250 cm^{-1}; ^{1}H NMR ($CDCl_3$, 300 MHz) 7.43 (d, 2 H, *J* = 8.4 Hz), 7.31-7.25 (m, 7 H), 6.82

(d, 4 H, *J* = 8.7 Hz), 5.40-5.30 (m, 2 H), 5.29-5.22 (m, 1 H), 4.34 (dd, 1 H, *J* = 3.6, 11.7 Hz), 4.23 (dd, 1 H, *J* = 6.6, 12.0 Hz), 3.79 (s, 6 H), 3.23-3.21 (m, 2 H), 2.33 (t, 2 H, *J* = 7.5 Hz), 2.23 (t, 2 H, *J* = 7.7 Hz), 2.02-2.00 (m, 4 H), 1.67-1.53 (m, 4 H), 1.29 (m, 40 H), 0.88 (t, 6 H, *J* = 6.8 Hz); ^{13}C NMR ($CDCl_3$, 125 MHz) 173.4, 173.0, 158.5, 144.6, 135.8, 135.7, 130.0, 129.7 128.1, 127.8, 126.8, 113.1, 86.1, 70.5, 62.9, 62.0, 55.2, 34.4, 34.1, 31.9, 31.8, 29.8-29.0 (multiple peaks), 27.2, 25.0, 24.9, 22.7, 22.6, 14.1.

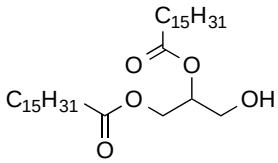

1,2-*O*-Dipalmitoylglycerol (3a) (Roodsari et al., 1999). General Procedure C. To a solution of **2a** (7.94 g, 9.11 mmol, 1.0 eq.) in $CHCl_3$:MeOH (1:1, 90 mL) was added Amberlite IR-120H (4.0 g). The reaction mixture was stirred for 2.5 h, then filtered through basic alumina (EtOAc). The resulting yellow oil was precipitated from Et_2O:hexanes (3:1) and filtered to give 1,2-*O*-dipalmitoylglycerol (**3a**, 3.75 g, 5.50 mmol, 60%, purity by ^{1}H NMR: 90%) as a colorless solid: ^{1}H NMR ($CDCl_3$, 400 MHz) 5.10-5.06 (m, 1 H), 4.32 (dd, 1 H, *J* = 4.8, 12.0 Hz), 4.24 (dd, 1 H, *J* = 6.0, 12.0 Hz), 3.74-3.73 (m, 2 H), 2.33 (apparent q, 4 H, *J* = 8 Hz), 1.65-1.58 (m, 4 H), 1.28-1.25 (m, 48 H), 0.88 (t, 3 H, *J* = 6.6 Hz).

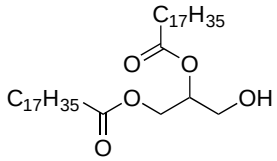

1,2-*O*-Distearoylglycerol (3b) (Lee et al., 2007). According to General Procedure C but using **2b**, and purification by trituration with Et_2O:hexanes (3:1) gave 1,2-*O*-

distearoylglycerol (**3b**, 2.08 g, 3.39 mmol, 72%) as a colorless solid: ^{1}H NMR ($CDCl_3$, 500 MHz) 5.10-5.06 (m, 1 H), 4.32 (dd, 1 H, J_1 = 4.5 Hz, J_2 = 12 Hz), 4.24 (dd, 1 H, J_1 = 5.5 Hz, J_2 = 12 Hz), 3.79-3.72 (m, 2 H), 2.34 (m, 4 H), 1.99 (t, 1 H, J = 4.0 Hz), 1.64-1.54 (m, 4 H), 1.29-1.25 (m, 56 H), 0.88 (t, 3 H, J = 7.0 Hz).

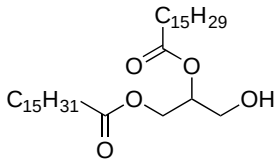

1-*O*-Palmitoyl-2-*O*-palmitoleoylglycerol (3c). According to General Procedure C but using **2c** and purification by chromatography on SiO_2 (1:0 to 5:1, CH_2Cl_2:ethyl acetate) gave 1-*O*-palmitoyl-2-*O*-palmitoleoylglycerol (**3c**, 64 mg, 0.113 mmol, 98%) as a light yellow oil: IR 3502, 2919, 2850, 2093, 1737, 1163 cm^{-1}; ^{1}H NMR ($CDCl_3$, 300 MHz) 5.40-5.30 (m, 2 H), 5.10-5.05 (m, 1 H), 4.32 (dd, 1 H, J = 4.8, 12.3 Hz), 4.24 (dd, 1 H, J = 5.4, 11.7 Hz), 3.73 (m, 2 H), 2.33 (apparent q, 4 H, J = 7.3 Hz), 2.02-2.00, (m, 4 H), 1.64-1.54 (m, 4 H), 1.30-1.27 (m, 40 H), 0.88 (t, 6 H, J = 6.7 Hz); ^{13}C NMR ($CDCl_3$, 125 MHz) 173.8, 173.4, 130.0, 129.7 128.1, 72.1, 62.0, 61.6, 34.3, 34.1, 31.9, 29.7-29.0 (multiple peaks), 27.2, 25.0, 24.9, 22.7, 22.6, 14.1; HRMS (ESI^{+}) *m/z* calculated for $C_{35}H_{67}O_5$ [M+H] 567.4983, found 567.4960.

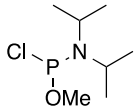

N, N-Diisopropylamidomethylchlorophosphite (4) (Stadlbauer et al., 2009). To a solution of PCl_3 (3.2 mL, 36 mmol, 1.04 eq.) and pyridine (2.9 mL, 36 mmol, 1.04 eq.) in Et_2O (120 mL) at -78 °C under argon was added dry MeOH (1.4 mL, 35 mmol, 1.0 eq.) in Et_2O (4 mL) over 30 min. The reaction mixture was stirred for 3 h at room temperature.

diluted with Et_2O (40 mL) and cooled to 0 °C. Diisopropylamine (9.6 mL, 67.9 mmol, 2.0 eq.) was added over 0.5 h and stirring was continued for 22 h at room temperature. The salts were filtered off under argon, rinsed with Et_2O (50 mL) and the solvent was distilled off. The resulting yellow oil was purified by vacuum distillation to give *N,N*-diisopropylamidomethylchlorophosphite (**4**, 3.73 g, 18.9 mmol, 56%) as a clear colorless oil: Bp 88 °C (12 Torr); ^{1}H NMR (CD_2Cl_2, 400 MHz) 3.74-3.64 (m, 2 H), 3.51 (d, 3 H, *J* = 14.4 Hz), 1.20-1.16 (m, 12 H); ^{31}P NMR (CD_2Cl_2, 162 MHz) 183.8.

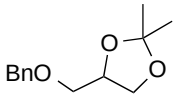

4-((Benzyloxy)methyl)-2,2-dimethyl-1,3-dioxolane (5). (Lee et al., 2007) A slurry of 60% NaH in mineral oil (360 mg, 9.00 mmol, 1.2 eq.) in THF (10 mL) at 0 °C under nitrogen was added to a solution of 2,2-dimethyl-1,3-dioxolane-4-methanol (1.0 mL, 7.8 mmol, 1.0 eq.) in THF (5 mL). The reaction mixture was stirred for 30 min, then BnBr (0.98 mL, 1.4 mmol, 1.05 eq.) was added in a drop wise fashion. The reaction mixture was warmed to room temperature and stirred for 2.5 h. The reaction was quenched with water (8 mL), diluted with Et_2O (20 mL), and the layers were separated. The aqueous layer was extracted with Et_2O (25 mL) and the combined organic layers were rinsed with brine (10 mL), dried ($MgSO_4$), and concentrated. Purification by chromatography on SiO_2 (95:5 to 9:1 to 85:15, hexanes:ethyl acetate) gave 4-((benzyloxy)methyl)-2,2-dimethyl-1,3-dioxolane (**5**, 1.15 g, 5.17 mmol, 67%) as a clear colorless oil: ^{1}H NMR ($CDCl_3$, 400 MHz) 7.35-7.29 (m, 5 H), 4.59, 4.56 (AB, 2 H, *J* = 12.0 Hz), 4.34-4.28 (m, 1 H), 4.06 (dd, 1 H, *J* = 6.4, 8.0 Hz), 3.75 (dd, 1 H, *J* = 6.4, 8.4 Hz), 3.56, 3.45 (ABd, 2 H, *J* = 5.6, 9.6 Hz), 3.46 (dd, 1 H, *J* = 5.6, 9.6 Hz), 1.42 (s, 3 H), 1.37 (s, 3 H).

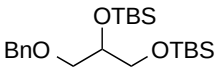

1-*O*-Benzyl-2,3-*O*-bis(*tert*-butyldimethylsilyl)glycerol (6). A solution of **5** (1.15 g, 5.17 mmol, 1.0 eq.) in THF:H_2O (2:1, 10 mL) was treated with 12 M HCl (2.1, 25 mmol, 4.9 eq.), and the reaction mixture was stirred for 1 h at room temperature, poured into sat. $NaHCO_3$ (30 mL) and extracted with Et_2O (3x 25 mL). The combined organic layers were rinsed brine (25 mL), dried ($MgSO_4$), and concentrated. The resulting yellow oil was dissolved in CH_2Cl_2 (8.7 mL) at 0 °C under nitrogen and treated with Et_3N (1.4 mL, 9.9 mmol, 2.3 eq.) and TBSOTf (2.2 mL, 9.5 mmol, 2.2 eq.). The cloudy white reaction mixture was then stirred for 3 h at room temperature, quenched with H_2O (8 mL) and diluted with CH_2Cl_2 (10 mL). The organic layer was rinsed with brine (8 mL), dried ($MgSO_4$), and concentrated. Purification by chromatography on SiO_2 (99:1 to 95:5, hexanes:ethyl acetate) gave 1-*O*-benzyl-2,3-*O*-bis(*tert*-butyldimethylsilyl)glycerol (**6**, 1.72, 4.31 mmol, 83% over 2 steps) as a clear colorless oil: ^{1}H NMR ($CDCl_3$, 500 MHz) 7.35-7.33 (m, 4 H), 7.28-7.26 (m, 1 H), 4.54 (s, 2 H), 3.89-3.84 (m, 1 H), 3.61 (dd, 1 H, *J* = 6.0, 10.0 Hz), 3.57-3.52 (m, 2 H), 3.42 (dd, 1 H, *J* = 5.5, 10.0 Hz), 0.87 (s, 18 H), 0.070 (d, 6 H, *J* = 1.5 Hz), 0.042 (s, 6 H).

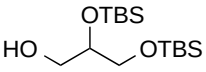

2,3-*O*-Bis(*tert*-butyldimethylsilyl)glycerol (7). (Harried et al., 2009) To a solution of **6** (1.62 g, 4.06 mmol, 1.0 eq.) in ethyl acetate (20 mL) was added 10% Pd/C (0.161 g, 0.152 mmol, 0.037 eq.). The reaction mixture was submitted to hydrogenation on a Parr hydrogenator under H_2 (5 atm) for 1 h, filtered through Celite (ethyl acetate) and

concentrated to give 2,3-*O*-bis(*tert*-butyldimethylsilyl)glycerol (**7**, 1.15 g, 3.59 mmol, 88%) as a clear colorless oil that was used without further purification. An analytically pure sample was obtained by chromatography on SiO_2 (95:5 to 9:1, hexanes:ethyl acetate): ^{1}H NMR ($CDCl_3$, 300 MHz) 3.79-3.74 (m, 1 H), 3.69-3.53 (m, 4 H), 2.10 (bs, 1 H), 0.90 (s, 18 H), 0.1-0.06 (m, 12 H).

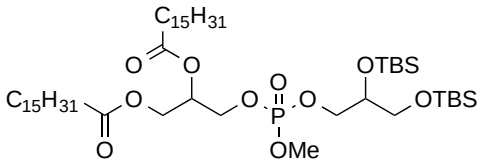

3-(((2,3-Bis((*tert*-butyldimethylsilyl)oxy)propoxy)(methoxy)phosphoryl)oxy)propane-1,2-diyl dipalmitate (8a).[7] General Procedure D. To a solution of **3a** (1.73 g, 2.89 mmol, 1.0 eq.) and diisopropylethylamine (DIPEA, 0.53 mL, 3.2 mmol, 1.1 eq.) in CH_2Cl_2 (30 mL) under nitrogen was added **7** (6.0 mL, 3.0 mmol, 1.1 eq.). The reaction mixture was stirred for 1 h, and treated dropwise with a solution of **6** (0.921 g, 2.87 mmol, 0.99 eq.) and 4,5-dicyanoimidazole (0.700 g, 5.80 mmol, 2 eq.) in THF (4.9 mL). The solution was stirred for 1 h, cooled to 0 °C, treated with Bu_4NIO_4 (1.46 g, 3.36 mmol, 1.2 eq.), and stirring was continued for 30 min. The mixture was diluted with water (15 mL) and the combined organic layers were rinsed with sat. $Na_2S_2O_3$ (15 mL), sat. $NaHCO_3$ (15 mL), and brine (15 mL), dried ($MgSO_4$), and concentrated. The crude residue was filtered through a plug of SiO_2 (1:1, hexanes:ethyl acetate) and concentrated. Purification by chromatography on SiO_2 (5:1 to 3:1, hexanes:ethyl acetate) gave 3-(((2,3-bis((*tert*-butyldimethylsilyl)oxy)propoxy)(methoxy) phosphoryl)oxy)propane-1,2-diyl dipalmitate (**8a**, 1.42 g, 1.47 mmol, 51%) as a clear colorless oil: IR 2922, 2854, 1741, 1252, 835 cm^{-1}; ^{1}H NMR ($CDCl_3$, 300 MHz) 5.25-5.19 (m, 1 H), 4.36-4.30 (m, 1 H), 4.19-4.09 (m, 4

H), 3.97-3.83 (m, 2 H), 3.76 (d, 3 H, *J* =11.1 Hz; diasteromers), 3.56-3.54 (m, 2 H), 2.34-2.27 (m, 4 H), 2.23 (t, 2 H, *J* = 7.5 Hz), 1.61-1.56 (m, 4 H), 1.28-1.25 (m, 48 H), 0.88-0.85 (m, 24 H), 0.08 (s, 3 H), 0.07 (s, 3 H), 0.05 (s, 6 H); ^{13}C NMR ($CDCl_3$, 125 MHz) 173.2, 172.7, 72.0 (d, *J* = 7.5 Hz), 69.4 (d, *J* = 7.5 Hz), 69.1 (d, *J* = 6.5 Hz), 65.4-65.3 (multiple peaks), 64.0, 61.6, 55.4 (d, *J* = 6.3 Hz) 34.1, 34.0, 31.9, 31.6, 29.7-29.1 (multiple peaks), 25.8, 25.7, 24.8, 22.6, 18.3, 18.1,14.1, -4.7, -4.8, -5.5; HRMS (ESI$^+$) *m/z* calculated for $C_{51}H_{106}O_{10}PSi_2$ $[M+H]^+$ 965.7057, found 965.7086.

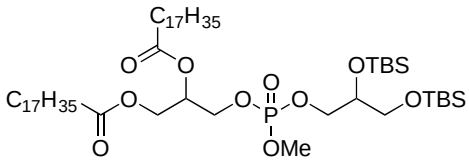

3-(((2,3-Bis((*tert*-butyldimethylsilyl)oxy)propoxy)(methoxy)phosphoryl)oxy)propane-1,2-diyl distearate (8b). (Harried et al., 2009) According to General Procedure D but using **3b** and purification by chromatography on SiO_2 (5:1, hexanes:ethyl acetate) gave 3-(((2,3-bis((*tert*-butyldimethylsilyl)oxy)propoxy)(methoxy)phosphoryl)oxy)propane-1,2-diyl distearate (**8b**, 0.605 g, 0.592 mmol, 67%) as a waxy colorless solid: Mp 31.0-31.9 °C; IR 2923, 2852, 1743, 1252, 835 cm^{-1}; ^{1}H NMR ($CDCl_3$, 300 MHz) 5.24-5.20 (m, 1 H), 4.37-4.31 (m, 1 H), 4.22-4.09 (m, 4 H), 3.97-3.84 (m, 2 H), 3.76 (d, 3 H, *J* =11.1 Hz; diasteromers), 3.57-3.54 (m, 2 H), 2.31 (apparent q, 4 H, *J* = 7.0 Hz), 1.61-1.57 (m, 4 H), 1.28-1.25 (m, 56 H), 0.88-0.86 (m, 24 H), 0.09 (s, 3 H), 0.08 (s, 3 H), 0.05 (s, 6 H); ^{13}C NMR ($CDCl_3$, 125 MHz) 173.2, 172.2, 72.0 (d, *J* = 8.8 Hz), 69.4 (d, *J* = 7.5 Hz), 69.2-69.1 (m), 65.4-65.3 (m), 64.0, 61.6, 54.4 (d, *J* = 5.0 Hz), 34.2, 34.0, 31.9, 29.7-29.1 (multiple peaks), 25.9, 25.7, 24.8, 22.7, 22.6, 18.3, 18.1,14.1, -4.7, -4.8, -5.4, -5.5; HRMS (ESI$^+$) *m/z* calculated for $C_{55}H_{114}O_{10}PSi_2$ $[M+H]^+$ 1021.7688, found 1021.7766.

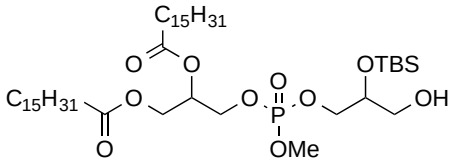

3-(((2-((*Tert*-butyldimethylsilyl)oxy)-3-hydroxypropoxy)(methoxy)phosphoryl)oxy) propane-1,2-diyl dipalmitate (9a). General Procedure E. To a solution of **8a** (800 mg, 0.829 mmol, 1.0 eq.) in CH_2Cl_2:MeOH (1:1, 8.3 mL) at 0 °C was added camphorsulfonic acid (195 mg, 0.823 mmol, 1.0 eq.). The reaction mixture was maintained between -5 and 5 °C and stirred for 5.5 h. The solution was filtered through a small plug of basic alumina (ethyl acetate) and concentrated. Purification by chromatography on SiO_2 (3:1 to 1:1, hexanes:ethyl acetate) gave 3-(((2-((*tert*-butyldimethylsilyl)oxy)-3-hydroxypropoxy)(methoxy)phosphoryl)oxy)propane-1,2-diyl dipalmitate (**9a**, 435 mg, 0.511 mmol, 62%) as a colorless solid: Mp 27.8-28.0 °C; IR 2922, 2854, 1741, 1252, 835 cm^{-1}; ^1H NMR ($CDCl_3$, 400 MHz) 5.29-5.20 (m, 1 H), 4.33 (dd, 1 H, *J* = 4.4, 12.0 Hz), 4.21-4.14 (m, 3 H), 4.06-4.01 (m, 2 H), 3.93-3.89 (m, 1 H), 3.80-3.76 (m, 3 H), 3.67-3.50 (m, 2 H), 2.35-2.31 (m, 5 H), 1.62-1.60 (m, 4 H), 1.28-1.25 (m, 48 H), 0.90-0.86 (m, 15 H), 0.11 (s, 6 H); ^{13}C NMR ($CDCl_3$, 100 MHz) 173.2, 172.8, 71.1 (d, *J* = 7.0 Hz), 69.4-69.3 (multiple peaks), 67.7 (m), 65.6-65.5 (multiple peaks), 63.0, 61.6, 54.6 (multiple peaks), 34.1, 34.0, 31.9, 29.7-29.1 (multiple peaks), 25.7, 24.8, 22.7, 18.0, 14.1, -4.8, -4.9; HRMS (ESI^+) *m/z* calculated for $C_{45}H_{92}O_{10}PSi$ $[M+H]^+$ 851.6192, found 851.6180.

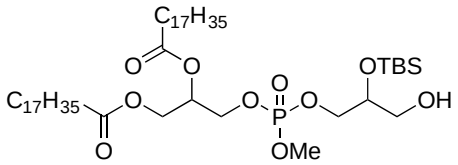

3-(((2-((*Tert*-butyldimethylsilyl)oxy)-3-hydroxypropoxy)(methoxy)phosphoryl)oxy) propane-1,2-diyl distearate (9b). According to General Procedure E but using **8b** and purification by chromatography on SiO_2 (4:1 to 1:1, hexanes:ethyl acetate) gave 3-(((2-((*tert*-butyldimethylsilyl)oxy)-3-hydroxypropoxy)(methoxy)phosphoryl)oxy)propane-1,2-diyl distearate (**9b**, 470 mg, 0.518 mmol, 55%) as a waxy colorless solid: Mp = 41.2-41.7 °C; IR 3535, 2921, 2850, 1739, 733 cm^{-1}; ^1H NMR ($CDCl_3$, 300 MHz) 5.25-5.22 (m, 1 H), 4.34 (dd, 1 H, *J* = 4.2, 12.0 Hz), 4.19-4.11 (m, 3 H), 4.05-4.02 (m, 2 H), 3.95-3.90 (m, 1 H), 3.78 (d, 3 H, *J* = 11.4 Hz; diasteromers), 3.67-3.60 (m, 2 H), 2.36-2.29 (m, 5 H), 1.62-1.58 (m, 4 H), 1.28-1.25 (m, 56 H), 0.90-0.86 (m, 15 H), 0.11 (s, 6 H); ^{13}C NMR ($CDCl_3$, 125 MHz) 173.3, 172.8, 71.1 (d, *J* = 7.1 Hz), 69.4 (multiple peaks), 67.7 (multiple peaks), 65.6 (multiple peaks), 63.0, 61.6, 54.6 (multiple peaks), 34.2, 34.0, 31.9, 29.7-29.1 (multiple peaks), 25.7, 24.8, 22.7, 18.0, 14.1, -4.7, -4.9; HRMS (ESI^+) *m/z* calculated for $C_{49}H_{100}O_{10}PSi$ $[M+H]^+$ 907.6818, found 907.6785.

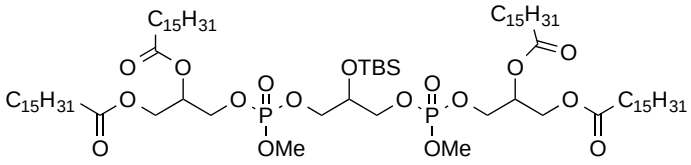

3-(((3-(((2,3-(Palmitoyloxy)propoxy)(methoxy)phosphoryl)oxy)-2-((*tert*-butyldimethylsilyl)oxy)propoxy)(methoxy)phosphoryl)oxy)propane-1,2-diyl dipalmitate (10a). (Harried et al., 2009) To a solution of **9a** (322 mg, 0.378 mmol, 1.0 eq.) in CH_2Cl_2 (3.7 mL) at 0 °C under nitrogen was added DIPEA (0.069 mL, 0.42 mmol, 1.1 eq.) and a 0.5 M solution of **7** in CH_2Cl_2 (0.83 mL, 0.42 mmol, 1.1 eq.). The reaction mixture was warmed to room temperature, stirred for 1.5 h, and treated with a solution of **3a** (364 mg, 0.416 mmol, 1.1 eq.) and 4,5-dicyanoimidazole (90 mg, 0.76 mmol, 2.0 eq.) in THF (1.5

mL) in a drowpwise fashion. The reaction mixture was stirred for 2 h, cooled to 0 °C, treated with Bu_4NIO_4 (186 mg, 0.429 mmol, 1.1 eq.) and stirred for 40 min. The mixture was diluted with water (3 mL) and CH_2Cl_2 (5 mL) and and the organic layer was rinsed with sat. $Na_2S_2O_3$ (3 mL) and brine (3 mL), dried ($MgSO_4$), and concentrated. The crude product was filtered through a plug of SiO_2 (1:1 hexanes:ethyl acetate) and concentrated. Purification by chromatography on SiO_2 (3:1 to 2:1 to 1:1, hexanes:ethyl acetate) gave 3-(((3-(((2,3-(palmitoyloxy)propoxy)(methoxy) phosphoryl)oxy)-2-((*tert*-butyldimethylsilyl)oxy)propoxy)(methoxy)phosphoryl)oxy)propane-1,2-diyl dipalmitate (**10a**, 381 mg, 0.255 mmol, 67%) as a colorless solid: Mp 36.5-37.5 °C; IR 2913, 2848, 1737, 1465, 913, 744 cm^{-1}; ^1H NMR ($CDCl_3$, 400 MHz) 5.25-5.22 (m, 2 H), 4.36-4.31 (m, 2 H), 4.22-4.12 (m, 6 H), 4.05-3.97 (m, 5 H), 3.78 (d, 6 H, *J* = 11.2 Hz; diasteromers), 2.32 (apparent q, 8 H, *J* = 7.9 Hz), 1.61-1.57 (m, 8 H), 1.28-1.25 (m, 96 H), 0.89-0.86 (m, 21 H), 0.11 (s, 6 H); ^{13}C NMR ($CDCl_3$, 125 MHz) 173.1, 172.7, 69.8 (multiple peaks), 69.4 (d, *J* = 6.3 Hz), 67.8 (2, *J* = 6.3 Hz), 65.7 (multiple peaks), 61.6, 54.6 (d, *J* = 6.3 Hz), 34.2, 34.0, 31.9, 29.7-29.1 (multiple peaks), 25.6, 24.9, 22.7, 18.0, 14.1, -4.9; HRMS (ESI^+) *m/z* calculated for $C_{81}H_{161}O_{17}P_2Si$ $[M+H]^+$ 1496.0973, found 1496.0903.

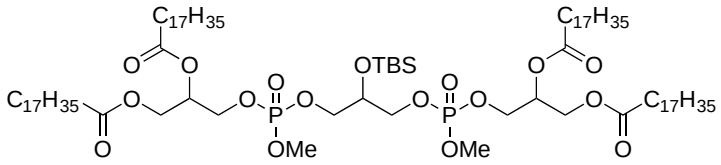

3-(((3-(((2,3-(Stearoyloxy)propoxy)(methoxy)phosphoryl)oxy)-2-((*tert*-butyldimethylsilyl)oxy)propoxy)(methoxy)phosphoryl)oxy)propane-1,2-diyl distearate (10b). General Procedure F (Abe et al., 2011). To a solution of **3b** (356 mg, 0.570 mmol,

1.0 eq.) and DIPEA (0.10 mL, 0.63 mmol, 1.1 eq.) under nitrogen was added a 0.5 M solution of **7** (1.2 mL, 0.63 mmol, 1.1 eq.) in CH_2Cl_2. The reaction was mixture stirred for 1 h, and treated drowpwise with a solution of **9b** (470 mg, 0.518 mmol, 1.0 eq.) and 4,5-dicyanoimidazole (125 mg, 1.04 mmol, 2.0 eq.) in THF (1.5 mL). The mixture was stirred for 3 h, cooled to 0 °C, treated with Bu_4NIO_4 (173 mg, 0.399 mmol, 1.2 eq.), stirred for 45 min and diluted with water (2 mL) and CH_2Cl_2 (5 mL). The organic layer was rinsed with sat. $Na_2S_2O_3$ (2x3 mL), sat. $NaHCO_3$ (3 mL), and brine (3 mL), dried (MgSO4), and concentrated. The crude residue was filtered through a plug of SiO_2 (1:1, hexanes:ethyl acetate), concentrated, dissolved in CH_2Cl_2 (4 mL) and treated with TBSCl (43 mg, 0.29 mmol 0.5 eq.), imidazole (21 mg, 0.31 0.6 eq.) and DMAP (3 mg, 0.024 mmol 0.04 eq.). The reaction mixture was stirred for 4.5 h, quenched with water (4 mL) and diluted with CH_2Cl_2 (4 mL). The organic layer was rinsed with brine (4 mL), dried ($MgSO_4$), and concentrated. Purification by chromatography on SiO_2 (5:1 to 3:1 to 1:1, hexanes:ethyl acetate) gave 3-(((3-(((2,3-(stearoyloxy)propoxy)(methoxy)phosphoryl)oxy)-2-((*tert*-butyldimethylsilyl) oxy)propoxy) (methoxy)phosphoryl)oxy)propane-1,2-diyl distearate (**10b**, 335 mg, 0.208 mmol, 40%) as a waxy colorless solid: Mp 48.1-48.2 °C; IR 2918, 2851, 1741, 1043 cm^{-1}; ^1H NMR ($CDCl_3$, 300 MHz) 5.25-5.22 (m, 2 H), 4.35-4.30 (m, 2 H), 4.29-4.04 (m, 11 H), 3.78 (d, 6 H, *J* = 11.4 Hz; diasteromers), 2.32 (apparent q, 8 H, *J* = 7.2 Hz), 1.61-1.57 (m, 8 H), 1.25 (m, 112 H), 0.89-0.86 (m, 21 H), 0.11 (s, 6 H); ^{13}C NMR ($CDCl_3$, 125 MHz) 173.2, 172.8, 69.7 (multiple peaks), 69.4 (multiple peaks), 67.9 (multiple peaks), 65.6 (multiple peaks), 61.6, 54.6 (d, *J* = 5.9 Hz), 34.1, 34.0, 31.9, 29.7-29.1 (multiple peaks), 25.6,

24.8, 22.7, 18.0, 14.1, -4.9; HRMS (ESI$^+$) *m/z* calculated for $C_{89}H_{177}O_{17}P_2Si$ $[M+H]^+$ 1608.2225, found 1608.2190.

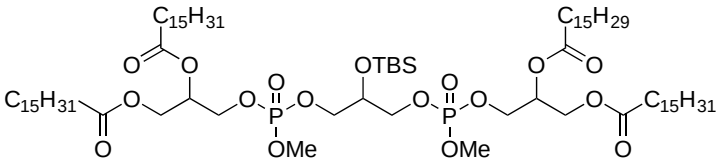

3-(((3-(((2-Palmitoleoyloxy-3-(palmitoyloxy)propoxy)(methoxy)phosphoryl)oxy)-2-((*tert*-butyldimethylsilyl)oxy)propoxy)(methoxy)phosphoryl)oxy)propane-1,2-diyl dipalmitate (10c). According to General Procedure F using **3c** and **9c** and a purification by chromatography on SiO_2 (5:1 to 3:1 to 1:1, hexanes:ethyl acetate) gave 3-(((3-(((2-palmitoleoyloxy-3-(palmitoyloxy)propoxy)(methoxy)phosphoryl)oxy)-2-((*tert*-butyldimethylsilyl)oxy)propoxy) (methoxy)phosphoryl)oxy)propane-1,2-diyl dipalmitate (**10c**,145 mg, 0.0970 mmol, 39%) as a clear colorless oil: IR 2919, 2850, 1741, 1465, 1034 cm^{-1}; ^{1}H NMR ($CDCl_3$, 300 MHz) 5.35-5.33 (m, 2 H), 5.25-5.22 (m, 2 H), 4.36-4.32 (m, 2 H), 4.23-4.12 (m, 6 H), 4.05-4.00 (m, 5 H), 3.78 (d, 6 H, *J* = 11.4 Hz; diasteromers visible), 2.32 (apparent q, 8 H, *J* = 7.2 Hz), 2.02-2.00 (m, 4 H), 1.61-1.54 (m, 8 H), 1.30-1.26 (m, 88 H), 0.89-0.86 (m, 21 H), 0.11 (s, 6 H); ^{13}C NMR ($CDCl_3$, 125 MHz) 173.2, 172.8, 130.0, 129.7, 69.7 (m), 69.4 (d, *J* = 6.5 Hz), 67.8 (d, *J* = 5.5 Hz), 65.6 (m), 61.6, 54.6 (d, *J* = 6.0 Hz), 34.1, 34.0, 31.8, 29.7-29.0 (multiple peaks), 25.6, 24.8, 22.7, 22.6 18.0, 14.1, -4.9; HRMS (ESI$^+$) *m/z* calculated for $C_{81}H_{159}O_{17}P_2Si$ $[M+H]^+$ 1494.0816, found 1494.0825.

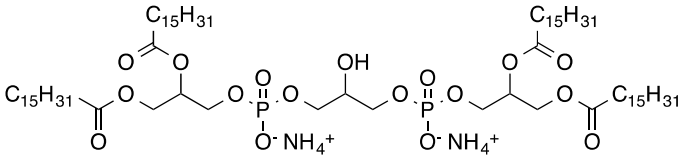

Tetrapalmitoylcardiolipin diammonium salt (11a). General Procedure G. A solution of **10a** and NaI (24 mg, 0.16 mmol, 4 eq.) in 2-butanone (0.8 mL) was heated at reflux for 13.5 h and concentrated. The crude waxy yellow solid was dissolved in 1 M HCl:THF:H_2O (0.1:2:1, 1 mL) and the resulting yellow solution was stirred for 12 h, and quenched with 30% NH_4OH (2 mL). The resulting white slurry was extracted with $CHCl_3$ (3x5 mL), concentrated, and triturated with Et_2O to give tetrapalmitoylcardiolipin diammonium salt (**11a**, 40 mg, 0.029 mmol, 73%) as a colorless solid containing 5-7% (ESI-MS) monolyso (tripalmitoyl) cardiolipin as an impurity that was removed by thin layer chromatography: ^{1}H NMR ($CDCl_3$, 400 MHz) 7.46 (bs, 8 H), 5.21(bs, 2 H), 4.37 (m, 2 H), 4.17-4.13 (m, 2 H), 3.91 (bs, 9 H), 2.29 (apparent q, 8 H, *J* = 8.5 Hz), 1.58 (m, 8 H), 1.28-1.25 (m, 98 H), 0.87 (t, 12 H, *J* = 6.8 Hz); HRMS (ESI^-) *m/z* calculated for $C_{73}H_{141}O_{17}P_2$ $[M-H]^-$ 1351.9639, found 1351.9648.

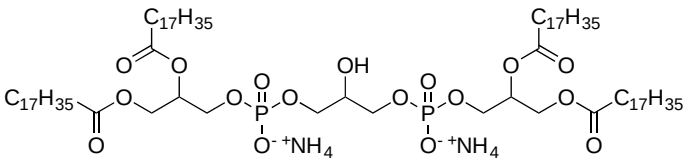

Tetrastearoylcardiolipin diammonium salt (11b) (Abe et al., 2011), According to General Procedure G using **10b** and purification by precipitation from hot THF gave tetrastearoylcardiolipin diammonium salt (**11b**, 53 mg, 0.035 mmol, 38%) as a colorless powder containing 5-7% (ESI-MS) monolyso (tristearoylcardiolipin) cardiolipin as an impurity that was removed by thin layer chromatography: ^{1}H NMR ($CDCl_3$, 400 MHz) 7.44 (bs, 8 H), 5.21 (bs, 2 H), 4.37-4.35 (m, 2 H), 4.17-4.13 (m, 2 H), 3.92 (bs, 9 H),

2.30 (apparent q, 8 H, *J* = 8.3 Hz), 1.59-1.58 (m, 8 H), 1.28-1.25 (m, 112 H), 0.88 (t, 12 H, *J* = 6.8 Hz); MS (ESI$^-$) *m/z* calculated for $C_{81}H_{156}O_{17}P_2$ $[M-2H]^{2-}$ 731.5, found 731.8.

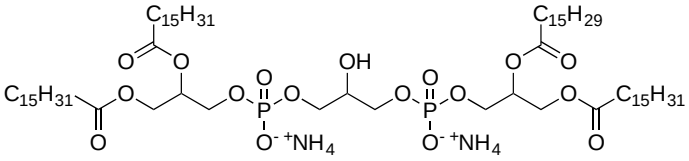

Tripalmitoyl-monopalmitoleoylcardiolipin diammonium salt (11c). According to General Procedure G using **10c** and purification by trituration with Et_2O gave tripalmitoyl-monopalmitoleoylcardiolipin diammonium salt (**11c**, 83 mg, 0.060 mmol, 70%) as a colorless powder containing 5-7% (ESI-MS) monolyso-**11c** as an impurity that was removed by thin layer chromatography: ^{1}H NMR ($CDCl_3$, 400 MHz) 7.44 (bs, 8 H), 5.35-5.32 (m, 2 H), 5.21 (bs, 2 H), 4.39-4.35 (m, 2 H), 4.17-4.13 (m, 2 H), 3.84 (bs, 9 H), 2.30 (apparent q, 8 H, *J* = 8.1 Hz), 2.01-1.99 (m, 4 H), 1.66-1.58 (m, 8 H), 1.28-1.25 (m, 106 H), 0.88 (t, 12 H, *J* = 6.4 Hz); MS (ESI$^-$) *m/z* calculated for $C_{73}H_{138}O_{17}P_2$ $[M-2H]^{2-}$ 674.5, found 674.7.

Assessment of Substrate Specificity of Purified Cld1—Activity of Cld1 was detected in liposomes by accumulation of MLCL after CL hydrolysis. Liposomes containing DOPC and CL (10 µM, 1:1) were prepared by sonication (Ultrasonic Homogenizer 4710 series, Cole-Parmer Instrument Co., Chicago, IL) and treated with Cld1 (0.1−0.5 µg of protein per 250µl sample) in 50 mM HEPES pH 7.45, containing 100 µM DTPA for 20 min at 37°C. After incubation with CLD1, lipids were extracted by Folch procedure and analysis of MLCL was performed using LC−ESI-MS. Internal standards of MLCLs were prepared from respective CLs in PLA_2 (porcine pancreatic, Sigma) driven reaction as described by Kim and Hoppel (2011) (Kim and Hoppel, 2011) with slight modifications.

Molecular modeling—The homology model of *CLD1* was built using I-TASSER (Yang et al., 2015) webserver. Hsad, a steroid-degrading hydrolase from Mycobacterium Tuberculosis (PDB ID: 2VF2 (Lack et al., 2008)), was utilized as a template. C-score for the constructed model was equal to 1.78. The C-score is a confidence score to estimate the quality of predicted models by I-TASSER, in the range of [-5,2], where a C-score of higher value defines a model with a high confidence (Yang et al., 2015). The model showed a TM-score equal to 0.5. TM-score is a scale for measuring the structural similarity of two protein models, with lower sensitivity to the local error compared to RMSD (a TM-score >0.5 indicates a model of correct topology independent from protein length) (Zhang and Skolnick, 2004). The overlay of the cavities and cartoon representations was employed to explore the active site and a possible channel facilitating access of CL acyl chain to the hydrolase domain of *CLD1*. Three homo-acylated-CL species, including (C14:0)4-CL, (C16:0)4-CL and (C18:2)4-CL were docked to the predicted structure of CLD1 using default settings by AutoDock Vina (http://vina.scripps.edu) (Trott and Olson, 2010). The pdb into pdbqt format conversion of lipids and protein structures was performed using MGL Tools. A grid box was centered at coordinates 39.861, 40.057, 74.975 with 100Å, 80Å and 90Å units in x, y and z directions, respectively, to cover the entire protein structure. AutoDock Vina reports the 9 lowest energy conformations, which were inspected using PyMOL software (www.pymol.org).

Statistical Analysis—The results are presented as mean ± S.D. values from at least three experiments, and statistical analyses were performed by paired/unpaired

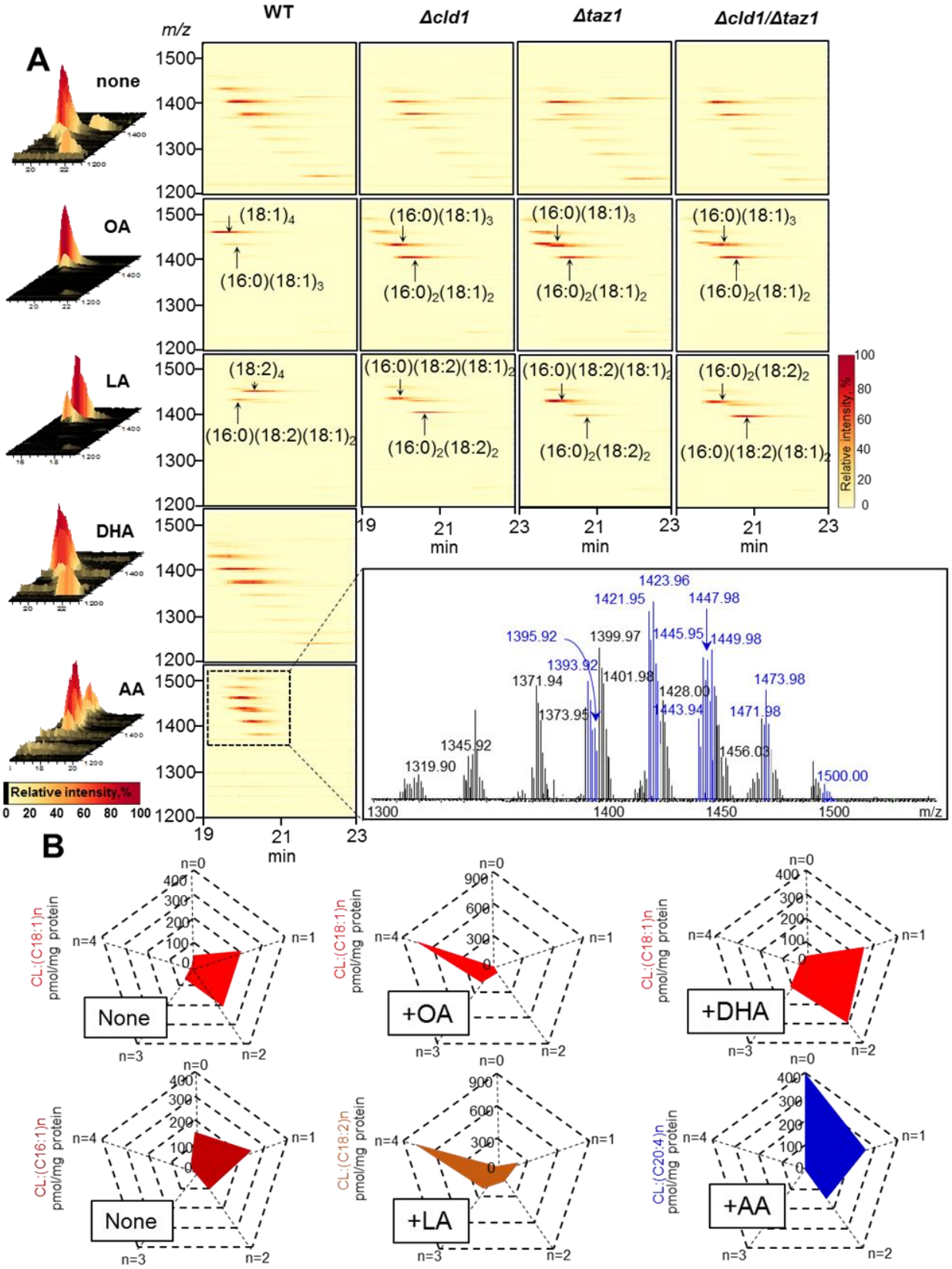
A
WT
Δcld1
Δtaz1
Δcld1/Δtaz1
m/z
none
OA
LA
DHA
AA
(18:1)4
(16:0)(18:1)3
(16:0)2(18:1)2
(18:2)4
(16:0)(18:2)(18:1)2
(16:0)2(18:2)2
Relative intensity,%
min
1423.96
1421.95
1447.98
1395.92
1399.97
1445.95
1449.98
1393.92
1371.94
1401.98
1473.98
1428.00
1373.95
1443.94
1471.98
1345.92
1319.90
1456.03
1500.00
m/z
B
CL:(C18:1)n pmol/mg protein
None
+OA
+DHA
CL:(C16:1)n pmol/mg protein
+LA
CL:(C18:2)n pmol/mg protein
+AA
CL:(C20:4)n pmol/mg protein
n=0
n=1
n=2
n=3
n=4

Figure 3-1. LC/MS analysis of CL in S. cerevisiae.

A. 3D-mass spectra (left panels) and MS maps (right panels) of CL obtained from wild type and *cld1Δ, taz1Δ, cld1Δ/taz1Δ mutants* before and after supplementation with different fatty acids. (OA, oleic acid C18:1; LA, linoleic acid C18:2, DHA, docosahexaenoic acid C22:6, AA, arachidonic acid C20:4). Insert: Mass spectrum of CL from yeast supplemented with C20:4 (AA). MS signals of C20:4 containing CL molecular species with m/z 1393.92, 1395.92, 1421.95, 1423.95, 1445.95, 1447.95, 1449.98, 1471.98, 1473.98, 1500.00 identified as C16:1/C16:1/C16:1/C20:4, C16:1/C16:1/C16:0/C20:4, C16:1/C16:1/C18:1/C20:4, C16:0/C16:1/C18:1/C20:4, C16:0/C16:1/C20:4/C20:4, C16:0/C16:0/C20:4/C20:4, C16:1/C18:1/C18:1/C20:4, C16:1/C18:1/C20:4/C20:4, C16:0/C18:1/C20:4/C20:4 and C18:1/C18:1/C20:4/C20:4, respectively and shown in blue. B. Quantitative assessment of hetero- and homo-acylated molecular species of CLs in wt yeast cells before and after supplementation with different FAs.

Student's t-test. The statistical significance of differences was set at $p < 0.05$.

RESULTS

Exogenous FAs define the molecular speciation of CLs in wt and mutant S. cerevisiae cells.

In wt *S. cerevisiae* cells grown without FA supplementation, there is an assortment of CL molecular species with different FA residues ranging from C10 to C18. Among those, only singly-unsaturated CL species were present whereas PUFA were not detected (Figure 3-1A). To gain insight into the mechanisms of CL remodeling and biosynthesis, we chose to expose yeast cells to FAs with different chain lengths as well as unsaturation. In particular, we employed oleic (18:1), linoleic (18:2), arachidonic (20:4) and docosahexaenoic (22:6) acids as components of the growth medium and established their effects on the phospholipidomes of *S. cerevisiae* cells.

Supplementation of the growth medium with either 18:1 or 18:2 FAs caused dramatic changes in CLs composition (Figure 3-1B). Only CL molecular species containing from one to four 18:1 or C18:2 were detectable, while essentially all other

molecular species of CLs with shorter chains and devoid of C18-containing species were not found (Figure3- 1). Notably, a huge preponderance of homo-acylated – $(18:1)_4$-CL- and $(18:2)_4$-TLCL species – was observed (Figure 3-1B). The second largest cluster of CLs included hetero-acylated - tri-C18:1 and tri-C18:2-species, respectively (Figure 3-1). These robust effects of exogenously added C18 FAs in wt cells were much less pronounced when C20:4 was used (Figure 3-1). In fact, only singly- and doubly- 20:4-acylated CL species were detectable; no tri- or tetra-20:4-CL species were observed (Figure 3-1B, Supplementary Figure 4). Upon treatment with 22:6, CLs speciation remained unchanged *vs* untreated w/t cells (Figure 3-1B); 22:6-contaning CL species were not detectable. Overall, these data indicate that the remodeling and biosynthetic pathways for CLs are very specific and favor the synthesis of C18-containing molecular species. The balance of natural processes of CL hydrolysis and re-acylation yields only very low concentrations of MLCLs – as intermediates of these reactions. Supplementation with FAs did not significantly affect the MLCL content in wt cells (Figure 3-2).

CL remodeling from MLCL in yeast cells occurs via a single metabolic reaction catalyzed by Taz1 (Ren et al., 2014):

$$\text{PL-2FA} + \text{MLCL-3FA} \rightarrow \text{LPL-1FA} + \text{CL-4FA}$$

where PL-2FA is a donor di-acylated phospholipid, MLCL-3FA is an acceptor MLCL, LPL is lyso-phospholipid formed, and CL-4FA is a remodeled CL. For CL reacylation, the enzyme utilizes donor phospholipids, particularly PC and PE. Therefore, we also studied the effects of C18:1 and C18:2 supplementations on the phospholipidome of

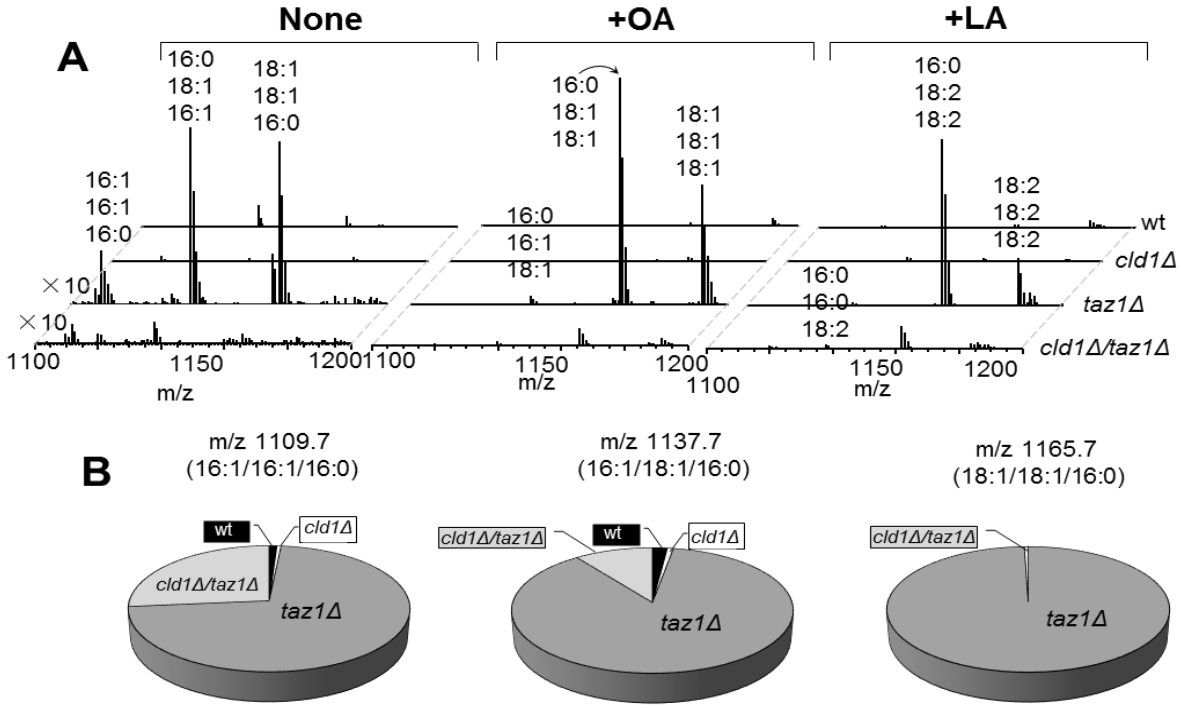

Figure 3-2. LC/MS analysis of mono-lyso-CL (MLCL) in S. cerevisiae.

A. Mass spectra of MLCL obtained from wt (left panel) yeast cells and *cld1Δ, taz1Δ, cld1Δ/taz1Δ* mutants supplemented with C18:1 (OA) (middle panel) and C18:2 (LA) (right panel). B. Quantitative assessments of MLCL performed for wild type yeast cells and *cld1Δ, taz1Δ, cld1Δ/taz1Δ* mutants.

these cells. We found no changes in the total content of phosphatidylcholine (PC) and phosphatidylethanolamine (PE) in supplemented cells. However, supplementation with 18:1 resulted in the accumulation of PE and PC species containing 18:1 FA residues (Figure 3-3). Similarly, addition to the medium of 18:2 was associated with higher levels of 18:2-containing PE and PC (Figure 3-3). The enrichment with C18 FA residues was at the expense of the decreased contents of PE and PC species containing 16:0 and 16:1 (Figure 3-3). Further, we found that supplementation of cells with either 18:1 or 18:2 resulted in the accumulation of homo-acylated PC and PE molecular species (containing either 18:1 or 18:2 in both *sn*-1 and *sn*-2 positions). Subsequently, we

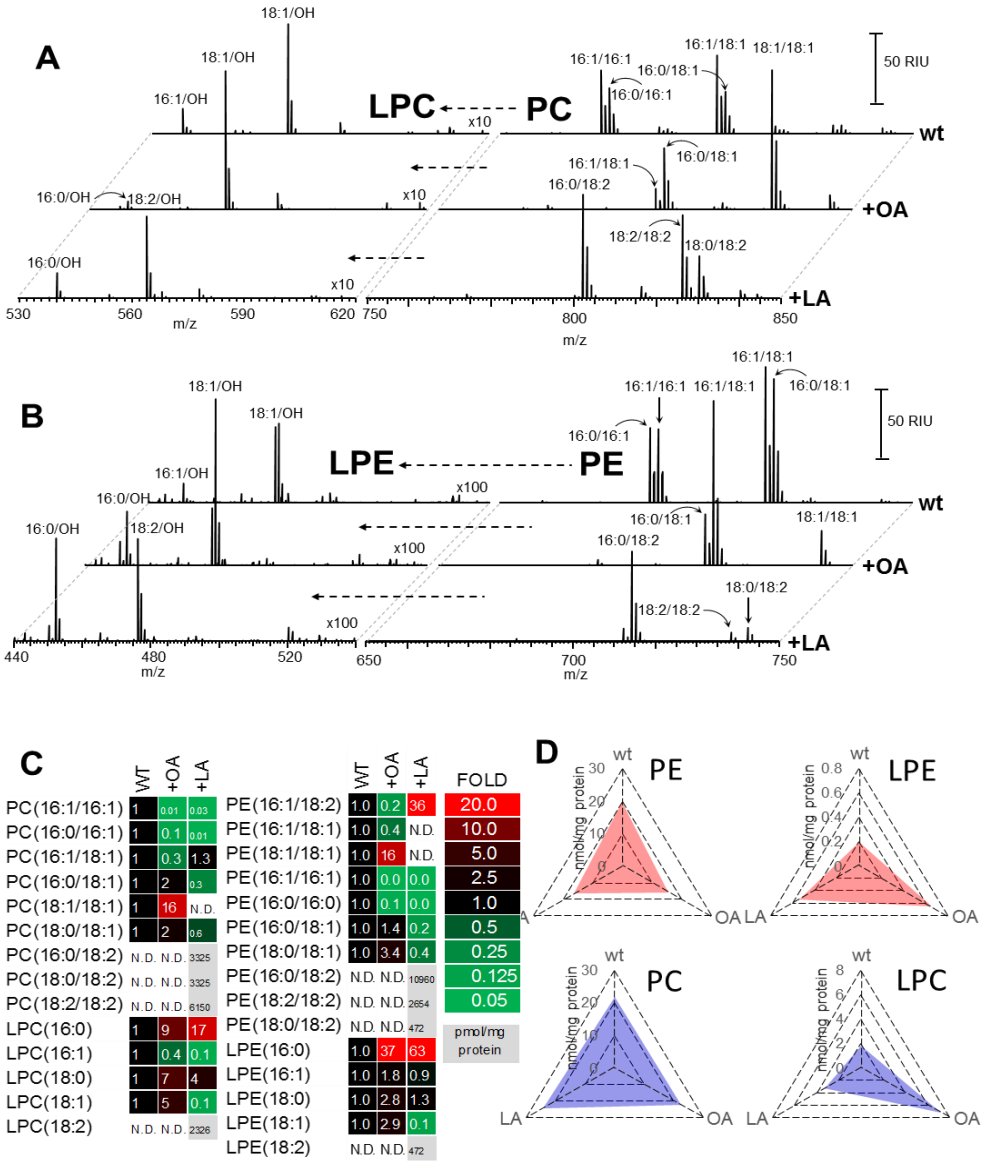

Figure 3-3. LC/MS analysis and quantitative assessment of phosphatidylcholine (PC) and phosphatidylethanolamine (PE) as well as their hydrolysis products – lyso-PC (LPC) and lyso-PE (LPE) - in S. cerevisiae.

A. Mass spectra of PC (left panels) and LPC (right panels) for wild type yeast cells before and after supplementation with either C18:1 (OA) or C18:2 (LA). B. A. Mass spectra of PE (left panels) and LPE (right panels) for wild type yeast cells before and after supplementation with either C18:1 (OA) or C18:2 (LA). C, D. Heat maps of PC, PE, LPC and LPE for wild type yeast cells before and after supplementation with either C18:1 (OA) or C18:2 (LA). Values in heat maps pixels show the fold change in phospholipid content in supplemented yeast cells compared to non-supplemented wild type cells. Red pixels without numbers inside designate lipid species produced only after LA supplementation (but not detectable in non-C18:2-supplemented cells).

detected an increased content of 18:1-LPC/LPE and 18:2-LPC/LPE after supplementation of cells with these FAs. This suggests that homo-acylated species of PC and PE were effectively utilized by Taz1 as preferred substrates for the re-acylation of MLCL. It is also possible that these FAs were readily incorporated via *de novo* biosynthesis (presumably of phosphatidic acid (PA)). Direct experimental assessment of the contribution of these alternative pathways can be deduced from our lipidomics data obtained from wt and mutant cells supplemented with FA, as shown below.

Both Cld1 and Taz1 modify the cardiolipinome.

Cld1 is a critical participant of the CL remodeling process, as it catalyzes phospholipid hydrolysis with a significant selectivity towards 16:0 and 16:1-containing molecular species (Beranek et al., 2009). This suggests that disruption of this process in the *cld1Δ* mutant should result in an altered molecular speciation of CLs, particularly with regards to longer-chain (C16 and C18) species. However, according to a recently reported shotgun lipidomics study, the lipid profile of *cld1Δ* was similar to that of wt, whereas *taz1Δ* had a reduction of CL and an accumulation of MLCL (Baile et al., 2014). To resolve this apparent conundrum, we performed detailed LC-MS based characterization of cardiolipinomes in wt and mutant *S. cerevisiae* cells. We found that composition of CL from wt cells was different from that detected in either *cld1Δ, taz1Δ* or *cld1Δ/taz1Δ* mutants. In addition, *cld1Δ* contained slightly (but significantly) higher levels of CLs compared to wt cells (Figure 3-1B). In line with published data, the changes in the total content of CL and MLCL found in *taz1Δ* mutants were no longer detectable in *cld1Δ/taz1Δ* mutants. Indeed, dramatic accumulation of MLCL was

detected in taz1Δ but not in cld1Δ or cld1Δ/taz1Δ mutants (Figure 3-2). However molecular speciation of CLs in wt cells vs double-mutant cells were markedly different. Similar results were obtained with wt cells and mutants supplemented with OA or LA (Figure 3-2). These data are compatible with the role of Cld1 in "preparing" CLs for remodeling via hydrolysis/reacylation, and suggest that elimination of the hydrolytic pathway by deletion of Cld1 would lead to "conservation" of CLs. Consistent with this prediction, *cld1Δ* mutant cells were essentially unable to produce remodeled tetra- and tri-18:1 species of CLs (Figure 3-1B). Instead, their CLs were enriched with 16:0 and 16:1 containing molecular species (Figure 3-1B).

Assuming that Cld1 is a participant in the only remodeling process in *S. cerevisiae* cells, one can distinguish between the contribution of *de novo* biosynthesis *vs* remodeling processes in the overall diversification of CLs. In wt cells, both the biosynthesis and *de novo* remodeling reactions contribute to the overall diversity and content of CLs. Deletion of Cld1 would eliminate the remodeling process, thus revealing the nascent CL species generated via its de novo biosynthesis. Thus, two categories of CLs can be determined by comparison of LC-MS spectra of CLs from wt and *cld1Δ* cells (Figure 3-4), including: i) those produced by the biosynthetic pathway, revealed in the *cld1Δ* mutant, ii) those generated as products (increased) or utilized as substrates by the remodeling pathway (decreased). These latter respective categories of CLs can be identified in the LC-MS spectra of CLs in ± (wt minus *cld1Δ)* by the differential analysis.

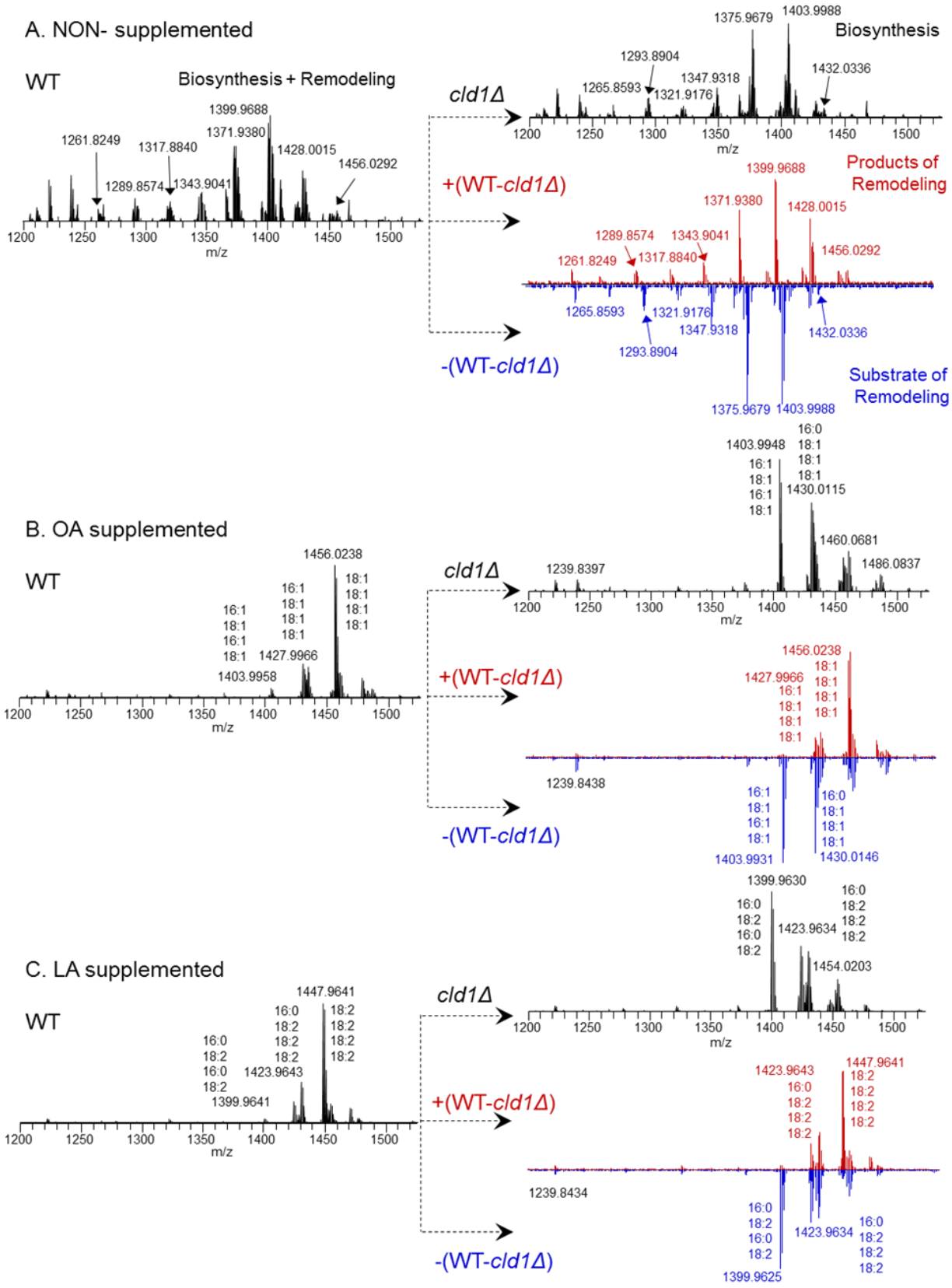
A. NON- supplemented
WT
Biosynthesis + Remodeling
cld1Δ
Biosynthesis
Products of Remodeling
+(WT-cld1Δ)
-(WT-cld1Δ)
Substrate of Remodeling
B. OA supplemented
WT
cld1Δ
+(WT-cld1Δ)
-(WT-cld1Δ)
C. LA supplemented
WT
cld1Δ
+(WT-cld1Δ)
-(WT-cld1Δ)
m/z

Figure 3-4. Contribution of de novo biosynthesis vs remodeling processes to the diversification of CLs in S. cerevisiae.

Mass spectra of CL obtained from wild type yeast cells and *cld1Δ* mutant cells with or without oleic/linoleic acid (OA/LA) supplementation. The resulting differential mass spectra of CL species produced and consumed by the remodeling process were obtained, as shown in the positive and negative spectra of w/t minus *cld1Δ* mutants, respectively. A. Mass spectra of CL obtained from non-supplemented wild type yeast cells and *cld1Δ* mutant. CL molecular species were identified as C10:0/C16:1/C16:1/C16:1 (m/z 1261.8249); C10:0/C16:0/C16:0/C16:1 (m/z 1265.8593); C10:0/C16:1/C16:1/C18:1 (m/z 1289.8574); C12:0/C16:0/C16:0/C16:1 (m/z1293.8904); C12:0/C16:1/C16:1/C18:1 (m/z 1317.8840); C12:0/C16:0/C16:1/C16:1 (m/z 1321.9176); C16:1/C16:1/C16:1/C16:1 (m/z 1343.9041); C12:0/C16:1/C18:1/C18:1 (m/z 1345.9184); C12:0/C16:0/C16:1/C18:0 (m/z 1347.9318); C16:1/C16:1/C16:1/C18:1 (m/z 1371.9380); C16:0/C16:1/C16:0/C18:1 (m/z 1375.9669); C16:1/C18:1/C16:1/C18:1 (m/z 1399.9688); C16:0/C18:1/C16:0/C18:1 (m/z 1403.9988); C16:1/C18:1/C18:1/C18:1 (m/z 1428.0015); C16:0/C18:1/C18:0/C18:1 (m/z 1432.0336); C18:1/C18:1/C18:1/C18:1 (m/z 1456.0292). B. Mass spectra of CL obtained from OA supplemented w/t yeast cells and *cld1Δ* mutant. Major CL species are annotated on mass spectra. C. Mass spectra of CL obtained from LA supplemented w/t yeast cells and *cld1Δ* mutant. Major CL species are annotated on mass spectra

By applying these differential (subtraction) protocols[1], we found significant differences in molecular speciation of CLs in wt and mutant cells. In cld1Δ cells *(lacking the remodeling pathway),* CLs formed in the reaction catalyzed by CL synthase were mainly represented by molecular species containing 16:0, 16:1 and 18:1 FA residues (Figure 3-4). This was supported by LC/MS analysis of the CL biosynthesis precursor, –phosphatidylglycerol (PG). We found that PGs were predominantly represented by 16:1/18:1, 16:1/18:1 and 16:0/16:1 molecular species in wt cells (Figure 3-5). On the other hand, during the remodeling, esterified 16:0 was substituted with the 16:1 fatty acid residue (Figure 3-5). These data suggest that in non-FA-supplemented w/t cells,

[1] Please note that the specific feature of the software utilized for the subtraction disallows plotting of the negative spectra; therefore -(WT- *cld1Δ*) plots were used as explained in detail in Materials and Methods.

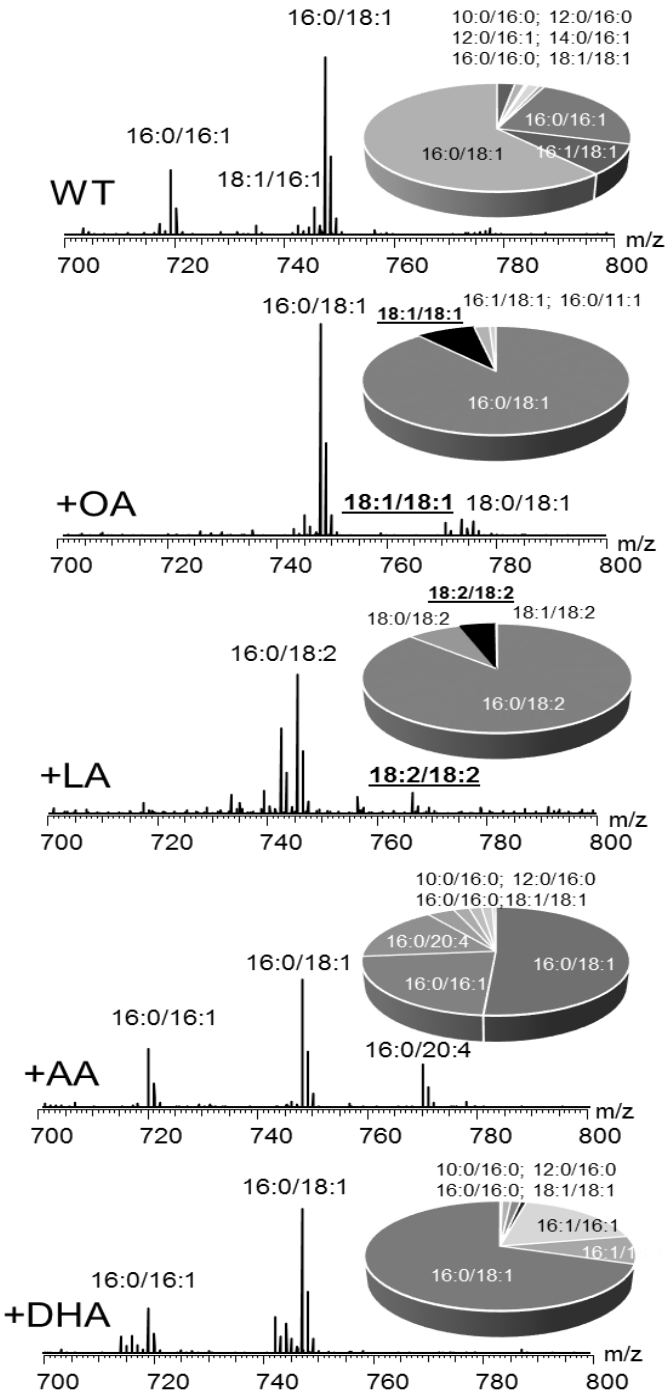

Figure 3-5. LC/MS analysis of phosphatidylglycerol (PG) in wild type S. cerevisae before and after supplementation with different fatty acids.

Mass spectra and quantitative assessments (inserts) of PG obtained from control wild type yeast cells and wild type yeast cells supplemented with C18:1 (OA), C18:2 (LA), C20:4 (AA) and C22:6 (DHA).

Cld1 predominantly hydrolyzed 16:0-containing CLs that were then remodeled with 16:1 by Taz1-catalyzed re-acylation.

We further applied the same approach to distinguish between the CL species formed through either biosynthetic or remodeling pathways in wt cells supplemented with either 18:1 or 18:2. This analysis revealed that the remodeling route was entirely accountable for the replacement of fatty acid residues in CLs yielding predominantly homo-acylated tetra-18:1 or tetra-18:2 molecular species of CLs, respectively (Figure 3-1B, Figure 3-4B, C). Based on these newly developed protocols for the assessment of biosynthetic *vs* remodeling origins of the CL species, we compared the relative contributions of these two pathways to all CLs in determining the pool of homo-acylated species. We found that biosynthesis was the major (wt cells, 18:2-treated cells) or significant (C18:1-treated cells) contributor to the entire pool of CLs. Interestingly, the remodeling process was, by far, the most important contributor to the pool of homo-acylated CLs. Specifically, we found that CL(18:1/18:1/18:1/18:1) was the major product (Figure 3-4B, WT-*cld1Δ*), while CL(16:1_18:1_16:1_18:1) and CL(16:0_18:1_18:1_18:1) were the major substrates of the remodeling process (Figure 3-4B, -(WT-*cld1Δ)*). Based on the *cld1Δ* spectra, we determined that both major substrates of the remodeling originated from CL biosynthesis. For LA-supplemented cells, we found that CL (18:2/18:2/18:2/18:2) was the major product (Figure 4C, WT-*cld1Δ*), while CL(16:0/18:2/16:0/18:2) and CL(16:0/18:2/18:2/18:2) were the major substrates of the remodeling process (Figure 3-4C, -(WT-*cld1Δ)*). Similar to OA-supplementation, both major remodeling substrates represented the products of CL

biosynthesis. Further, the differential analysis demonstrated that after OA- or LA-supplementation, Cld1 had preferentially hydrolyzed C16:0- and C16:1-fatty acid residues over C18:1- and C18:2-containing CL species. As a result, the remodeling process tended to convert hetero-acylated CL to homo-acylated CLs, provided C18:1 or C18:2 were available.

As all major phospholipids can serve as acyl sources for Taz1-catalyzed remodeling, we further looked at the content of several phospholipids as well as their monolyso-forms in wt and *taz1Δ* mutant cells. Included in our phospholipidomics analyses were several major classes of phospholipids: i) a biosynthetic precursor of CL, phosphatidylglycerol (PG); ii) two major phospholipids present in both mitochondria and extra-mitochondrial compartments, PE and PC, and iii) an extra-mitochondrial phospholipid, phosphatidylserine (PS). We found that the effects of *taz1Δ* deletion were CL specific. Other phospholipids such as PC, PG, PS were not sensitive to *taz1Δ* deletion.

Exogenous FAs do not affect molecular speciation of CL in remodeling of mutant S. cerevisiae cells.

While Cld1 and Taz1 represent the two major components of the machinery involved in the CL remodeling process, the immediate motive force(s) triggering the process remain unknown. As exogenously added C18 FAs caused efficient remodeling of CL to generate mostly homo-acylated tetra-18:1 and tetra-18:2 molecular species in wt cells, we further explored the CL composition in mutant cells. The dramatic changes in molecular speciation of CLs induced by exogenous C18-FAs in wt cells were

essentially not found in any of the remodeling mutant cells, including *cld1Δ, taz1Δ*, and *cld1Δ/taz1Δ* (Figure 3-1).

Because Cld1 is specific for the hydrolysis and remodeling of CLs but Taz1 can participate in remodeling of other phospholipids (Ye et al., 2014), we were interested in assessing the effects of deletion of Cld1 as well as Taz1 on the phospholipidomes of the mutant cells grown in the presence of 18:1 and 18:2 FAs. Our findings clearly demonstrate that deletion of *cld1Δ* did not cause any changes in PE and PC molecular species in either 18:1- or 18:2-supplemented cells. The absence of Taz1 also did not substantially affect the content or molecular speciation of PC and PE (except for the accumulation of 16:0/16:1 and 16:1/16:1 PC molecular species but in cells supplemented with C18:1).

Specificity of Cld1 for different molecular species of CLs.

Because of the apparent preference of CL remodeling triggered by exogenous fatty acids for C18 species, we further investigated the specificity of Cld1 in the hydrolysis of different molecular species of CLs. We used commercially available homo-acylated CLs - $(14:0)_4$-CL, $(18:1)_4$-CL, $(18:2)_4$-CL and also synthesized several molecular species of CL - $(16:0)_4$-CL, $(18:0)_4$-CL, and (16:1) $(16:0)_3$-CL. The multistep preparations of $(16:0)_4$-CL, $(18:0)_4$-CL and (16:1) $(16:0)_3$-CL followed a modular approach to achieve optimal synthetic efficiency. Selectively protected glycerol building blocks were loaded with palmitoate, stearate, and palmitoleoate in the presence of 1-ethyl-3-(3-dimethyl-aminopropyl) carbodiimide (EDCI) and *N, N*-dimethyl-4-aminopyridine (DMAP) and then condensed with 1-chloro-*N*,*N*-diisopropyl-1-

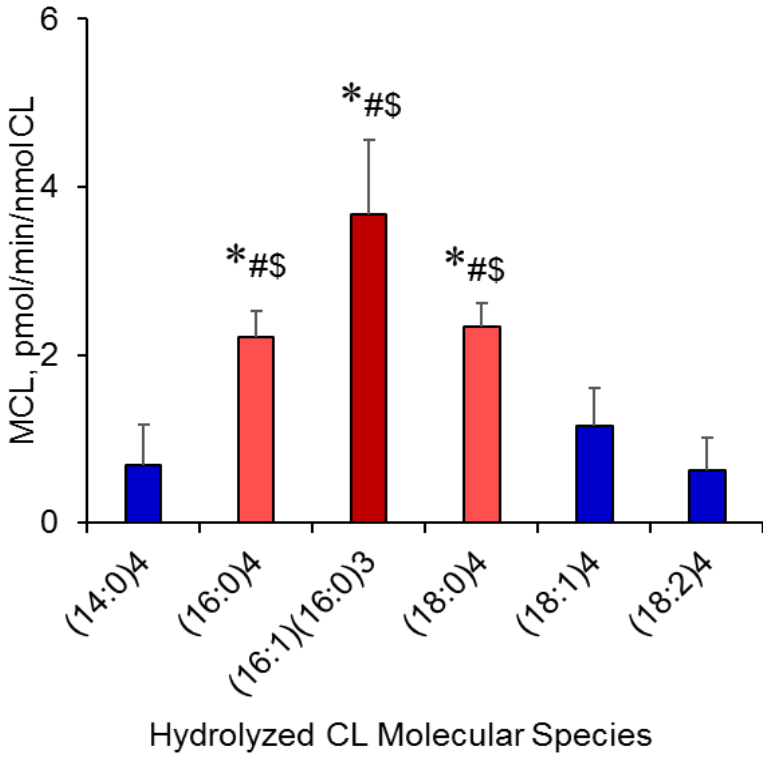

Figure 3-6. Effect of Cld1 isolated from S. cerevisiae on accumulation of mono-lyso-CLs after hydrolysis of different CLs in a biochemical system in vitro.

*$p<0.05$ vs $(14:0)_3$, $^{\#}p<0.002$ vs. $(18:1)_3$, $^{\$}p<0.005$ vs $(18:2)_3$, (n=4-10).

methoxyphosphinamine. The formation of the second phosphoester bond utilized 4,5-dicyanoimidazole, and the resulting phosphite was subsequently peroxidized to the phosphate with tetrabutylammonium periodate. Iterative couplings generated a fully protected CL precursor that was *O*-demethylated with sodium iodide to release the phosphate anions and *O*-desilylated under mild, carefully controlled acidic conditions to generate the secondary alcohol in the glycerol moiety. Ammonium hydroxide was used to prepare the final CL diammonium salts that were used for biological analysis.

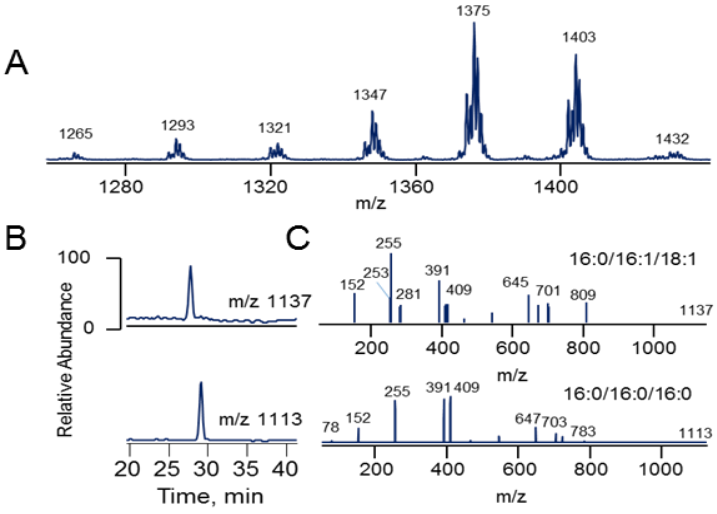

D

Hydrolyzed Acyl chain	Molecular Species	m/z	pmol/nmol CL/min
	Mono-lyso-CLs		
Yeast $^{-/-}$ CLD1 Cells (*S. cerevisiae*)			
16:0	10:0_16:1_16:0	1027.6252	
16:0	12:0_14:0_18:1	1055.6565	
18:1	14:0_14:0_16:0	1057.6721	
16:0	14:0_14:0_18:1	1083.6878	
16:0	14:0_16:1_18:1	1109.7034	
14:0	14:0_16:0_18:1	1111.7191	
16:0	16:0_16:0_16:0	1113.7347	
16:0	16:0_16:1_18:1	1137.7347	
16:0	16:0_16:0_18:1	1139.7504	
16:0	16:0_18:1_18:1	1165.766	
16:0	16:0_18:0_18:1	1167.7817	
16:0	18:1_18:1_18:1	1191.7817	
16:0	18:0_18:1_18:1	1193.7973	
Heart of Northern Red Snapper (*Lufjanus campechanus*)			
18:1	16:1_18:2_18:1	1161.7347	
16:0	16:1_18:1_18:1	1163.7504	
18:2	16:0_18:2_20:3	1187.7504	
16:0	18:1_18:1_18:2	1189.7660	
18:1	16:1_18:1_22:6	1209.7347	
16:0	18:2_18:2_20:3	1211.7504	
18:1	18:1_18:2_22:6	1235.7504	
16:0	18:1_18:1_22:6	1237.7660	
18:1	16:1_22:5_22:6	1257.7347	
20:3	18:1_20:4_22:6	1259.7504	
18:2	18:1_20:3_22:6	1261.7660	
18:1	20:3_20:4_22:6	1283.7504	
16:0	18:1_22:5_22:6	1285.7660	
18:1	20:3_22:6_22:6	1307.7504	

Unit: pmol/nmol CL/min

Minimum 0.014 | 50% Value | Maximum 16.89

Figure 3-7. Typical LC-ESI-MS spectrum of CL isolated from *cld1Δ* mutants

(A), LC-MS profiles (B) and MS/MS spectra (C) of MLCLs after CL hydrolysis by Cld1 and heat map of mono-lyso-CLs molecular species (D) after the release fatty acids from CLs induced by Cld1 in the CLs isolated from *cld1Δ* mutants and from the heart of Northern Red Snapper (*Lutjanus campechanus).*

We found that $(14:0)_4$-CL, $(18:1)_4$-CL, $(18:2)_4$-CL were very poor substrates for Cld1 (Figure 3-6). Both $(16:0)_4$-CL and (16:1) $(16:0)_3$-CL and also $(18:0)_4$-CL were readily hydrolyzed by Cld1 (Figure 3-6). To verify the specificity of Cld1 toward CL containing palmitic acid, we performed experiments using several types of mixtures of different CLs. In particular, we were interested in testing Cld1 substrate specificity towards different CL species present in *S. cerevisiae* cells as well as long-chain polyunsaturated CL species "unusual" for these cells. To this end, we prepared two types of liposomes, DOPC liposomes containing either CLs isolated from *cld1Δ* yeast mutant (to obtain the most diversified set of yeast CLs in conditions of suppressed remodeling process) or long chain polyunsaturated CLs isolated from fish heart (Northern Red Snapper, *Lutjanus campechanus*) (Figure 3-7). These experiments provided interesting details regarding the specificity of Cld1 towards different molecular species of CLs as substrates. We found that hydrolysis of yeast CLs by Cld1 resulted in the release of predominantly palmitic acid (16:0) and the formation of four major MLCL species such as 12:0_14:0_18:1; (14:0_14:0__18:1; 16:0_16:1_18:1 and 18:1_18:1_18;1. We did not observe significant accumulation of MLCL and free fatty acids or decreased CL content when liposomes containing fish heart CLs (with highly diversified CLs containing C22:5 and C22:6 fatty acid residues) were treated with Cld1. Thus, Cld1 specifically hydrolyzed CL species containing palmitic acid.

Computational studies of the interactions of homo-acylated-CL with Cld1.

To get insights into specifics of Cld1 hydrolysis of CL and its molecular species, a homology model of full-length structure of the protein was generated using Hsad, a

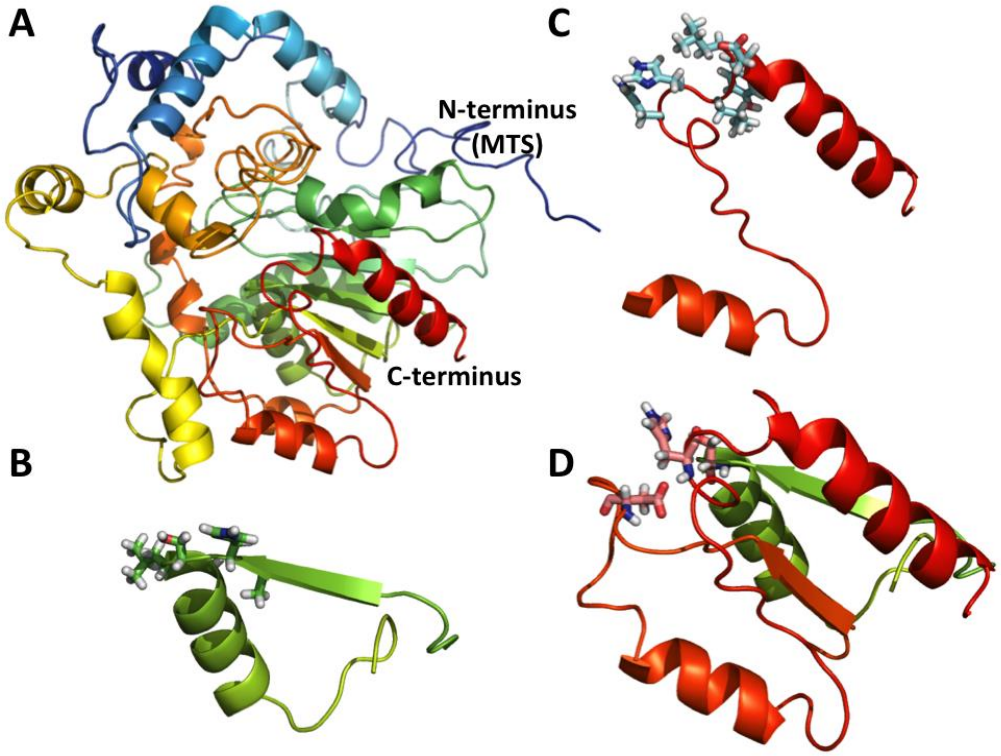

Figure 3-8. A homology model of Cld1, generated using iTassar server.

A. A full-length structure of Cld1 and its N-terminus region called mitochondrial target signal (MTS). B. The known lipase motif (^{228}AHSLG^{232}). C. Acyl transferase motif (^{424}HHLYLD^{429}). D. The catalytic triad, including S230, D392 and H424, introduced by Baile et al.

steroid-degrading hydrolase, from *Mycobacterium tuberculosis* as a template (Figue 3-8A) (Lack et al., 2008). The choice was based on the sequence analysis using the Protein BLAST tool (Altschul et al., 1990). This resulted in five templates with the highest levels of identities to Cld1. Accordingly, five homology models of Cld1 were built using I-TASSER 31 webserver. The model based on Hsad, a steroid-degrading hydrolase from Mycobacterium Tuberculosis (PDB ID: 2VF2 13), demonstrated the greatest C-score (C-score was equal to -1.78). Therefore, it was selected for molecular

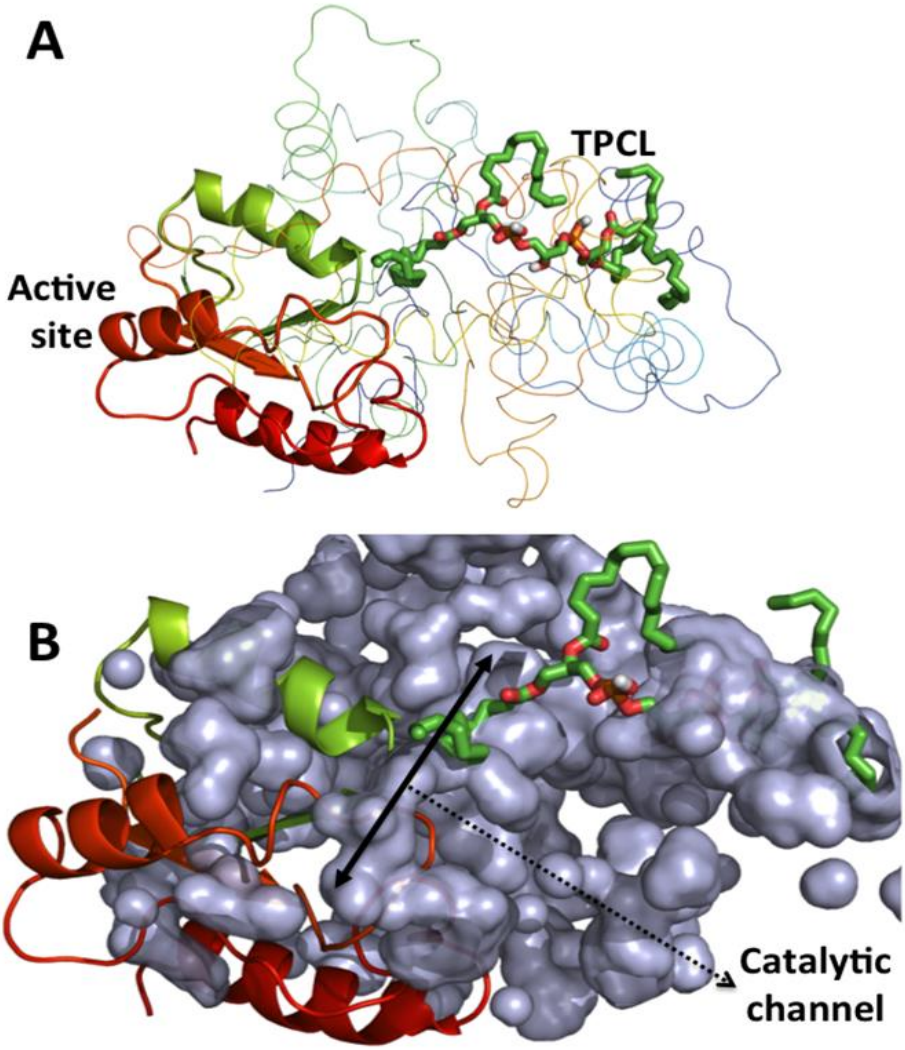

Figure 3-9. Interactions of (C16:0)4-CL with Cld1 structure, generated using homology modeling.
A. One of the acyl chains of TPCL aligned toward the active site. B. A channel represents the CL acyl chain to the active site, which may define the specificity of Cld1 toward particular fatty acids based upon its size.

docking modeling. The known lipase motif (^{228}AHSLG^{232}) and acyl transferase motif (^{424}HHLYLD^{429}) are shown in Figure 3-8B-C, respectively. According to Baile et al. (Baile et al., 2014), S230, H424 and D329 are the catalytic triad of Cld1 (Figure 3-8D).

Intriguingly, the overlay of cavity and cartoon representation of the model structure revealed a channel toward the catalytic site. Subsequently, molecular docking method was utilized to investigate the interactions of three homo-acylated-CL species - $(14:0)_4$-CL, $(16:0)_4$-CL and $(18:2)_4$-CL. Notably, a palmitoyl residue (16:0) perfectly fit in this cavity (Figure 3-9). However, neither chains of tetra-myristoyl CL, nor chains of tetra-linoleoyl CL penetrated the active site channel. This indicates that the channel can introduce a CL acyl chain to the active site. Moreover, the length of the channel may function as a "ruler" defining the specificity of Cld1 towards particular molecular species of CLs – in reasonable agreement with the experimentally tested homo- and hetero-acylated CLs.

Effects of C18:1, C18:2 and C20:4 FAs supplementation on mitochondrial bioenergetic function in S. cerevisiae cells.

As CL is an essential structural component of the OxPhos machinery, we tested one possible effect of fatty acid supplementation on intact cell respiration of yeast cells. Interestingly, yeast cells analyzed in stationary phase in YPD media showed 45% and 21% increased respiration rates when the media was supplemented with linoleic acid and arachidonic acid, respectively, but not with oleic acid, where respiration was decreased by -26% compared to control (Figure 3-10). These data suggest that CL composition plays an important role for mitochondrial function at the level of the oxidative phosphorylation system, and that linoleic acid supplementation produces highest respiration rates.

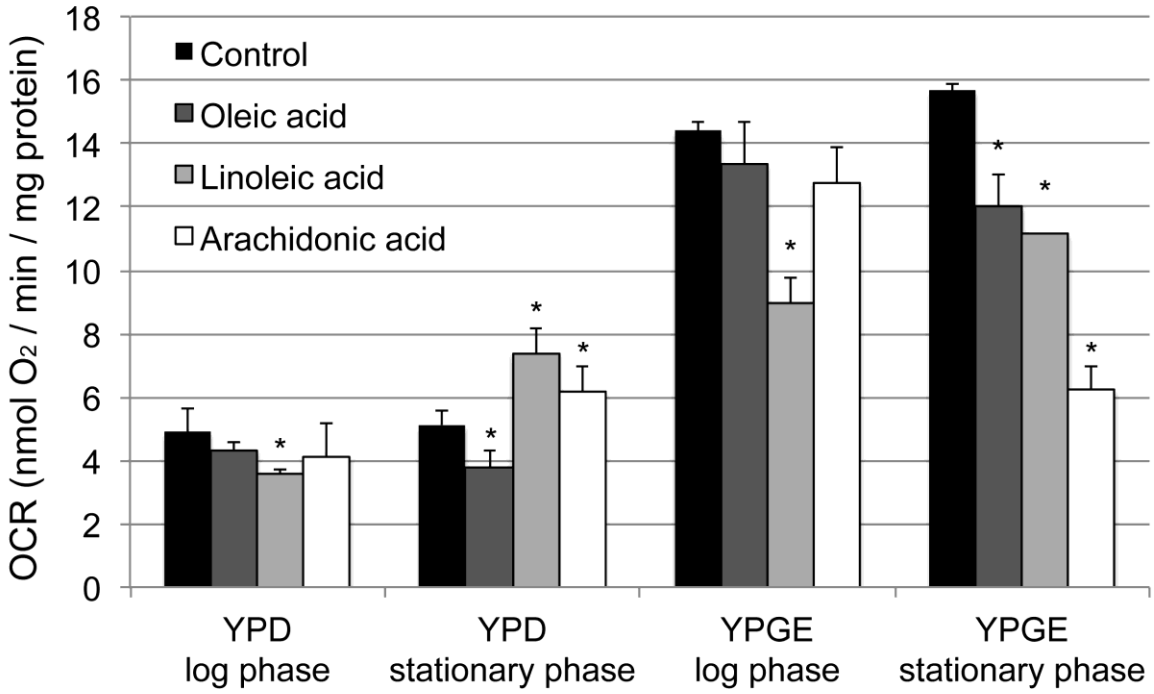

Figure 3-10. Yeast cells were grown in synthetic fermentable (YPD) media supplemented with tergitol alone (control), or tergitol plus oleic acid, linoleic acid, or arachidonic acid.

Respiration of intact cells was analyzed via the polarographic method. *$p<0.05$ versus control (n=3).

DISCUSSION

Predominantly localized in mitochondria, CLs interact with numerous mitochondrial proteins (Eble et al., 1990; Mileykovskaya and Dowhan, 2014; Pfeiffer et al., 2003; Poyry et al., 2013; Sharpley et al., 2006; Shinzawa-Itoh et al., 2007) thus defining their role and significance in mitochondrial structural organization and metabolic/signaling functions. Similar to other phospholipids, CLs are subject to continuous turnover, resulting in changes in their molecular species that may be associated with their modified interactions with proteins. The molecular mechanisms

and the significance of these changes – also called remodeling – in normal physiology and disease conditions are the subject of intensive investigation (Barth et al., 2004). We discovered that nutritional “pressure” by high levels of free FAs in the growth medium triggered massive synthesis of unusual homo-acylated di-oleoyl- and di-linoleoyl-molecular species in all major classes of phospholipids, including direct CL precursors as well as donors of acyl-groups for the remodeling reactions. Not surprisingly, this resulted in the preponderant accumulation of the respective homo-acylated CL species.

By employing detailed phospholipidomics analysis, this work established that the availability of specific FA precursors is the major factor defining the diversity and molecular speciation of CLs in *S. cerevisiae*. Supplementation with C18 FAs resulted in the predominant accumulation of homo-tetra-acylated 18:1 and 18:2 species of CL. Based on the engagement of only one biosynthetic and one remodeling pathway for CLs in *S. cerevisiae*, the specific contributions of these respective mechanisms to the overall molecular diversification/speciation of CLs in different growth conditions as well as in mutant forms can be established. For example, we established that the remodeling process is the major contributor to the pool of homo-acylated $(C18:1)_4$-CL and $(C18:2)_4$-CL in cells supplemented with these FAs.

The hydrolase is a major part of the remodeling pathway. To convert nascent CL, containing short saturated FA, to homo-acylated CL with log chain polyunsaturated FAs, CL first has to undergo deacylation. In yeast, Cld1 fulfills this function and has been identified as a CL-specific hydrolase enzyme. Modeling data revealed the presence of a channel adjacent to the active site of Cld1, which may introduce a fatty acid of CL to the

active site to be hydrolyzed. In line with LC/MS data demonstrating preferable hydrolysis of 16:0 fatty acids by Cld1, and modeling results revealing most likely interactions of 16:0 fatty acid with the channel it is tempting to speculate that the channel acts as a “molecular ruler” defining the specificity of Cld1 to particular fatty acid residues in CLs.

By appropriately designing genetic manipulations (e.g., creating and producing appropriate deletion mutants such as *cld1Δ*and targeted transfection with mammalian remodeling genes such as $iPLA_{2\beta}$ or $iPLA_{2\gamma}$), yeast cells supplemented with desired PUFA can be used as effective models in studies of mammalian CL metabolism. Similarly, the *taz1Δ* mutant transfected with acyltransferases *alcat1* or *mlcat1* may lead to the elucidation of their specific contributions to CL metabolic processes. In all these cases, the approach based on differential (subtractive) lipidomics analysis may be particularly powerful in examination of remodeling and biosynthesis.

Supplementation with exogenous C18 FAs stimulated CL remodeling. As FAs can be integrated into yeast CLs only via MLCL/Taz1-driven reactions, the acyl-CoA-dependent pathways are not utilized to remodel CL. However, it has been reported that acyl-CoAs are essential for reacylation of other phospholipids (Rijken et al., 2009). Thus, detailed lipidomic analyses of other phospholipids in addition to CL are essential for comprehensive analysis of CL remodeling pathways.

It has been well established that *taz1Δ* cells are characterized by lower levels of CLs and markedly increased content of MLCL relative to wt cells (Ye et al., 2014). Our results are in full agreement with these earlier studies. In terms of molecular speciation

of CLs, the same altered features of CLs molecular speciation were also characteristic of *taz1Δ* mutant and double mutant *cld1Δtaz1Δ* cells, suggesting that the selectivity of Cld1 for C16-containing CLs is the major factor defining the overall molecular speciation and remodeling of CLs in *S. cerevisiae.* This is clearly illustrated by the analysis of MLCL molecular species that accumulate in *taz1Δ* cells, in which 16:1_16:1_16:0, 16:1_16:0_18:1, and 16:1_18:1_18:1 individual species dominated. Only minimal amounts of MLCLs were detected in *cld1Δ* and *cld1Δ/taz1Δ* mutant cells, reconfirming that the Taz1-catalyzed reaction was the major contributor to the re-acylation/remodeling of CLs in *S. cerevisiae.*

A recent study demonstrated that simultaneous deletion of *cld1Δ and taz1Δ* provided protection against mitochondrial injury triggered by single deletion of *taz1Δ (Ye et al., 2014)*. However, molecular speciation of CLs in w/t and double mutant cells *cld1Δ/taz1Δ* was markedly different. This suggests that the accumulated MLCL – rather than the changed CL speciation – are the major contributors to mitochondrial dysfunction. A recent study demonstrated that unremodeled CLs are functionally indistinguishable from remodeled CLs for yeast major bioenergetic functions (Baile et al., 2014). In contrast, we found that mitochondrial respiration rates were altered in the presence of different FA. Surprisingly, monounsaturated oleic acid had a small inhibitory effect on intact cell respiration whereas the PUFAs - linoleic acid and arachidonic acid - significantly increased mitochondrial respiration. This may give yeast cells a survival advantage by shifting metabolism from glycolysis to the much more efficient OxPhos process under non-proliferating conditions. Interestingly, CL with four linoleic acid

chains is the primary CL species in some mammalian tissues including cow heart (Schlame et al., 1993), a tissue that fully depends on aerobic energy production, suggesting that linoleic acid is the evolutionarily preferred CL side chain to support optimal high levels of oxidative phosphorylation. It should be noted that the effect of the studied fatty acids on mitochondrial function can be the result of several independent mechanisms. One primary mechanism is likely through changes in CL fatty acid composition (i.e., length and saturation versus unsaturation state), which will affect the structure of the OxPhos complexes. Another mechanism may be through cell signaling. For example, it is known that arachidonic acid, a well-studied signaling molecule in higher organisms, also affects cell signaling in yeast, where it leads to changes in the phosphorylation state of many proteins and in particular protein kinase C (PKC) signaling (Kuo et al., 1994). PKC has been shown to regulate mitochondrial respiration by acting on OxPhos complexes both in mammals and yeast (Machida et al., 1998; Ogbi and Johnson, 2006), suggesting that cell signaling may contribute to the observed changes in the presence of arachidonic acid.

Interestingly, these general considerations can be applied to specific pathogenic pathways in disease conditions such as, for example, the one likely operating in patients suffering from the X-linked disease Barth syndrome (BTHS) leading to a rare childhood cardiomyopathy with cyclic neutropenia (Barth et al., 2004). Recent detailed studies have identified seven functional classes of BTHS mutations with several distinct loss-of-function mechanisms leading to a partial or total loss of catalytic activity (Claypool et al., 2011; Whited et al., 2013). It has also been demonstrated that accumulation of MLCL

(decreased CL/MLCL ratio) rather than deficiency of “correct” unsaturated CL species is the major reason of mitochondrial dysfunction in yeast cells (Ye et al., 2014). Based on our data on the effective remodeling of CLs supplemented with PUFA, one may wonder whether the supplementation with C18:2 may be of therapeutic value, particularly in cases with a partial loss of TAZ catalytic activity (Valianpour et al., 2003).

It has been long believed that remodeling of PUFA phospholipids is driven, at least in part, by their peroxidation with subsequent hydrolysis of oxidatively modified FA residues and re-acylation (Kagan et al., 1978; Salgo et al., 1993; Vankuijk et al., 1987). The results of this work clearly indicate that the remodeling process occurs even in the absence of peroxidizable PUFA. This suggests that different mechanisms, independent of peroxidation, may drive the CL recycling process yielding the molecular species of CL optimized in response to specific cell/tissue demands. Our results are compatible with the dominant role of Taz in re-acylation of Cld1-hydrolyzed CLs and explain the high selectivity of the overall remodeling process towards homo-acylated 18:2 species of CLs and the role of the *tazΔ* mutations in the pathogenesis of Barth syndrome. However, further detailed studies of the specificity and the role of PLAs in the re-acylation of peroxidized *vs* non-peroxidized polyunsaturated CL species may be necessary to better understand these intriguing and important general mechanisms of biological adaptation.

ACKNOWLEGMENTS

This study was conceived and designed in collaboration with Valerian E. Kagan (University of Pittsburgh). I prepared all yeast samples for the experiments, constructed the *CLD1* expression vector, purified Cld1 protein, and measured respiration assisted by Jenney Liu (Wayne State University Medical School). Dr. Valerian E. Kagan's lab performed the LC-MS to analyze the CL profile and the computational studies of the interactions of CL with Cld1.

CHAPTER 4 EXPRESSION OF Δ^{12}-DESATURASE PROMOTES CARDIOLIPIN PEROXIDATION IN *SACCHAROMYCES CEREVISIAE*: A MODEL FOR CL SIGNALING

INTRODUCTION

The dimeric mitochondrial phospholipid cardiolipin (CL) is most abundant in the mammalian heart, where it was first discovered (Pangborn, 1942); however, it is present in nearly all mammalian tissues and throughout the eukaryotic kingdom (Schlame et al., 2000b). The cellular and subcellular functions of CL have been studied for decades using the powerful yeast genetic model, *Saccharomyces cerevisiae* (Schlame and Greenberg, 2017). Yeast genes encoding the CL biosynthetic enzymes (Figure 4-1) have been identified, and well-characterized mutants are available for each step of the pathway, enabling *in vivo* studies of CL function that are not easily carried out in mammalian cells (Joshi et al., 2009b). The yeast model has, thus, been pivotal in demonstrating the critical role of CL in mitochondrial bioenergetics (Claypool et al., 2008b; Gohil et al., 2004; Jiang et al., 2000; Patil et al., 2013; Raja et al., 2017), mitochondrial protein import (Gebert et al., 2009), mitochondrial dynamics (Joshi et al., 2016; Joshi et al., 2012), cell cycle progression (Chen et al., 2010), cellular aging (Zhou et al., 2009), mitophagy (Shen et al., 2017), and apoptosis (Gonzalvez and Gottlieb, 2007; Schug and Gottlieb, 2009), among other essential functions.

CL that is synthesized *de novo* undergoes remodeling, in which it is deacylated to monolysocardiolipin (MLCL), which is reacylated by the transacylase tafazzin, thus forming CL species that are more highly unsaturated (Baile et al., 2013; Beranek et al., 2009; Brandner et al., 2005; Gu et al., 2004; Testet et al., 2005). Unsaturated

tetralinoleoyl-CL is the major CL species detected in the heart, skeletal muscle and liver; however, the physiological significance of tetralinoleoyl-CL remains unclear. It is absent in cells from patients with Barth syndrome (BTHS), an X-linked recessive disorder associated with variable cardiomyopathy, skeletal myopathy, neutropenia, and organic aciduria (Barth et al., 1983). BTHS is caused by mutations in the *TAZ* gene that codes for tafazzin (Bione et al., 1996). Accordingly, BTHS patient cells accumulate MLCL and are devoid of tetralinoleoyl-CL, owing to a loss in the final step of the CL remodeling pathway (Shen et al., 2015). In yeast, unremodeled and remodeled CL are thought to be functionally indistinguishable (Baile et al., 2014), and deletion of the CL-specific phospholipase, Cld1*,* was found to rescue the defects caused by loss of the CL-transacylase, Taz1 (Ye et al., 2014). This raises the question of why cells remodel CL, and how CL-enriched with polyunsaturated fatty acid (PUFA) is functionally distinct from that of saturated or mono-unsaturated fatty acyl CL species. Recent studies implicate peroxidation of CL, yielding CL_{OX}, in the cellular signaling events that initiate apoptosis, as enzymatic hydrolysis of CL_{OX} results in the release of lipid mediators with diverse signaling properties (Kagan et al., 2014; Kagan et al., 2005a).

In the wild, yeast cells proliferate in diverse environments (Huffnagle and Noverr, 2013; Spencer and Spencer, 2013; Spencer and Spencer, 1997; Vadkertiova et al., 2012), from which PUFAs may be readily incorporated into CL. We previously demonstrated that yeast cells supplemented with PUFAs linoleic acid (C18:2) or arachidonic acid (C20:4) readily incorporate these fatty acids into CL (Tyurina et al., 2017), suggesting that the yeast model may be exploited to dissect the mechanisms

underlying the generation and function of CL_{OX}. Cipak and co-workers demonstrated that yeast cells expressing the *H. brasiliensis* Δ^{12}-desaturase synthesize PUFA and exhibit sensitivity to oxidative stress (Andrisic et al., 2015; Cipak et al., 2006). In the current study, we show that *S. cerevisiae* yeast cells that express the *H. brasiliensis* Δ^{12}-desaturase synthesize CL acyl species containing PUFA. Furthermore, multiple species of CL_{OX}, including CL-hydroperoxides and CL-dihydroperoxides, are present in these cells. Peroxidized species of mitochondrial phospholipids PC and PE were also detected, but peroxidized PS (which is largely non-mitochondrial) was not. Importantly, the presence of PUFA-containing CL and the production of CL_{OX} were not associated with major growth defects under optimum conditions. However, mild temperature sensitivity and increased sensitivity to mitochondral lipid peroxidation were observed. Thus, our findings illustrate that yeast cells synthesizing PUFA readily generate phospholipid hydroperoxides and dihydroperoxides, including various CLox species, within the mitochondira. Moreover, yeast provides a powerful genetic model that can be exploited to elucidate mechanisms underlying the generation and function of CL peroxidation.

METHODS AND MATERIALS

Strains, Media, and Growth Conditions—The *S. cerevisiae* strain used in this work is BY4741(*MATa his3Δ1 leu2Δ0 met15Δ0 ura3Δ0*). The plasmids pYES2-EV and pYES2-desa employed in this study were kindly given by Dr. Ana Cipak Gasparovic from the Rudjer Boskovic Institute in Zagreb, Croatia. Expression of the Δ^{12}-desaturase is controlled by a Gal promoter and is induced by growth on galactose-containing media.

Complex media contained yeast extract (1%), peptone (2%), and glucose (2%) (YPD). The solid medium contained agar (2%) in addition to the ingredients mentioned above. Synthetic complete (SC) ura- medium contained adenine (20.25 mg/liter), histidine (20 mg/liter), arginine (20 mg/liter), lysine (200 mg/liter), leucine (60 mg/liter), methionine (20 mg/liter), tryptophan (20 mg/liter), threonine (300 mg/liter) all the essential components of yeast nitrogen base without amino acids (Difco), 0.2% ammonium sulfate, and glucose/galactose (2%). Yeast strains were grown at 30°C. *E. coli* strain DH5 was used for plasmid maintenance and amplifications. Bacteria were grown at 37°C in LB medium (0.5% yeast extract, 1% tryptone, 1% NaCl), supplemented with ampicillin (100 μg/ml) for selection purposes. For growth on plates, media were supplemented with 1.5 and 2% agar for *E. coli* and yeast, respectively. Growth in liquid cultures was monitored spectrophotometrically. Cells were harvested and centrifuged at 4°C (4,300 rpm, 5 min). The supernatant was discarded, and glass beads (0.3g) were added to the centrifuge tubes. Samples were vortexed (5 X 1 min intervals) and frozen at -80 ℃ for lipidomic analysis.

Chronological Life Span—As described in Chapter 2

Spotting Assay—As described in Chapter 2

Determination of mitochondrial membrane potential (MMP)—Cells were grown in SC Gal Ura- medium to log phase and incubated with 500 nM TMRM for 30 min at 30°C. Cells were washed, resuspended in warm medium and divided in half. One group was treated with 6 μM FCCP and the other group was untreated. The TMRM fluorescence intensity was determined in 30,000 cells from each group using LSR II flow cytometer at

the Wayne State University Microscopy, Imaging and Cytometry Resources Core. Median fluorescence intensity was calculated after correcting for background TMRM fluorescence (values obtained after treatment with FCCP) using FlowJo v10.2.

Determination of O_2 consumption—Cells were grown in SC Gal Ura- medium to the mid-log phase to obtain a suspension containing 1.4 x 10^7 cells/ml. Cell respiration was measured in a 5 mL glass chamber using a Clark-type electrode (YSI 5300) operated by TracerDAQ software at 30 °C. After measurements of basal respiration, 5 µM FCCP was added to measure maximal respiration. KCN (0.2 mM) was added to measure cytochrome c oxidase-independent oxygen consumption.

Synthesis of Mito-AAPH—

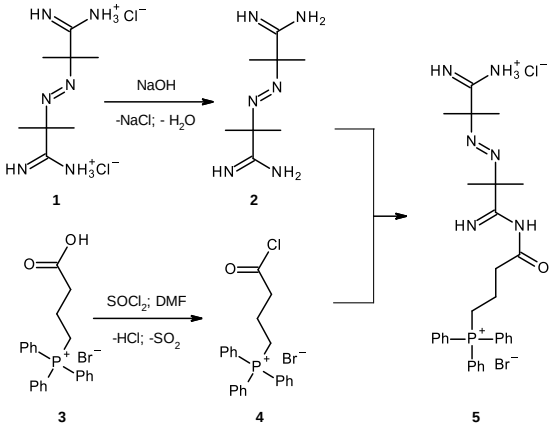

2-[(*E*)-(2-amino-2-imino-1,1-dimethyl-ethyl)azo]-2-methyl-propanamidine hydrochloride (2; yield, 82%): In ice-cold methanol (100 mL), 2,2'-azobis-2-methyl-propanimidamide (AAPH; 2,2'-azobis-2-methyl-propanimidamide, **1**; 1 g; 3.7 mmol) was neutralized with NaOH (0.3 g; 7.4 mmol). The solvent was rotor-evaporated (25 ºC; 10 torr) and the crystals formed were suspended in chloroform (100 mL). Undissolved **1** and NaCl were

filtered off. Rotor-evaporation of the filtrate afforded **2** (0.6 g; 3 mmol), which was used immediately for the preparation of **5**.

(4-chloro-4-oxo-butyl)-triphenyl-phosphonium bromide (4; yield, 65%): 3-carboxypropyl(triphenyl)phosphonium bromide (**3**, 1 g; 2.3 mmol) was dissolved in chloroform (50 mL) containing thionyl chloride (3 g; 25 mmol) and dimethylformamide (DMF; 0.05 g; 0.68 mmol), and the reaction solution was refluxed for 4 hours. The volume of the solvent was reduced to ~ 5 mL (rotor-evaporation; 25 ^{o}C; 150 torr) and trituration with n-hexane afforded **4** (0.68 g), which was dried under vacuum (40 ^{o}C; 10 torr) for 1 hour.

[2-[(*E*)-[2-imino-1,1-dimethyl-2-(4-triphenylphosphaniumylbutanoylamino)ethyl]azo]-2-methyl-propanimidoyl]ammonium chlorobromide (5; yield 45%): Chloroform (50 mL) containing **2** (0.5 g; 2.5 mmol) and **4** (1.12 g; 2.5 mmol) was incubated for 24 hours at 0 ^{o}C. Thereafter, the solvent was rotor-evaporated (20 ^{o}C; 10 torr) and the dry residue was redissolved in minimal volume of ethanol. Trituration of the solution with diethyl ether afforded **5 (**0.69 g), which was filtered and dried under vacuum (20 ^{o}C; 1 torr) for 30 min. ESI MS calculated for the triphenylphosphonium cation of **5** ($C_{30}H_{38}N_6OP^+$), 529.64; found, 529.80.

Mito-AAPH Treatment—Mito-AAPH was diluted with ethanol to make a 50 mM stock. For the spotting assay, 50 µM Mito-AAPH was directly spread on the plate before the experiment. For liquid culture, 50 µM Mito-AAPH was added at log phase ($A_{550} \approx 0.5$).

Statistical Analysis—All results are presented as mean ± S.D. from at least three experiments. Statistical analyses were performed by paired and unpaired Student's t-tests, and the level of statistical significance was set at $p< 0.05$.

LC/MS assessment of phospholipids—Lipids were extracted from yeast and LC/MS of phospholipids was performed as previously described (Tyurina et al., 2017). Briefly, phospholipids were analyzed in negative mode using a Dionex UltimateTM 3000 RSLCnano system coupled online to Q-Exactive hybrid quadrupole-orbitrap mass spectrometer (ThermoFisher Scientific, San Jose, CA). Lipids were separated on a normal phase column (Silica Luna 3 µm, 100A, 150x2 mm, (Phenomenex, Torrance CA)) with flow rate 0.2 mL/min using gradient solvents containing 5 mM CH_3COONH_4 (A – *n*-hexane:2-propanol: water, 43:57:1 (v/v/v) and B - *n*-hexane:2-propanol: water, 43:57:10 (v/v/v). MS lipid standards used in this study were from Avanti polar lipids (Alabaster, AL). Analysis of LC-MS data was performed using software package Compound Discoverer^{TM} (ThermoFisher Scientific) with an in-house generated analysis workflow and peroxidized phospholipid database.

RESULTS

Expression of the *H. brasiliensis* Δ^{12}-desaturase alters the molecular speciation of CL in *S. cerevisiae* cells

Yeast cells that are not supplemented with exogenous fatty acids produce only saturated and Δ^9-mono-unsaturated fatty acyl residues, as these cells cannot synthesize PUFA (Tyurina et al., 2017). To construct a yeast model with PUFA-

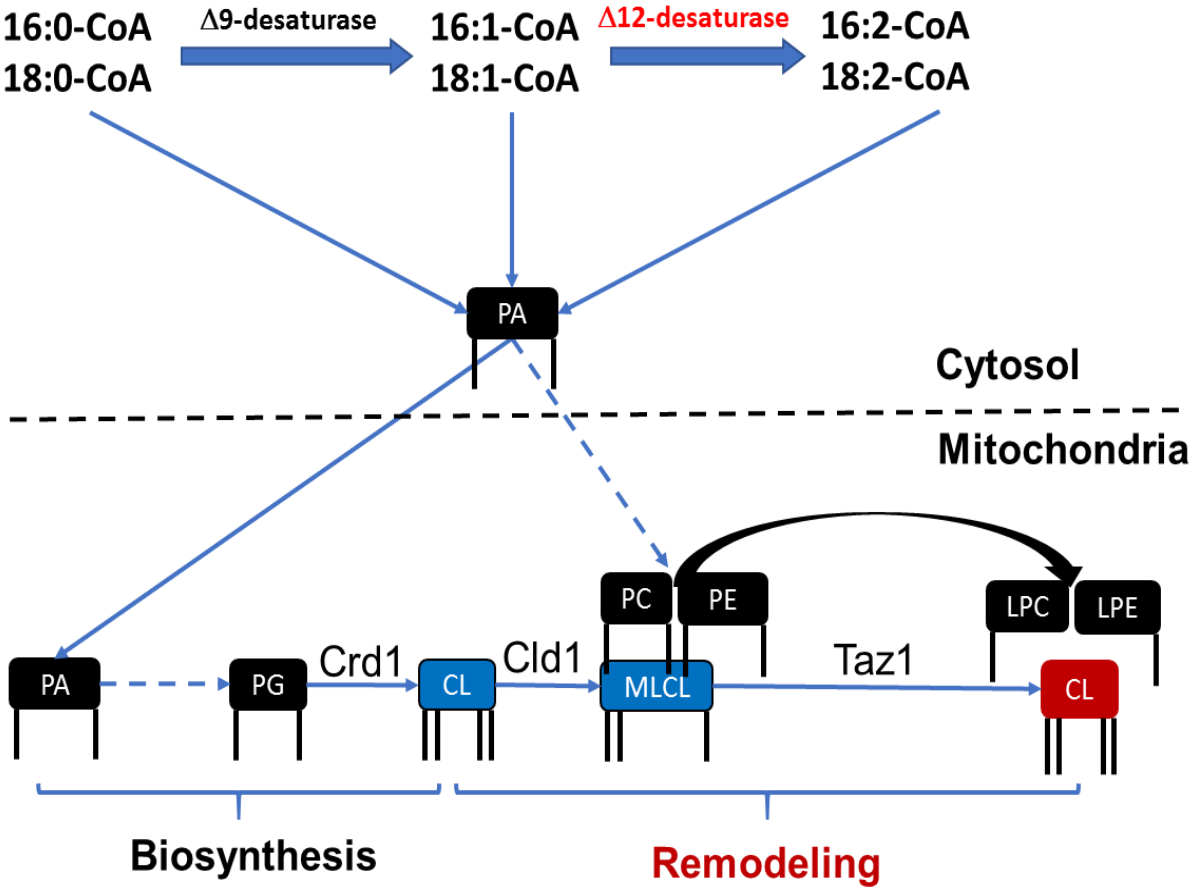

Figure 4-1 Cardiolipin biosynthesis and remodeling in *S. cerevisiae*.
Yeast cells readily produce 16:0-CoA and 18:0-CoA, which can be converted to 16:1-CoA and 18:1-CoA via endogenous Δ^9-desaturase activity or the expressed D^{12}-desaturase. 16:1-CoA and 18:1-CoA can be further converted to 16:2-CoA and 18:2-CoA following a second, complementary desaturation. All available acyl-CoA species can be incorporated into PA and used in the *de novo* synthesis of CL via CL synthase (Crd1). Newly synthesized CL contains predominantly unsaturated fatty acyl chains. Nascent CL may undergo Cld1-catalyzed deacylation to form MLCL. The transacylase, Taz1, utilizes donor phospholipids, particularly PC and PE, to reacylate MLCL to CL. PC and PE are also synthesized from PA. Multiple cycles of deacylation-reacylation generate CL that contains mainly unsaturated acyl chains.

containing CL, we expressed the *H. brasiliensis* Δ^{12}-desaturase gene in yeast (Cipak et al., 2006) and established its effect on the phospholipidome of these cells.

As described in Figure 4-1, yeast readily produces 16:0-CoA and 18:0-CoA, which can be converted to 16:1-CoA and 18:1-CoA via endogenous Δ^{9}-desaturase activity. These acyl-CoA species can be incorporated into phosphatidic acid (PA) and used in the *de novo* synthesis of CL via the CL synthase (Crd1)-catalyzed reaction to form nascent CL, which contains predominately unsaturated fatty acyl chains (Chang et al., 1998b; Jiang et al., 1997; Tamai and Greenberg, 1990; Tuller et al., 1998). Nascent CL is deacylated by the phospholipase Cld1 to form monolysocardiolipin (MLCL) (Baile et al., 2013; Beranek et al., 2009). The transacylase Taz1 utilizes donor phospholipids, particularly PC and PE, to acylate MLCL to form CL (Brandner et al., 2005; Gu et al., 2004; Testet et al., 2005). Multiple cycles of deacylation-reacylation lead to the synthesis of mature CL containing mainly unsaturated acyl chains (Beranek et al., 2009; Gu et al., 2004; Vaz et al., 2003). As we showed previously, Cld1 has a greater affinity for C16-containing acyl chains than for C18-containing acyl chains (Tyurina et al., 2017). Accordingly, the predominant CL species detected in yeast contain C18 acyl chains.

The expression of Δ^{12}-desaturase results in the production of 16:2-CoA and 18:2-CoA, which are incorporated into CL through *de novo* synthesis or via CL remodeling. As shown in Figure 4-2A-B, expression of the Δ^{12}-desaturase caused dramatic changes in CL composition. WT yeast cells have predominantly CL64:3, CL66:4, CL68:4, CL70:4 and CL72:4, while cells expressing the Δ^{12}-desaturase contained predominantly CL66:5, CL68:5, CL70:6 and CL72:8. The CL species detected in WT and Δ^{12}-desaturase-

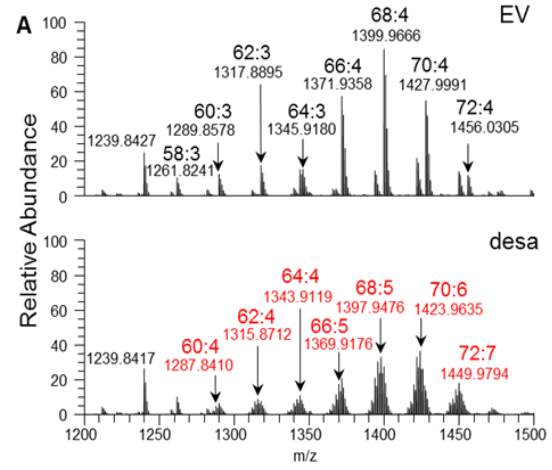

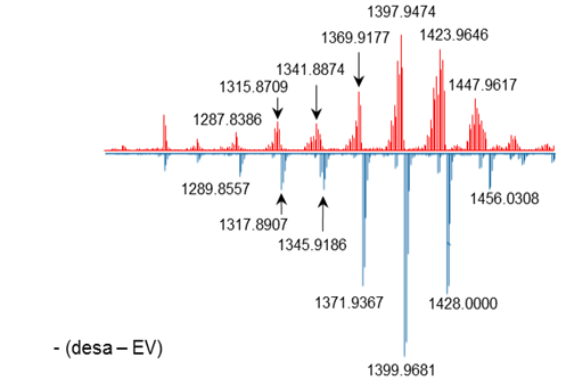

C

CN:DB	m/z	EV	desa
58:1	1265.8557	0.07	0.05
58:2	1263.8401	0.49	0.36
58:3	1261.8232	1.00	1.04
58:4	1259.8109	N.D.	0.10
60:1	1293.8858	0.15	0.13
60:2	1291.8707	0.78	0.42
60:3	1289.8565	1.62	0.73
60:4	1287.8397	N.D.	0.55
60:5	1285.8236	N.D.	0.28
60:6	1283.8084	N.D.	0.12
60:7	1281.7919	N.D.	0.02
62:1	1321.9158	0.16	0.09
62:2	1319.9010	0.98	0.38
62:3	1317.8873	2.17	0.86
62:4	1315.8702	N.D.	0.99
62:5	1313.8544	N.D.	0.83
62:6	1311.8392	N.D.	0.43
62:7	1309.8231	N.D.	0.14
62:8	1307.8076	N.D.	0.06
64:1	1349.9414	0.08	0.03
64:2	1347.9317	0.66	0.21
64:3	1345.9171	1.99	0.65
64:4	1343.9023	1.93	1.17
64:5	1341.8854	N.D.	0.94
64:6	1339.8704	N.D.	0.67
64:7	1337.8538	N.D.	0.29
64:8	1335.8385	N.D.	0.20

CN:DB	m/z	EV	desa
66:1	1377.9709	0.08	0.04
66:2	1375.9621	0.55	0.25
66:3	1373.9466	3.43	0.96
66:4	1371.9334	6.88	2.13
66:5	1369.9165	N.D.	1.76
66:6	1367.9009	N.D.	1.13
66:7	1365.8856	N.D.	0.63
66:8	1363.8699	N.D.	0.29
68:2	1403.9929	0.62	0.25
68:3	1401.9769	4.51	1.05
68:4	1399.9643	9.77	2.66
68:5	1397.9465	N.D.	3.20
68:6	1395.9307	N.D.	2.98
68:7	1393.9163	N.D.	2.01
68:8	1391.9010	N.D.	0.77
70:2	1432.0255	0.28	0.05
70:3	1430.0070	2.68	0.44
70:4	1427.9964	6.08	1.40
70:5	1425.9774	N.D.	2.49
70:6	1423.9619	N.D.	3.43
70:7	1421.9481	N.D.	3.18
70:8	1419.9327	N.D.	1.56
72:3	1458.0362	0.59	0.06
72:4	1456.0287	1.30	0.22
72:5	1454.0082	N.D.	0.53
72:6	1451.9918	N.D.	1.13
72:7	1449.9793	N.D.	1.63
72:8	1447.9638	N.D.	1.28

pmol/nmol PLs

N.D. – not detected

Figure 4-2. CL species synthesized in Δ^{12}-desaturase-expressing cells.

(A) Mass spectra of CL obtained from wild type yeast cells expressing the empty vector (EV) or Δ^{12}-desaturase (desa). Major CL molecular species are identified: CL58:3 (m/z 1261.8241); CL60:3 (m/z 1289.8578); CL62:3 (m/z 1317.8895); CL64:3 (m/z 1345.9180); CL66:4 (m/z 1371.9358); CL68:4 (m/z 1399.9666); CL70:4 (m/z 1427.9991); CL72:4 (m/z 1456.0305); CL60:4 (m/z 1287.8410); CL62:4 (m/z 1315.8712); CL64:4 (m/z 1343.9119); CL66:5 (m/z 1369.9176); CL68:5 (m/z 1397.9476); CL70:6 (m/z 1423.9635); CL72:7 (m/z 1449.9794). (B) A differential mass spectra of CL species was obtained by highlighting individual CL species that were increased [+(desa-EV)] or decreased [-(desa-EV)] by the expression of the D^{12}-desaturase. (C) Heat map of CL quantified from wild type yeast cells expressing the empty vector (EV) or Δ^{12}-desaturase (desa). (D) Quantitative comparison of CL molecular species in cells expressing the empty vector (EV) or Δ^{12}-desaturase (desa).

expressing cells are shown in Figure 4-2C. Quantitative comparison of individual CL species indicates that Δ^{12}-desaturase expression resulted in the production of multiple PUFA-containing CL species and a concomitant reduction in the abundance of CL species containing saturated or monounsaturated fatty acids (Figure 4-2C-D).

MLCL species were also altered by Δ^{12}-desaturase expression (Figure 4-3). Total MLCL was significantly reduced in Δ^{12}-desaturase-expressing cells when compared to WT. Furthermore, quantitative comparison of individual MLCL species indicates that Δ^{12}-desaturase expression resulted in the reduction of MLCL species containing saturated or monounsaturated fatty acids. Additionally, PUFA-containing MLCL species were detected (in low abundance) in the Δ^{12}-desaturase-expressing cells.

Because phosphatidylglycerol (PG) is the precursor of nascent CL produced via *de novo* synthesis (Chang et al., 1998b; Jiang et al., 1997; Osman et al., 2010; Tamai and Greenberg, 1990; Tuller et al., 1998), we also examined the effect of Δ^{12}- desaturase

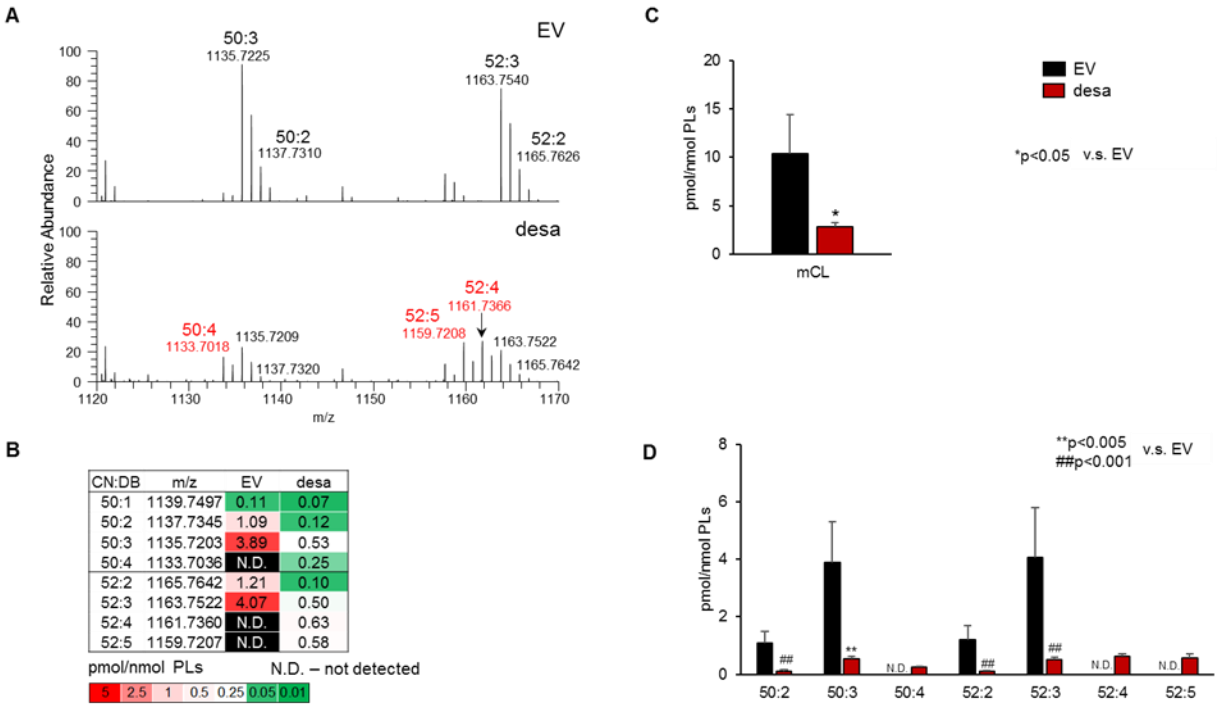

Figure 4-3. MLCL species in Δ^{12}-desaturase-expressing cells.

(A) Mass spectra of MLCL. Major MLCL molecular species are identified: MLCL50:2 (m/z 1137.7310); MLCL50:3 (m/z 1135.7225); MLCL50:4 (m/z 1133.7018); MLCL52:2 (m/z 1165.7626); MLCL52:3 (m/z 1163.7540); MLCL52:4 (m/z 1161.7366); MLCL52:5 (m/z 1159.7208). (B) Heat map of MLCL. (C) Quantitative assessment of total MLCL. (D) Quantitative comparison of MLCL molecular species.

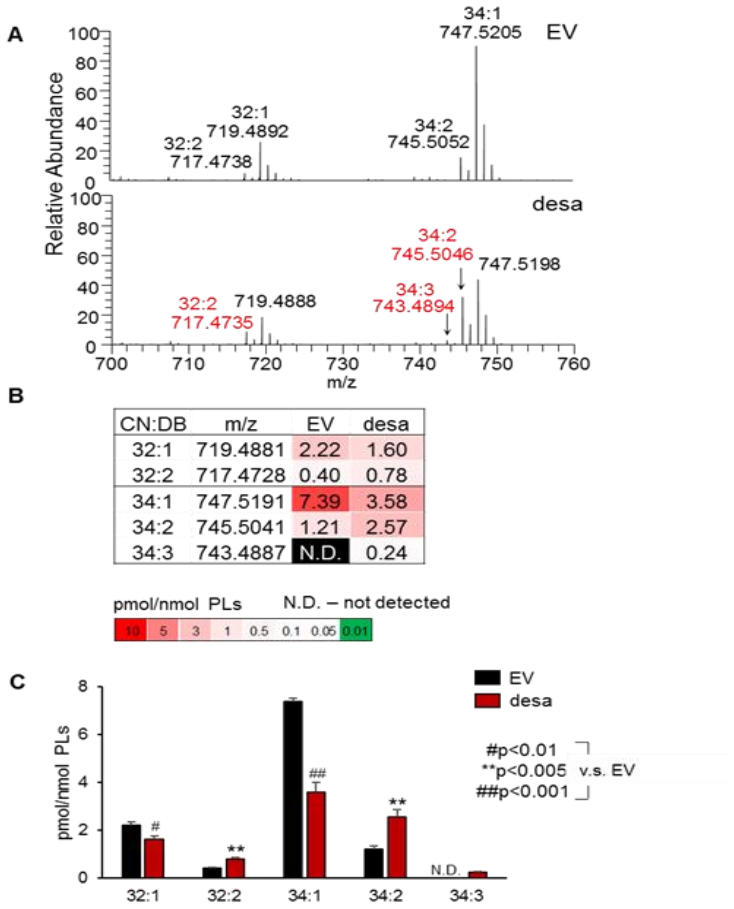

Figure 4-4. PG in Δ^{12}-desaturase-expressing cells.

(A) Mass spectra of PG. Major PG molecular species identified: PG32:1 (m/z 719.5); PG32:2 (m/z 717.5); PG34:1 (m/z 747.5); PG34:2 (m/z 745.5); PG34:3 (m/z 743.5). (B) Heat map of PG. (C) Quantitative assessment of PG.

expression on PG (Figure 4-4). In WT cells, the predominant PG species (34:1 and 32:1) contain one saturated acyl chain and one mono-unsaturated acyl chain. The expression of Δ^{12}-desaturase resulted in a significant reduction of PG34:1 and PG32:1. Furthermore, when compared to WT, Δ^{12}-desaturase-expressing cells had significantly increased PG32:2 and PG34:2. Additionally, PG34:3 was detected in Δ^{12}-desaturase-

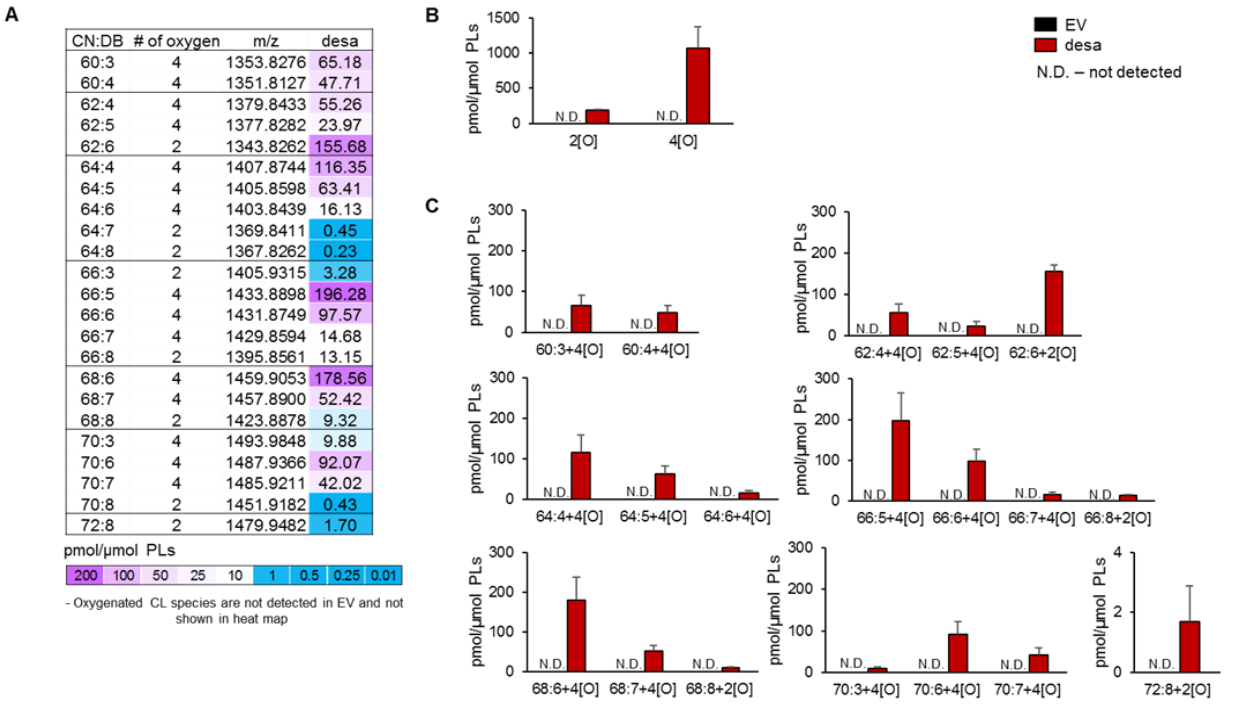

Figure 4-5. Oxygenated CL (CL_{ox}) in Δ^{12}-desaturase-expressing cells.

(A) Heat map of CLox. (B) Quantitative assessment of total. (C) Quantitative assessment of CLox molecular.

expressing cells but not WT cells.

Δ^{12}-desaturase expression leads to accumulation of peroxidized CL.

The accumulation of CL_{OX} was readily observed in cells expressing the Δ^{12}-desaturase (Figure 4-5A-C). CL-hydroperoxide and CL-dihydroperoxide species were observed in these cells. As anticipated, peroxidized CL species were not detected in

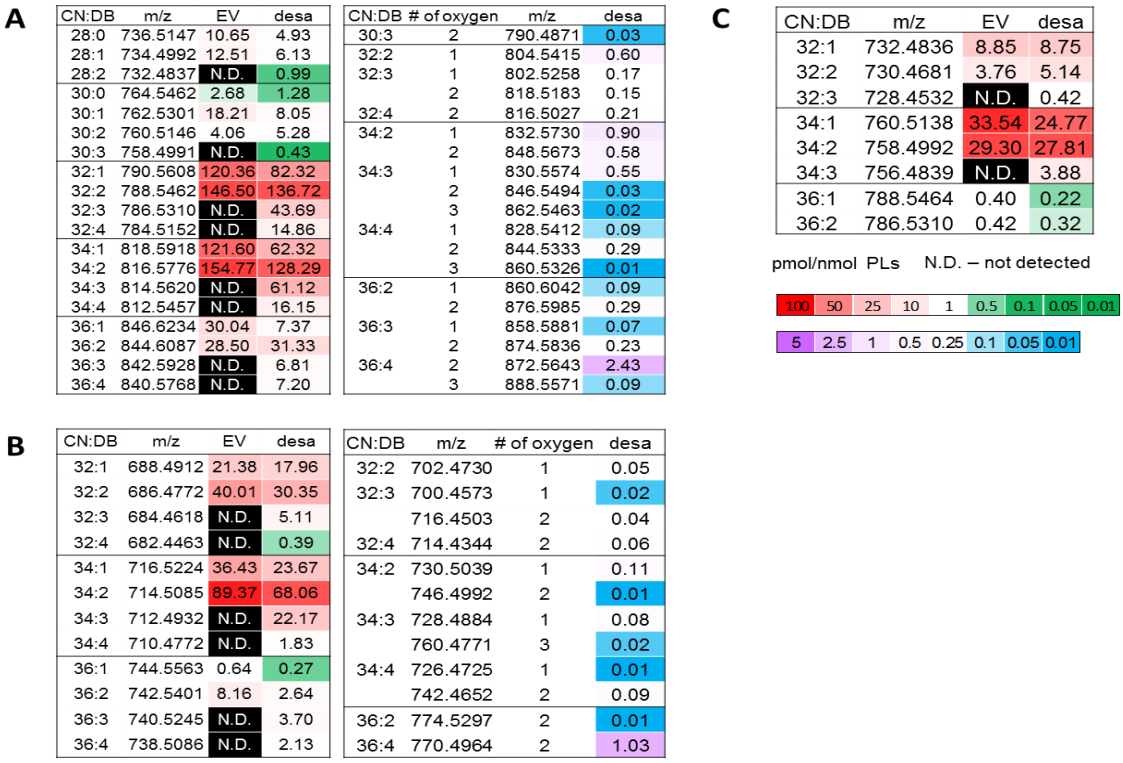

Figure 4-6. PC, PE, and PS in Δ^{12}-desaturase-expressing cells.

Heat map of PC (A), PE (B), and PS (C).

WT cells. Neither peroxidized MLCL nor peroxidized PG was detected in the Δ^{12}-desaturase-expressing cells. As the lipid profile has been altered in Δ^{12}-desaturase expression yeast cells, we next sought to determine if presence of PUFA-containing or peroxidized CL species affected yeast growth

Detection of other peroxidized phospholipids in Δ^{12}-desaturase-expressing cells.

The effects of Δ^{12}-desaturase expression on PC, PE, and PS (Figure 4-6) were determined. All phospholipids analyzed in these cells contained C16:2 and/or C18:2 fatty acyl chains. Peroxidized species of PC and PE were readily detected in Δ^{12}-desaturase-expressing cells. Interestingly, however, peroxidized PS species were not

detected. Given that PC and PE species are enriched within mitochondrial membranes while PS species contribute minimally to the mitochondrial phospholipidome (Carman and Zeimetz, 1996; Wright and McMaster, 2002), this finding suggests that phospholipid peroxidation observed in Δ^{12}-desaturase-expressing cells likely occurs within the mitochondrial subcellular compartment.

Δ^{12}-desaturase expression results in a mild growth phenotype and increased sensitivity to mitochondria-targeted lipid peroxidation.

In accordance with the findings of Cipak and coworkers (Andrisic et al., 2015; Cipak et al., 2006), we observed a mild growth phenotype in the Δ^{12}-desaturase cells, characterized by a prolonged lag phase and a slower rate of growth during stationary phase in liquid growth medium (Figure 4-7A). Growth on solid medium was unaffected at 30℃ but was decreased at 39℃ (Figure 4-7B). Interestingly, chronological lifespan was largely unaffected by Δ^{12}-desaturase expression at 30℃ (Figure 4-7C). The expression of Δ^{12}-desaturase resulted in an increase in the mitochondrial membrane potential, which was associated with minimal changes in basal mitochondrial respiration (Figure 4-7D-E). We next used the mitochondria-targeted lipid peroxidation reagent, mito-AAPH, to further examine how CL peroxidation and growth are affected in Δ^{12}-desaturase-expressing cells. We determined that Δ^{12}-desaturase-expressing cells exhibit increased sensitivity to mito-AAPH (Figure 4-8A). Exposure to mito-AAPH

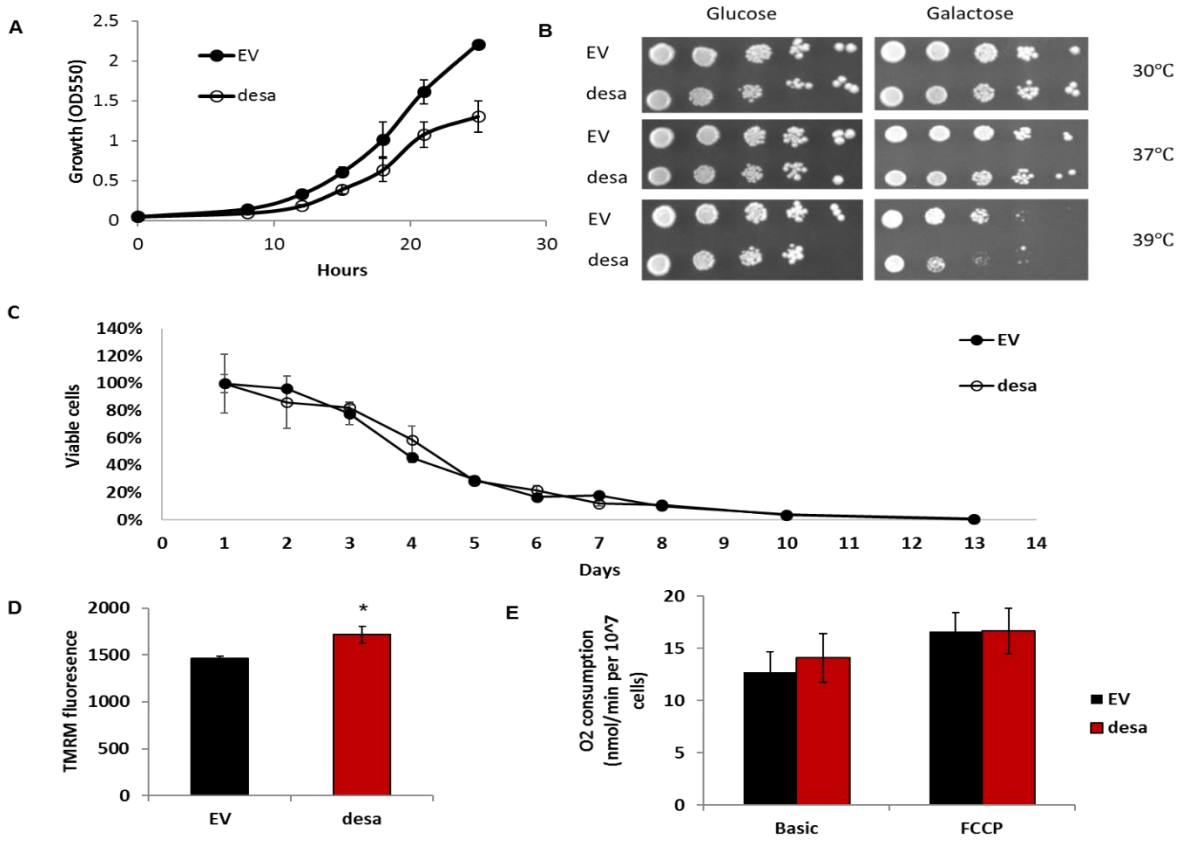

Figure 4-7. Physiologic phenotype in desaturase-expressing cells.

(A) Cell growth. Cells were inoculated at an initial A_{550} of 0.05, and A_{550} was measured at the indicated times. The growth curves shown are representative of three experiments. (B) Serial 10-fold dilutions of cells were spotted on SC medium containing 2% glucose or 2% galactose as carbon source. Plates were incubated at the indicated temperature for 5 days. (C) Chronological life span. The data depicted are representative of three experiments. (D) Membrane potential was determined in logarithmically growing cells by measuring the TMRM fluorescence intensity in 30,000 cells from each group using LSR II flow cytometer. (E) Oxygen consumption was measured in logarithmically growing cells using a Clark-type electrode.

resulted in an increased generation of specific CL-dihydroperoxide species, including CL(62:6)+2[O], CL (64:8)+2[O], CL(66:7)+2[O], CL(66:8)+2[O], CL(68:8)+2[O] (Figure 4-8B). PC(36:4)+2[O] (Figure 4-8C), PE(32:4)+2[O], and PE(34:4)+2[O] (Figure 4-8D) were also increased. CL(66:7)+2[O] and PE(34:3)+2[O] were found only in desaturase-

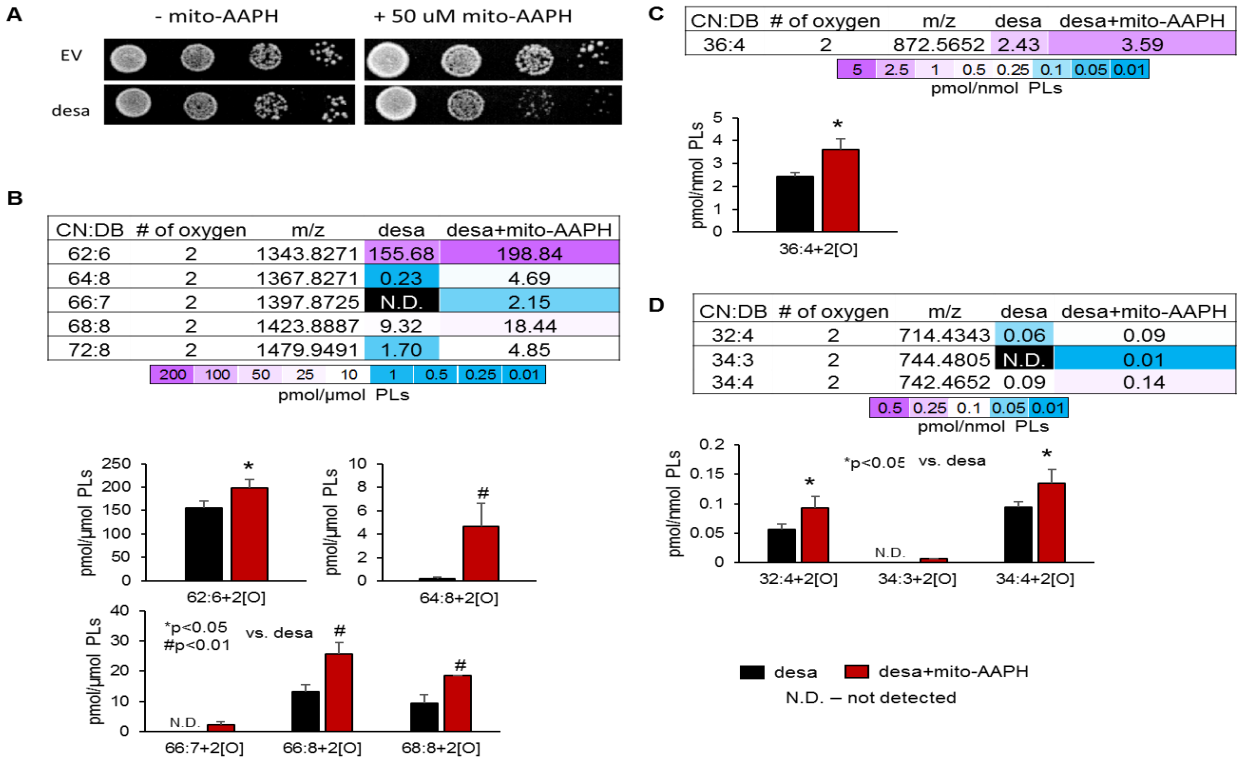

Figure 4-8. Effect of mito-AAPH on desaturase-expressing cells.

(A) Serial 10-fold dilutions of cells were spotted on SC medium containing 2% galactose as carbon source. Mito-AAPH was spread on the plates immediately before spotting. Plates were incubated at 30°C for 3 days. (B) Quantitative assessment of CLox molecular species in cells expressing the Δ^{12}-desaturase (desa) treated with or without mito-AAPH. (C) Quantitative assessment of PCox molecular species in cells expressing the Δ^{12}-desaturase (desa) treated with or without mito-AAPH. (D) Quantitative assessment of PEox molecular species in cells expressing the Δ^{12}-desaturase (desa) treated with or without mito-AAPH.

expressing cells exposed to mito-AAPH. Oxygenated mCL, PG, and PS were not found in desaturase-expressing cells exposed to mito-AAPH. These results suggest that the increased mitochondrial lipid peroxidation contributes to the overall growth defects observed in the Δ^{12}-desaturase-expressing cells.

DISCUSSION

This study demonstrates for the first time that Δ^{12}-desaturase expression in yeast promotes the formation of PUFA-containing CL species that are readily peroxidized *in vivo*. To date, the study of processes governing CL peroxidation and the various cellular signaling functions of CL_{OX} and CL_{OX}-derived lipid mediators has not been carried out using yeast model systems. We have confirmed that 16:2-CoA and 18:2-CoA produced by yeast expressing the Δ^{12}-desaturase are incorporated into CL. This likely occurs, in part, during *de novo* synthesis of CL from PUFA-containing PG and CDP-diacylglycerol by CL synthase. Subsequent enrichment of CL with PUFA occurs during CL remodeling. Consistent with our previous observations in yeast cells supplemented with exogenous PUFA (Tyurina et al., 2017), in the current study, MLCL levels were significantly decreased in Δ^{12}-desaturase-expressing cells compared to WT. This may suggest that CL remodeling is down-regulated in cells containing PUFA. Alternatively, the relative activities of Cld1 and Taz1 may be altered by the availability of PUFA. Nonetheless, the enrichment of PUFA-containing CL combined with reduced detection of the CL remodeling intermediate, MLCL, in Δ^{12}-desaturase-expressing cells supports a model in which a major role of CL remodeling is to generate PUFA-enriched CL, which may serve to increase mitochondrial membrane potential.

This is the first report of CL peroxidation in the yeast *S. cerevisiae.* CL peroxidation provides a critical signal for the initiation of apoptosis (Kagan et al., 2004; Mao et al., 2016; Nakagawa, 2004), and therapeutic reduction of CL peroxidation is being explored to treat human diseases associated with apoptosis (Jiang et al., 2014;

Maddalena et al., 2017; Zhong et al., 2017). Additionally, hydrolysis of CL_{OX} likely serves as a key mitochondrial source of peroxidized fatty acid lipid signaling molecules (Tyurina et al., 2014). Given that in their natural environments, yeast cells likely encounter PUFA, it is reasonable to speculate that yeast may readily synthesize CL-enriched with PUFA in these environments and produce CLox in the absence of stressors. The Δ^{12}-desaturase-expressing yeast provides a powerful tool for the study of CL peroxidation and CL_{OX} signaling Future studies will explore potential inducers of CL peroxidation as well as functions of CLox using this model system.

The expression of exogenous desaturase enzymes in yeast has variable effects on cellular function and viability depending on the yeast strain and growth conditions used (Andrisic et al., 2015; Cipak et al., 2006; Cipak et al., 2008; Johansson et al., 2016). Johansson and coworkers observed severe growth defects in cells expressing both Δ^{12} and Δ^{6}-desaturase enzymes (Johansson et al., 2016). Cipak and coworkers report distinct effects of Δ^{12}-desaturase expression depending on the yeast strain used (Andrisic et al., 2015; Cipak et al., 2006; Cipak et al., 2008). The current study is the first to perform unbiased lipidomic analysis of yeast cells expressing an exogenous desaturase enzyme. Our findings indicate that CL_{OX} is readily detected in the Δ^{12}-desaturase-expressing yeast under normal growth conditions, suggesting that CL peroxidation may occur in the absence of cytotoxic stressors.

The accumulation of CL_{OX} may be subject to factors beyond the rate of CL peroxidation. Peroxidized forms of other phospholipids known to localize within the mitochondrial membranes (PC and PE) were detected in the Δ^{12}-desaturase-expressing

cells. As Taz1, the yeast CL-transacylase transfers fatty acids from phospholipids to MLCL without specificity (Xu et al., 2006b), CL_{OX} may be formed in a Taz1-dependent manner during the transmission of a peroxidized fatty acid residue from a donor phospholipid. However, because PC_{OX} and PE_{OX} are relatively non-abundant, this mechanism likely contributes minimally to the total pool of CL_{OX}.

Increased sensitivity to lipid peroxidation were previously reported using this genetic yeast model (Andrisic et al., 2015). However, our comprehensive lipidomic approach provides compelling evidence to implicate mitochondrial free radicals and CL peroxidation in contributing to the growth defects observed in Δ^{12}-desaturase-expressing cells. Excessive generation of CL_{OX} in response to mitochondrial oxidative stress likely contributes to the small but significant growth defect observed under these conditions. In the current study, we found that Δ^{12}-desaturase-expressing cells exhibit increased sensitivity to mito-AAPH (Figure 4-8A), and treatment with mito-AAPH was associated with an increase in specific CL_{OX} species (Figure 4-8B). The absence of peroxidized PS supports a model of mitochondria-localized phospholipid peroxidation. PS species are confined almost exclusively to the cell membrane and secretory vesicles (Zinser et al., 1991). Although PS is imported into mitochondrial membranes, its intramitochondrial transport is linked to enzymatic conversion to PE by PS decarboxylase (Atkinson et al., 1980; Carman and Henry, 1989; Simbeni et al., 1993). Thus, the relative abundance of PS within the mitochondrial membranes is minimal when compared to PC and PE (Zinser et al., 1991). Peroxidation of CL, PC, and PE but

not PS suggests that phospholipid peroxidation observed in Δ^{12}-desaturase-expressing cells likely occurs within the mitochondrial subcellular compartment.

While hydrolysis of CL may be driven, at least in part, by CL peroxidation (Kagan et al., 1978), in the current study, we detected decreased MLCL in the Δ^{12}-desaturase-expressing cells containing CL_{OX}, indicating that some degree of CL_{OX} can be tolerated in yeast. Future *in vitro* studies will focus on the specificity of CL hydrolysis for peroxidized vs. non-peroxidized CL substrates. Additionally, using the *in vivo* Δ^{12}-desaturase expression system, the relationship between CL remodeling and CL peroxidation will be further explored.

ACKNOWLEDGMENTS

This study was conceived and designed in collaboration with Valerian E. Kagan (University of Pittsburg). Specifically, Christian A. Reynolds and I prepared samples for lipid profile analysis, performed all yeast growth analysis. Mitochondrial membrane potential was measured by my previous lab colleague Wenxi Yu. Our new lab member, Zhuqing Liang, performed measurement of chronological life span. Collaborators from Dr. Kagan's lab performed the LC-MS to analyze the CL profile.

CHAPTER 5 LOSS OF *CLD1* IN Δ^{12}-DESATURASE EXPRESSION CELLS LEADS TO INCREASED PEROXIDIZED CL SPECIES THAT DECREASES CELLULAR MEMBRANE POTENTIAL AND CHRONOLOGICAL LIFE SPAN

INTRODUCTION

As the signature lipid of mitochondria, cardiolipin (CL) plays a critical role in mitochondrial bioenergetics (Claypool et al., 2008b; Gohil et al., 2004; Jiang et al., 2000), mitochondrial protein import (Gebert et al., 2009), cell cycle progression (Chen et al., 2010), cellular aging (Zhou et al., 2009) and apoptosis (Gonzalvez and Gottlieb, 2007; Schug and Gottlieb, 2009). Following *de novo* synthesis, CL undergoes remodeling in which acyl chains are exchanged. Cld1 is the only known CL-specific phospholipase in yeast and is required to initiate the CL remodeling pathway. In this process, CL is deacylated by Cld1 on the matrix side of the inner mitochondrial membrane to form monolysocardiolipin (MLCL) (Baile et al., 2013; Beranek et al., 2009). The transacylase, Taz1, reacylates MLCL to reform CL using acyl groups from donor phospholipids, particularly PC and PE (Brandner et al., 2005; Gu et al., 2004; Testet et al., 2005). In addition to its role in CL remodeling, deacylation of CL results in the generation of mitochondria-derived free fatty acids, which may modulate various cellular functions. Peroxidation of CL, yielding CL_{OX}, has been implicated in the cellular signaling events that initiate apoptosis, and CL_{OX} can undergo enzymatic hydrolysis, resulting in the release of various lipid mediators with diverse signaling properties (Kagan et al., 2014; Kagan et al., 2005a). Cancer cells evade apoptosis through modulation of CL oxidation and subsequent formation of reactive lipid electrophiles, especially 4-hydroxy-nonenal (4-HNE) (Zhong et al., 2017). Attenuating CL peroxidation

is being explored as a potential treatment to manage the clinical effects of aberrant apoptosis. For instance, 3-hydroxypropyl-triphenylphosphonium-conjugated imidazole-substituted oleic acid (TPP-IOA) was developed as an apoptosis-specific inhibitor that prevents CL oxidation (Maddalena et al., 2017).

Previous studies showed that unremodeled and remodeled CL are functionally indistinguishable in the yeast *S. cerevisiae* (Baile et al., 2014; Ye et al., 2014). However, the CL species of unsupplemented yeast contain only saturated and Δ^9-mono-unsaturated fatty acids, enriched primarily with palmitic (C16:0), stearic (C18:0), palmitoleic (C16:1) and oleic acids (C18:1) (Tyurina et al., 2017). In the wild, yeast proliferate in diverse environments (Huffnagle and Noverr, 2013; Spencer and Spencer, 2013; Spencer and Spencer, 1997; Vadkertiova et al., 2012), from which polyunsaturated fatty acids (PUFA)'s may be readily incorporated into CL. Yeast supplemented with PUFA-containing CL readily synthesize peroxidized CL (unpublished). However, the functions of PUFA-containing CL and peroxidized CL are not clear. A recent study showed that the mammalian CL phospholipase iPLA2γ deacylates peroxidized CL, initiating diverse signaling pathways, including activation of caspase-3, expression of stress response genes, accumulation of ceramide, loss of mitochondrial membrane potential, and induction of apoptosis (Song et al., 2014). Accordingly, we speculated that Cld1 may function to deacylate peroxidized CL and regulate cellular signaling in yeast. We demonstrated that cells expressing the *H. brasiliensis* Δ^{12}-desaturase synthesize C16:2 and C18:2 fatty acids, which are readily incorporated into CL. Multiple species of CLox, including CL-hydroperoxides and CL-

dihydroperoxides, were detected in these cells (unpublished). However, the specific functions of Cld1 and CL remodeling in yeast cells with PUFA-containing CL have not been explored.

In this study, we compared the CL profiles of Δ^{12}-desaturase-expressing WT and *cld1Δ* cells to determine if Cld1 removes peroxidized CL. Δ^{12}-desaturase-expressing *cld1Δ* cells contain increased amount of discrete peroxidized CL species, which leads to decreased growth, chronological life span and membrane potential. Furthermore, purified Cld1 protein exhibits higher affinity for peroxidized CL than non-peroxidized CL $(C18:2)_4$. These results indicate a novel role for Cld1 in mitigating the effects of CL peroxidation. Additionally, MLCL levels were increased in desaturase-expressing *cld1Δ* cells, suggesting the existence of an alternate, unidentified CL phospholipase that is capable of deacylating PUFA-containing CL. The findings from this study will serve as the basis on which we will improve our understanding of CL remodeling and its mechanistic roles in mitigating oxidative stress.

METHODS AND MATERIALS

Strains, Media, and Growth Conditions— The *S. cerevisiae* strain used in this work is BY4741(*MATa his3Δ1 leu2Δ0 met15Δ0 ura3Δ0*). The plasmids pYES2-EV and pYES2-desa employed in this study were kindly given by Dr. Ana Cipak Gasparovic (Rudjer Boskovic Institute, Zagreb, Croatia). Expression of the Δ^{12}-desaturase is controlled by a Gal promoter and is induced by growth on galactose-containing medium. Complex medium contained yeast extract (1%), peptone (2%), and glucose (2%) (YPD). Solid medium contained agar (2%) in addition to the ingredients mentioned above. Synthetic

complete (SC) ura- medium contained adenine (20.25 mg/liter), histidine (20 mg/liter), arginine (20 mg/liter), lysine (200 mg/liter), leucine (60 mg/liter), methionine (20 mg/liter), tryptophan (20 mg/liter), threonine (300 mg/liter), all the essential components of yeast nitrogen base without amino acids (Difco), 0.2% ammonium sulfate, and glucose/galactose (2%). Yeast strains were grown at 30°C. *E. coli* strain DH5 was used for plasmid maintenance and amplifications. Bacteria were grown at 37°C in LB medium (0.5% yeast extract, 1% tryptone, 1% NaCl), supplemented with ampicillin (100 μg/ml) for selection purposes. For growth on plates, media were supplemented with 1.5 and 2% agar for *E. coli* and yeast, respectively. Growth in liquid cultures was monitored spectrophotometrically. For lipidomic analysis, cells were harvested and centrifuged at 4°C (4,300 rpm, 5 min). The supernatant was discarded, and glass beads (0.3g) were added to the centrifuge tubes. Samples were vortexed (5 X 1 min intervals) and centrifuged again at 4°C (4,300 rpm, 5 min). Supernatants were collected and frozen at -80 ℃ for lipidomic analysis.

Construction of Plasmids and Expression of Yeast His$_6$-tagged Cld1 in S. cerevisiae—As described in Chapter 3

Purification of His$_6$-tagged Cld1—As described in Chapter 3.

Chronological Life Span—As described in Chapter 2

Spotting Assay—As described in Chapter 2

Real Time Quantitative PCR (RT-qPCR) Analysis—As described in Chapter 2

Determination of mitochondrial membrane potential (MMP)—As described in Chapter 4

Determination of O_2 consumption— As described in Chapter 4

Mito-AAPH Treatment—Mito-AAPH was diluted with ethanol to make a 50 mM stock. For the spotting assay, 50 µM Mito-AAPH was directly spread on the plate before the experiment. For liquid culture, 50 µM Mito-AAPH was added at log phase ($A_{550} \approx 0.5$).

Statistical Analysis—The results are presented as mean ± S.D. values from at least three experiments, and statistical analyses were performed by paired/unpaired Student's t-test. The statistical significance of differences was set at $p < 0.05$.

LC/MS assessment of phospholipids—Lipids were extracted from cells and LC/MS of phospholipids was performed as previously described (Tyurina et al., 2017). Briefly, phospholipids were analyzed in negative mode using a Dionex UltimateTM 3000 RSLCnano system coupled online to Q-Exactive hybrid quadrupole-orbitrap mass spectrometer (ThermoFisher Scientific, San Jose, CA). Lipids were separated on a normal phase column (Silica Luna 3 µm, 100A, 150x2 mm, (Phenomenex, Torrance CA)) with flow rate 0.2 mL/min using gradient solvents containing 5 mM CH_3COONH_4 (A – *n*-hexane:2-propanol: water, 43:57:1 (v/v/v) and B - *n*-hexane:2-propanol: water, 43:57:10 (v/v/v). MS lipid standards used in this study were from Avanti polar lipids (Alabaster, AL). Analysis of LC-MS data was performed using software package Compound Discoverer^{TM} (ThermoFisher Scientific) with an in-house generated analysis workflow and peroxidized phospholipid database. LC/MS was carried out by collaborators from Dr. Valerian Kagan's lab from Pittsburgh University.

RESULTS

Expression of Δ^9-desaturase in *cld1*Δ cells leads to increased levels of specific peroxidized CL species

We have previously shown that expression of *CLD1* is highest when cells are actively respiring (Ye et al., 2014). These conditions lead to increased generation of ROS and, concomitantly, increased oxidation of lipids. Increased *CLD1* in these conditions suggests the possibility that this phospholipase deacylates peroxidized CL, in which case the loss of *CLD1* would lead to increased peroxidized CL. Yeast cells can synthesize only saturated and Δ^9-mono-unsaturated fatty acids, but when engineered to express Δ^{12}-desaturase, they can synthesize PUFAs (Andrisic et al., 2015; Cipak et al., 2006). Furthermore, when supplemented with PUFA, they can synthesize PUFA-containing phospholipid species (Tyurina et al., 2017). To investigate the role of Cld1 in deacylating peroxidized CL, we expressed the Δ^{12}-desaturase in *cld1*Δ cells. PUFA-containing CL species were detected in the Δ^{12}-desaturase-expressing *cld1*Δ cells, likely because some incorporation of PUFA into CL occurs during *de novo* CL biosynthesis. However, the level of PUFA-containing CL was significantly decreased in *cld1*Δ cells expressing Δ^{12}-desaturase (*cld1*Δ+desa) compared to WT cells expressing the desaturase (Figure 5-1). Surprisingly, although *cld1*Δ+desa cells had decreased total

A

CLox	wt+desa	cld1Δ+desa
CL(58:3)+4[O]	30.04	0.38
CL(60:3)+4[O]	65.18	0.86
CL(60:4)+4[O]	47.71	0.10
CL(62:4)+4[O]	55.26	1.85
CL(62:5)+4[O]	23.97	0.10
CL(62:6)+2[O]	155.68	174.35
CL(64:4)+4[O]	116.35	36.15
CL(64:5)+4[O]	63.41	1.87
CL(64:6)+4[O]	16.13	0.28
CL(64:7)+2[O]	0.45	51.30
CL(64:8)+2[O]	0.23	N.D.
CL(66:3)+2[O]	3.28	5.48
CL(66:5)+4[O]	196.28	5.33
CL(66:6)+4[O]	97.57	3.68
CL(66:7)+2[O]	0.10	91.36
CL(66:7)+4[O]	14.68	1.46
CL(66:8)+2[O]	13.15	N.D.
CL(68:6)+4[O]	178.56	3.90
CL(68:7)+2[O]	0.10	36.50
CL(68:7)+4[O]	52.42	4.60
CL(68:8)+2[O]	9.32	51.64
CL(70:3)+4[O]	9.88	0.10
CL(70:6)+4[O]	92.07	0.25
CL(70:7)+4[O]	42.02	0.61
CL(70:8)+2[O]	0.43	78.85
CL(72:8)+2[O]	1.70	N.D.

pmol/μmol PLs: 200, 100, 50, 25, 10, 1, 0.5, 0.25, 0.01

B

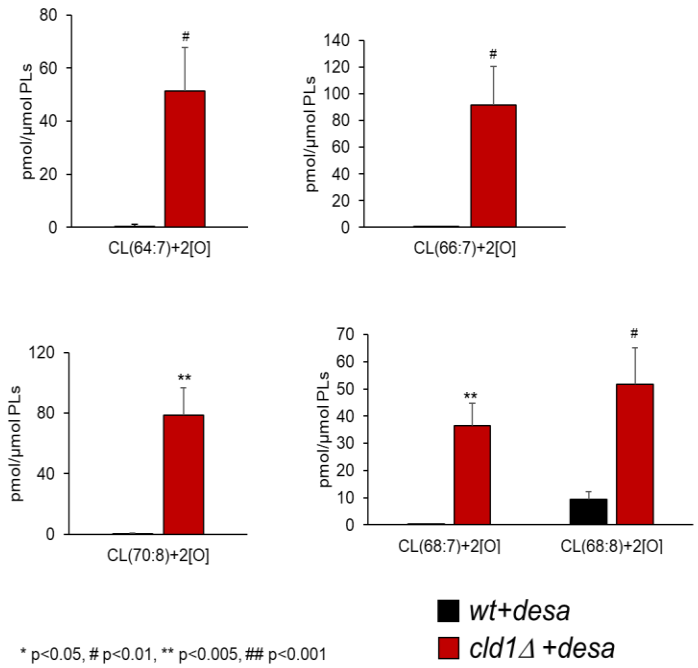

C

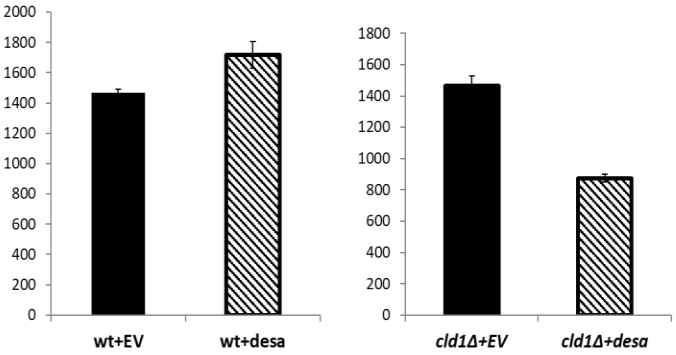

D

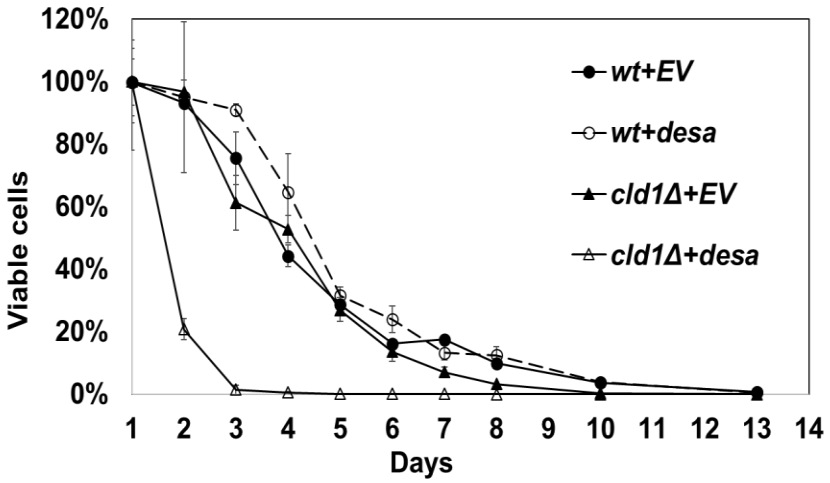

Figure 5-1. Oxygenated CL (CLOX) in Δ^{12}-desaturase-expressing cells.

(A) Heat map of all CLox species quantified. (B) Quantitative assessment of specific molecular species of CLox that are increased in *cld1Δ* yeast cells expressing Δ^{12}-desaturase (desa). (C) Mitochondrial membrane potential was determined in logarithmically growing cells by measuring the TMRM fluorescence intensity. Analysis of 30,000 cells from each group demonstrated that mitochondrial membrane potential is significantly affected by the presence of Δ^{12}-desaturase expression. (D) Chronological life span of wt and *cld1Δ* yeast cells expressing Δ^{12}-desaturase (desa) or empty vector (EV). The data depicted are representative of three experiments.

levels of peroxidizable CL, they contained significantly more CLox species within highly unsaturated CL species (64:7, 66: 7, 68:7, 68:8, 70:8) (Figure 5-2A-B).

The expression of Δ^{12}-desaturase increased the incorporation of PUFA not only into CL but also into other phospholipids known to localize to the mitochondrial membranes (e.g. PG and PC) in both wt and *cld1Δ* cells (need data for *cld1Δ*). Interestingly, while desaturase expression increased the mitochondrial membrane potential in wt cells, the membrane potential in *cld1Δ* cells was decreased (Figure 5-2C). These results suggest that mitochondrial membrane potential is directly affected by the extent to which CL is enriched with PUFA and/or peroxidized.

Increased MLCL in *cld1Δ* cells expressing Δ^{12}-desaturase indicate a novel CL phospholipase that prefer to deacylate PUFA-containing CL.

Cld1 is the only known CL phospholipase capable of deacylating CL to form MLCL (Baile et al., 2013; Beranek et al., 2009; Ye et al., 2014). Although *cld1Δ* cells have decreased levels of MLCL compared to wt cells, small amounts of MLCL were

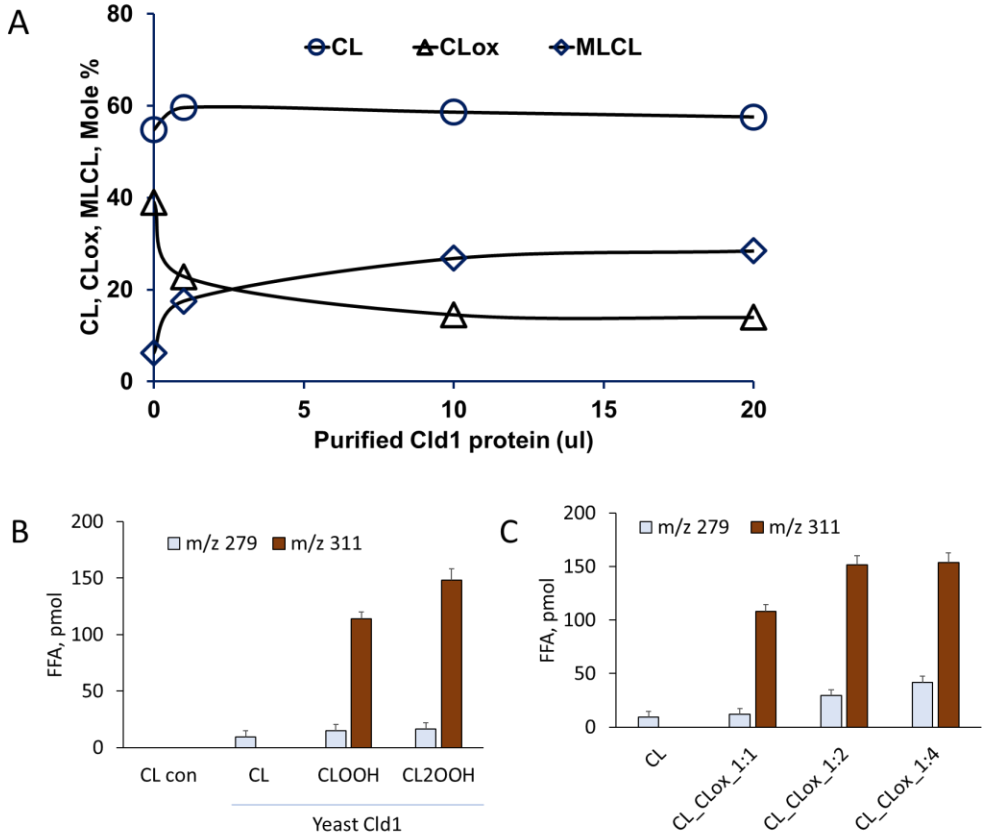

Figure 5-2. Cld1 exhibits greater affinity for oxidized than non-oxidized CL in vitro.

(A) Mixture of 10 μM cardiolipin (TLCL/TLCLox) in HEPES buffer pH 7.45 was incubated at 37℃ for 45 min with an increasing amount of Cld1. Total TLCL was extracted by the Folch procedure and TLCL, TLCLox, and MLCL were quantified by LCMS. Hydrolysis of CL was evident by an accumulation of MCL and concomitant reduction of CL. (B) Isolated Cld1 was incubated with non-oxidized TLCL (CL), TLCL containing one hydroperoxy-LA residue (CLOOH), or TLCL containing two hydroperoxy-LA residues (CL2OOH). In the presence of oxygenated CL (CLOOH or CL2OOH) Cld1 generated significantly increased free hydroperoxy-LA (m/z 311) than non-oxidized-LA (m/z 279). (C) Isolated Cld1 was incubated with increasing ratios of oxidized TLCL (CL_{OX}) to non-oxidized TLCL (CL). As the CL: CLOX ratio was increased from 1:1 to 1:2, the generation of free hydroperoxy-LA (m/z 311) increased by nearly 50%. Further increasing the CL: CLOX ratio (1:4) had little effect on the generation of free hydroperoxy-LA. As the CL: CL_{OX} ratio was increased, the generation of free non-oxidized-LA (m/z 279) was also increased.

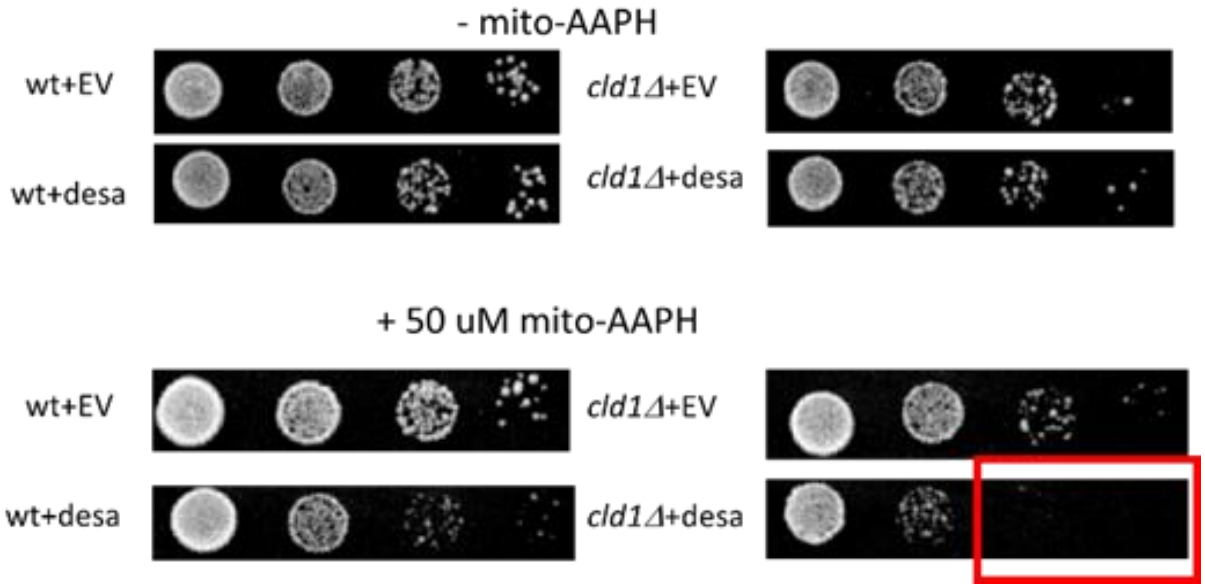

Figure 5-3. Expression of desaturase increases the sensitivity of cells to mito-AAPH.

Serial 10-fold dilutions of wt and cld1Δ yeast cells expressing Δ12-desaturase (desa) or empty vector (EV) were spotted on SC medium containing 2% galactose as carbon source. Mito-AAPH was spread on the plates immediately before spotting. Plates were incubated at 30°C for 3 days.

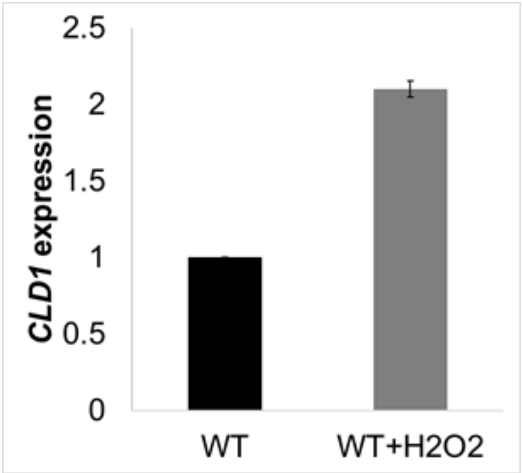

Figure 5-4. CLD1 expression is increased by exposure to H_2O_2.

WT cells were grown to the mid-logarithmic phase and treated with 1 mM H_2O_2 for 1 h. Analyses *CLD1* expression in H_2O_2-treated cells and non-treated cells was determined using RT-qPCR.

A

MLCL	wt	cld1Δ
MLCL(32:3)	0.25	0.20
MLCL(34:3)	0.09	0.08
MLCL(36:3)	0.07	0.06
MLCL(40:3)	0.26	0.21
MLCL(42:1)	0.05	0.11
MLCL(42:2)	0.18	0.04
MLCL(44:1)	0.18	0.16
MLCL(44:2)	0.26	0.17
MLCL(44:3)	2.15	1.75
MLCL(46:2)	0.39	0.27
MLCL(48:3)	0.74	0.33
MLCL(50:1)	0.14	0.30
MLCL(50:2)	1.41	1.09
MLCL(50:3)	5.06	0.35
MLCL(52:2)	1.53	0.57
MLCL(52:3)	5.08	0.15
MLCL(54:3)	1.24	N.D.

MLCL	wt+desa	cld1Δ+desa
MLCL(32:3)	0.19	0.37
MLCL(34:3)	0.08	0.18
MLCL(36:3)	0.04	0.09
MLCL(40:3)	0.20	0.07
MLCL(42:1)	0.05	0.25
MLCL(42:2)	0.07	0.06
MLCL(44:1)	0.14	0.20
MLCL(44:2)	0.20	0.19
MLCL(44:3)	2.03	2.94
MLCL(46:2)	0.30	0.66
MLCL(48:3)	0.34	0.67
MLCL(50:1)	0.13	0.79
MLCL(50:2)	0.27	0.88
MLCL(50:3)	0.98	0.89
MLCL(50:4)	0.47	0.50
MLCL(52:2)	0.16	0.24
MLCL(52:3)	0.99	0.34
MLCL(52:4)	1.30	0.49
MLCL(52:5)	1.16	0.53
MLCL(52:6)	0.25	0.33
MLCL(54:3)	0.23	0.00
MLCL(54:4)	0.44	0.01
MLCL(54:5)	0.59	0.22
MLCL(54:6)	0.59	0.22

pmol/nmol PLs
10
5
2.5
1
0.5
0.25
0.05
0.01

B

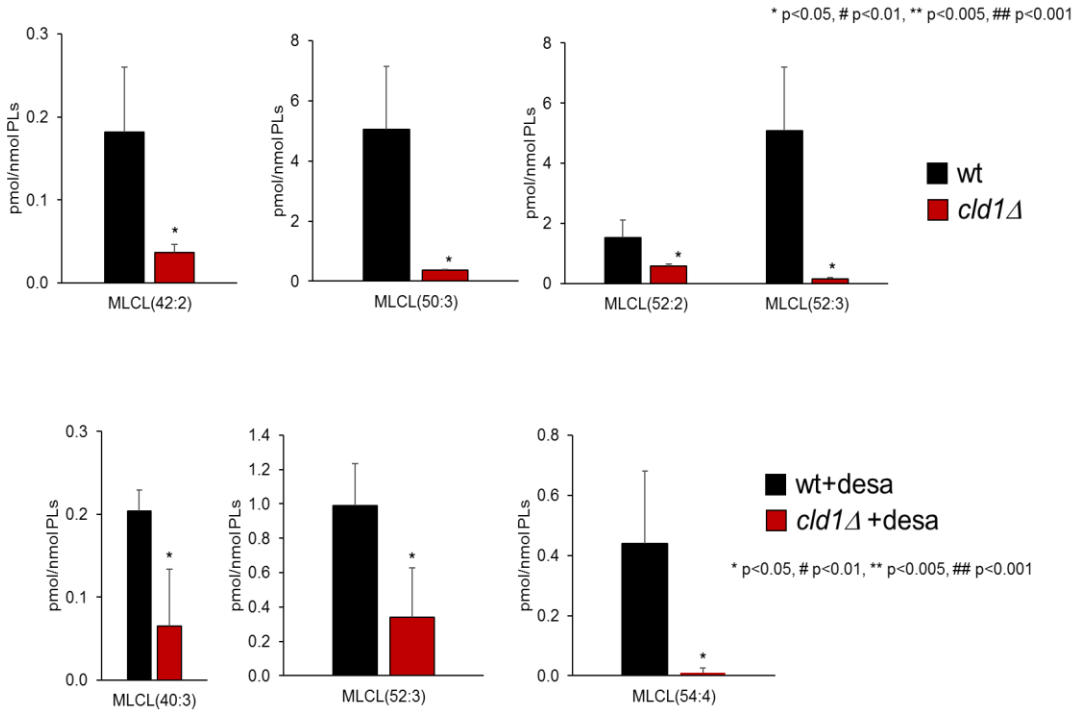

Figure 5-5. MLCL species in Δ^{12}-desaturase-expressing cells.

(A) Heat map of all MLCL species quantified. (B) Quantitative assessment of total MLCL in wt and *cld1Δ* yeast cells expressing Δ^{12}-desaturase (desa) or empty vector (EV).

detectable in the mutant (Figure 5-3). Interestingly, the expression of Δ^{12}-desaturase in *cld1*Δ cells increased MLCL levels by more than 100%, suggesting that an alternate, unidentified CL phospholipase may exist that is capable of deacylating PUFA-containing CL.

Cld1 mitigates the effects of CL peroxidation

In vitro experiments revealed that Cld1 exhibits greater affinity for peroxidized than non-peroxidized CL (Figure 5-4). Thus, $(18:2)_4$-CL was a poor substrate for Cld1, but peroxidized $(18:2)_4$-CL was an excellent substrate.

We have previously shown that *CLD1* expression is increased during respiratory growth and regulated by the HAP complex (Ye et al., 2014). It is plausible that increased *CLD1* expression during respiratory growth mitigates the effects of superoxides generated by respiratory complex III, which likely contribute to the peroxidation of CL. Consistent with this possibility, wt cells treated in the log phase with H_2O_2 for 1 hr exhibited a 2-fold increase in *CLD1* expression (Figure 5-5). Furthermore, the expression of desaturase increased the sensitivity of *cld1*Δ cells to mito-AAPH (Figure 5-6), which has been shown to generate CLox (unpublished). The chronological life span of *cld1*Δ was dramatically decreased by expression of desaturase (Figure 5-2D), while the life span of wt cells expressing the desaturase was not affected.

Taken together, these findings support a role for Cld1 in mitigating the effects of CL peroxidation.

DISCUSSION

This study demonstrates, for the first time, a role for Cld1 in mitigating the effects of CL peroxidation. Previously, we demonstrated that deletion of *CLD1* rescues the respiratory growth defect of tafazzin deficient yeast cells, indicating that an increased MLCL/CL ratio, not decreased CL with unsaturated fatty acyl chains, is detrimental in tafazzin deficient cells (Ye et al., 2014). Similarly, a study by Baile and colleagues illustrated that unremodeled and remodeled cardiolipin are functionally indistinguishable in yeast (Baile et al., 2014). An interesting question arises from these observations: why do yeast require CL remodeling if there is no adaptive advantage of accumulating CL dominated by unsaturated fatty acyl chains. A clue to this question comes from our findings, it further indicate that expression of *CLD1* is increased in response to respiratory growth conditions, and this increase is mediated by the HAP and Mig1 transcriptional factors. Baile and coworkers revealed that Cld1 protein level and function are decreased in glucose and increased in lactate (Baile et al., 2013). They observed that CL remodeling is regulated by available carbon source and membrane potential. Mitochondria are the major producer of cellular ROS, and CL-hydroperoxides are known to reduce oxidative metabolism by inactivating complex IV (Musatov, 2006). Similarly, respiratory chain defects have been shown to increase ROS production and decrease the membrane potential (Grivennikova and Vinogradov, 2006; Minners et al., 2007). These findings support a model in which decreased membrane potential resulting from the accumulation of CL-hydroperoxides serves as a signal to activate CL remodeling. This model is further supported by the notion that CL remodeling may function to

remove peroxidized fatty acyl residues from CL, thereby mitigating the downstream consequences of mitochondrial CL-hydroperoxide accumulation, possibly including mitophagy or apoptosis. However, it is unclear if this model applies to yeast cells because loss of *CLD1* does not cause any detectable functional defects (Baile et al., 2014). CL-hydroperoxides are not produced in either WT or *cld1Δ* cells unless PUFA is supplied in the growth medium or an exogenous-desaturase is expressed (Tyurina et al., 2017). WT yeast cells readily incorporate PUFA into CL, which suggests that CL enriched with PUFA may influence cellular function in *S. cerevisiae*. In the current study, we used Δ^{12}-desaturase-expressing cells to study the functions of Cld1 and CL remodeling in the presence of PUFA-containing CL, and reveal that loss of Cld1 causes an accumulation of specific CLox species, decreased membrane potential, and decreased chronological life span (Figure 2). These results suggest that Cld1 is involved in removing specific CLox species. This is supported by the demonstration that purified Cld1 has a higher affinity for peroxidized than non-peroxidized $(C18:2)_4CL$ (Figure 3). This may explain the previous observation that *CLD1* expression is upregulated during stationary phase and that *CLD1* upregulation is respiration dependent (Ye et al., 2014). Consistent with this model, H_2O_2 treatment increases *CLD1*expression, which suggests that increased oxidative stress upregulates *CLD1* expression.

We previously demonstrated that expression of Δ^{12}-desaturase enables WT *S. cerevisiae* cells to make C16:2- and C18:2- containing phospholipids, including CL, PC, PE, and PS, and CLox (Chapter 4, unpublished). The LC-MS data showed that *cld1Δ*

cells exhibit decreased PUFA-containing CL, but increased levels of specific CLox species. In our previous study, we showed that WT yeast cells expressing Δ^{12}-desaturase readily accumulate CLox, yet these cells do not exhibit detectable defects under optimum growth conditions (Chapter 4, unpublished). In this study, we showed that Cld1 is involved in removing specific CLox species, and that loss of *CLD1* in Δ^{12}-desaturase-expressing cells led to severe physiological defects, including decreased mitochondrial membrane potential and decreased chronological life span.

As Cld1 functions to removed CLox, we speculate that *CLD1* expression is regulated by the cellular ROS level. This is supported by the finding that treatment of H_2O_2 increased *CLD1* expression (Figure 5). This observation is consistent with the previous finding that *CLD1* expression is upregulated in stationary phase, as cellular ROS are accumulated during respiration and reach high concentrations during this phase. Furthermore, upregulation of *CLD1* expression is respiration dependent, and the transcription factor Mig1 is required for *CLD1* upregulation. Mig1 has been shown to sense ROS and regulate gene expression in response to increased ROS production.

Although Cld1 is the only known phospholipase that deacylates CL in yeast, MLCL was still detectable in *cld1Δ*, and the MLCL level was significantly increased in Δ^{12}-desaturase-expressing *cld1Δ* cells. This observation suggests the existence of an unidentified phospholipase capable of deacylating CL containing PUFA.

ACKNOWLEDGMENTS

In this chapter, we conceived and designed the experiments in collaboration with Dr. Valerian E. Kagan (University of Pittsburg). Christian A. Reynolds, Wenxi Yu, Zhuqing Liang and I performed yeast growth experiments. Collaborators from Valerian E. Kagan's lab performed the LC-MS to analyze the CL profile.

CHAPTER 6 LOSS OF CARDIOLIPIN REMODELING RESULTS IN DECREASED C2C12 MYOBLAST DIFFERENTIATION: A MYOBLAST MODEL FOR BARTH SYNDROME AND CARDIOLIPIN DEFICIENCY

INTRODUCTION

Cardiolipin (CL) is a dimeric mitochondrial membrane phospholipid with multiple functions that are conserved from yeast to humans (Acehan et al., 2011; Chen et al., 2008; Gebert et al., 2009; Jiang et al., 2000; Joshi et al., 2009a; Koshkin and Greenberg, 2000; Koshkin and Greenberg, 2002; McKenzie et al., 2006; Pfeiffer et al., 2003; Soustek et al., 2011; Xu et al., 2006a). Newly synthesized CL contains predominately saturated fatty acyl chains, and acyl remodeling of CL is required to produce “mature”, highly unsaturated CL species. Deficient CL remodeling causes Barth syndrome (BTHS), a rare X-linked genetic disorder associated with a broad range of clinical manifestations, including cardiomyopathy, skeletal myopathy, neutropenia, and 3-methylglutaconic aciduria (Barth et al., 1983; Mazzocco et al., 2007b). Specifically, BTHS results from mutations in the *tafazzin* gene (*TAZ)* encoding the transacylase responsible for remodeling of CL. Mutations in *TAZ* lead to reduced total CL content and an accumulation of monolyso-CL (MLCL), an intermediate of the CL remodeling pathway.

Most patients diagnosed with BTHS exhibit pronounced skeletal myopathy, low muscle mass, delayed gross motor development, exercise intolerance, muscle weakness, and focal myofibrillar degeneration (Barth et al., 1999b; Spencer et al., 2006b). Consistent with decreased mitochondrial function, skeletal muscle O_2 utilization and peak work rate are significantly lower in BTHS patients than control participants

(Spencer et al., 2011). While it is widely accepted that skeletal myopathy associated with BTHS stems from mitochondrial dysfunction, the mechanisms linking defective CL remodeling and skeletal myopathy have not been clearly elucidated and likely extend beyond compromised ATP generation. Myogenic differentiation is largely controlled by myogenic transcription factors and is accompanied by major changes in mitochondrial metabolism (Abdel Khalek et al., 2014; Hamai et al., 1997; Philp et al., 2011; Zhu et al., 2013), mitochondrial energy production (Abdel Khalek et al., 2014; Murray and Huss, 2011), and mitochondria-mediated activation of apoptotic pathways (Camara et al., 2007; Ciavarra and Zacksenhaus, 2011; Griffiths et al., 2015). Given the central role of mitochondria in regulating myoblast differentiation, we hypothesized that mitochondrial defects associated with BTHS may contribute to skeletal myopathy by interfering with normal myocyte differentiation.

To determine the effect of defective CL remolding on myogenic determination, we sought to develop a tafazzin-deficient mammalian skeletal myoblast model. The C2C12 cell line was derived from murine skeletal myoblast cells and represents a widely used model for the study of skeletal muscle development (Burattini et al., 2004), skeletal myopathy (Arya et al., 2013; Bathe et al., 2007; Mullen et al., 2010), and skeletal muscle differentiation (Ardite et al., 2004; Jasmer and Kwak, 2006; Wallace et al., 2016). The cells readily proliferate in high-serum conditions, and differentiate and fuse in low-serum conditions. Tafazzin-deficient C2C12 myocytes would provide a metabolic model for which isogenic cells are available as controls, in contrast to currently used BTHS patient-derived lymphoblast cells. Furthermore, they are

experimentally easier and cheaper to manipulate than tafazzin-deficient induced pluripotent stem cells (iPSCs) (Dudek et al., 2013b).

In this study, we constructed a CRISPR-generated stable tafazzin knockout (TAZ-KO) C2C12 myocyte cell line. The TAZ-KO cell line exhibits an increased MLCL/CL ratio, decreased mitochondrial respiratory capacity, increased mitochondrial ROS production, and defective myocyte differentiation. These results indicate that loss of CL remodeling influences myogenic determination and form the foundation for future studies exploring potential mechanisms by which CL remodeling is required for regulating myocyte differentiation. Although BTHS is the only known genetic disorder directly linked to CL, aberrant myocyte differentiation may contribute to the development of skeletal myopathy associated with other mitochondrial diseases.

METHODS AND MATERIALS

Cell line and growth conditions—Wild type C2C12 cell lines were kindly provided by Dr. Steven Cala, Wayne State University. Growth medium consisted of DMEM (Gibco) containing 10% FBS (Hyclone), 2 mM glutamine (Gibco), penicillin, (100 units/ml) and streptomycin (100 µg/ml) (Invitrogen). Cells were grown at 37°C in a humidified incubator with 5% CO_2. C2C12 myoblast differentiation was induced by shifting cells to DMEM medium containing 2% horse serum (Gibco).

Construction of TAZ-KO C2C12 cell line using CRISPR—A gRNA targeting mouse TAZ exon 3 was identified using the clustered regulatory interspaced short palindromic repeats (CRISPR) design tool at crispr.mit.edu (G2: TCCTAAAACTCCGCCACATC). To express Cas9 and guide RNA in the mouse-derived C2C12 myoblast cells,

complementary oligonucleotides containing the gRNA sequence preceded by a G (for expression from the U6 promoter) were cloned into the *Bbs*I site of plasmid pX330 (Cong et al., 2013) (a gift from Feng Zhang; Massachusetts Institute of Technology, Cambridge, Massachusetts, USA) [Addgene plasmid # 42230]). The sequence was verified using oligonucleotide primer 330/335 (ACTATCATATGCTTACCGTAAC).–The plasmid pPGKpurobpa (a gift from Allan Bradley; Wellcome Trust Sanger Institute, Cambridge, UK) was co-transfected to allow selection under puromycin. Cells were transfected with plasmid pX330-TAZ and pPGKpurobpa using Lipofectamine 2000 (Life Technologies, Inc.). Cells were selected in puromycin-containing DMEM with 10% FBS. Cells were then diluted and put into 96-well plates. Single colonies were picked for screening. To screen for insertions or deletions at the target sites, the following oligonucleotide primers flanking mouse Taz exon 3 were used: FOR: CCAACCACCAGTCTTGCATG. REV: ATCCCTGCCTCCAAGACTTC. Wild type genomic DNA generates a product of 547 bp. Cells that did not generate this product were selected for further analysis.

Real Time Quantitative PCR (RT-qPCR) Analysis—As described in Chapter 2

Mitochondria extraction—Cells were grown to 100% confluency in 150 mm dishes, and collected by scraping followed by centrifugation at 800 rpm for 5 min. The cell pellets were washed with cold PBS and suspended in mitochondrial isolation buffer (280 mM sucrose, 0.25 mM EDTA, 20 mM Tris-HCl, pH 7.2). Cells were manually homogenized with a glass homogenizer. Cell debris was removed by centrifugation at 800 rpm for 5 min. Mitochondria were subsequently collected by centrifugation at

11,500 rpm for 10 min. Protein concentration was determined using the DC protein assay kit (BIO-RAD).

Determination of CL by mass spectrometry—Transacylation products were quantified by MALDI-TOF mass spectrometry using the method of Sun et al. (Sun et al., 2008). Lipid extracts were dissolved in chloroform/methanol (1:1) and mixed 1:1 with matrix solution containing 20 g/L 9-aminoacridine in 2-propanol/acetonitrile (3:2, v/v). An aliquot of 1 µL or less of this mixture was spotted on a target plate. Measurements were performed with a MALDI Micro MX mass spectrometer (Waters) operated in reflectron mode. The pulse voltage was set to 2000 V, the detector voltage was set to 2200 V, and the TLF delay was set to 700 ns. The nitrogen laser (337 nm) was fired at a rate of 5 Hz and 10 laser shots were acquired per sub-spectrum. The instrument was operated in negative ion mode with a flight tube voltage of 12 kV, a reflectron voltage of 5.2 kV, and a negative anode voltage of 3.5 kV, and calibrated daily. We typically acquired 100 sub-spectra (representing 1000 laser shots) per sample in a mass range from 400 to 2000 Da. Spectra were only acquired if their base-peak-intensity was within 10–95% of the saturation level. Data were analyzed with the MassLynx 4.1 software.

Western Blot—Mitochondrial protein concentration was measured using the DC Protein Assay Kit (BIO-RAD). Cell extract corresponding to 30 µg protein was analyzed by SDS-PAGE on a 10% gel. Immunoblotting was performed using primary antibodies against tafazzin, NDUFB6, and corresponding secondary antibodies conjugated to horseradish peroxidase. Immunoreactivity was visualized using enhanced chemiluminescence (ECL) substrate (Thermo).

MTT assay—3000 cells were suspended in 100 µL of growth medium and seeded into 96-well plates. Viable cells were measured in triplicate using MTT (Fisher) after 3, 24, and 48 h. In brief, 10 µL of 5 mg/mL MTT were added to each well. Inclusion of an additional set of wells treated with MTT but containing no cells served as a negative control. The plate was incubated for 4 h at 37°C in a culture hood. The medium was carefully removed and 150 µL DMSO were added to dissolve the MTT product. The plate was covered with foil and incubated for 10 min at 37°C. Samples from each well were mixed well with a pipette, and absorbance was read at 570 nm.

Mitochondrial respiration measurements— Intact cell respiration was analyzed in a closed 500 µL chamber equipped with a micro Clark-type oxygen electrode (Oxygraph Plus System, Hansatech Instruments) at 35 °C as described (Lee et al., 2010). Cells were cultured in high glucose DMEM medium (100 units/mL penicillin-streptomycin, 10% fetal bovine serum), trypsinized, and washed with PBS. Cells were then suspended in measuring buffer (120 mM KCl, 3 mM Hepes, 3 mM $MgSO_4$ 5 mM KPi), to a final protein concentration of 2 mg/mL. Following measurements of basal cell respiration, 0.5 µM FCCP was added to analyze uncoupled respiration. Oxygen consumption was recorded on a computer and analyzed with the Oxygraph plus software. Oxygen consumption rate (OCR) is defined as nM consumed O_2/min/mg protein).

Measurement of mitochondrial membrane potential via TMRM florescence—Cells were plated at 40% confluency in 96-well plates in growth medium. After 24 h, the mitochondrial membrane potential was measured using the fluorescent dye Tetramethylrhodamine methyl ester (TMRM) as described previously (Brown, 1999). Briefly, cells were treated with 150 nM TMRM in growth medium for 30 min at 37°C. The

cells were then washed 3 times in PBS and TMRM fluorescence was measured on a microplate reader (Excitation: 544 nm and Emission: 590 nm). Each assay was performed in parallel with samples containing 10 μM carbonyl-cyanide-4-(trifluoromethoxy)phenylhydrazone (FCCP), which collapses the mitochondrial membrane potential. All data were expressed as the total TMRM fluorescence minus the FCCP treated TMRM fluorescence.

Measurement of ROS production using MitoSOX—ROS production was measured with MitoSOX™ mitochondrial superoxide indicator (M36008) (Fisher Scientific) following the manufacture ’s guide. In brief, the 5 mM MitoSOX™ reagent stock solution was diluted in growth medium to make a 5 μM MitoSOX™ reagent working solution. 1.0 mL of 5 μM MitoSOX™ reagent working solution was applied to cover cells adhering to coverslips. Cells were incubated for 10 min at 37˚C, protected from light, then washed gently three times with warm buffer, counterstained with DAPI, and imaged using a Z1 AxioObserver inverted fluorescence microscope equipped with an AxioVision MRm camera (Zeiss). Images were taken using a 20X objective. MitoSOX fluorescence was quantified in all cells within five randomly selected fields of view from three biological replicates using florescence density analysis with ZenPro software (Zeiss).

Immunofluorescence imaging of myotubes—Cells were seeded on gelatin and fibronectin coated glass coverslips at 40% confluency. Following overnight culture, the growth media containing 10% FBS were replaced with differentiation media containing 2% horse serum. At the indicated times, the cells were fixed with 4% paraformaldehyde. The coverslips were washed three times in buffer (PBS + 0.3% Triton) and then blocked

using 10% horse serum (Invitrogen). Coverslips were incubated with primary antibody, mouse anti-MHC (Novus Biologicals; MAB4470), diluted in PBS supplemented with 10% horse serum for 24 h. After washing with PBS, coverslips were incubated with an AlexaFluor 488®-conjugated donkey anti-mouse secondary antibody (1:1000, Jackson ImmunoResearch Laboratories) overnight. Fluorescence microscopy was performed using a Z1 AxioObserver inverted fluorescence microscope equipped with an AxioVision MRm camera (Zeiss) operated by ZenPro software (Zeiss). All images were taken using a 20X objective.

RESULTS

Construction of a tafazzin knockout C2C12 cell line using CRISPR technology.

We generated a TAZ-KO C2C12 myocyte cell line in order to interrogate a potential link between CL remodeling and myocyte differentiation. C2C12 is a well characterized myoblast cell line that exhibits a high metabolic demand, similar to skeletal muscle cells (Burattini et al., 2004). These cells proliferate as undifferentiated myoblast cells when grown in media containg high concentrations of serum (10%), and terminally differentiate into multinucleated myotubes when cultured in low serum-containing media. We used the CRISPR approach to generate tafazzin-deficient C2C12 myoblast cells. The pX330-TAZ and pPGKpurobpa plasmids were transfected into C2C12 myoblasts, which were grown in selective medium. Following serial dilution, cultures derived from single cells were picked and PCR was used to identify the gene knockout. Tafazzin mRNA levels were measured using RT-qPCR. The TAZ-KO C2C12 myoblast cells exhibited a 90% decrease in tafazzin mRNA levels (Figure 6-1A).

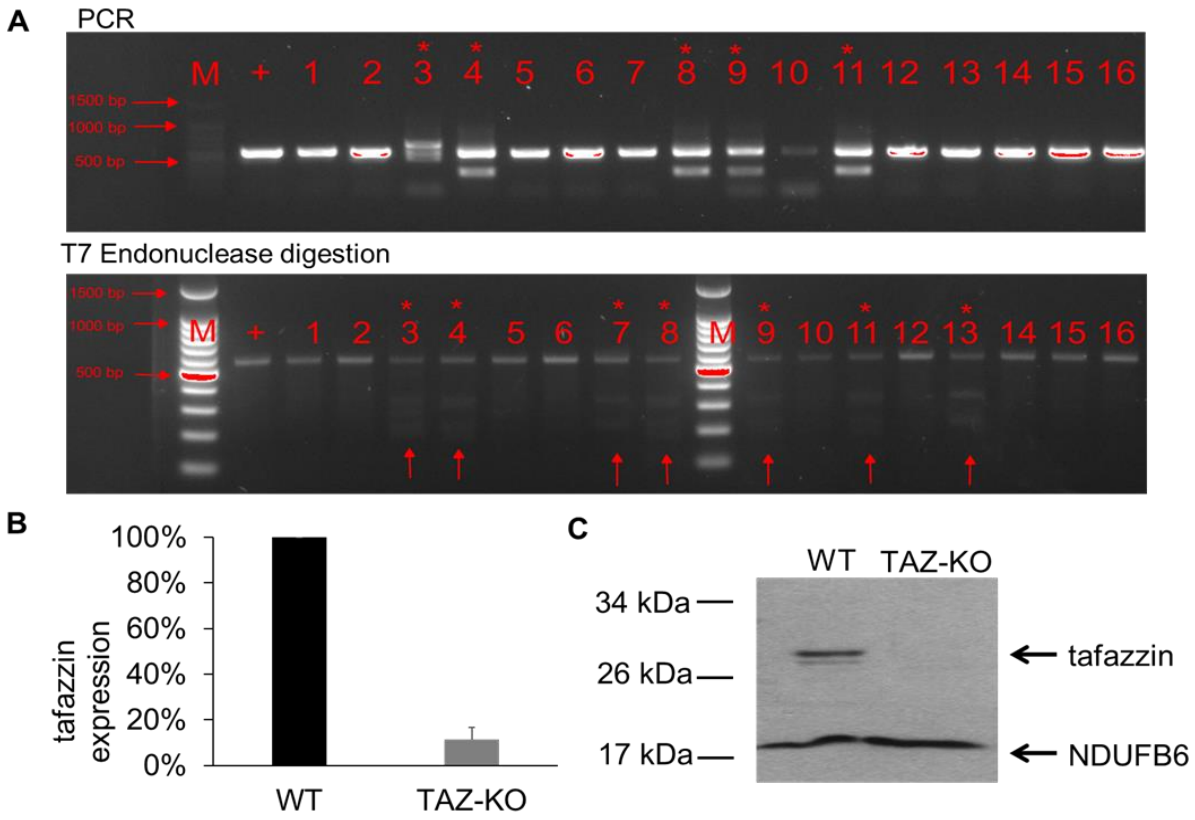

Figure 6-1. Construction of TAZ-KO C2C12 cells.

Mouse C2C12 myoblast cells were transfected with CRISPR plasmid targeting the tafazzin gene. (A) Genomic TAZ is altered in TAZ-KO cells. Cells were selected in puromycin-containing DMEM with 10% FBS. The knockout strain was identified by PCR using the 547 bp region of the tafazzin gene targeted by the Cas9 gRNA followed by a T7 endonuclease digestion. (B) Tafazzin mRNA levels were decreased in TAZ-KO cells. WT and TAZ-KO cells were grown in DMEM with 10% FBS and harvested for mRNA extraction. Tafazzin mRNA levels were quantified by RT-qPCR and normalized to mRNA levels of the internal control GAPDH (three independent experiments with three replicates each). (C) Tafazzin protein was not detectable in TAZ-KO cells. Cells were grown in DMEM with 10% FBS, harvested, and lysed for protein extraction. 30 µg of total cell extract from each sample were subjected to Western blot analysis using 10% polyacrylamide gels. The mitochondrial protein NDUFB6 was used as a loading control.

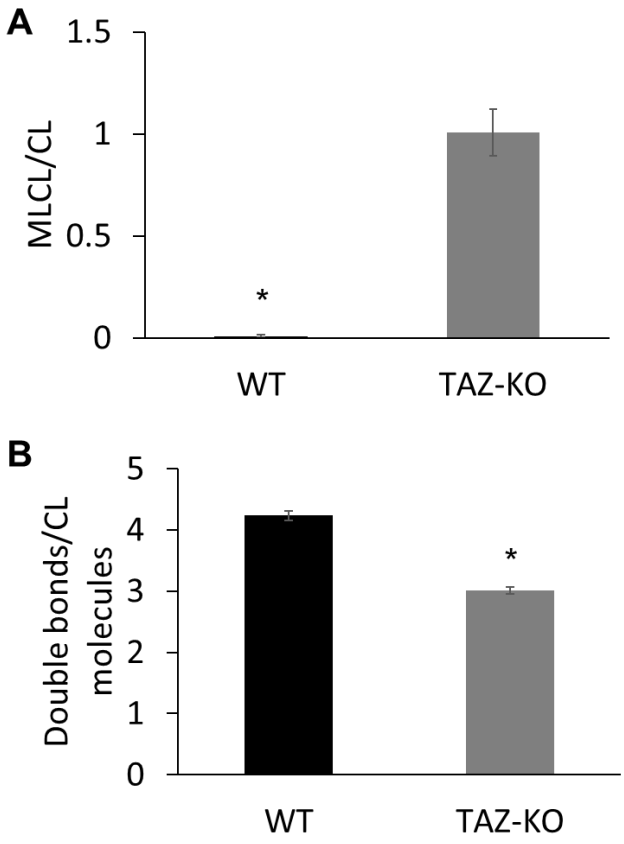

Figure 6-2.CL profile of TAZ-KO cells.

(A) MLCL/CL ratio of TAZ-KO cells was increased compared to WT controls. WT and TAZ-KO cells grown in DMEM to confluence were extracted for CL and MLCL content analysis by MALDI-TOF mass spectrometry. (B) CL saturation of TAZ-KO cells is increased, consistent with defective CL remodeling.

Tafazzin protein was not detectable via Western blot analysis (Figure 6-1B).

Increased MLCL/CL ratio in TAZ-KO cells.

The most direct biochemical phenotype associated with tafazzin deficiency is an accumulation of MLCL and a concomitant reduction in CL species containing unsaturated fatty acyl chains. Using MALDI-TOF mass spectrometry we confirmed the TAZ-KO C2C12 myoblast cells exhibit reduced tafazzin function, as indicated by the characteristic CL profile of tafazzin deficiency. The MLCL/CL ratio was significantly

increased in TAZ-KO cells compared to controls, and the degree of CL unsaturation was significantly reduced (Figure 6-2).

Characterization of tafazzin-deficient C2C12 cells.

We measured the proliferative growth of TAZ-KO myoblast cells using the MTT assay to determine if loss of tafazzin directly affects myoblast proliferation. Deletion of tafazzin did not significantly influence the doubling time of C2C12 cells (Figure 6-3A). In other BTHS models, including BTHS patient-derived lymphoblast cells and iPSCs, loss of tafazzin results in decreased mitochondrial respiration, increased mitochondrial ROS production and decreased mitochondrial membrane potential (Dudek et al., 2013b; Xu et al., 2005). We assayed these parameters in the TAZ-KO myoblast cells. Mitochondrial respiration was measured in intact cells using a Clark-type electrode. Basal mitochondrial respiration was not significantly affected by tafazzin deficiency in the myoblast cells; however, maximal respiratory capacity of the TAZ-KO myoblast cells was significantly decreased compared to controls (Figure 6-3B). This observation contrasts with other BTHS models in which both basal and maximal mitochondrial respiration is compromised by tafazzin deficency (Dudek et al., 2013b). Assessment of mitochondrial membrane potential using TMRM fluorescence indicated a significant reduction in membrane potential in TAZ-KO myoblasts compared to controls (Figure 6-3C). To quantify mitochondrial ROS production in the myoblast cells, we employed MitoSOX fluorescence staining. Mitochondrial ROS production was significantly increased in TAZ-KO myoblast cells compared to controls (Figure 6-4).

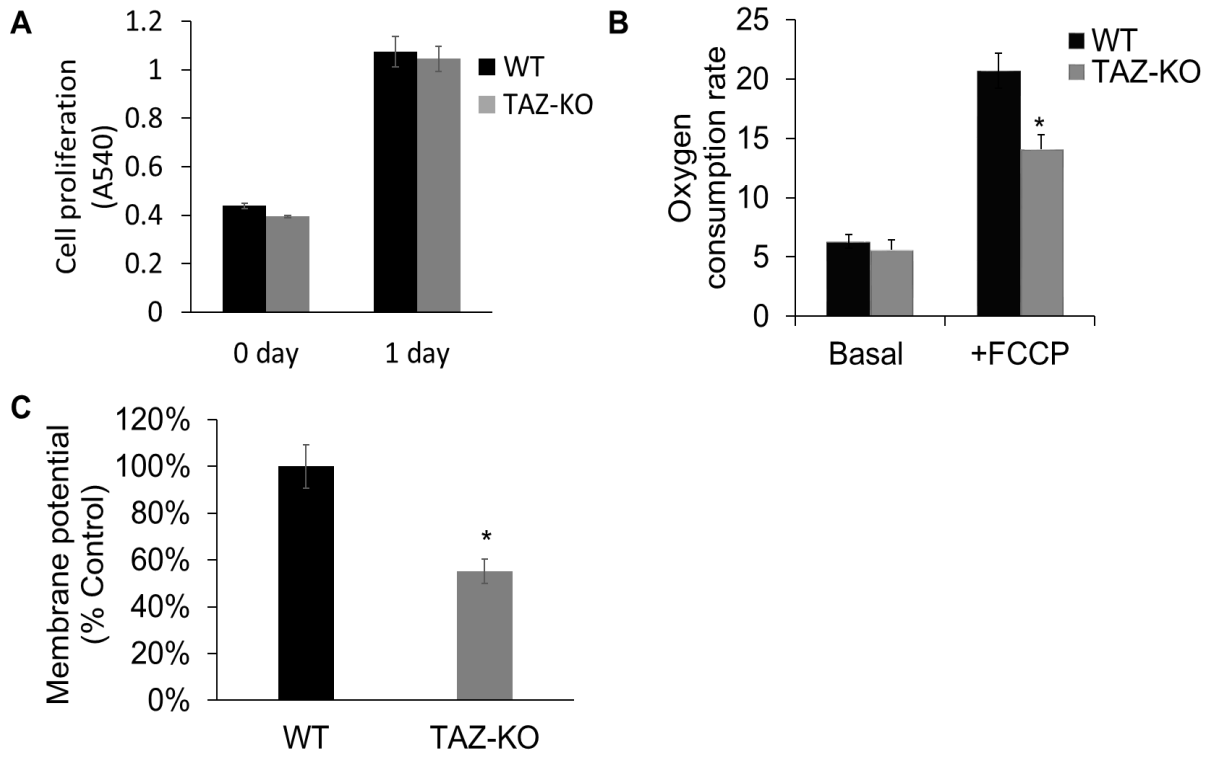

Figure 6-3. Mitochondrial function is decreased in TAZ-KO cells.

(A) C2C12 myoblast proliferation was not affected by tafazzin deficiency. WT and TAZ-KO cell proliferation in DMEM media with 10% FBS was measured using the MTT assay. (B) Mitochondrial respiratory capacity is decreased in TAZ-KO cells. Oxygen consumption was measured in intact cells using a Clark-type electrode. While basal mitochondrial respiration was not affected by tafazzin deficiency, maximal respiratory capacity was significantly decreased in TAZ-KO compared to control cells ($p=<0.05$). (C) Mitochondrial membrane potential is significantly reduced in TAZ-KO cells. Membrane potential of growing WT and TAZ-KO cells was determined by fluorescence quantification of the $\Delta\psi$ dependent dye TMRM.

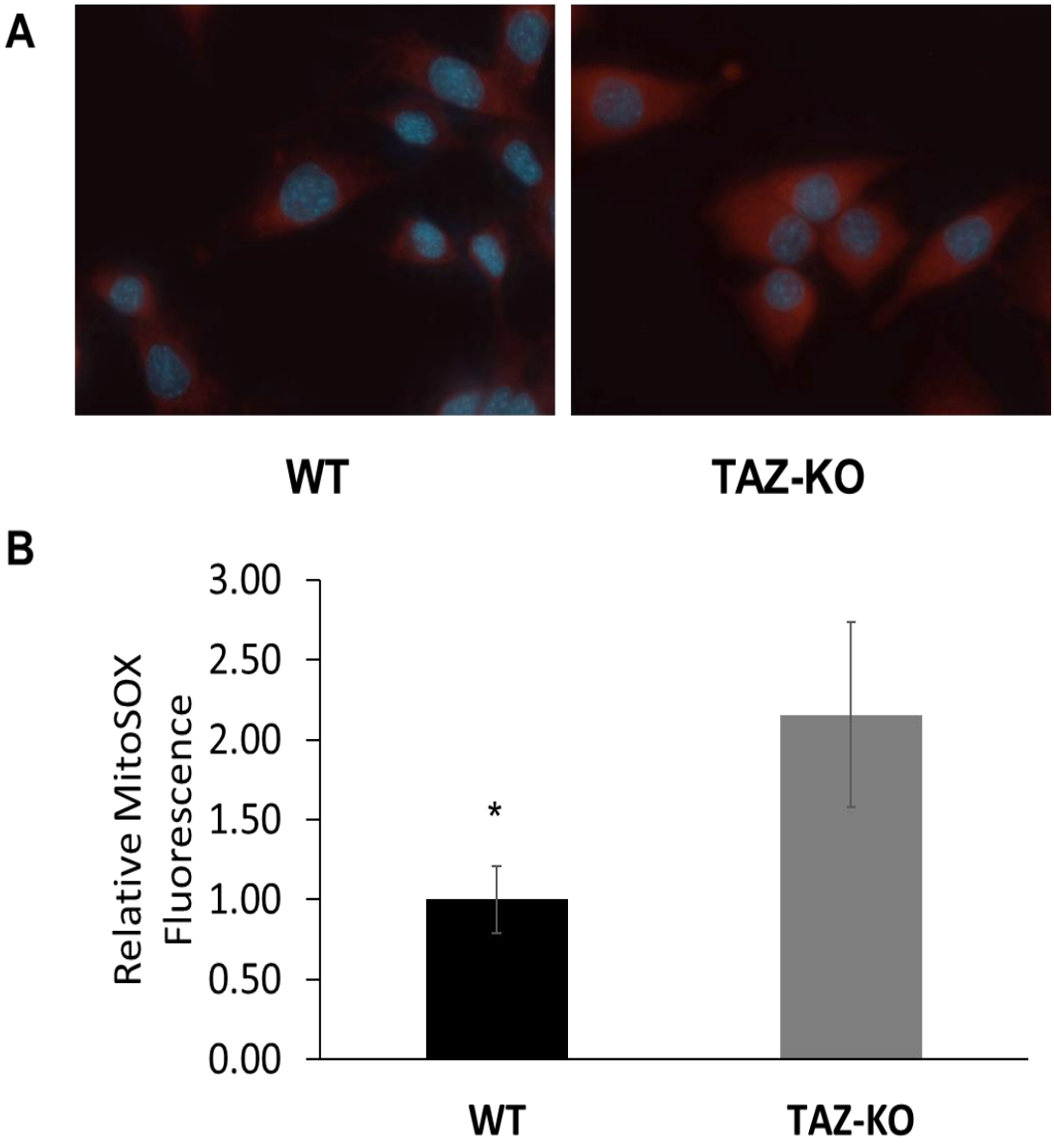

Figure 6-4. Mitochondrial ROS production is increased in TAZ-KO cells.

(A) An increase of mitochondrial ROS was observed in TAZ-KO cells. ROS production was measured via MitoSOX fluorescence using a Z1 AxioObserver inverted fluorescence microscope equipped with an AxioVision MRm camera (Zeiss). (B) Quantitative assesment of MitoSOX fluorescence was performed in all cells within five randomly selected fields of view from three biological replicates using fluorescence density analysis with ZenPro software (Zeiss).

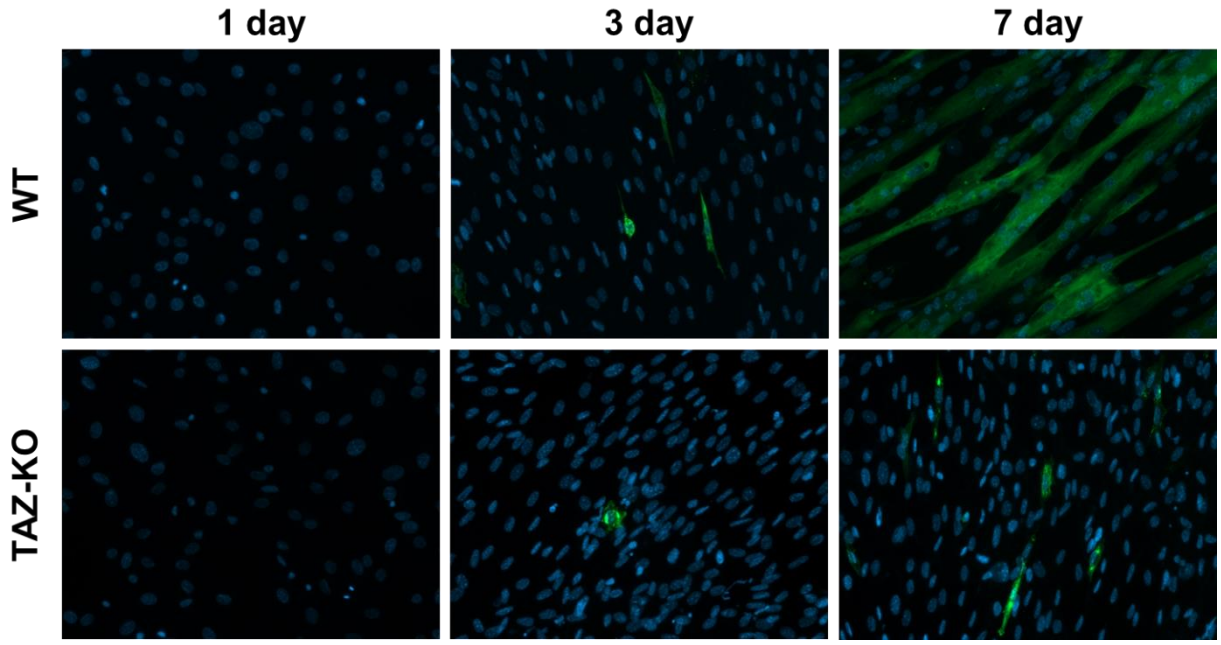

Figure 6-5. Myogenic differentiation is reduced in TAZ-KO cells.

Myogenic differentiation was initiated in cells reaching confluence by switching the cells to DMEM medium containing 2% horse serum. Cells were cultured for 1, 3, or 7 days. Antibody detection of skeletal muscle contractile protein myosin heavy chain (MHC) was used for immunofluorescent staining of differentiated myotubes.

CL remodeling is required for myocyte differentiation.

C2C12 myoblast cells are routinely used to study skeletal muscle differentiation. These cells grow as undifferentiated myoblasts in growth medium containing 10% fetal bovine serum and myogenic differentiation can be initiated in cells reaching confluence by shifting the cells to medium containing 2% horse serum (Travaglione et al., 2005). To investigate how myocyte differentiation is affected by the loss of tafazzin, we initiated myogenic differentiation using the widely-used protocol outlined above. As shown by fluorescence microscopy (Figure 6-5), control myoblast cells morphologically responded to the serum depletion and expressed the skeletal muscle contractile protein myosin

heavy chain (MHC). In striking contrast, TAZ-KO myoblast cells exhibited severely impaired phenotypic differentiation into myotubes.

DISCUSSION

Previous studies have utilized TAZ-KO or BTHS patient-derived iPSCs to generate cardiomyocytes for studying the pathophysiology underlying the cardiomyopathy in BTHS (Acehan et al., 2009; Dudek et al., 2013a; Moffat et al., 2014). The TAZ-KO C2C12 cell line generated in the current study represents the first tafazzin-deficient mammalian cell culture model system established in an immortalized skeletal myoblast cell line. Skeletal myopathy associated with BTHS is presumed to result primarily from impaired ATP production owing to alterations in mitochondrial oxidative phosphorylation. In the present study, we provide evidence for an additional link between dysfunctional CL remodeling and disturbed myocyte ontogenesis. Our findings suggest that myocyte differentiation may be affected in BTHS and may contribute to the skeletal myopathy observed in these patients. The current study has generated a new BTHS model for the study of skeletal myopathy. The TAZ-KO C2C12 cells provide an isogenic model system for exploring the muscle-specific effects of tafazzin-deficiency. C2C12 cells are widely used for biochemical and metabolic studies of skeletal myocytes, and are relatively easy and inexpensive to manipulate. TAZ-KO C2C12 myoblast cells display a mitochondrial phenotype similar to that of BTHS patient tissues and other mammalian models of BTHS. Loss of tafazzin was associated with a significant increase in the MLCL/CL ratio, and a reduction in the number of unsaturated fatty acyl chains incorporated into CL. Furthermore, TAZ-KO myoblast cells display decreased

membrane potential, decreased mitochondrial respiratory capacity, and increased mitochondrial ROS production.

Although we found that loss of CL remodeling leads to defective skeletal myocyte differentiation, the mechanism by which myocyte differentiation is affected remains to be elucidated. CL content is an important determinant of mitochondrial membrane structure and cristae density (Schlame, 2013), and structural changes resulting from the loss of remodeled CL or from the accumulation of monolyso-CL may physically interfere with normal mitochondrial network fusion status. In BTHS patient-derived lymphoblast cells, mitochondrial hyperproliferation and increased mitochondrial network fragmentation are observed (Acehan et al., 2007; Xu et al., 2005). Currently, little is known regarding the role of mitochondrial network dynamics in controlling cellular differentiation. However, actively dividing blast cells have highly fragmented mitochondrial networks that progressively fuse during terminal differentiation, which is associated with increased respiratory capacity (Zhang, 2011). In general, highly fused mitochondrial networks are associated with maximal respiratory capacity (Chen et al., 2005a; Chen et al., 2003; Yu et al., 2006). Thus, it is tempting to speculate that loss of tafazzin may interfere with normal differentiation owing to a reduced ability to form highly fused mitochondrial networks. Consistent with this notion, increased mitochondrial network fragmentation and hyperproliferation have been linked to IKK/NF-κB signaling, which partially inhibits myocyte differentiation (34).

What is the relationship between tafazzin deficiency, cellular energy metabolism, and myocyte differentiation? To meet the anabolic demands of proliferation, actively

dividing blast cells limit mitochondrial oxidative metabolism to increase cellular biomass via anabolic pathways. Consequently, differentiation requires remodeling of mitochondrial oxidative metabolism to support oxidation of glycolysis-derived pyruvate to CO_2. Differentiation is associated with a spectrum of changes in mitochondrial metabolic machinery, including upregulation of enzymes of the tricarboxylic acid (TCA) cycle and subunits of the mitochondrial respiratory chain, and downregulation of glycolytic enzymes (Armstrong et al., 2010; Chung et al., 2007; Prigione et al., 2010; Tormos et al., 2011). This metabolic transition from glycolysis to mitochondrial oxidative metabolism is necessary for cellular differentiation. Studies of pluripotent stem cell differentiation confirm that inhibition of key glycolytic enzymes promotes differentiation, while impairment of mitochondrial function with respiratory inhibitors improves pluripotency and inhibits differentiation (Chung et al., 2007; Mandal et al., 2011). Accordingly, it is plausible that defective mitochondrial oxidative metabolism contributes to the observed differentiation defect in tafazzin deficient C2C12 myoblast cells.

Given their roles as energy and redox sensors, AMP-activated kinase (AMPK), and the sirtuin family of NAD-dependent deacetylases have been implicated in regulating skeletal muscle differentiation in response to metabolic status (Ryall, 2013). Although very little is known about the role of these proteins in the development of skeletal myopathy, increased AMPK and sirtuin activity have been proposed to inhibit differentiation (Fulco et al., 2003; Williamson et al., 2009). It it possible that metabolic and/or redox signaling pathways that regulate myoblast differentation are affected in tafazzin-dificient cells. Future studies will determine what effect tafazzin-deficiency has

on cellular metabolism and redox in order to further elucidate the molecular mechanisms regulating myogenic determination in the TAZ-KO C2C12 cells.

CHAPTER 7 UNFINISHED PROJECTS AND FUTURE DIRECTIONS

The studies described in this thesis elucidate functions of *CLD1* and CL remodeling in the yeast *S. cerevisiae* and murine myoblasts. Our data demonstrated that an increased MLCL/CL ratio, but not decreased CL unsaturation, is likely the primary cause of growth defects observed in yeast *taz1Δ*. This suggests that the physiological defects in BTHS patients is possibly caused by an increased MLCL/CL ratio, and possibly amenable to treatment by attenuation of CL phospholipases. Through nutritional and genetic manipulation of yeast CL species, we identified a novel role for Cld1 in mitigating the effects of CL peroxidation, suggesting that elucidating the role of CL remodeling may shed light on approaches for mitigating oxidative stress. The findings from this study will serve as the basis on which we will improve our understanding of CL remodeling and its mechanistic roles in mitigating oxidative stress. The tafazzin knockout C2C12 cells provides a mammalian model with a congenic control for future studies, and the link between CL deficiency to myotube differentiation is identified.

Additionally, an important function of CL remodeling is to accumulate CL with unsaturated fatty acyl chains. It is still a mystery why cells need PUFA-containing CL. In this chapter, I summarize several interesting projects pertaining to CL remodeling that are left unfinished. These projects can be considered for future studies that could lead to a better understanding of CL remodeling and potential BTHS treatments.

1. Identification of human CL phospholipase that is deleterious to tafazzin-deficient cells

My previous study indicated that deletion of *CLD1* rescues growth, life span, and respiratory defects of the *taz1Δ* mutant, suggesting that these defects in tafazzin-deficient cells are caused by increased MLCL/CL (Ye et al., 2014). This led to the hypothesis that the deleterious effects of the loss of tafazzin can be alleviated by inhibiting the deacylation of CL. A large number of phospholipases complicate the ability to test this hypothesis in mammalian cells. A 50% decrease in MLCL levels was observed in mouse cells carrying a deletion in iPLA2γ, suggesting that phospholipase not yet identified deacylate CL (Kiebish et al., 2013a). Several other phospholipases were shown to deacylate CL *in vitro,* including sPLA2-GIA and iPLA2-GVIA (Hsu et al., 2013). Treatment of BTHS lymphoblasts with the iPLA2 inhibitor, BEL, partially restored the MLCL/CL ratio (Malhotra et al., 2009). Taken together, these published studies indicate that there are several human CL phospholipases and that inhibition of their activities may alleviate deficiencies in BTHS cells.

I have developed a method utilizing a yeast functional bioassay to identify the human phospholipases that deacylate CL *in vivo* and determine if inhibiting their expression alleviates the respiratory defects in BTHS cells. iPLA2γ was cloned into the yeast high copy expression vector pYPGK18. Expression of iPLA2γ leads to decreased growth of *taz1Δ* cells at elevated temperature (Figure 7-1). This is a straightforward and inexpensive bioassay that can be used as a functional screen for CL phospholipases.

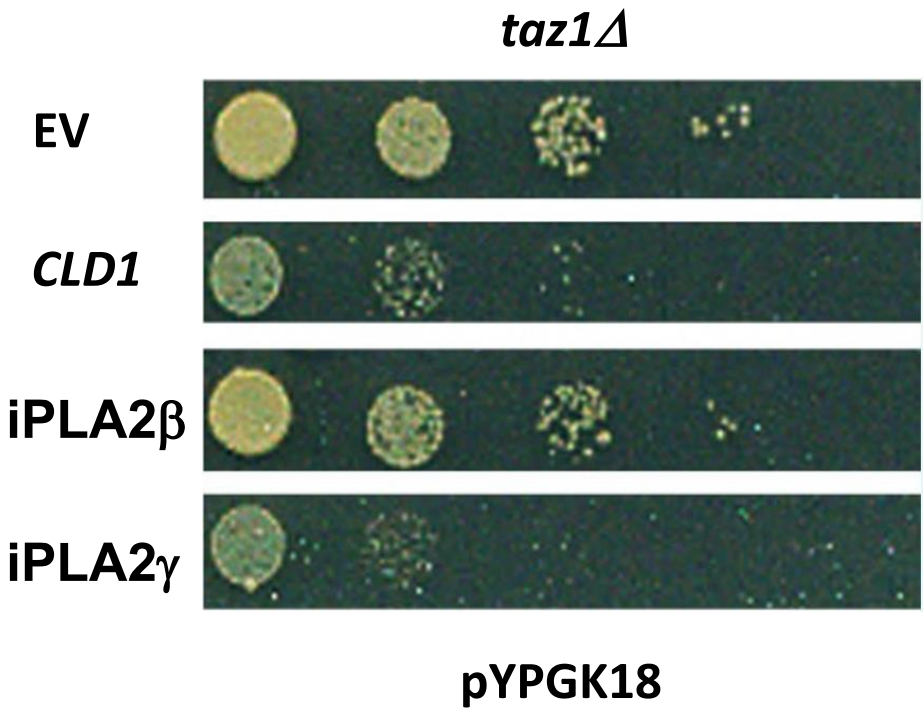

Figure 7-1. Expression of iPLA2γ leads to decreased growth of *taz1Δ* at elevated temperature

To identify the human phospholipases that deacylate CL, the previously described PLA2 phospholipases (Hsu et al., 2013) were cloned into the yeast expression vector pYPGK18. The yeast bioassay was utilized to identify those that exacerbate yeast *taz1Δ* growth defects, which may be deleterious to BTHS cells. This can be tested by inhibiting their expression. To do so, BTHS lymphoblasts and TAZ-KO C2C12 cells can be transfected with lentivirus-derived small hairpin RNA (shRNA) against specific CL phospholipase genes. The effects of knocking down these phospholipases on parameters that are defective in BTHS lymphoblasts, including MLCL/CL ratio, CL acyl composition, respiration, and mitochondrial membrane potential can be assayed (Xu et

al., 2005). The identification of new CL phospholipases will facilitate the understanding of CL remodeling pathways in mammalian cells, possibly leading to new strategies for BTHS treatment.

2. Does loss of *PGS1* function correlate with low HDL-C level?

High-Density Lipoprotein-Cholesterol (HDL-C) alleviates plaque build up in arteries, while low HDL-C levels correlate with heart disease (Ahmed et al., 2016; Hashemi Nazari et al., 2015). A study from the laboratory of Dr. E Shyong Tai in the Department of Medicine at the National University of Singapore identified 250 people with the highest HDL levels and 250 with the lowest HDL from a population of 3000. The *PGS1* gene was sequenced, and four rare *PGS1* variants were found in patients with low HDL. These variants had amino acid substitutions A2E, I114V, A302V, and R343H. Due to the decreased levels of HDL in these patients, these variants were predicted to be harmful to humans. Based on the above finding, it was hypothesized that loss of *PGS1* function correlates with low HDL-C level.

To test the hypothesis, Pgs1 activity and CL levels were assayed in *pgs1Δ* yeast cells expressing human PGS1 variants. To determine if the yeast model is appropriate for testing this hypothesis, we first compared the mammalian and yeast *PGS1* sequence. 33% of the human *PGS1* amino acid sequence is identical to yeast Pgs1. The conserved sequences include the 96 – 269 amino acid and 349 - 534 amino acid catalytic domains. Overexpression of human *PGS1* rescues yeast *pgs1Δ* growth defects, showing that human *PGS1* is functional in yeast (Figure 7-2A). Furthermore, results from thin layer chromatography (TLC) demonstrated that yeast *pgs1Δ* cells do not

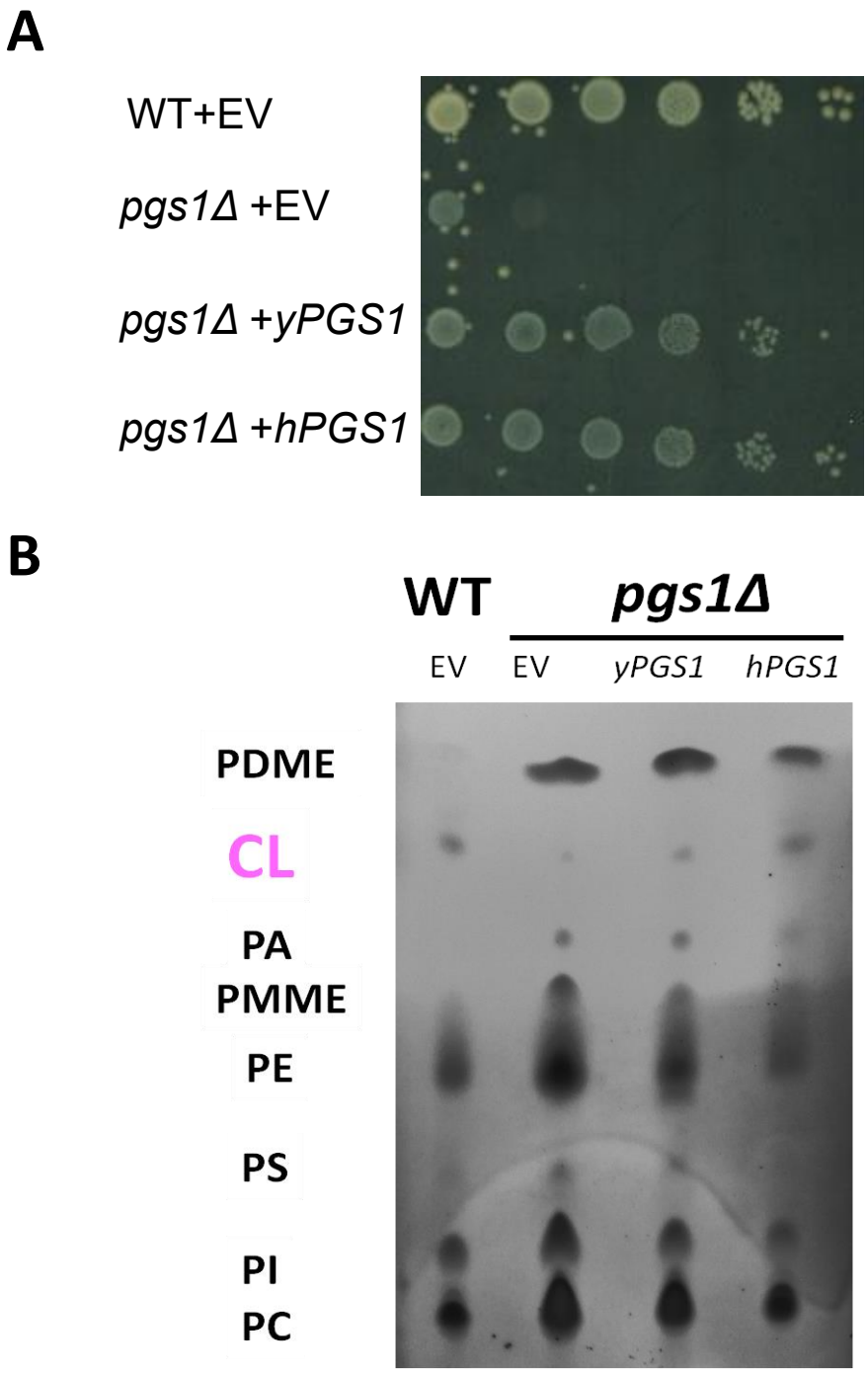

Figure 7-2. Overexpression of human *PGS1* rescues yeast *pgs1Δ* growth defects

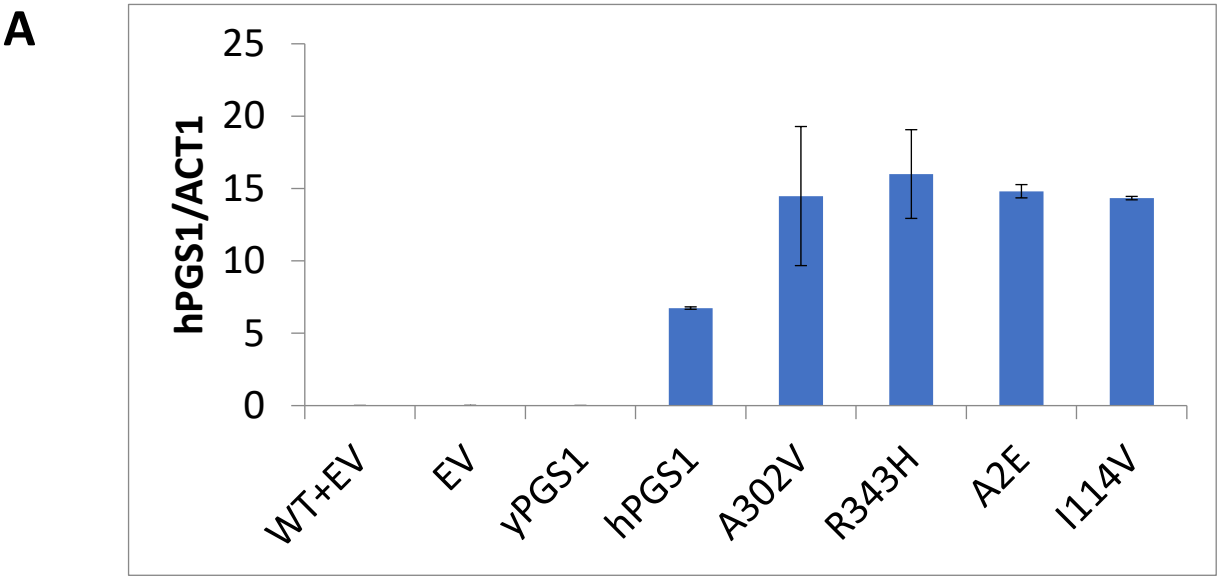

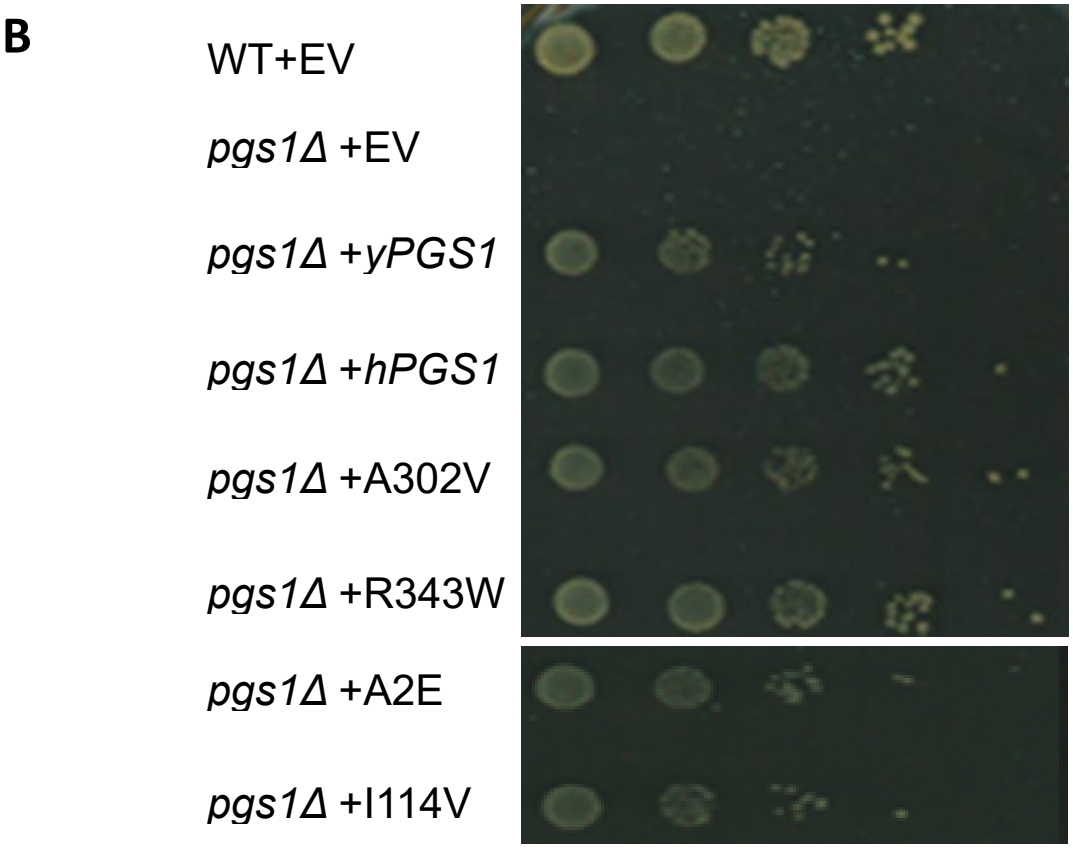

Figure 7-3. Overexpression of human *PGS1* variants rescues yeast *pgs1Δ* growth defects

synthesize CL; however, expression of human *PGS1* leads to CL synthesis in yeast (Figure 7-2B). The difference between wild type human *PGS1* and the four variants (A2E, I114V, A302V, and R343H) in complementing yeast *pgs1Δ* was determined. All 4 variants were successfully expressed in yeast *pgs1Δ* (qRT-PCR) (Figure 7-3A). However, overexpression of all four variants rescued yeast *pgs1Δ* growth defects (Figure 7-3B). Although the overexpression of all four hPGS1 variants rescued *pgs1Δ*, the possibility of defective enzymatic activity of Pgs1 variants, expressed at endogenous levels, cannot be excluded. In addition, suppressors frequently arising in the *pgs1Δ* mutant can easily affect growth. As a result, growth phenotype is not an effective indicator for determining the functionality of human *PGS1* variants. In order to continue with this project, the CL profile in strains expressing variant human *PGS1* should be measured. An alternative strategy is to complement a diploid heterozygous *pgs1Δ* mutant with a human *PGS1* variant. Tetrad analysis can be performed with the diploid cells carrying the *PGS1* variant in a low copy expression vector followed by observing colony growth. A decrease in colony growth (of haploid *pgs1Δ* expressing the *PGS1* variant) can identify variants that leads to defective Pgs1 activity.

Pgs1 ablation eliminates *de novo* synthesis of PG, the CL precursor, and decreased CL is correlated with decreased HDL level (Chang et al., 1998a; Hauff and Hatch, 2010). Therefore, identification of human *PGS1* variants that have decreased Pgs1 activity may provide a molecular marker for decreased HDL level. People who carry the defective *PGS1* variant can then be diagnosed using these molecular markers and receive corresponding treatment.

3. Does ferroptosis exist in yeast?

Ferroptosis is a unique iron-dependent form of nonapoptotic cell death that is dependent on intracellular iron but is not affected by other metals. It is morphologically, biochemically, and genetically distinct from apoptosis, necrosis, and autophagy (Cao and Dixon, 2016; Dixon et al., 2012). Ferroptosis was initially identified in cancer cells. In these cells, classic features of apoptosis, including cytochrome c release, caspase activation, and chromatin fragmentation, were not observed. Ferroptosis is prevented by iron chelation or genetic inhibition of cellular iron uptake (Dixon et al., 2012). The manipulation of ferroptosis could be exploited to selectively destroy tumor cells. Additionally, inhibition of ferroptosis could be utilized to preserve neuronal cells exposed to specific oxidative conditions. The mechanism of ferroptosis regulation is not fully understood. Yeast can serve as a powerful model in studying ferroptosis because most essential cellular functions are conserved from yeast to humans. Additionally, lipid species and intracellular iron can be readily manipulated in yeast. However, it is not known if ferroptosis exists in yeast cells.

Previous studies identified mammalian Gpx4 as a key regulator in ferroptotic cell death. Depletion of Gpx4 leads to peroxidation of arachidonic acid (AA) and ferroptosis in mammalian cells (2017; Conrad and Friedmann Angeli, 2015; Imai et al., 2017; Maiorino et al., 2017; Sakai et al., 2017; Yang et al., 2014). Yeast Gpx3 is the homolog of mammalian Gpx4. To determine if ferroptosis exists in yeast, spotting experiments were

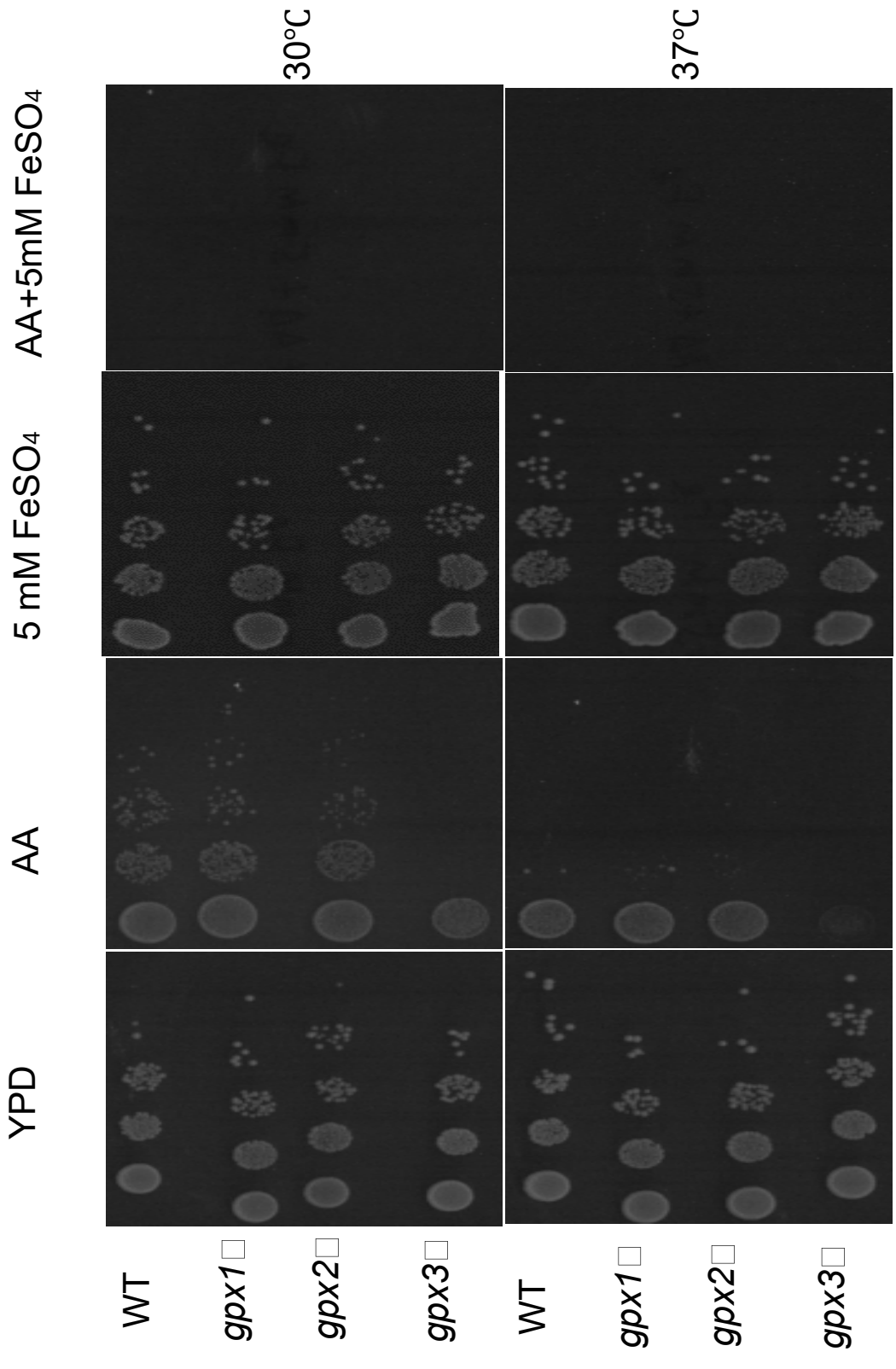

Figure 7-4. Deletion of GPX3 increases the sensitivity of cells to arachidonic acid.

performed to test if Gpx3 deficient yeast exhibit growth retardation when supplemented with AA. Briefly, cell cultures were grown to stationary phase. Serial dilutions of the culture were plated on YPD plates in the presence or absence of AA or $FeSO_4$. Cells were incubated at 30 ℃ or 37 ℃ for 2 days. The results showed that deletion of *GPX3* increased the sensitivity of cells to AA. Sensitivity was more pronounced at the elevated temperature. Supplementation with 5 mM $FeSO_4$ was lethal in the presence of AA (Figure 7-4). These data suggest that deletion of GPX3 possibly leads to ferroptosis of yeast cells supplementated with AA.

To confirm that *GPX3* deletion in yeast leads to ferroptosis in the presence of AA, cells should be grown with an iron chelator that has been shown to inhibit ferroptosis. A finding that growth of *gpx3Δ* in medium containing AA is restored when an iron chelator is supplemented would support the hypothesis that ferroptosis exists in yeast, which can then serve as a potent model to study the mechanism and regulation of this death pathway.

4. Does Drosophila ABHD5 have CL phospholipase activity?

Alpha beta hydrolase domain-containing 5 (ABHD5), also known as comparative gene identification 58 (CGI-58), belongs to the AB hydrolase superfamily, which is composed of hydrolytic enzymes of widely differing phylogenetic origin and catalytic functions (Brown and Mark Brown, 2017; Ollis et al., 1992). Mutations in ABHD5 have been associated with Chanarin-Dorfman syndrome, a triglyceride storage disease with impaired long-chain fatty acid oxidation (Lefevre et al., 2001) and neutral lipid storage disease (Schweiger et al., 2009). Understanding functions and regulation of ABHD5

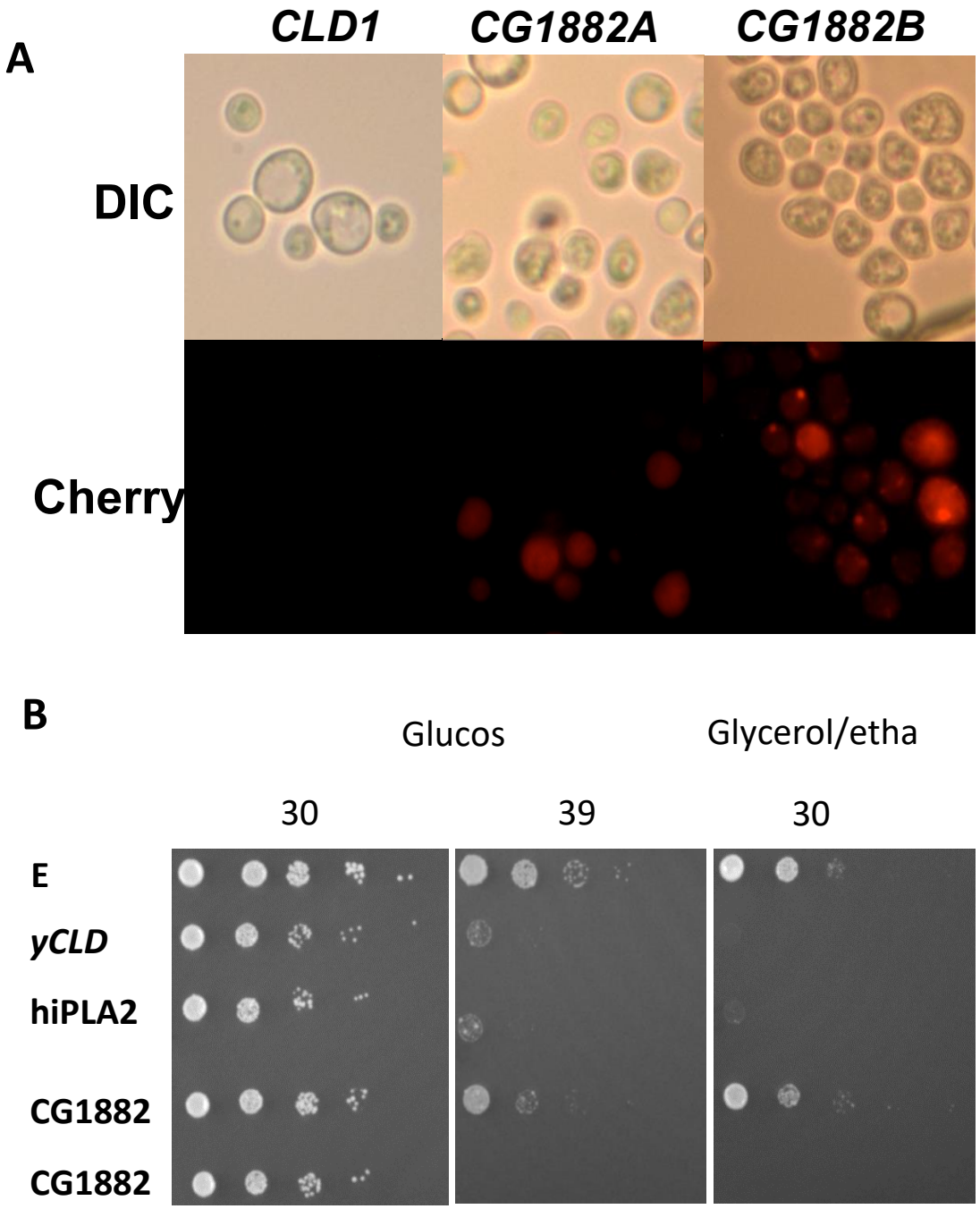

Figure 7-5. Overexpression of B-isoform of the ABHD5 ortholog exhibits a growth defect like overexpression of *CLD1* and iPLA2γ in *taz1Δ*

may provide clues for deciphering physiological defects caused by ABHD5 mutations. Dr. James G. Granneman (Center for Molecular Medicine and Genetics, Wayne State University School of Medicine) recently identified a Drosophila AB hydrolase (CG1882) that is likely an ortholog of human ABHD5. Interestingly, the yeast mitochondrial phospholipase Cld1 is more closely related to ABHD5 than any other protein in the database. ABHD5, however, is not considered a mitochondrial lipase (deacylase) because it lacks a nucleophilic serine and is not targeted to mitochondria. Unlike ABHD5 CG1882 has the nucleophilic serine and a splice variant that is specifically targeted to mitochondria. Given the evolution of this gene and the targeting of a specific splice variant to mitochondria, it might function as a CL lipase.

Our previous study showed that expression of yeast *CLD1* or human iPLA2γ in yeast *taz1Δ* leads to decreased growth (unpublished). In collaboration with Dr. Granneman, we determined if expression of CG1882 in *taz1Δ* leads to decreased growth. There are two isoforms of CG1882, A and B, which have the same sequence except that isoform B has a mitochondrial targeting sequence. *CLD1*, iPLA2γ, and CG1882 (isoforms A and B, with a RFP tag) were expressed on pYPGK18. Both CG1882 isoforms were expressed in *taz1Δ* cells and the B isoform localized to mitochondria. Cells were spotted on solid synthetic complete Leu- medium with either glucose or glycerol/ethanol as a carbon source and incubated at 30 ℃, 37 ℃, and 39℃. The results showed that overexpression of the B-isoform exhibits a growth defect similar to overexpression of *CLD1* and iPLA2γ in *taz1Δ* (Figure 7-5). This suggests that CG1882 and yeast Cld1 may have similar functions.

Future experiments using confocal microscopy could be performed to confirm mitochondrial targeting. In addition, CG1882 enzymatic activity could be determined by targeted mutation of the catalytic domain. Enzymatic activity can be verified by *in vitro* studies followed by assaying phospholipase activity *in vivo*. The CG1882B CL phospholipase activity could be confirmed in Drosophila cell lines followed by characterization of CG1882-null Drosophila. The outcome of this study may provide insight for deciphering physiological defects of Chanarin-Dorfman syndrome and neutral lipid storage disease to develop potential therapeutic treatment.

5. Using genetically-modified yeast cells to screen for iPLA2γ inhibitors

We have shown that a high level of expression of CL phospholipase (*CLD1* or iPLA2γ) is lethal to *TAZ1* deficient cells. To identify iPLA2γ inhibitors, a yeast bioassay strain was genetically manipulated to express the *H. brasiliensis* Δ^{12}-desaturase gene. My colleague Wenxi Yu engineered the pBEVY-L plasmid, which contains a bi-directional promoter, to constitutively express the human iPLA2$_\gamma$ and the *H. brasiliensis* Δ^{12}-desaturase genes in the *cld1*Δ*taz1*Δ double mutant. The Δ^{12}-desaturase expressing strain exhibited decreased growth on non-fermentable carbon sources in the presence of tert-butyl-hydroperoxide (TBHP), a mitochondrial oxidant (**Figure 7-6**). It was especially interesting to discover that dose-dependent sensitivity to TBHP was observed only on non-fermentable growth medium, suggesting that the lipid mediators generated

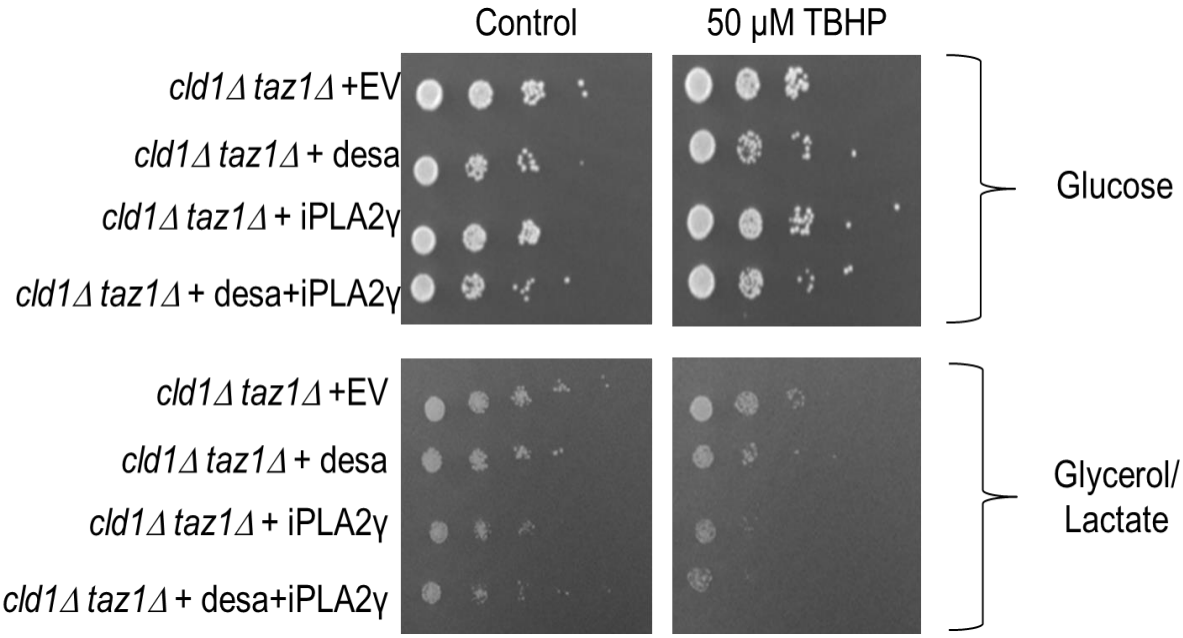

Figure 7-6. Humanized yeast bioassay strain displays sensitivity to mitochondrial oxidative stress.

Serial dilutions of *cld1*Δ*taz1*Δ double mutant yeast cells expressing the H. brasiliensis Δ12-fatty acid desaturase gene (desa), the human iPLA2$_\gamma$ gene (iPLA2$_\gamma$), or both genes (desa + iPLA2$_\gamma$) were spotted on synthetic complete media containing either 2% glucose or 2% glycerol and lactate. *cld1*Δ*taz1*Δ double mutant yeast cells containing the empty pBEVY-L plasmid (EV) served as a control. Plates were treated with either 50 μM TBHP or vehicle control and immediately spotted. Following 5 days of incubation at 30C, plates were imaged for subsequent analysis.

by iPLA2γ impact cell metabolism only during respiratory conditions.

The laboratory of Dr. Valerian Kagan (University of Pittsburg) demonstrated that R-BEL, an inhibitor of iPLA2γ, suppressed hydrolysis of peroxidized CL and the production of peroxidized free fatty acids in a radiation-induced injury mouse model (Buland et al., 2016). To test the hypothesis that inhibitors of iPLA2γ protect against cell damage caused by CL peroxidation, we examined whether the sensitivity of the Δ^{12}-desaturase expressing strain to TBHP is affected by supplementation of R-BEL. In

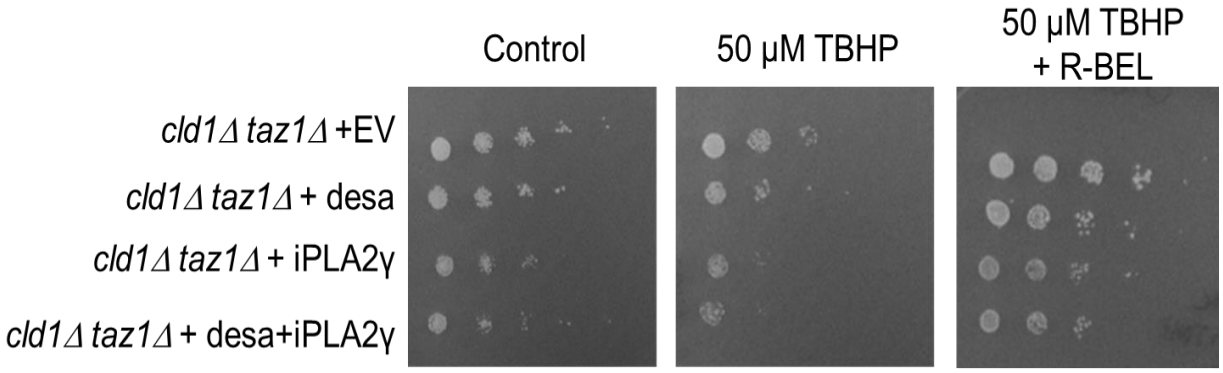

Figure 7-7. Humanized yeast bioassay strain displays sensitivity to mitochondrial oxidative stress.

Serial dilutions of *cld1*Δ*taz1*Δ double mutant yeast cells expressing the H. brasiliensis Δ12-fatty acid desaturase gene (desa), the human iPLA2$_\gamma$ gene (iPLA2$_\gamma$), or both genes (desa + iPLA2$_\gamma$) were spotted on synthetic complete media containing 2% glycerol and lactate. *cld1*Δ*taz1*Δ double mutant yeast cells containing the empty pBEVY-L plasmid (EV) served as a control. Plates were treated with either 50 μM TBHP, 50 μM TBHP + R-BEL, or vehicle control and immediately spotted. Following 5 days of incubation at 30C, plates were imaged for subsequent analysis.

accordance with our hypothesis, we found that the sensitivity of the Δ^{12}-desaturase expressing strain to TBHP on non-fermentable medium was rescued by R-BEL supplementation (**Figure 7-7**). These experiments highlight the utility of this powerful yeast model. Future experiments will seek to screen other potential inhibitors of iPLA2$_\gamma$ using this strain.

Pathways that negatively regulate iPLA2$_\gamma$ activity can be identified by transforming the bioassay strain with a mammalian cDNA library and screening for suppressors of the iPLA2$_\gamma$-mediated lethality phenotype.

It is possible to identify activators of iPLA2γ through assessing mutants that rescue cells from iPLA2$_\gamma$-mediated growth inhibition by synthetic genetic array (SGA) analysis. Genes and associated pathways that are identified in the yeast screens can

A

MLCL	wt	cld1Δ
MLCL(32:3)	0.25	0.20
MLCL(34:3)	0.09	0.08
MLCL(36:3)	0.07	0.06
MLCL(40:3)	0.26	0.21
MLCL(42:1)	0.05	0.11
MLCL(42:2)	0.18	0.04
MLCL(44:1)	0.18	0.16
MLCL(44:2)	0.26	0.17
MLCL(44:3)	2.15	1.75
MLCL(46:2)	0.39	0.27
MLCL(48:3)	0.74	0.33
MLCL(50:1)	0.14	0.30
MLCL(50:2)	1.41	1.09
MLCL(50:3)	5.06	0.35
MLCL(52:2)	1.53	0.57
MLCL(52:3)	5.08	0.15
MLCL(54:3)	1.24	N.D.

MLCL	wt+desa	cld1Δ+desa
MLCL(32:3)	0.19	0.37
MLCL(34:3)	0.08	0.18
MLCL(36:3)	0.04	0.09
MLCL(40:3)	0.20	0.07
MLCL(42:1)	0.05	0.25
MLCL(42:2)	0.07	0.06
MLCL(44:1)	0.14	0.20
MLCL(44:2)	0.20	0.19
MLCL(44:3)	2.03	2.94
MLCL(46:2)	0.30	0.66
MLCL(48:3)	0.34	0.67
MLCL(50:1)	0.13	0.79
MLCL(50:2)	0.27	0.88
MLCL(50:3)	0.98	0.89
MLCL(50:4)	0.47	0.50
MLCL(52:2)	0.16	0.24
MLCL(52:3)	0.99	0.34
MLCL(52:4)	1.30	0.49
MLCL(52:5)	1.16	0.53
MLCL(52:6)	0.25	0.33
MLCL(54:3)	0.23	0.00
MLCL(54:4)	0.44	0.01
MLCL(54:5)	0.59	0.22
MLCL(54:6)	0.59	0.22

pmol/nmol PLs
10
5
2.5
1
0.5
0.25
0.05
0.01

B

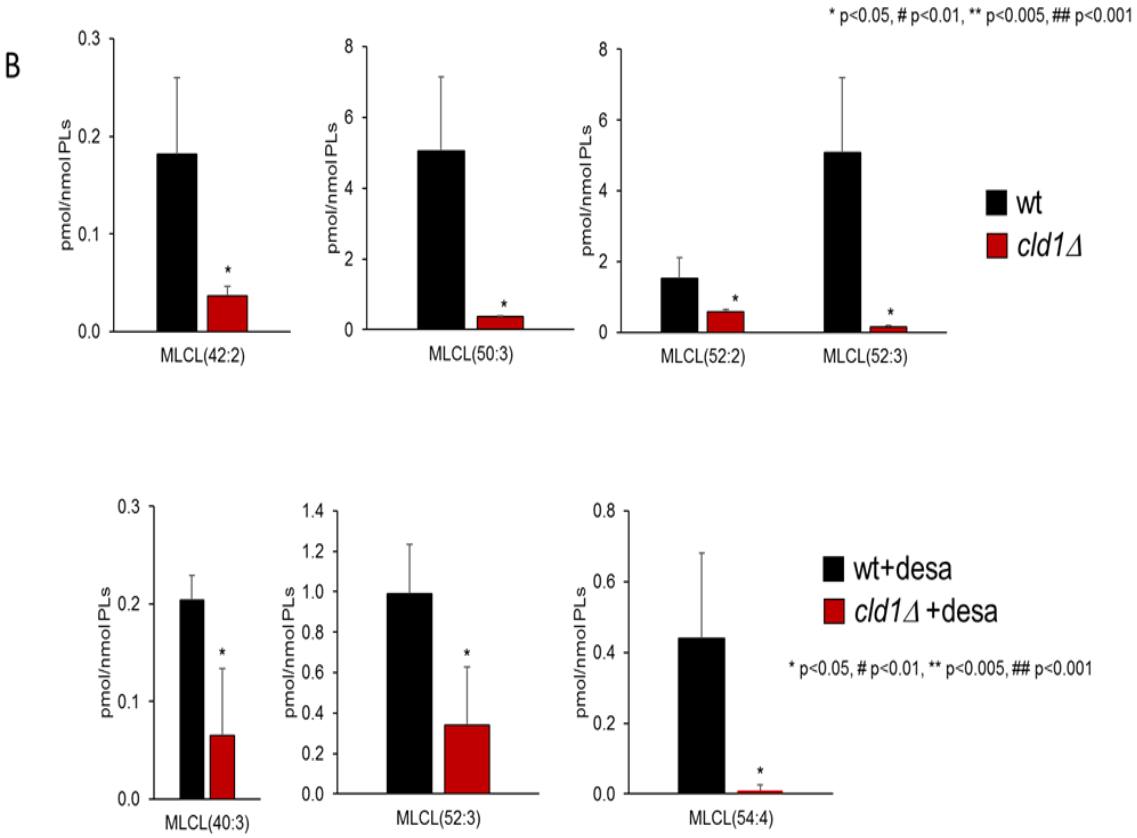

Figure 7-8. MLCL species in Δ^{12}-desaturase-expressing cells.

(A) Heat map of MLCL. (B) Quantitative assessment of total MLCL.

be further characterized. Subsequent studies testing the suppressive effects of human homologs on the iPLA2γ phenotype would help identify regulatory pathways of iPLA2γ present in human cells.

The yeast bioassay can also be utilized to identify new inhibitors of iPLA2γ that protect against oxidative damage of CL. Furthermore, a possible outcome of this study is the identification of new pathways that regulate iPLA2γ, which will contribute broadly to our understanding of lipid mediators. These inhibitors and regulators could be examined in animal models to elucidate their role in radiation-induced injury.

6. Is there a novel CL phospholipase in yeast?

Cld1 is the only known CL phospholipase that deacylates CL to form MLCL in yeast. Although *cld1Δ* has decreased levels of MLCL, MLCL is still detectable (Figure 7-8). Interestingly, the expression of Δ^{12}-desaturase increased levels of MLCL (Figure 7-8) suggesting that there is an unidentified CL phospholipase that prefers to deacylate CL with polyunsaturated fatty acyl chains. Future studies to identify this novel CL phospholipase will understand functions and regulations of CL remodeling, possibly leading to treatment for BTHS.

7. Novel roles of CL and CL remodeling

Although roles of CL remodeling have been shown in removal of damaged CL acyl chains and in cell differentiation in this dissertation, the functions of CL, CLox and CL remodeling in cellular signaling pathways are still unclear. My lab colleagues, Cunqi Ye and Jiajia Ji, determined that Cld1 is required for activation of the PKC pathway by SGA analysis. Additional genetic interactions of *CLD1* have yet to be uncovered and

further analysis of the SGA data can be used to identify functions of CL and CL remodeling.

Although we are at the end of this dissertation, people in our lab will not stop studying functions and regulation of CL and CL remodeling. I will be excited if future researchers are interested in joining in the world of CL research because of my studies. It will be a great pleasure if my findings stimulate creative ideas in the minds of fellow researchers.

REFERENCES

2017. GPX4 Blocks Ferroptosis to Drive the Survival of Chemoresistant Cells. *Cancer Discov*.

Abdel Khalek, W., F. Cortade, V. Ollendorff, L. Lapasset, L. Tintignac, B. Chabi, and C. Wrutniak-Cabello. 2014. SIRT3, a mitochondrial NAD(+)-dependent deacetylase, is involved in the regulation of myoblast differentiation. *PLoS One*. 9:e114388.

Abe, M., Y. Hasegawa, M. Oku, Y. Sawada, E. Tanaka, Y. Sakai, and H. Miyoshi. 2016. Mechanism for Remodeling of the Acyl Chain Composition of Cardiolipin Catalyzed by Saccharomyces cerevisiae Tafazzin. *J Biol Chem*. 291:15491-15502.

Abe, M., R. Niibayashi, S. Koubori, I. Moriyama, and H. Miyoshi. 2011. Molecular mechanisms for the induction of peroxidase activity of the cytochrome c-cardiolipin complex. *Biochemistry*. 50:8383-8391.

Acehan, D., Z. Khuchua, R.H. Houtkooper, A. Malhotra, J. Kaufman, F.M. Vaz, M. Ren, H.A. Rockman, D.L. Stokes, and M. Schlame. 2009. Distinct effects of tafazzin deletion in differentiated and undifferentiated mitochondria. *Mitochondrion*. 9:86-95.

Acehan, D., F. Vaz, R.H. Houtkooper, J. James, V. Moore, C. Tokunaga, W. Kulik, J. Wansapura, M.J. Toth, A. Strauss, and Z. Khuchua. 2011. Cardiac and skeletal muscle defects in a mouse model of human Barth syndrome. *J Biol Chem*. 286:899-908.

Acehan, D., Y. Xu, D.L. Stokes, and M. Schlame. 2007. Comparison of lymphoblast mitochondria from normal subjects and patients with Barth syndrome using electron microscopic tomography. *Lab Invest*. 87:40-48.

Ahmed, H.M., M. Miller, K. Nasir, J.W. McEvoy, D. Herrington, R.S. Blumenthal, and M.J. Blaha. 2016. Primary Low Level of High-Density Lipoprotein Cholesterol and Risks of Coronary Heart Disease, Cardiovascular Disease, and Death: Results From the Multi-Ethnic Study of Atherosclerosis. *Am J Epidemiol*. 183:875-883.

Altschul, S.F., W. Gish, W. Miller, E.W. Myers, and D.J. Lipman. 1990. Basic local alignment search tool. *J Mol Biol*. 215:403-410.

Andrisic, L., E.J. Collinson, O. Tehlivets, E. Perak, T. Zarkovic, I.W. Dawes, N. Zarkovic, and A. Cipak Gasparovic. 2015. Transcriptional and antioxidative responses to endogenous polyunsaturated fatty acid accumulation in yeast. *Mol Cell Biochem*. 399:27-37.

Ardite, E., J.A. Barbera, J. Roca, and J.C. Fernandez-Checa. 2004. Glutathione depletion impairs myogenic differentiation of murine skeletal muscle C2C12 cells through sustained NF-kappaB activation. *Am J Pathol*. 165:719-728.

Armstrong, L., K. Tilgner, G. Saretzki, S.P. Atkinson, M. Stojkovic, R. Moreno, S. Przyborski, and M. Lako. 2010. Human induced pluripotent stem cell lines show stress defense mechanisms and mitochondrial regulation similar to those of human embryonic stem cells. *Stem Cells*. 28:661-673.

Arya, M.A., A.K. Tai, E.C. Wooten, C.D. Parkin, E. Kudryavtseva, and G.S. Huggins. 2013. Notch pathway activation contributes to inhibition of C2C12 myoblast differentiation by ethanol. *PLoS One*. 8:e71632.

Athenstaedt, K., and G. Daum. 1999. Phosphatidic acid, a key intermediate in lipid metabolism. *Eur J Biochem*. 266:1-16.

Atkinson, J., A.A. Kapralov, N. Yanamala, Y.Y. Tyurina, A.A. Amoscato, L. Pearce, J. Peterson, Z. Huang, J. Jiang, A.K. Samhan-Arias, A. Maeda, W. Feng, K. Wasserloos, N.A. Belikova, V.A. Tyurin, H. Wang, J. Fletcher, Y. Wang, Vlasova, II, J. Klein-Seetharaman, D.A. Stoyanovsky, H. Bayir, B.R. Pitt, M.W. Epperly, J.S. Greenberger, and V.E. Kagan. 2011. A mitochondria-targeted inhibitor of cytochrome c peroxidase mitigates radiation-induced death. *Nat Commun*. 2:497.

Atkinson, K., S. Fogel, and S.A. Henry. 1980. Yeast mutant defective in phosphatidylserine synthesis. *J Biol Chem*. 255:6653-6661.

Baile, M.G., M. Sathappa, Y.W. Lu, E. Pryce, K. Whited, J.M. McCaffery, X. Han, N.N. Alder, and S.M. Claypool. 2014. Unremodeled and remodeled cardiolipin are functionally indistinguishable in yeast. *J Biol Chem*. 289:1768-1778.

Baile, M.G., K. Whited, and S.M. Claypool. 2013. Deacylation on the matrix side of the mitochondrial inner membrane regulates cardiolipin remodeling. *Mol Biol Cell*. 24:2008-2020.

Barth, P.G., H.R. Scholte, J.A. Berden, J.M. Van der Klei-Van Moorsel, I.E. Luyt-Houwen, E.T. Van 't Veer-Korthof, J.J. Van der Harten, and M.A. Sobotka-Plojhar. 1983. An X-linked mitochondrial disease affecting cardiac muscle, skeletal

muscle and neutrophil leucocytes. *Journal of the neurological sciences*. 62:327-355.

Barth, P.G., F. Valianpour, V.M. Bowen, J. Lam, M. Duran, F.M. Vaz, and R.J. Wanders. 2004. X-linked cardioskeletal myopathy and neutropenia (Barth syndrome): an update. *Am J Med Genet A*. 126A:349-354.

Barth, P.G., R.J. Wanders, P. Vreken, E.A. Janssen, J. Lam, and F. Baas. 1999a. X-linked cardioskeletal myopathy and neutropenia (Barth syndrome) (MIM 302060). *J Inherit Metab Dis*. 22:555-567.

Barth, P.G., R.J. Wanders, P. Vreken, E.A. Janssen, J. Lam, and F. Baas. 1999b. X-linked cardioskeletal myopathy and neutropenia (Barth syndrome)(MIM 302060). *Journal of inherited metabolic disease*. 22:555-567.

Basova, L.V., I.V. Kurnikov, L. Wang, V.B. Ritov, N.A. Belikova, Vlasova, II, A.A. Pacheco, D.E. Winnica, J. Peterson, H. Bayir, D.H. Waldeck, and V.E. Kagan. 2007. Cardiolipin switch in mitochondria: shutting off the reduction of cytochrome c and turning on the peroxidase activity. *Biochemistry*. 46:3423-3434.

Bathe, F.S., H. Rommelaere, and L.M. Machesky. 2007. Phenotypes of myopathy-related actin mutants in differentiated C2C12 myotubes. *BMC Cell Biol*. 8:2.

Bayir, H., V.A. Tyurin, Y.Y. Tyurina, R. Viner, V. Ritov, A.A. Amoscato, Q. Zhao, X.J. Zhang, K.L. Janesko-Feldman, H. Alexander, L.V. Basova, R.S. Clark, P.M. Kochanek, and V.E. Kagan. 2007. Selective early cardiolipin peroxidation after traumatic brain injury: an oxidative lipidomics analysis. *Ann Neurol*. 62:154-169.

Beranek, A., G. Rechberger, H. Knauer, H. Wolinski, S.D. Kohlwein, and R. Leber. 2009. Identification of a cardiolipin-specific phospholipase encoded by the gene CLD1 (YGR110W) in yeast. *J Biol Chem*. 284:11572-11578.

Beyer, K., and M. Klingenberg. 1985. ADP/ATP carrier protein from beef heart mitochondria has high amounts of tightly bound cardiolipin, as revealed by 31P nuclear magnetic resonance. *Biochemistry*. 24:3821-3826.

Bione, S., P. D'Adamo, E. Maestrini, A.K. Gedeon, P.A. Bolhuis, and D. Toniolo. 1996. A novel X-linked gene, G4.5. is responsible for Barth syndrome. *Nat Genet*. 12:385-389.

Boettcher, C., C. Pries, and C.M. Vangent. 1961. A Rapid and Sensitive Sub-Micro Phosphorus Determination. *Anal Chim Acta*. 24:203-&.

Bolhuis, P.A., G.W. Hensels, T.J. Hulsebos, F. Baas, and P.G. Barth. 1991. Mapping of the locus for X-linked cardioskeletal myopathy with neutropenia and abnormal mitochondria (Barth syndrome) to Xq28. *Am J Hum Genet*. 48:481-485.

Botstein, D., S.A. Chervitz, and J.M. Cherry. 1997. Yeast as a model organism. *Science*. 277:1259-1260.

Brandner, K., D.U. Mick, A.E. Frazier, R.D. Taylor, C. Meisinger, and P. Rehling. 2005. Taz1, an outer mitochondrial membrane protein, affects stability and assembly of inner membrane protein complexes: implications for Barth Syndrome. *Mol Biol Cell*. 16:5202-5214.

Brown, A.L., and J. Mark Brown. 2017. Critical Roles for alpha/beta Hydrolase Domain 5 (ABHD5)/Comparative Gene Identification-58 (CGI-58) at the Lipid Droplet Interface and Beyond. *Biochim Biophys Acta*.

Brown, G.C. 1999. Nitric oxide and mitochondrial respiration. *Biochim Biophys Acta*. 1411:351-369.

Bu, Y., and M.C. Schmidt. 1998. Identification of cis-acting elements in the SUC2 promoter of Saccharomyces cerevisiae required for activation of transcription. *Nucleic acids research*. 26:1002-1009.

Buland, J.R., K.J. Wasserloos, V.A. Tyurin, Y.Y. Tyurina, A.A. Amoscato, R.K. Mallampalli, B.B. Chen, J. Zhao, Y. Zhao, S. Ofori-Acquah, V.E. Kagan, and B.R. Pitt. 2016. Biosynthesis of oxidized lipid mediators via lipoprotein-associated phospholipase A2 hydrolysis of extracellular cardiolipin induces endothelial toxicity. *Am J Physiol Lung Cell Mol Physiol*. 311:L303-316.

Burattini, S., P. Ferri, M. Battistelli, R. Curci, F. Luchetti, and E. Falcieri. 2004. C2C12 murine myoblasts as a model of skeletal muscle development: morpho-functional characterization. *Eur J Histochem*. 48:223-233.

Camara, Y., C. Duval, B. Sibille, and F. Villarroya. 2007. Activation of mitochondrial-driven apoptosis in skeletal muscle cells is not mediated by reactive oxygen species production. *Int J Biochem Cell Biol*. 39:146-160.

Cao, J.Y., and S.J. Dixon. 2016. Mechanisms of ferroptosis. *Cell Mol Life Sci*. 73:2195-2209.

Carman, G.M., and S.A. Henry. 1989. Phospholipid biosynthesis in yeast. *Annu Rev Biochem*. 58:635-669.

Carman, G.M., and G.M. Zeimetz. 1996. Regulation of phospholipid biosynthesis in the yeast Saccharomyces cerevisiae. *J Biol Chem*. 271:13293-13296.

Chan, R.B., and G. Di Paolo. 2012. Knockout punch: cardiolipin oxidation in trauma. *Nat Neurosci*. 15:1325-1327.

Chang, S.C., P.N. Heacock, C.J. Clancey, and W. Dowhan. 1998a. The PEL1 gene (renamed PGS1) encodes the phosphatidylglycero-phosphate synthase of Saccharomyces cerevisiae. *J Biol Chem*. 273:9829-9836.

Chang, S.C., P.N. Heacock, E. Mileykovskaya, D.R. Voelker, and W. Dowhan. 1998b. Isolation and characterization of the gene (CLS1) encoding cardiolipin synthase in Saccharomyces cerevisiae. *J Biol Chem*. 273:14933-14941.

Chen, H., A. Chomyn, and D.C. Chan. 2005a. Disruption of fusion results in mitochondrial heterogeneity and dysfunction. *The Journal of biological chemistry*. 280:26185-26192.

Chen, H., S.A. Detmer, A.J. Ewald, E.E. Griffin, S.E. Fraser, and D.C. Chan. 2003. Mitofusins Mfn1 and Mfn2 coordinately regulate mitochondrial fusion and are essential for embryonic development. *The Journal of cell biology*. 160:189-200.

Chen, S., D. Liu, R.L. Finley, Jr., and M.L. Greenberg. 2010. Loss of mitochondrial DNA in the yeast cardiolipin synthase crd1 mutant leads to up-regulation of the protein kinase Swe1p that regulates the G2/M transition. *J Biol Chem*. 285:10397-10407.

Chen, S., M. Tarsio, P.M. Kane, and M.L. Greenberg. 2008. Cardiolipin mediates cross-talk between mitochondria and the vacuole. *Mol Biol Cell*. 19:5047-5058.

Chen, X.J., X. Wang, B.A. Kaufman, and R.A. Butow. 2005b. Aconitase couples metabolic regulation to mitochondrial DNA maintenance. *Science*. 307:714-717.

Cheng, H., D.J. Mancuso, X. Jiang, S. Guan, J. Yang, K. Yang, G. Sun, R.W. Gross, and X. Han. 2008. Shotgun lipidomics reveals the temporally dependent, highly diversified cardiolipin profile in the mammalian brain: temporally coordinated postnatal diversification of cardiolipin molecular species with neuronal remodeling. *Biochemistry*. 47:5869-5880.

Chu, C.T., J. Ji, R.K. Dagda, J.F. Jiang, Y.Y. Tyurina, A.A. Kapralov, V.A. Tyurin, N. Yanamala, I.H. Shrivastava, D. Mohammadyani, K.Z.Q. Wang, J. Zhu, J. Klein-Seetharaman, K. Balasubramanian, A.A. Amoscato, G. Borisenko, Z. Huang, A.M. Gusdon, A. Cheikhi, E.K. Steer, R. Wang, C. Baty, S. Watkins, I. Bahar, H. Bayir, and V.E. Kagan. 2013. Cardiolipin externalization to the outer mitochondrial membrane acts as an elimination signal for mitophagy in neuronal cells. *Nat Cell Biol*. 15:1197-1205.

Chung, S., P.P. Dzeja, R.S. Faustino, C. Perez-Terzic, A. Behfar, and A. Terzic. 2007. Mitochondrial oxidative metabolism is required for the cardiac differentiation of stem cells. *Nat Clin Pract Cardiovasc Med*. 4 Suppl 1:S60-67.

Ciavarra, G., and E. Zacksenhaus. 2011. Multiple pathways counteract cell death induced by RB1 loss: implications for cancer. *Cell Cycle*. 10:1533-1539.

Cipak, A., M. Hasslacher, O. Tehlivets, E.J. Collinson, M. Zivkovic, T. Matijevic, W. Wonisch, G. Waeg, I.W. Dawes, N. Zarkovic, and S.D. Kohlwein. 2006. Saccharomyces cerevisiae strain expressing a plant fatty acid desaturase produces polyunsaturated fatty acids and is susceptible to oxidative stress induced by lipid peroxidation. *Free Radic Biol Med*. 40:897-906.

Cipak, A., M. Jaganjac, O. Tehlivets, S.D. Kohlwein, and N. Zarkovic. 2008. Adaptation to oxidative stress induced by polyunsaturated fatty acids in yeast. *Biochim Biophys Acta*. 1781:283-287.

Claypool, S.M. 2009. Cardiolipin, a critical determinant of mitochondrial carrier protein assembly and function. *Biochim Biophys Acta*. 1788:2059-2068.

Claypool, S.M., P. Boontheung, J.M. McCaffery, J.A. Loo, and C.M. Koehler. 2008a. The cardiolipin transacylase, tafazzin, associates with two distinct respiratory components providing insight into Barth syndrome. *Molecular biology of the cell*. 19:5143-5155.

Claypool, S.M., Y. Oktay, P. Boontheung, J.A. Loo, and C.M. Koehler. 2008b. Cardiolipin defines the interactome of the major ADP/ATP carrier protein of the mitochondrial inner membrane. *J Cell Biol*. 182:937-950.

Claypool, S.M., K. Whited, S. Srijumnong, X. Han, and C.M. Koehler. 2011. Barth syndrome mutations that cause tafazzin complex lability. *J Cell Biol*. 192:447-462.

Cong, L., F.A. Ran, D. Cox, S. Lin, R. Barretto, N. Habib, P.D. Hsu, X. Wu, W. Jiang, L.A. Marraffini, and F. Zhang. 2013. Multiplex genome engineering using CRISPR/Cas systems. *Science*. 339:819-823.

Conrad, M., and J.P. Friedmann Angeli. 2015. Glutathione peroxidase 4 (Gpx4) and ferroptosis: what's so special about it? *Mol Cell Oncol*. 2:e995047.

DeVay, R.M., L. Dominguez-Ramirez, L.L. Lackner, S. Hoppins, H. Stahlberg, and J. Nunnari. 2009. Coassembly of Mgm1 isoforms requires cardiolipin and mediates mitochondrial inner membrane fusion. *J Cell Biol*. 186:793-803.

Diekert, K., A.I. de Kroon, G. Kispal, and R. Lill. 2001. Isolation and subfractionation of mitochondria from the yeast Saccharomyces cerevisiae. *Methods Cell Biol*. 65:37-51.

Dimitrov, L.N., R.B. Brem, L. Kruglyak, and D.E. Gottschling. 2009. Polymorphisms in multiple genes contribute to the spontaneous mitochondrial genome instability of Saccharomyces cerevisiae S288C strains. *Genetics*. 183:365-383.

Dixon, S.J., K.M. Lemberg, M.R. Lamprecht, R. Skouta, E.M. Zaitsev, C.E. Gleason, D.N. Patel, A.J. Bauer, A.M. Cantley, W.S. Yang, B. Morrison, 3rd, and B.R. Stockwell. 2012. Ferroptosis: an iron-dependent form of nonapoptotic cell death. *Cell*. 149:1060-1072.

Dudek, J., I.-F. Cheng, M. Balleininger, F.M. Vaz, K. Streckfuss-Bömeke, D. Hübscher, M. Vukotic, R.J. Wanders, P. Rehling, and K. Guan. 2013a. Cardiolipin deficiency affects respiratory chain function and organization in an induced pluripotent stem cell model of Barth syndrome. *Stem cell research*. 11:806-819.

Dudek, J., I.F. Cheng, M. Balleininger, F.M. Vaz, K. Streckfuss-Bomeke, D. Hubscher, M. Vukotic, R.J. Wanders, P. Rehling, and K. Guan. 2013b. Cardiolipin deficiency

affects respiratory chain function and organization in an induced pluripotent stem cell model of Barth syndrome. *Stem Cell Res*. 11:806-819.

Eble, K.S., W.B. Coleman, R.R. Hantgan, and C.C. Cunningham. 1990. Tightly associated cardiolipin in the bovine heart mitochondrial ATP synthase as analyzed by 31P nuclear magnetic resonance spectroscopy. *J Biol Chem*. 265:19434-19440.

Fabrizio, P., and V.D. Longo. 2003. The chronological life span of Saccharomyces cerevisiae. *Aging cell*. 2:73-81.

Folch, J., M. Lees, and G.H. Sloane Stanley. 1957. A simple method for the isolation and purification of total lipides from animal tissues. *The Journal of biological chemistry*. 226:497-509.

Fontanesi, F., C. Jin, A. Tzagoloff, and A. Barrientos. 2008. Transcriptional activators HAP/NF-Y rescue a cytochrome c oxidase defect in yeast and human cells. *Hum Mol Genet*. 17:775-788.

Fulco, M., R.L. Schiltz, S. Iezzi, M.T. King, P. Zhao, Y. Kashiwaya, E. Hoffman, R.L. Veech, and V. Sartorelli. 2003. Sir2 regulates skeletal muscle differentiation as a potential sensor of the redox state. *Mol Cell*. 12:51-62.

Garcia Fernandez, M., L. Troiano, L. Moretti, M. Nasi, M. Pinti, S. Salvioli, J. Dobrucki, and A. Cossarizza. 2002. Early changes in intramitochondrial cardiolipin distribution during apoptosis. *Cell Growth Differ*. 13:449-455.

Gardner, P.R. 2002. Aconitase: sensitive target and measure of superoxide. *Methods in enzymology*. 349:9-23.

Gebert, N., A.S. Joshi, S. Kutik, T. Becker, M. McKenzie, X.L. Guan, V.P. Mooga, D.A. Stroud, G. Kulkarni, M.R. Wenk, P. Rehling, C. Meisinger, M.T. Ryan, N. Wiedemann, M.L. Greenberg, and N. Pfanner. 2009. Mitochondrial cardiolipin involved in outer-membrane protein biogenesis: implications for Barth syndrome. *Curr Biol*. 19:2133-2139.

Gohil, V.M., P. Hayes, S. Matsuyama, H. Schagger, M. Schlame, and M.L. Greenberg. 2004. Cardiolipin biosynthesis and mitochondrial respiratory chain function are interdependent. *J Biol Chem*. 279:42612-42618.

Gonzalvez, F., and E. Gottlieb. 2007. Cardiolipin: setting the beat of apoptosis. *Apoptosis*. 12:877-885.

Griffiths, G.S., J. Doe, M. Jijiwa, P. Van Ry, V. Cruz, M. de la Vega, J.W. Ramos, D.J. Burkin, and M.L. Matter. 2015. Bit-1 is an essential regulator of myogenic differentiation. *J Cell Sci*. 128:1707-1717.

Grivennikova, V.G., and A.D. Vinogradov. 2006. Generation of superoxide by the mitochondrial Complex I. *Biochim Biophys Acta*. 1757:553-561.

Gu, Z., F. Valianpour, S. Chen, F.M. Vaz, G.A. Hakkaart, R.J. Wanders, and M.L. Greenberg. 2004. Aberrant cardiolipin metabolism in the yeast taz1 mutant: a model for Barth syndrome. *Mol Microbiol*. 51:149-158.

Hamai, N., M. Nakamura, and A. Asano. 1997. Inhibition of mitochondrial protein synthesis impaired C2C12 myoblast differentiation. *Cell Struct Funct*. 22:421-431.

Harried, S.S., M.D. Croghan, M.R. Kaller, P. Lopez, W. Zhong, R. Hungate, and P.J. Reider. 2009. Stereoselective synthesis of anti-N-protected 3-amino-1,2-

epoxides by nucleophilic addition to N-tert-butanesulfinyl imine of a glyceraldehyde synthon. *J Org Chem*. 74:5975-5982.

Hashemi Nazari, S.S., M. Shakiba, D. Khalili, F. Hadaegh, M. Tohidi, and F. Azizi. 2015. High-density lipoprotein cholesterol, a protective or a risk factor for developing coronary heart disease? Tehran Lipid and Glucose Study. *J Clin Lipidol*. 9:553-558.

Hauff, K.D., and G.M. Hatch. 2010. Reduction in cholesterol synthesis in response to serum starvation in lymphoblasts of a patient with Barth syndrome. *Biochem Cell Biol*. 88:595-602.

Hostetler, K.Y., H. van den Bosch, and L.L. van Deenen. 1972. The mechanism of cardiolipin biosynthesis in liver mitochondria. *Biochim Biophys Acta*. 260:507-513.

Houtkooper, R.H., H. Akbari, H. van Lenthe, W. Kulik, R.J. Wanders, M. Frentzen, and F.M. Vaz. 2006. Identification and characterization of human cardiolipin synthase. *FEBS Lett*. 580:3059-3064.

Houtkooper, R.H., R.J. Rodenburg, C. Thiels, H. van Lenthe, F. Stet, B.T. Poll-The, J.E. Stone, C.G. Steward, R.J. Wanders, J. Smeitink, W. Kulik, and F.M. Vaz. 2009. Cardiolipin and monolysocardiolipin analysis in fibroblasts, lymphocytes, and tissues using high-performance liquid chromatography-mass spectrometry as a diagnostic test for Barth syndrome. *Analytical biochemistry*. 387:230-237.

Houtkooper, R.H., and F.M. Vaz. 2008. Cardiolipin, the heart of mitochondrial metabolism. *Cell Mol Life Sci*. 65:2493-2506.

Hovius, R., H. Lambrechts, K. Nicolay, and B. de Kruijff. 1990. Improved methods to isolate and subfractionate rat liver mitochondria. Lipid composition of the inner and outer membrane. *Biochim Biophys Acta*. 1021:217-226.

Hsu, Y.H., D.S. Dumlao, J. Cao, and E.A. Dennis. 2013. Assessing phospholipase A2 activity toward cardiolipin by mass spectrometry. *PLoS One*. 8:e59267.

Hu, J., M. Wei, M.G. Mirisola, and V.D. Longo. 2013. Assessing chronological aging in Saccharomyces cerevisiae. *Methods in molecular biology*. 965:463-472.

Huang, Y., C. Powers, S.K. Madala, K.D. Greis, W.D. Haffey, J.A. Towbin, E. Purevjav, S. Javadov, A.W. Strauss, and Z. Khuchua. 2015. Cardiac metabolic pathways affected in the mouse model of barth syndrome. *PLoS One*. 10:e0128561.

Huffnagle, G.B., and M.C. Noverr. 2013. The emerging world of the fungal microbiome. *Trends in microbiology*. 21:334-341.

Huttemann, M., I. Lee, L.I. Grossman, J.W. Doan, and T.H. Sanderson. 2012. Phosphorylation of mammalian cytochrome c and cytochrome c oxidase in the regulation of cell destiny: respiration, apoptosis, and human disease. *Adv Exp Med Biol*. 748:237-264.

Imai, H., M. Matsuoka, T. Kumagai, T. Sakamoto, and T. Koumura. 2017. Lipid Peroxidation-Dependent Cell Death Regulated by GPx4 and Ferroptosis. *Curr Top Microbiol Immunol*. 403:143-170.

Jakovcic, S., G.S. Getz, M. Rabinowitz, H. Jakob, and H. Swift. 1971. Cardiolipin content of wild type and mutant yeasts in relation to mitochondrial function and development. *J Cell Biol*. 48:490-502.

Jasmer, D.P., and D. Kwak. 2006. Fusion and differentiation of murine C2C12 skeletal muscle cells that express Trichinella spiralis p43 protein. *Exp Parasitol*. 112:67-75.

Ji, J., Y.Y. Tyurina, M. Tang, W. Feng, D.B. Stolz, R.S. Clark, D.F. Meaney, P.M. Kochanek, V.E. Kagan, and H. Bayir. 2012. Mitochondrial injury after mechanical stretch of cortical neurons in vitro: biomarkers of apoptosis and selective peroxidation of anionic phospholipids. *J Neurotrauma*. 29:776-788.

Jiang, F., Z.M. Gu, J.M. Granger, and M.L. Greenberg. 1999. Cardiolipin synthase expression is essential for growth at elevated temperature and is regulated by factors affecting mitochondrial development. *Molecular Microbiology*. 31:373-379.

Jiang, F., H.S. Rizavi, and M.L. Greenberg. 1997. Cardiolipin is not essential for the growth of Saccharomyces cerevisiae on fermentable or non-fermentable carbon sources. *Mol Microbiol*. 26:481-491.

Jiang, F., M.T. Ryan, M. Schlame, M. Zhao, Z. Gu, M. Klingenberg, N. Pfanner, and M.L. Greenberg. 2000. Absence of cardiolipin in the crd1 null mutant results in decreased mitochondrial membrane potential and reduced mitochondrial function. *J Biol Chem*. 275:22387-22394.

Jiang, J., A. Bakan, A.A. Kapralov, K.I. Silva, Z. Huang, A.A. Amoscato, J. Peterson, V.K. Garapati, S. Saxena, H. Bayir, J. Atkinson, I. Bahar, and V.E. Kagan. 2014. Designing inhibitors of cytochrome c/cardiolipin peroxidase complexes: mitochondria-targeted imidazole-substituted fatty acids. *Free Radic Biol Med*. 71:221-230.

Johansson, M., X. Chen, S. Milanova, C. Santos, and D. Petranovic. 2016. PUFA-induced cell death is mediated by Yca1p-dependent and -independent pathways, and is reduced by vitamin C in yeast. *FEMS Yeast Res*. 16:fow007.

Joshi, A.S., N. Fei, and M.L. Greenberg. 2016. Get1p and Get2p are required for maintenance of mitochondrial morphology and normal cardiolipin levels. *FEMS Yeast Res*. 16.

Joshi, A.S., M.N. Thompson, N. Fei, M. Huttemann, and M.L. Greenberg. 2012. Cardiolipin and mitochondrial phosphatidylethanolamine have overlapping functions in mitochondrial fusion in Saccharomyces cerevisiae. *J Biol Chem*. 287:17589-17597.

Joshi, A.S., J. Zhou, V.M. Gohil, S. Chen, and M.L. Greenberg. 2009a. Cellular functions of cardiolipin in yeast. *Biochim Biophys Acta*. 1793:212-218.

Joshi, A.S., J. Zhou, V.M. Gohil, S. Chen, and M.L. Greenberg. 2009b. Cellular functions of cardiolipin in yeast. *Biochimica et biophysica acta*. 1793:212-218.

Kagan, V.E., H.A. Bayir, N.A. Belikova, O. Kapralov, Y.Y. Tyurina, V.A. Tyurin, J. Jiang, D.A. Stoyanovsky, P. Wipf, P.M. Kochanek, J.S. Greenberger, B. Pitt, A.A. Shvedova, and G. Borisenko. 2009. Cytochrome c/cardiolipin relations in mitochondria: a kiss of death. *Free Radic Biol Med*. 46:1439-1453.

Kagan, V.E., G.G. Borisenko, Y.Y. Tyurina, V.A. Tyurin, J. Jiang, A.I. Potapovich, V. Kini, A.A. Amoscato, and Y. Fujii. 2004. Oxidative lipidomics of apoptosis: redox catalytic interactions of cytochrome c with cardiolipin and phosphatidylserine. *Free Radic Biol Med*. 37:1963-1985.

Kagan, V.E., C.T. Chu, Y.Y. Tyurina, A. Cheikhi, and H. Bayir. 2014. Cardiolipin asymmetry, oxidation and signaling. *Chem Phys Lipids*. 179:64-69.

Kagan, V.E., A.A. Shvedova, and K.N. Novikov. 1978. [Participation of phospholipases in the "repair" of photoreceptor membranes subjected to peroxidation]. *Biofizika*. 23:279-284.

Kagan, V.E., V.A. Tyurin, J. Jiang, Y.Y. Tyurina, V.B. Ritov, A.A. Amoscato, A.N. Osipov, N.A. Belikova, A.A. Kapralov, and V. Kini. 2005a. Cytochrome c acts as a cardiolipin oxygenase required for release of proapoptotic factors. *Nature chemical biology*. 1:223-232.

Kagan, V.E., V.A. Tyurin, J. Jiang, Y.Y. Tyurina, V.B. Ritov, A.A. Amoscato, A.N. Osipov, N.A. Belikova, A.A. Kapralov, V. Kini, Vlasova, II, Q. Zhao, M. Zou, P. Di, D.A. Svistunenko, I.V. Kurnikov, and G.G. Borisenko. 2005b. Cytochrome c acts as a cardiolipin oxygenase required for release of proapoptotic factors. *Nat Chem Biol*. 1:223-232.

Kagan, V.E., Y.Y. Tyurina, V.A. Tyurin, D. Mohammadyani, J.P. Angeli, S.V. Baranov, J. Klein-Seetharaman, R.M. Friedlander, R.K. Mallampalli, M. Conrad, and H. Bayir. 2015. Cardiolipin signaling mechanisms: collapse of asymmetry and oxidation. *Antioxid Redox Signal*. 22:1667-1680.

Kapralov, A.A., N. Yanamala, Y.Y. Tyurina, L. Castro, A. Samhan-Arias, Y.A. Vladimirov, A. Maeda, A.A. Weitz, J. Peterson, D. Mylnikov, V. Demicheli, V. Tortora, J. Klein-Seetharaman, R. Radi, and V.E. Kagan. 2011. Topography of tyrosine residues and their involvement in peroxidation of polyunsaturated cardiolipin in

cytochrome c/cardiolipin peroxidase complexes. *Biochim Biophys Acta*. 1808:2147-2155.

Kelley, R.I., J.P. Cheatham, B.J. Clark, M.A. Nigro, B.R. Powell, G.W. Sherwood, J.T. Sladky, and W.P. Swisher. 1991. X-linked dilated cardiomyopathy with neutropenia, growth retardation, and 3-methylglutaconic aciduria. *The Journal of pediatrics*. 119:738-747.

Kelly, B.L., and M.L. Greenberg. 1990. Characterization and regulation of phosphatidylglycerolphosphate phosphatase in Saccharomyces cerevisiae. *Biochim Biophys Acta*. 1046:144-150.

Kiebish, M.A., X. Han, H. Cheng, J.H. Chuang, and T.N. Seyfried. 2008. Cardiolipin and electron transport chain abnormalities in mouse brain tumor mitochondria: lipidomic evidence supporting the Warburg theory of cancer. *J Lipid Res*. 49:2545-2556.

Kiebish, M.A., K. Yang, X. Liu, D.J. Mancuso, S. Guan, Z. Zhao, H.F. Sims, R. Cerqua, W.T. Cade, X. Han, and R.W. Gross. 2013a. Dysfunctional cardiac mitochondrial bioenergetic, lipidomic, and signaling in a murine model of Barth syndrome. *J Lipid Res*. 54:1312-1325.

Kiebish, M.A., K. Yang, X. Liu, D.J. Mancuso, S. Guan, Z. Zhao, H.F. Sims, R. Cerqua, W.T. Cade, X. Han, and R.W. Gross. 2013b. Dysfunctional cardiac mitochondrial bioenergetic, lipidomic, and signaling in a murine model of Barth syndrome. *J Lipid Res*. 54:1312-1325.

Kim, J., and C.L. Hoppel. 2011. Monolysocardiolipin: improved preparation with high yield. *J Lipid Res*. 52:389-392.

Klingenberg, M. 2009. Cardiolipin and mitochondrial carriers. *Biochim Biophys Acta*. 1788:2048-2058.

Kohrer, K., and H. Domdey. 1991. Preparation of high molecular weight RNA. *Methods Enzymol*. 194:398-405.

Koshkin, V., and M.L. Greenberg. 2000. Oxidative phosphorylation in cardiolipin-lacking yeast mitochondria. *Biochem J*. 347 Pt 3:687-691.

Koshkin, V., and M.L. Greenberg. 2002. Cardiolipin prevents rate-dependent uncoupling and provides osmotic stability in yeast mitochondria. *Biochem J*. 364:317-322.

Krebs, J.J., H. Hauser, and E. Carafoli. 1979. Asymmetric distribution of phospholipids in the inner membrane of beef heart mitochondria. *J Biol Chem*. 254:5308-5316.

Kriska, T., W. Korytowski, and A.W. Girotti. 2005. Role of mitochondrial cardiolipin peroxidation in apoptotic photokilling of 5-aminolevulinate-treated tumor cells. *Arch Biochem Biophys*. 433:435-446.

Kuo, W.N., D.L. Walbey, D.L. Davis, and L.K. McCall. 1994. Dual modulation of the phosphorylation of endogenous yeast proteins by arachidonic acid and phosphatidylinositol. *Cytobios*. 78:241-247.

Kutik, S., M. Rissler, X.L. Guan, B. Guiard, G. Shui, N. Gebert, P.N. Heacock, P. Rehling, W. Dowhan, M.R. Wenk, N. Pfanner, and N. Wiedemann. 2008. The translocator maintenance protein Tam41 is required for mitochondrial cardiolipin biosynthesis. *J Cell Biol*. 183:1213-1221.

Kwast, K.E., P.V. Burke, B.T. Staahl, and R.O. Poyton. 1999. Oxygen sensing in yeast: evidence for the involvement of the respiratory chain in regulating the transcription of a subset of hypoxic genes. *Proc Natl Acad Sci U S A*. 96:5446-5451.

Lack, N., E.D. Lowe, J. Liu, L.D. Eltis, M.E. Noble, E. Sim, and I.M. Westwood. 2008. Structure of HsaD, a steroid-degrading hydrolase, from Mycobacterium tuberculosis. *Acta Crystallogr Sect F Struct Biol Cryst Commun*. 64:2-7.

Lange, C., J.H. Nett, B.L. Trumpower, and C. Hunte. 2001. Specific roles of protein-phospholipid interactions in the yeast cytochrome bc1 complex structure. *EMBO J*. 20:6591-6600.

Leary, S.C., B.J. Battersby, R.G. Hansford, and C.D. Moyes. 1998. Interactions between bioenergetics and mitochondrial biogenesis. *Biochim Biophys Acta*. 1365:522-530.

Lecocq, J., and C.E. Ballou. 1964. On the Structure of Cardiolipin. *Biochemistry*. 3:976-980.

Lee, I., A. Pecinova, P. Pecina, B.G. Neel, T. Araki, R. Kucherlapati, A.E. Roberts, and M. Huttemann. 2010. A suggested role for mitochondria in Noonan syndrome. *Biochim Biophys Acta*. 1802:275-283.

Lee, J.D., M. Ueno, Y. Miyajima, and H. Nakamura. 2007. Synthesis of boron cluster lipids: closo-dodecaborate as an alternative hydrophilic function of boronated liposomes for neutron capture therapy. *Org Lett*. 9:323-326.

Lefevre, C., F. Jobard, F. Caux, B. Bouadjar, A. Karaduman, R. Heilig, H. Lakhdar, A. Wollenberg, J.L. Verret, J. Weissenbach, M. Ozguc, M. Lathrop, J.F. Prud'homme, and J. Fischer. 2001. Mutations in CGI-58, the gene encoding a new protein of the esterase/lipase/thioesterase subfamily, in Chanarin-Dorfman syndrome. *Am J Hum Genet*. 69:1002-1012.

Liebisch, G., J.A. Vizcaino, H. Kofeler, M. Trotzmuller, W.J. Griffiths, G. Schmitz, F. Spener, and M.J. Wakelam. 2013. Shorthand notation for lipid structures derived from mass spectrometry. *J Lipid Res*. 54:1523-1530.

Liu, C.T., and G.A. Brooks. 2012. Mild heat stress induces mitochondrial biogenesis in C2C12 myotubes. *J Appl Physiol (1985)*. 112:354-361.

Liu, G.Y., S.H. Moon, C.M. Jenkins, M. Li, H.F. Sims, S. Guan, and R.W. Gross. 2017. The phospholipase iPLA2gamma is a major mediator releasing oxidized aliphatic chains from cardiolipin, integrating mitochondrial bioenergetics and signaling. *J Biol Chem*. 292:10672-10684.

Lok, C.M., A.P.J. Mank, and J.P. Ward. 1985. Synthesis of Glycidol Esters and Mono-Di-Acylglycerols from Glycidol. *Chemistry and Physics of Lipids*. 36:329-334.

Lu, Y.W., and S.M. Claypool. 2015. Disorders of phospholipid metabolism: an emerging class of mitochondrial disease due to defects in nuclear genes. *Front Genet*. 6:3.

Machida, K., T. Tanaka, K. Fujita, and M. Taniguchi. 1998. Farnesol-induced generation of reactive oxygen species via indirect inhibition of the mitochondrial electron transport chain in the yeast Saccharomyces cerevisiae. *J Bacteriol*. 180:4460-4465.

Maddalena, L.A., M. Ghelfi, J. Atkinson, and J.A. Stuart. 2017. The mitochondria-targeted imidazole substituted oleic acid 'TPP-IOA' affects mitochondrial bioenergetics and its protective efficacy in cells is influenced by cellular dependence on aerobic metabolism. *Biochim Biophys Acta*. 1858:73-85.

Maguire, J.J., Y.Y. Tyurina, D. Mohammadyani, A.A. Kapralov, T.S. Anthonymuthu, F. Qu, A.A. Amoscato, L.J. Sparvero, V.A. Tyurin, J. Planas-Iglesias, R.R. He, J. Klein-Seetharaman, H. Bayir, and V.E. Kagan. 2017. Known unknowns of cardiolipin signaling: The best is yet to come. *Biochim Biophys Acta*. 1862:8-24.

Maiorino, M., M. Conrad, and F. Ursini. 2017. GPx4, Lipid Peroxidation, and Cell Death: Discoveries, Rediscoveries, and Open Issues. *Antioxid Redox Signal*.

Malhotra, A., I. Edelman-Novemsky, Y. Xu, H. Plesken, J. Ma, M. Schlame, and M. Ren. 2009. Role of calcium-independent phospholipase A2 in the pathogenesis of Barth syndrome. *Proc Natl Acad Sci U S A*. 106:2337-2341.

Mandal, S., A.G. Lindgren, A.S. Srivastava, A.T. Clark, and U. Banerjee. 2011. Mitochondrial function controls proliferation and early differentiation potential of embryonic stem cells. *Stem Cells*. 29:486-495.

Mao, G., F. Qu, C.M. St Croix, Y.Y. Tyurina, J. Planas-Iglesias, J. Jiang, Z. Huang, A.A. Amoscato, V.A. Tyurin, A.A. Kapralov, A. Cheikhi, J. Maguire, J. Klein-Seetharaman, H. Bayir, and V.E. Kagan. 2016. Mitochondrial Redox Opto-Lipidomics Reveals Mono-Oxygenated Cardiolipins as Pro-Apoptotic Death Signals. *ACS Chem Biol*. 11:530-540.

Mazzocco, M.M., A.E. Henry, and R.I. Kelly. 2007a. Barth syndrome is associated with a cognitive phenotype. *J Dev Behav Pediatr*. 28:22-30.

Mazzocco, M.M., A.E. Henry, and R.I. Kelly. 2007b. Barth syndrome is associated with a cognitive phenotype. *Journal of developmental and behavioral pediatrics: JDBP*. 28:22.

McKenzie, M., M. Lazarou, D.R. Thorburn, and M.T. Ryan. 2006. Mitochondrial respiratory chain supercomplexes are destabilized in Barth Syndrome patients. *J Mol Biol*. 361:462-469.

Mileykovskaya, E., and W. Dowhan. 2014. Cardiolipin-dependent formation of mitochondrial respiratory supercomplexes. *Chem Phys Lipids*. 179:42-48.

Minners, J., L. Lacerda, D.M. Yellon, L.H. Opie, C.J. McLeod, and M.N. Sack. 2007. Diazoxide-induced respiratory inhibition - a putative mitochondrial K(ATP) channel independent mechanism of pharmacological preconditioning. *Mol Cell Biochem*. 294:11-18.

Moffat, C., L. Bhatia, T. Nguyen, P. Lynch, M. Wang, D. Wang, O.R. Ilkayeva, X. Han, M.D. Hirschey, S.M. Claypool, and E.L. Seifert. 2014. Acyl-CoA thioesterase-2 facilitates mitochondrial fatty acid oxidation in the liver. *J Lipid Res*. 55:2458-2470.

Mori, K. 2012. , Pheromone synthesis. Part 253: Synthesis of the racemates and enantiomers of triglycerides of male Drosophila fruit flies with special emphasis on the preparation of enantiomerically pure 1-monoglycerides. *Tetrahedron*. 68 8441-8449.

Mullen, P.J., B. Luscher, H. Scharnagl, S. Krahenbuhl, and K. Brecht. 2010. Effect of simvastatin on cholesterol metabolism in C2C12 myotubes and HepG2 cells, and consequences for statin-induced myopathy. *Biochem Pharmacol*. 79:1200-1209.

Murray, J., and J.M. Huss. 2011. Estrogen-related receptor alpha regulates skeletal myocyte differentiation via modulation of the ERK MAP kinase pathway. *Am J Physiol Cell Physiol*. 301:C630-645.

Musatov, A. 2006. Contribution of peroxidized cardiolipin to inactivation of bovine heart cytochrome c oxidase. *Free Radic Biol Med*. 41:238-246.

Nakagawa, Y. 2004. Initiation of apoptotic signal by the peroxidation of cardiolipin of mitochondria. *Ann N Y Acad Sci*. 1011:177-184.

Nehlin, J.O., and H. Ronne. 1990. Yeast MIG1 repressor is related to the mammalian early growth response and Wilms' tumour finger proteins. *The EMBO journal*. 9:2891-2898.

Nicholls, D.G., V.M. Darley-Usmar, M. Wu, P.B. Jensen, G.W. Rogers, and D.A. Ferrick. 2010. Bioenergetic profile experiment using C2C12 myoblast cells. *J Vis Exp*.

Ocampo, A., J. Liu, E.A. Schroeder, G.S. Shadel, and A. Barrientos. 2012. Mitochondrial respiratory thresholds regulate yeast chronological life span and its extension by caloric restriction. *Cell Metab*. 16:55-67.

Ogbi, M., and J.A. Johnson. 2006. Protein kinase Cepsilon interacts with cytochrome c oxidase subunit IV and enhances cytochrome c oxidase activity in neonatal cardiac myocyte preconditioning. *Biochem J*. 393:191-199.

Ollis, D.L., E. Cheah, M. Cygler, B. Dijkstra, F. Frolow, S.M. Franken, M. Harel, S.J. Remington, I. Silman, J. Schrag, J.L. Sussman, K.H.G. Verschueren, and A. Goldman. 1992. The α/β hydrolase fold. *Protein Engineering, Design and Selection*. 5:197-211.

Osman, C., M. Haag, F.T. Wieland, B. Brugger, and T. Langer. 2010. A mitochondrial phosphatase required for cardiolipin biosynthesis: the PGP phosphatase Gep4. *EMBO J*. 29:1976-1987.

Palsdottir, H., C.G. Lojero, B.L. Trumpower, and C. Hunte. 2003. Structure of the yeast cytochrome bc1 complex with a hydroxyquinone anion Qo site inhibitor bound. *J Biol Chem*. 278:31303-31311.

Pangborn, M.C. 1942. Isolation and purification of a serologically active phospholipid from beef heart. *J Biol Chem*. 143:247-256.

Pangborn, M.C. 1947. The composition of cardiolipin. *J Biol Chem*. 168:351-361.

Pangborn, M.C. 1948. Method of recovering and refining cardiolipin. No. 2,456,836. *J Pat Off Soc*. 108:Unknown.

Paradies, G., G. Petrosillo, M. Pistolese, and F.M. Ruggiero. 2000. The effect of reactive oxygen species generated from the mitochondrial electron transport chain on the cytochrome c oxidase activity and on the cardiolipin content in bovine heart submitochondrial particles. *FEBS Lett*. 466:323-326.

Paradies, G., G. Petrosillo, M. Pistolese, and F.M. Ruggiero. 2001. Reactive oxygen species generated by the mitochondrial respiratory chain affect the complex III

activity via cardiolipin peroxidation in beef-heart submitochondrial particles. *Mitochondrion*. 1:151-159.

Paradies, G., F.M. Ruggiero, G. Petrosillo, and E. Quagliariello. 1998. Peroxidative damage to cardiac mitochondria: cytochrome oxidase and cardiolipin alterations. *FEBS letters*. 424:155-158.

Patil, V.A., J.L. Fox, V.M. Gohil, D.R. Winge, and M.L. Greenberg. 2013. Loss of cardiolipin leads to perturbation of mitochondrial and cellular iron homeostasis. *J Biol Chem*. 288:1696-1705.

Patil, V.A., and M.L. Greenberg. 2013. Cardiolipin-mediated cellular signaling. *Adv Exp Med Biol*. 991:195-213.

Petrosillo, G., P. Portincasa, I. Grattagliano, G. Casanova, M. Matera, F.M. Ruggiero, D. Ferri, and G. Paradies. 2007. Mitochondrial dysfunction in rat with nonalcoholic fatty liver Involvement of complex I, reactive oxygen species and cardiolipin. *Biochim Biophys Acta*. 1767:1260-1267.

Petrosillo, G., F.M. Ruggiero, M. Pistolese, and G. Paradies. 2001. Reactive oxygen species generated from the mitochondrial electron transport chain induce cytochrome c dissociation from beef-heart submitochondrial particles via cardiolipin peroxidation. Possible role in the apoptosis. *FEBS Lett*. 509:435-438.

Pfeifer, K., K.S. Kim, S. Kogan, and L. Guarente. 1989. Functional dissection and sequence of yeast HAP1 activator. *Cell*. 56:291-301.

Pfeiffer, K., V. Gohil, R.A. Stuart, C. Hunte, U. Brandt, M.L. Greenberg, and H. Schagger. 2003. Cardiolipin stabilizes respiratory chain supercomplexes. *J Biol Chem*. 278:52873-52880.

Philp, A., M.Y. Belew, A. Evans, D. Pham, I. Sivia, A. Chen, S. Schenk, and K. Baar. 2011. The PGC-1alpha-related coactivator promotes mitochondrial and myogenic adaptations in C2C12 myotubes. *Am J Physiol Regul Integr Comp Physiol*. 301:R864-872.

Poyry, S., O. Cramariuc, P.A. Postila, K. Kaszuba, M. Sarewicz, A. Osyczka, I. Vattulainen, and T. Rog. 2013. Atomistic simulations indicate cardiolipin to have an integral role in the structure of the cytochrome bc1 complex. *Biochim Biophys Acta*. 1827:769-778.

Prigione, A., B. Fauler, R. Lurz, H. Lehrach, and J. Adjaye. 2010. The senescence-related mitochondrial/oxidative stress pathway is repressed in human induced pluripotent stem cells. *Stem Cells*. 28:721-733.

Raja, V., A.S. Joshi, G. Li, K.R. Maddipati, and M.L. Greenberg. 2017. Loss of Cardiolipin Leads to Perturbation of Acetyl-CoA Synthesis. *J Biol Chem*. 292:1092-1102.

Ren, M., C.K. Phoon, and M. Schlame. 2014. Metabolism and function of mitochondrial cardiolipin. *Prog Lipid Res*. 55:1-16.

Rijken, P.J., R.H. Houtkooper, H. Akbari, J.F. Brouwers, M.C. Koorengevel, B. de Kruijff, M. Frentzen, F.M. Vaz, and A.I. de Kroon. 2009. Cardiolipin molecular species with shorter acyl chains accumulate in Saccharomyces cerevisiae mutants

lacking the acyl coenzyme A-binding protein Acb1p: new insights into acyl chain remodeling of cardiolipin. *J Biol Chem*. 284:27609-27619.

Roodsari, F.S., D.P. Wu, G.S. Pum, and J. Hajdu. 1999. A new approach to the stereospecific synthesis of phospholipids. The use of L-glyceric acid for the preparation of diacylglycerols, phosphatidylcholines, and related derivatives. *J Org Chem*. 64:7727-7737.

Ryall, J.G. 2013. Metabolic reprogramming as a novel regulator of skeletal muscle development and regeneration. *FEBS J*. 280:4004-4013.

Sakai, O., T. Yasuzawa, Y. Sumikawa, T. Ueta, H. Imai, A. Sawabe, and S. Ueshima. 2017. Role of GPx4 in human vascular endothelial cells, and the compensatory activity of brown rice on GPx4 ablation condition. *Pathophysiology*. 24:9-15.

Salgo, M.G., F.P. Corongiu, and A. Sevanian. 1993. Enhanced interfacial catalysis and hydrolytic specificity of phospholipase A2 toward peroxidized phosphatidylcholine vesicles. *Arch Biochem Biophys*. 304:123-132.

Santangelo, G.M. 2006. Glucose signaling in Saccharomyces cerevisiae. *Microbiol Mol Biol Rev*. 70:253-282.

Schlame, M. 2008. Cardiolipin synthesis for the assembly of bacterial and mitochondrial membranes. *J Lipid Res*. 49:1607-1620.

Schlame, M. 2013. Cardiolipin remodeling and the function of tafazzin. *Biochim Biophys Acta*. 1831:582-588.

Schlame, M., S. Brody, and K.Y. Hostetler. 1993. Mitochondrial cardiolipin in diverse eukaryotes. Comparison of biosynthetic reactions and molecular acyl species. *Eur J Biochem*. 212:727-735.

Schlame, M., and M.L. Greenberg. 2017. Biosynthesis, remodeling and turnover of mitochondrial cardiolipin. *Biochim Biophys Acta*. 1862:3-7.

Schlame, M., R.I. Kelley, A. Feigenbaum, J.A. Towbin, P.M. Heerdt, T. Schieble, R.J. Wanders, S. DiMauro, and T.J. Blanck. 2003. Phospholipid abnormalities in children with Barth syndrome. *J Am Coll Cardiol*. 42:1994-1999.

Schlame, M., and M. Ren. 2006. Barth syndrome, a human disorder of cardiolipin metabolism. *FEBS Lett*. 580:5450-5455.

Schlame, M., and M. Ren. 2009. The role of cardiolipin in the structural organization of mitochondrial membranes. *Biochim Biophys Acta*. 1788:2080-2083.

Schlame, M., M. Ren, Y. Xu, M.L. Greenberg, and I. Haller. 2005. Molecular symmetry in mitochondrial cardiolipins. *Chem Phys Lipids*. 138:38-49.

Schlame, M., D. Rua, and M.L. Greenberg. 2000a. The biosynthesis and functional role of cardiolipin. *Prog Lipid Res*. 39:257-288.

Schlame, M., D. Rua, and M.L. Greenberg. 2000b. The biosynthesis and functional role of cardiolipin. *Prog Lipid Res*. 39:257-288.

Schlame, M., J.A. Towbin, P.M. Heerdt, R. Jehle, S. DiMauro, and T.J. Blanck. 2002. Deficiency of tetralinoleoyl-cardiolipin in Barth syndrome. *Annals of neurology*. 51:634-637.

Schug, Z.T., and E. Gottlieb. 2009. Cardiolipin acts as a mitochondrial signalling platform to launch apoptosis. *Biochim Biophys Acta*. 1788:2022-2031.

Schuller, H.J. 2003. Transcriptional control of nonfermentative metabolism in the yeast Saccharomyces cerevisiae. *Curr Genet*. 43:139-160.

Schweiger, M., A. Lass, R. Zimmermann, T.O. Eichmann, and R. Zechner. 2009. Neutral lipid storage disease: genetic disorders caused by mutations in adipose triglyceride lipase/PNPLA2 or CGI-58/ABHD5. *Am J Physiol Endocrinol Metab*. 297:E289-296.

Sharpley, M.S., R.J. Shannon, F. Draghi, and J. Hirst. 2006. Interactions between phospholipids and NADH:ubiquinone oxidoreductase (complex I) from bovine mitochondria. *Biochemistry*. 45:241-248.

Shen, Z., Y. Li, A.N. Gasparski, H. Abeliovich, and M.L. Greenberg. 2017. Cardiolipin Regulates Mitophagy through the Protein Kinase C Pathway. *J Biol Chem*. 292:2916-2923.

Shen, Z., C. Ye, K. McCain, and M.L. Greenberg. 2015. The Role of Cardiolipin in Cardiovascular Health. *Biomed Res Int*. 2015:891707.

Shinzawa-Itoh, K., H. Aoyama, K. Muramoto, H. Terada, T. Kurauchi, Y. Tadehara, A. Yamasaki, T. Sugimura, S. Kurono, K. Tsujimoto, T. Mizushima, E. Yamashita, T. Tsukihara, and S. Yoshikawa. 2007. Structures and physiological roles of 13 integral lipids of bovine heart cytochrome c oxidase. *EMBO J*. 26:1713-1725.

Simbeni, R., K. Tangemann, M. Schmidt, C. Ceolotto, F. Paltauf, and G. Daum. 1993. Import of phosphatidylserine into isolated yeast mitochondria. *Biochim Biophys Acta*. 1145:1-7.

Song, H., M. Wohltmann, M. Tan, J.H. Ladenson, and J. Turk. 2014. Group VIA phospholipase A2 mitigates palmitate-induced beta-cell mitochondrial injury and apoptosis. *J Biol Chem*. 289:14194-14210.

Soustek, M.S., D.J. Falk, C.S. Mah, M.J. Toth, M. Schlame, A.S. Lewin, and B.J. Byrne. 2011. Characterization of a transgenic short hairpin RNA-induced murine model of Tafazzin deficiency. *Human gene therapy*. 22:865-871.

Spencer, C.T., R.M. Bryant, J. Day, I.L. Gonzalez, S.D. Colan, W.R. Thompson, J. Berthy, S.P. Redfearn, and B.J. Byrne. 2006a. Cardiac and clinical phenotype in Barth syndrome. *Pediatrics*. 118:e337-346.

Spencer, C.T., R.M. Bryant, J. Day, I.L. Gonzalez, S.D. Colan, W.R. Thompson, J. Berthy, S.P. Redfearn, and B.J. Byrne. 2006b. Cardiac and clinical phenotype in Barth syndrome. *Pediatrics*. 118:e337-e346.

Spencer, C.T., B.J. Byrne, R.M. Bryant, R. Margossian, M. Maisenbacher, P. Breitenger, P.B. Benni, S. Redfearn, E. Marcus, and W.T. Cade. 2011. Impaired cardiac reserve and severely diminished skeletal muscle O(2) utilization mediate exercise intolerance in Barth syndrome. *Am J Physiol Heart Circ Physiol*. 301:H2122-2129.

Spencer, J.F., and D.M. Spencer. 2013. Yeasts in natural and artificial habitats. Springer Science & Business Media.

Spencer, J.F.T., and D.M. Spencer. 1997. Ecology: Where Yeasts Live. *In* Yeasts in Natural and Artificial Habitats. J.F.T. Spencer and D.M. Spencer, editors. Springer Berlin Heidelberg, Berlin, Heidelberg. 33-58.

Stadlbauer, S., R. Frank, I. Maulana, P. Lonnecke, B. Kirchner, and E. Hey-Hawkins. 2009. Synthesis and Reactivity of ortho-Carbaborane-Containing Chiral Aminohalophosphines. *Inorg Chem*. 48:6072-6082.

Su, X., and W. Dowhan. 2006. Translational regulation of nuclear gene COX4 expression by mitochondrial content of phosphatidylglycerol and cardiolipin in Saccharomyces cerevisiae. *Molecular and cellular biology*. 26:743-753.

Sun, G., K. Yang, Z. Zhao, S. Guan, X. Han, and R.W. Gross. 2008. Matrix-assisted laser desorption/ionization time-of-flight mass spectrometric analysis of cellular glycerophospholipids enabled by multiplexed solvent dependent analyte-matrix interactions. *Anal Chem*. 80:7576-7585.

Szijgyarto, Z., A. Garedew, C. Azevedo, and A. Saiardi. 2011. Influence of inositol pyrophosphates on cellular energy dynamics. *Science*. 334:802-805.

Tamai, K.T., and M.L. Greenberg. 1990. Biochemical characterization and regulation of cardiolipin synthase in Saccharomyces cerevisiae. *Biochim Biophys Acta*. 1046:214-222.

Tamura, Y., Y. Harada, S. Nishikawa, K. Yamano, M. Kamiya, T. Shiota, T. Kuroda, O. Kuge, H. Sesaki, K. Imai, K. Tomii, and T. Endo. 2013. Tam41 is a CDP-diacylglycerol synthase required for cardiolipin biosynthesis in mitochondria. *Cell Metab*. 17:709-718.

Testet, E., J. Laroche-Traineau, A. Noubhani, D. Coulon, O. Bunoust, N. Camougrand, S. Manon, R. Lessire, and J.J. Bessoule. 2005. Ypr140wp, 'the yeast tafazzin', displays a mitochondrial lysophosphatidylcholine (lyso-PC) acyltransferase activity related to triacylglycerol and mitochondrial lipid synthesis. *Biochem J*. 387:617-626.

Tormos, K.V., E. Anso, R.B. Hamanaka, J. Eisenbart, J. Joseph, B. Kalyanaraman, and N.S. Chandel. 2011. Mitochondrial complex III ROS regulate adipocyte differentiation. *Cell Metab*. 14:537-544.

Travaglione, S., G. Messina, A. Fabbri, L. Falzano, A.M. Giammarioli, M. Grossi, S. Rufini, and C. Fiorentini. 2005. Cytotoxic necrotizing factor 1 hinders skeletal muscle differentiation in vitro by perturbing the activation/deactivation balance of Rho GTPases. *Cell Death Differ*. 12:78-86.

Trott, O., and A.J. Olson. 2010. AutoDock Vina: improving the speed and accuracy of docking with a new scoring function, efficient optimization, and multithreading. *J Comput Chem*. 31:455-461.

Tuller, G., C. Hrastnik, G. Achleitner, U. Schiefthaler, F. Klein, and G. Daum. 1998. YDL142c encodes cardiolipin synthase (Cls1p) and is non-essential for aerobic growth of Saccharomyces cerevisiae. *FEBS Lett*. 421:15-18.

Tyurina, Y.Y., W. Lou, F. Qu, V.A. Tyurin, D. Mohammadyani, J. Liu, M. Huttemann, M.A. Frasso, P. Wipf, H. Bayir, M.L. Greenberg, and V.E. Kagan. 2017. Lipidomics Characterization of Biosynthetic and Remodeling Pathways of

Cardiolipins in Genetically and Nutritionally Manipulated Yeast Cells. *ACS Chem Biol*. 12:265-281.

Tyurina, Y.Y., S.M. Poloyac, V.A. Tyurin, A.A. Kapralov, J. Jiang, T.S. Anthonymuthu, V.I. Kapralova, A.S. Vikulina, M.Y. Jung, M.W. Epperly, D. Mohammadyani, J. Klein-Seetharaman, T.C. Jackson, P.M. Kochanek, B.R. Pitt, J.S. Greenberger, Y.A. Vladimirov, H. Bayir, and V.E. Kagan. 2014. A mitochondrial pathway for biosynthesis of lipid mediators. *Nat Chem*. 6:542-552.

Vadkertiova, R., J. Molnarova, D. Vranova, and E. Slavikova. 2012. Yeasts and yeast-like organisms associated with fruits and blossoms of different fruit trees. *Can J Microbiol*. 58:1344-1352.

Valianpour, F., R.J. Wanders, P.G. Barth, H. Overmars, and A.H. van Gennip. 2002. Quantitative and compositional study of cardiolipin in platelets by electrospray ionization mass spectrometry: application for the identification of Barth syndrome patients. *Clin Chem*. 48:1390-1397.

Valianpour, F., R.J. Wanders, H. Overmars, F.M. Vaz, P.G. Barth, and A.H. van Gennip. 2003. Linoleic acid supplementation of Barth syndrome fibroblasts restores cardiolipin levels: implications for treatment. *J Lipid Res*. 44:560-566.

Vankuijk, F.J.G.M., A. Sevanian, G.J. Handelman, and E.A. Dratz. 1987. A New Role for Phospholipase-A2 - Protection of Membranes from Lipid-Peroxidation Damage. *Trends Biochem Sci*. 12:31-34.

Vaz, F.M., R.H. Houtkooper, F. Valianpour, P.G. Barth, and R.J. Wanders. 2003. Only one splice variant of the human TAZ gene encodes a functional protein with a role in cardiolipin metabolism. *J Biol Chem*. 278:43089-43094.

Vreken, P., F. Valianpour, L.G. Nijtmans, L.A. Grivell, B. Plecko, R.J. Wanders, and P.G. Barth. 2000. Defective remodeling of cardiolipin and phosphatidylglycerol in Barth syndrome. *Biochem Biophys Res Commun*. 279:378-382.

Wallace, M.A., P.A. Della Gatta, B. Ahmad Mir, G.M. Kowalski, J. Kloehn, M.J. McConville, A.P. Russell, and S. Lamon. 2016. Overexpression of Striated Muscle Activator of Rho Signaling (STARS) Increases C2C12 Skeletal Muscle Cell Differentiation. *Front Physiol*. 7:7.

Whited, K., M.G. Baile, P. Currier, and S.M. Claypool. 2013. Seven functional classes of Barth syndrome mutation. *Hum Mol Genet*. 22:483-492.

Williamson, D.L., D.C. Butler, and S.E. Alway. 2009. AMPK inhibits myoblast differentiation through a PGC-1alpha-dependent mechanism. *Am J Physiol Endocrinol Metab*. 297:E304-314.

Wright, M.M., and C.R. McMaster. 2002. PC and PE synthesis: mixed micellar analysis of the cholinephosphotransferase and ethanolaminephosphotransferase activities of human choline/ethanolamine phosphotransferase 1 (CEPT1). *Lipids*. 37:663-672.

Wu, J., and R.J. Trumbly. 1998. Multiple regulatory proteins mediate repression and activation by interaction with the yeast Mig1 binding site. *Yeast*. 14:985-1000.

Xu, Y., M. Condell, H. Plesken, I. Edelman-Novemsky, J. Ma, M. Ren, and M. Schlame. 2006a. A Drosophila model of Barth syndrome. *Proc Natl Acad Sci U S A*. 103:11584-11588.

Xu, Y., R.I. Kelley, T.J. Blanck, and M. Schlame. 2003. Remodeling of cardiolipin by phospholipid transacylation. *J Biol Chem*. 278:51380-51385.

Xu, Y., A. Malhotra, M. Ren, and M. Schlame. 2006b. The enzymatic function of tafazzin. *J Biol Chem*. 281:39217-39224.

Xu, Y., J.J. Sutachan, H. Plesken, R.I. Kelley, and M. Schlame. 2005. Characterization of lymphoblast mitochondria from patients with Barth syndrome. *Lab Invest*. 85:823-830.

Yang, J., R. Yan, A. Roy, D. Xu, J. Poisson, and Y. Zhang. 2015. The I-TASSER Suite: protein structure and function prediction. *Nature methods*. 12:7-8.

Yang, W.S., R. SriRamaratnam, M.E. Welsch, K. Shimada, R. Skouta, V.S. Viswanathan, J.H. Cheah, P.A. Clemons, A.F. Shamji, C.B. Clish, L.M. Brown, A.W. Girotti, V.W. Cornish, S.L. Schreiber, and B.R. Stockwell. 2014. Regulation of ferroptotic cancer cell death by GPX4. *Cell*. 156:317-331.

Ye, C., W. Lou, Y. Li, I.A. Chatzispyrou, M. Huttemann, I. Lee, R.H. Houtkooper, F.M. Vaz, S. Chen, and M.L. Greenberg. 2014. Deletion of the cardiolipin-specific phospholipase Cld1 rescues growth and life span defects in the tafazzin mutant: implications for Barth syndrome. *J Biol Chem*. 289:3114-3125.

Yu, T., J.L. Robotham, and Y. Yoon. 2006. Increased production of reactive oxygen species in hyperglycemic conditions requires dynamic change of mitochondrial

morphology. *Proceedings of the National Academy of Sciences of the United States of America*. 103:2653-2658.

Zhang, J.J. 2011. Seamless networks of myocardial bioenergetics. *J Physiol*. 589:5013-5014.

Zhang, M., E. Mileykovskaya, and W. Dowhan. 2002. Gluing the respiratory chain together. Cardiolipin is required for supercomplex formation in the inner mitochondrial membrane. *J Biol Chem*. 277:43553-43556.

Zhang, Y., and J. Skolnick. 2004. Scoring function for automated assessment of protein structure template quality. *Proteins*. 57:702-710.

Zhong, H., M. Xiao, K. Zarkovic, M. Zhu, R. Sa, J. Lu, Y. Tao, Q. Chen, L. Xia, S. Cheng, G. Waeg, N. Zarkovic, and H. Yin. 2017. Mitochondrial control of apoptosis through modulation of cardiolipin oxidation in hepatocellular carcinoma: A novel link between oxidative stress and cancer. *Free Radic Biol Med*. 102:67-76.

Zhong, Q., and M.L. Greenberg. 2005. Deficiency in mitochondrial anionic phospholipid synthesis impairs cell wall biogenesis. *Biochem Soc Trans*. 33:1158-1161.

Zhong, Q., J. Gvozdenovic-Jeremic, P. Webster, J. Zhou, and M.L. Greenberg. 2005. Loss of function of KRE5 suppresses temperature sensitivity of mutants lacking mitochondrial anionic lipids. *Mol Biol Cell*. 16:665-675.

Zhong, Q., G. Li, J. Gvozdenovic-Jeremic, and M.L. Greenberg. 2007. Up-regulation of the cell integrity pathway in saccharomyces cerevisiae suppresses temperature sensitivity of the pgs1Delta mutant. *J Biol Chem*. 282:15946-15953.

Zhou, J., Q. Zhong, G. Li, and M.L. Greenberg. 2009. Loss of cardiolipin leads to longevity defects that are alleviated by alterations in stress response signaling. *J Biol Chem*. 284:18106-18114.

Zhu, L.N., Y. Ren, J.Q. Chen, and Y.Z. Wang. 2013. Effects of myogenin on muscle fiber types and key metabolic enzymes in gene transfer mice and C2C12 myoblasts. *Gene*. 532:246-252.

Zinser, E., C.D. Sperka-Gottlieb, E.V. Fasch, S.D. Kohlwein, F. Paltauf, and G. Daum. 1991. Phospholipid synthesis and lipid composition of subcellular membranes in the unicellular eukaryote Saccharomyces cerevisiae. *J Bacteriol*. 173:2026-2034.

ABSTRACT

NOVEL FUNCTIONS OF CARDIOLIPIN REMODELING IN SACCHAROMYCES CEREVISIAE AND MAMMALIAN CELLS IMPLACATIONS FOR BARTH SYNDROME

by

WENJIA LOU

December 2017

Advisor: Dr. Miriam L. Greenberg

Major: Biological Sciences

Degree: Doctor of Philosophy

Cardiolipin (CL) is a unique phospholipid that is primarily localized within the inner mitochondrial membrane. Newly synthesized CL undergoes acyl remodeling to produce CL species enriched with unsaturated acyl groups. The tafazzin gene (TAZ) encodes a transacylase that remodels CL. Deficiencies in CL remodeling cause Barth syndrome (BTHS), an X-linked genetic disorder resulting from TAZ mutations that lead to reduced total CL content and an accumulation of monolysocardiolipin (MLCL), an intermediate of the CL remodeling pathway. However, which of these biochemical outcomes contributes to the physiological defects is not fully understood.

Deletion of yeast CL phospholipase rescues the *taz1Δ* growth phenotype. We concluded that an increased MLCL/CL, but not decreased CL unsaturation, is likely the primary cause of decreased respiratory growth and chronological life span observed in *taz1Δ*. This suggests that the physiological defects of BTHS patients is possibly due to increased MLCL/CL ratio instead of decreased unsaturated CL, and that attenuation of CL phospholipases may potentially treat BTHS.

Furthermore, our findings suggested a possibility that *CLD1* expression is upregulated in response to oxidative stress. CL peroxidation, resulting from oxidative stress, has been described in mammalian cells. Based on this, one of the physiological roles of CL remodeling is to remove peroxidized CL. Liquid chromatography−mass-spectrometry-based phospholipidomics was combined with genetic and nutritional manipulations to assay CL incorporation of PUFA during the CL biosynthetic and post-synthetic remodeling processes in yeast. Our results demonstrated that yeast readily incorporate PUFA to synthesize oxidizable CL. Although multiple CL-hydroperoxides and CL-dihydroperoxides were readily detected in these cells, cell growth and life span were not impacted. *cld1Δ* cells expressing Δ^{12}-desaturase were utilized to determine the effect of peroxidation on CL remodeling. Using this novel yeast model, in which cells expressed Δ^{12}-desaturase, the specificity of Cld1 to peroxidized CL, and its role in deacylating peroxidized CL, was determined. In cells expressing desaturase, loss of *CLD1* led to increased peroxidized CL species, as well as decreased cell growth and life span. The findings from this study may contribute to our understanding of CL remodeling and its mechanistic roles in mitigating oxidative stress.

To probe defects resulting from CL deficiency in mammalian cells, I constructed a tafazzin knockout C2C12 cell line, which exhibits an increased MLCL/CL ratio, decreased respiration capacity, increased ROS generation and decreased membrane potential. Although WT and TAZ-KO C2C12 cells can differentiate into myotubes, differentiation was significantly decreased in TAZ-KO C2C12 cells under certain

conditions. Taken together, these findings indicate that CL remodeling plays a role in myotube differentiation.

AUTOBIOGRAPHICAL STATEMENT

EDUCATION:

2010-2017 Ph.D. in Biology Wayne State University, Detroit, USA
2007-2010 M.S. in Zhejiang Sci-tech University, China
2002-2006 B.S. in Zhejiang University, China

HONORS AND AWARDS:

2015-2016 - Graduate School Graduate Research Assistant Award
2016 - Travel grant award from Barth Syndrome Foundation, 7th International Scientific, Medical and Family Conference, Clearwater, Florida.
2016 - ASBMB 2016 Graduate/Postdoctoral Travel Award
2015 - 2015-2016 Thomas C. Rumble University Graduate Fellowship
2014 - Travel grant award from Barth Syndrome Foundation, 7th International Scientific, Medical and Family Conference, Clearwater, Florida.
2009 - 3rd prize - Extracurricular Academic Science and Technology Work Competition, Zhejiang Province
2009 - 2nd prize - Graduate Scholarship - Zhejiang Sci-Tech University
2001 - 1st prize - National Biology Olympic Competition, China

Publications

1. Tyurina* Y. Y., **W. Lou***, et al., 2016. Lipidomics characterization of biosynthetic and remodeling pathways of cardiolipins in genetically and nutritionally manipulated yeast cells. *ACS Chemical Biology*. ***Equal contributors**
2. Ye*, C.**, W. Lou***, et al., 2014. Deletion of the cardiolipin-specific phospholipase Cld1 rescues growth and life span defects in the tafazzin mutant: implications for Barth syndrome. *The Journal of biological chemistry*. 289:3114-3125. ***Equal contributors** http://www.ncbi.nlm.nih.gov/pubmed/24318983
3. **Lou, W**., et al., 2013. Oncolytic adenovirus co-expressing miRNA-34a and IL-24 induces superior antitumor activity in experimental tumor model. *Journal of molecular medicine*. 91:715-725. http://www.ncbi.nlm.nih.gov/pubmed/23292172
4. Chen, Q., **W. Lou**, et al., 2010. Potent antitumor activity in experimental hepatocellular carcinoma by adenovirus-mediated coexpression of TRAIL and shRNA against COX-2. *Clinical cancer research.* 16:3696-3705. http://www.ncbi.nlm.nih.gov/pubmed/20515870
5. **Lou, W.J.**, Q. Chen, L. Liu, and C. Qian. 2010. [miR-34s--a tumor suppression protein p53 highly related microRNA]. *Yi chuan = Hereditas / Zhongguo yi chuan xue hui bian ji. 32:423-430.* http://www.ncbi.nlm.nih.gov/pubmed/20466628
6. **Lou, W**., et al., 2010 [Construction of Adenovirus Armed with miR-34a and Investigation of its Expression *in Vitro*]. *Journal of Zhejiang Institute of Science and Technology.*
7. Chen, Q.**, W**. **Lou**, C. Qian, L. Liu 2010 [Construction of Adenovirus Armed with shRNA (COX-2) and investigation of its Anti-tumor Activity *in Vitro*]. *Journal of Zhejiang Institute of Science and Technology.*